University of Southampton

Faculty of Engineering and Physical Sciences

Physics and Astronomy

Natural Theories of Physics Beyond the Standard Model

by

Simon James Douglas King

Thesis for the degree of Doctor of Philosophy

March 2021

University of Southampton

Abstract

Faculty of Engineering and Physical Sciences
Physics and Astronomy

Thesis for the degree of Doctor of Philosophy

Natural Theories of Physics Beyond the Standard Model
by **Simon James Douglas King**

We study natural models of physics beyond the Standard Model with several directions in mind. Firstly we study the supersymmetric extension of the $U(1)_Y \times U(1)_{B-L}$ model. This non-minimal supersymmetric model maintains the best features of the minimal supersymmetric Standard Model, but provides several new dark matter candidates. We compare metrics of fine-tuning in these two models and characterise these new candidates. We then focus in particular on the superpartner of the right-handed neutrino, the right-handed sneutrino and consider methods of indirect, direct and collider detection.

We then consider Z' signals at the LHC arising from two models, the aforementioned $B - L$ model, as well as one originating from the group $U(1)_R \times U(1)_{B-L}$, which comes from the breaking of $SO(10)$. These models may be distinguished by the axial couplings in the later case leading to different forward-backward asymmetry shapes.

Lastly, we consider neutrino masses and the flavour puzzle. Here we use the framework of modular symmetry to present new models of neutrino masses and mixing in addition to natural charged lepton masses. We then consider a new model scenario which also accommodates the observed quark masses and mixing angles in addition to the lepton sector, providing a natural solution to the fermion mass hierarchies.

Contents

List of Figures

List of Tables

Declaration of Authorship

I, **Simon James Douglas King**, declare that the thesis, entitled *Natural Theories of Physics Beyond the Standard Model*, and the work presented in it are both my own and have been generated by me as the result of my own original research.

I confirm that:

1. This work was done wholly or mainly while in candidature for a research degree at this University;
2. Where any part of this thesis has previously been submitted for a degree or any other qualification at this University or any other institution, this has been clearly stated;
3. Where I have consulted the published work of others, this is always clearly attributed;
4. Where I have quoted from the work of others, the source is always given. With the exception of such quotations, this thesis is entirely my own work;
5. I have acknowledged all main sources of help;
6. Where the thesis is based on work done by myself jointly with others, I have made clear exactly what was done by others and what I have contributed myself;
7. Parts of this work have been published as references [1–5].

Signed:

Date:

Acknowledgements

I would like to first thank my supervisor Stefano Moretti for his continued guidance over the last five years, providing me with every possible opportunity for personal and professional growth available. I would also like to thank my collaborator and father Steve King for his endless support throughout my life and for all his teachings, which have shaped the way I think about physics. I also extend my gratitude to Ferruccio Feruglio and Stefano Rigolin for their knowledge and expertise throughout my time in Padova.

I have had a wonderful selection of friends throughout my PhD which have made the time a thoroughly enjoyable experience, and I would like to thank all of those in office 4007 in Southampton. There are too many names to thank, but I make a special mention to Azaria Coupe, Billy Ford, Alex Mitchell, Elena Perdomo Méndez, James Richings, Ronnie Rodgers, Sam Rowley and Alex Titterton. In addition, I would like to thank all my friends from Elusiνes, including Rupert Coy, Sergio González Martín and Olcyr Sumensari.

Finally, I would like to thank Laura and my parents for their constant encouragement and support.

Nomenclature

SM	Standard Model	BSM	Beyond the Standard Model
EW	Electroweak	MSSM	Minimal Supersymmetric Standard Model
LH	Left-Handed	EWSB	Electroweak Symmetry Breaking
RH	Right-Handed	EWPO	Electroweak Precision Observable
BR	Branching Ratio	VEV	Vacuum Expectation Value
CP	Charge-Parity	SSB	Spontaneous Symmetry Breaking
DM	Dark Matter	RGE	Renormalisation Group Equations
FT	Fine-Tuning	SUSY	Supersymmetry
CL	Confidence Level	SUGRA	Supergravity
TM	Trimaximal	LSP	Lightest Supersymmetric Particle
16-D	16 Dimensional	$B-L$	Baryon minus Lepton number
MO	Mass Ordering	BLR	$U(1)_R \times U(1)_{B-L}$
NO	Normal Ordering	WIMP	Weakly Interacting Massive Particle
IO	Inverted Ordering	GUT	Grand Unified Theory
HB	HiggsBounds	FCNC	Flavour Changing Neutral Currents
HS	HiggsSignals	dSphs	Dwarf Spheroidal Galaxies
SK	Super-Kamiokande	GKM	Gauge-Kinetic Mixing
HL	High-Luminosity	2HDM	2-Higgs Doublet Model
BG	Barbieri-Giudice	LHC	Large Hadron Collider
DY	Drell-Yan	LEP	Large Electron–Positron Collider
PS	Pati-Salam	CKM	Cabibbo–Kobayashi–Maskawa
CG	Clebsch-Gordan	PMNS	Pontecorvo–Maki–Nakagawa–Sakata
FN	Froggatt-Nielsen	GIM	Glashow–Iliopoulos–Maiani

Chapter 1

Introduction

1.1 Overture

Despite the overwhelming success of the Standard Model (SM), there are many outstanding puzzles which remain to be solved. In this thesis, we investigate several interesting models which provide some natural solutions to some of the main challenges in modern High Energy Physics (HEP).

At the lowest energy scale lies neutrino physics. Predicted massless in the SM, but now known to have non-zero, $< \mathcal{O}(1)$ eV masses, this is perhaps the most direct evidence of Beyond the SM (BSM) physics we see. All of the models discussed in this thesis are motivated with solutions which can accommodate neutrino masses, directly or otherwise. One of the simplest SM extensions which can explain the masses is the $B-L$ model, which promotes the global symmetry in the SM of baryon minus lepton number into a gauge symmetry. For anomaly cancellation, this demands three new Right-Handed (RH) singlets of the SM, which are identified as the RH neutrinos. Breaking the gauged $U(1)_{B-L}$ symmetry sets a dynamic scale for the neutrino mass, as well as providing other interesting phenomenology related to the associated $B-L$ Higgs and massive gauge boson. Such a theory is well motivated, but does not provide concrete predictions on the nature of the neutrinos masses and mixing. Here, flavour symmetry models can produce falsifiable predictions of the properties of neutrinos. Discrete symmetries here attempt to match the currently measured neutrino properties, as well as providing predictions for parameters which will be directly measured by the next generation of neutrino experiments.

At the larger Electroweak (EW) and TeV scales, the Large Hadron Collider (LHC) is searching for BSM content both directly through production of new particles, as well as from deviations in quantities predicted by the SM. One of the most compelling theories here is low-scale Supersymmetry (SUSY). This theory addresses numerous problems in HEP, but perhaps the most immediate concern is the hierarchy problem. Introducing any heavy BSM content will lead to large corrections to the bare mass of the SM Higgs, such that the corrected Higgs mass must be very finely tuned to remain at the EW scale. The scale of this fine-tuning is considered unacceptably large (up to 1 part in 10^{34} for content around the Planck scale) and begs for a NP

explanation. In addition, SUSY can predict a suitable Dark Matter (DM) candidate, and modifies the running of the SM gauge couplings such that they appear to all unify, and is a necessary ingredient for many theories of Quantum Gravity (QG).

At the highest scale are Grand Unified Theories (GUTs). Motivated by the running of gauge couplings which almost meet in the SM and directly meet in low-scale SUSY models, GUTs aim to unify the three SM forces. There are numerous GUT groups which are considered, but $SO(10)$, $SU(5)$ and the Pati-Salam (PS) group $SU(4)_C \times SU(2)_L \times SU(2)_R$ are the most popular choices. Unification has been a guiding principle in physics since Maxwell's unification of electricity and magnetism into electromagnetism (EM) and EM combining with the weak force into the EW theory.

In chapter one we will present a full introduction to the SM, neutrino masses, SUSY and GUTs. We will then present five chapters based on models which relate to these topics. In chapter two we introduce the non-SUSY $B - L$ model, and then the SUSY version the $B - L$ Supersymmetric SM (BLSSM). We compare the Fine-Tuning (FT) of this model to the usual minimal supersymmetric SM (MSSM), as well as identify new DM candidates. We find that the levels of FT similar, however we see several features of the BLSSM model result in a larger parameter space for solutions which satisfy the relic density requirements for the DM candidate. In chapter three we continue with the the BLSSM, but focus on the RH sneutrino as the DM candidate. Here we study the direct, indirect and collider approaches to identify the RH sneutrino as DM and find several smoking gun signals of the BLSSM. In chapter four we investigate a comparison between the aforementioned $U(1)_Y \times U(1)_{B-L}$ model with the similar $U(1)_R \times U(1)_{B-L}$ model, dubbed the BLR. The later model has origins from $SO(10)$ whereas the former does not nicely embed itself into a GUT group. Both predict a Z' with similar phenomenology at the LHC and in this chapter we aim to discriminate the two similar models, should a signal be seen, by their forward-backward asymmetries. We then move on to models of neutrino masses in chapters five and six, and study the string-theory inspired framework of modular symmetry. In chapter five we present a new model which provides natural (ie with model parameters close to unity) models of charged lepton masses in addition to predicting neutrino masses and mixing parameters competitively, with a reduced χ^2 close to unity. We then go on, in chapter six, to study a model in the framework of modular symmetry which predicts all fermion masses (leptons and quarks) with natural inputs, close to unity and again find several solutions with a successful reduced $\chi^2 \approx 1$. Finally, we present our conclusions in chapter seven.

1.2 Standard Model

1.2.1 The Gauge Sector

The SM is a gauge theory based on the group $SU(3)_c \times SU(2)_L \times U(1)_Y$, comprising the strong interactions (where c is for colour), weak interactions (denoted by L, referring to the Left-Handed

(LH) fermions which couple to it [1]), and the hypercharge, denoted by Y.

We begin by considering the gauge sector of the SM. Their interactions are determined by the Lagrangian involving the field strength tensors,

$$\mathcal{L}^{\text{gauge}} = -\frac{1}{4}G^a_{\mu\nu}G^{a,\mu\nu} - \frac{1}{4}W^a_{\mu\nu}W^{a,\mu\nu} - \frac{1}{4}B_{\mu\nu}B^{\nu\mu}. \tag{1.1}$$

The forms of the field strength tensors are defined by their symmetry. The Abelian (where different elements of the group commute) hypercharge field strength tensor is defined as

$$B_{\mu\nu} = \partial_\mu B_\nu - \partial_\nu B_\mu, \tag{1.2}$$

where a local transformation of the hypercharge field takes the form

$$B_\mu \to B_\mu + \frac{1}{g'}\partial_\mu \omega_Y(x), \tag{1.3}$$

where g' is the hypercharge coupling and $\omega_Y(x)$ parametrises a local (space-time dependent) phase. With this transformation, the term $-\frac{1}{4}B_{\mu\nu}B^{\mu\nu}$ is invariant. We note here that as this is an Abelian group, all terms are quadratic derivatives of the gauge boson fields, and so there are no interactions between hypercharge bosons.

This is not the case for non-Abelian theories. The weak field strength tensor, now with index $a = 1,\ 2,\ 3$, which refers to the 3 different gauge fields (generally for $SU(N)$, the $N^2 - 1$ fields), is defined as

$$W^a_\mu = \partial_\mu W^a_\nu - \partial_\nu W^a_\mu + g\epsilon^{abc}W^b_\mu W^c_\nu, \tag{1.4}$$

where ϵ^{abc} is the totally antisymmetric three-index tensor (also known as the Levi-Civita symbol), such that $\epsilon^{123} = 1$. This is defined from the group generators T^a,

$$\left[T^a, T^b\right] = i\epsilon^{abc}T^c, \tag{1.5}$$

where the generators $T^a = \sigma^a/2$ and σ^a are the Pauli matrices,

$$\sigma_1 = \begin{pmatrix} 0 & 1 \\ 1 & 0 \end{pmatrix} \quad \sigma_2 = \begin{pmatrix} 0 & -i \\ i & 0 \end{pmatrix} \quad \sigma_3 = \begin{pmatrix} 1 & 0 \\ 0 & -1 \end{pmatrix}. \tag{1.6}$$

The fields $W^a_{\nu\mu}$ transform locally as

$$W^a_\mu \to W^a_\mu + \frac{1}{g}\partial_\mu \omega^a_L(x) + \epsilon^{abc}W^b_\mu \omega^c_L(x), \tag{1.7}$$

[1] The common choice to use the identifier L in the weak coupling gauge group can be confusing, as Right-Handed (RH) anti-fermions also couple to this, and in principle any new RH fermion could be charged, and any left-handed piece uncharged under $SU(2)$. An alternative, less commonly used, notation is to refer to the group as $SU(2)_W$, where W means weak, though we do not adopt this convention to keep consistent with the standard notation and avoid other confusions with the field strength tensor notation.

such that after a local transformation, one will also gain terms of the form

$$\delta\mathcal{L} \supset g\epsilon^{abc}(\partial_\mu W_\nu^a)W_\mu^b W_\nu^c - \frac{1}{4}g^2\epsilon^{abc}\epsilon_{ade}W_\mu^b W_\nu^c W_\mu^d W_\nu^e, \tag{1.8}$$

which are the three-point and four-point interaction terms. Here we find the crucial difference that while Abelian fields do not interact, non-Abelian gauge fields do. The strong interaction $SU(3)_c$, being non-Abelian, looks very similar to the weak interaction, however now the index a runs from $1 \dots 8$, since $N = 3$, and $t^a = \lambda^a/2$, the Gell-Mann matrices (see appendix),

$$G_\mu^a = \partial_\mu G_\nu^a - \partial_\nu G_\mu^a + g\epsilon^{abc}G_\mu^b G_\nu^c, \tag{1.9}$$

$$\left[t^a, t^b\right] = if^{abc}t^c, \tag{1.10}$$

$$G_\mu^a \to G_\mu^a + \frac{1}{g_s}\partial_\mu\omega_c^a(x) + \epsilon^{abc}G_\mu^b\omega_c^c(x). \tag{1.11}$$

A mass term in any gauge field, such as $\Omega_\mu = \left(B_\mu,\ W_\mu^a,\ G_\mu^a\right)$,

$$\mathcal{L} \supset \frac{1}{2}m_\Omega^2\Omega_\mu\Omega^\mu, \tag{1.12}$$

is not gauge-invariant, and thus forbidden to be entered in the Lagrangian, therefore all (unbroken) gauge bosons must be massless.

Fermions will transform in the following way under the three gauge transformations

$$U(1)_Y: \qquad \psi \to e^{i\omega_Y}\psi, \tag{1.13}$$

$$SU(2)_L: \qquad \psi \to e^{i\omega_L^a T^a}\psi, \tag{1.14}$$

$$SU(3)_c: \qquad \psi \to e^{i\omega_c^a t^a}\psi, \tag{1.15}$$

and interact with the gauge fields through the covariant derivative,

$$\mathcal{D}_\mu = \partial_\mu - ig'B_\mu Y - igW_\mu^a T^a - ig_s G_\mu^a t^a, \tag{1.16}$$

$$\mathcal{L}^{\text{fermion, gauge}} = i\bar{\psi}(\mathcal{D}_\mu\gamma^\mu)\psi. \tag{1.17}$$

1.2.2 The Fermion Sector

The fermionic content of the SM is summarised in table 1.1. There are three generations of chiral (LH and RH) fields transform in different ways, as opposed to vector-like where LH and RH fields transform in the same way) of quarks and leptons, where all three generations have the same representation. In Dirac notation, the Lagrangian for a fermion ψ with mass m has the form

$$\mathcal{L} = i\bar{\psi}\partial_\mu\gamma^\mu\psi - m\bar{\psi}\psi. \tag{1.18}$$

Generation			Representation under
1	2	3	$SU(3)_c \times SU(2)_L \times U(1)_Y$
$\begin{pmatrix} u \\ d \end{pmatrix}_L$	$\begin{pmatrix} c \\ s \end{pmatrix}_L$	$\begin{pmatrix} t \\ b \end{pmatrix}_L$	(**3**, **2** , 1/6)
$\begin{pmatrix} \nu_e \\ e \end{pmatrix}_L$	$\begin{pmatrix} \nu_\mu \\ \mu \end{pmatrix}_L$	$\begin{pmatrix} \nu_\tau \\ \tau \end{pmatrix}_L$	(**1**, **2**, -1/2)
u_R	c_R	t_R	(**3**, **1**, +2/3)
d_R	s_R	b_R	(**3**, **1**, -1/3)
e_R	μ_R	τ_R	(**1**, **1**, -1)

Table 1.1: Fermionic fields and representations in the SM, in the convention $Q = T^3 + Y$.

We may rewrite this mass term in Weyl notation

$$-m\bar{\psi}\psi = -m\bar{\psi}_R\psi_L - m\bar{\psi}_L\psi_R, \tag{1.19}$$

and can see that we may not write any mass term for any of the SM particle content, for example a term like me_Le_R would break gauge invariance of both $SU(2)_L$ and $U(1)_Y$. To generate both particle and gauge boson masses as observed, we need to consider the final piece of the SM, the Higgs sector.

1.2.3 The Higgs Sector

To the aforementioned gauge and fermionic sector, we add a complex, $SU(2)_L$ doublet scalar, Φ, with hypercharge $Y = 1/2$ and a colour singlet,

$$\Phi = \begin{pmatrix} \phi^+ \\ \phi^0 \end{pmatrix} = \frac{1}{\sqrt{2}} \begin{pmatrix} \phi_1 + i\phi_2 \\ \phi_3 + i\phi_4 \end{pmatrix}, \tag{1.20}$$

which has four real degrees of freedom $\phi_1 \dots \phi_4$. The Lagrangian for this new scalar is

$$\mathcal{L}_\Phi = |\mathcal{D}_\mu\Phi|^2 - V(\Phi) + \mathcal{L}_{\text{Yukawa}}, \tag{1.21}$$

with kinetic and gauge interactions contained in the first piece, the potential written in the second, and fermionic interactions contained in the final, Yukawa [2] Lagrangian. The normalisation $1/\sqrt{2}$ is chosen so that the kinetic piece of the Lagrangian has the correct normalisation, $\mathcal{L} \supset \frac{1}{2}\partial_\mu\phi_i\partial^\mu\phi_i$. A general potential for a complex scalar contains two allowed pieces,

$$V(\Phi) = -\mu^2\Phi^\dagger\Phi + \lambda(\Phi^\dagger\Phi)^2, \tag{1.22}$$

[2] Any interaction between a scalar field (or pseudoscalar) and a fermion is named after Hideki Yukawa, who predicted pion (pseudoscalar) interactions with protons and neutrons (fermions).

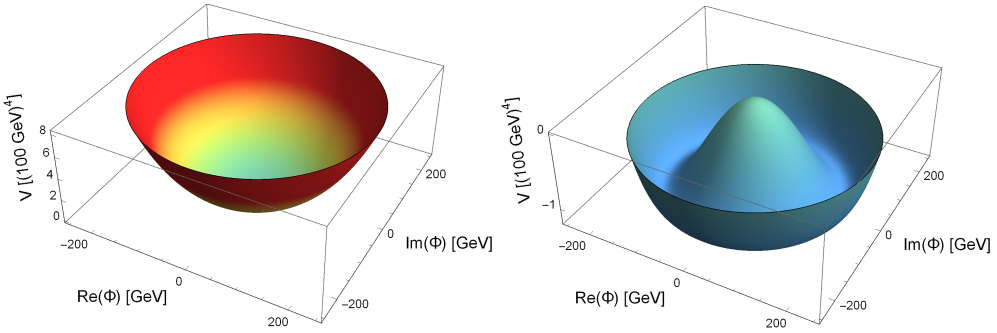

Figure 1.1: Plots of the Higgs potential, $V(\Phi) = -\mu^2\Phi^\dagger\Phi + \lambda(\Phi^\dagger\Phi)^2$ as a function of $\mathrm{Re}(\Phi)$ and $\mathrm{Im}(\Phi)$, for $-\mu^2 > 0$ (left and $-\mu^2 < 0$ (right). The parameters $\lambda \simeq 0.129$ and $|\mu^2| \simeq (88.4\mathrm{GeV})^2$ are obtained from the measured Higgs mass $m_h = 125$ GeV and vev, $v = 246$ GeV. In the right hand case, the minimum lies at $\Phi = v/\sqrt{2} \simeq 174$ GeV.

where μ and λ are fundamental parameters of the theory and

$$\Phi^\dagger\Phi = \frac{1}{2}(\phi_1^2 + \phi_2^2 + \phi_3^2 + \phi_4^2). \tag{1.23}$$

For a stable potential, we must have that $\lambda > 0$, which leave two scenarios where $-\mu^2 > 0$ and $-\mu^2 < 0$. This is shown in figure 1.1 on the left and right side respectively. In the former scenario, the minimum lies at $|\Phi| = \sqrt{\Phi^\dagger\Phi} = 0$ (coloured in turquoise), which does not break any symmetry as a gauge transformation acting on the vacuum $\Phi = 0$ does not change the state. Nature realises the other scenario, with negative $-\mu^2$ and positive λ. Here the ground state lies away from $\Phi = 0$, at the base of the "Mexican-hat" shaped potential, coloured in blue. Since now $\Phi_{\min} \neq 0$, $SU(2)_L \times U(1)_Y$ transformations rotate the vacuum around this minima ring, and the gauge symmetry is spontaneously broken in the vacuum.

We may find the vacuum state value of Φ in the ground state by minimising the potential,

$$\frac{dV(\Phi)}{d\sqrt{\Phi^\dagger\Phi}} = -\mu^2 + 2\lambda\Phi^\dagger\Phi = 0, \tag{1.24}$$

$$\sqrt{\Phi^\dagger\Phi} = \sqrt{\frac{\mu^2}{2\lambda}} \equiv \frac{v}{\sqrt{2}}. \tag{1.25}$$

We notice at this point there is a global $O(4)$ symmetry among the column vector $(\phi_1,\ \phi_2,\ \phi_3,\ \phi_4)^T$, i.e. $\phi_i \to O_{ij}\phi_j \implies \Phi^\dagger\Phi \to \Phi^\dagger\Phi$, if $O_{ij}O_{ik} = \delta_{jk}$, which is the $O(4)$ rotational symmetry group. This allows us to choose a single component to take the vacuum expectation value (VEV), rather than it lie in some combination of fields. Without loss of generality, we may choose the vev to lie in the ϕ_3 component,

$$\langle\phi_3\rangle = v, \qquad \langle\phi_1\rangle = \langle\phi_2\rangle = \langle\phi_4\rangle = 0, \tag{1.26}$$

which is why we chose the normalisation relating v and $V(\Phi)|_{\min}$. We also permit a new real scalar h, with zero vev $\langle h\rangle = 0$ related to excitations around the vacuum, $\phi_3 = h + v$, so that our

final Higgs doublet becomes

$$\Phi = \frac{1}{\sqrt{2}} \begin{pmatrix} \phi_1 + i\phi_2 \\ h + v + i\phi_4 \end{pmatrix}. \tag{1.27}$$

The form of a generic mass term to a scalar field is made from a quadratic piece in the field, $\mathcal{L}^{\varphi,\text{mass}} = \frac{1}{2}m^2\varphi^2$. From our Higgs potential, we find only one quadratic piece which is in the h field. The other three ϕ_i terms are massless.

$$V(\Phi)^{\text{quadratic}} = \lambda v^2 h^2 \longrightarrow m_h = \sqrt{2\lambda v^2}. \tag{1.28}$$

It is possible to remove the appearance of these massless modes by a gauge transformation. By writing $\xi^1 = \phi_2,\ \xi^2 = \phi_1,\ \xi^3 = -\phi_4$, and working to first order in $(h, \phi_i)/v$, then we may re-write Φ as

$$\Phi = \frac{1}{\sqrt{2}} \exp\left(\frac{i\xi^a\sigma^a}{v}\right) \begin{pmatrix} 0 \\ v + h \end{pmatrix}, \tag{1.29}$$

where σ^a are the Pauli matrices, and the repeated index is summed over $a = 1,\ 2,\ 3$. The gauge transformation in $SU(2)_L$ may now be straight forwardly calculated. Fixing the gauge to be $\omega_L^a(x) = -2\xi^a/v$ at all points in space-time, then we find

$$SU(2)_L: \qquad \Phi \to \exp\left(i\,\omega_L^a \frac{\sigma^a}{2}\right)\Phi = \frac{1}{\sqrt{2}} \begin{pmatrix} 0 \\ v + h \end{pmatrix}. \tag{1.30}$$

This process of "gauging-away" allows us to view the theory in some manner in which these fields are absent. This particular gauge is known as unitary gauge, and is sometimes referred to as the Goldstones being "eaten" by the gauge bosons. We will now describe this effect in detail.

1.2.4 Gauge Boson Masses

Using the covariant derivative, defined in eq. 1.16 on the unitary gauge Higgs field, and defining the combinations [3]

$$\frac{W_\mu^1 - iW_\mu^2}{\sqrt{2}} \equiv W_\mu^+ \qquad \frac{W_\mu^1 + iW_\mu^2}{\sqrt{2}} \equiv W_\mu^-, \tag{1.31}$$

then the gauge-kinetic term of the Higgs takes the form

$$|\mathcal{D}_\mu\Phi|^2 = \frac{1}{2}(\partial_\mu h)(\partial^\mu h) + \frac{g^2v^2}{4}W_\mu^+W^{-\mu} + \frac{g^2v}{2}hW_\mu^+W^{-\mu} + \frac{g^2}{4}hhW_\mu^+W^{-\mu} + \frac{1}{8}(v+h)^2(-g'B_\mu + gW_\mu^3)^2. \tag{1.32}$$

We note that the appearance of a two real scalar fields appearing together in the form $(\varphi_1 + i\varphi_2)$ may be identified as a single complex field $\Psi \equiv \frac{\varphi_1 + i\varphi_2}{\sqrt{2}}$, so the above combination is well justified.

[3] The charge may be correctly assigned to each combination of $W_\mu^1,\ W_\mu^2$ by requiring charge conservation in the fermion-gauge interactions.

The mass terms for this general complex (charged) gauge field Ψ, and real (neutral) field $\mathcal{Z}^0$ are

$$\mathcal{L}^{\text{gauge masses}} = m_\Psi^2 \Psi^\dagger \Psi + \frac{1}{2} m_{\mathcal{Z}}^2 \mathcal{Z}_\mu^0 \mathcal{Z}^{0\mu}. \tag{1.33}$$

Analogously to the masses of real versus complex scalar fields, there is no factor of $1/2$ for the complex field, as it can be written in terms of two real scalar fields and this normalisation generates the $1/2$ from the $1/\sqrt{2}$'s. We may thus extract a mass term for our W boson,

$$m_W = \frac{g^2 v^2}{4}. \tag{1.34}$$

We see that our VEV has given the W a mass, in addition to generating interactions with the Higgs boson. We may measure the parameters g and m_W experimentally, to derive that $v = 246$ GeV.

We now turn out attention to the B_μ and W_μ^3 fields. We may re-write this term as a mass matrix,

$$|\mathcal{D}_\mu \Phi|^2 \supset \frac{1}{8}(v+h)^2 \begin{pmatrix} B_\mu & W_\mu^3 \end{pmatrix} \begin{pmatrix} g'^2 & -gg' \\ -gg' & g^2 \end{pmatrix} \begin{pmatrix} B^\mu \\ W^{3\mu} \end{pmatrix}, \tag{1.35}$$

which we may diagonalise by making a field rotation. Defining

$$\begin{pmatrix} B_\mu \\ W_\mu^3 \end{pmatrix} = \begin{pmatrix} \cos\theta_W & -\sin\theta_W \\ \sin\theta_W & \cos\theta_W \end{pmatrix} \begin{pmatrix} A_\mu \\ Z_\mu \end{pmatrix}, \tag{1.36}$$

and requiring no mixed $A_\mu Z^\mu$ term, we find

$$\cos\theta_W = \frac{g}{\sqrt{g^2+g'^2}}, \quad \sin\theta_W = \frac{g'}{\sqrt{g^2+g'^2}}, \tag{1.37}$$

$$m_A = 0, \quad m_Z = \frac{v\sqrt{g^2+g'^2}}{2} = \frac{m_W}{\cos\theta_W}. \tag{1.38}$$

The physical fields we observe are the photon, A, the $Z-$boson, and the charged $W^\pm$. These fields will appear in the final covariant derivative expression and Feynman rules for all interactions with scalar and fermionic fields may be derived from this. Defining $\sin\theta_W \equiv s_W$, and $\cos\theta_W \equiv c_W$, we may focus on the photon term of the covariant derivative

$$\mathcal{D}_\mu = -iA_\mu(g s_W T^3 + g' c_W Y) + \dots. \tag{1.39}$$

By experiment, we may observe the photon coupling to be eQ where Q is the electric charge of the interacting field and e is the electromagnetic coupling. We may simplify the photon coupling which appears in the covariant derivative using this,

$$\left(g s_W T^3 + g' c_W Y\right) = \frac{gg'}{\sqrt{g^2+g'^2}}(T^3+Y) = eQ, \tag{1.40}$$

from which we identify

$$e = \frac{gg'}{\sqrt{g^2 + g'^2}} = gs_W = g'c_W, \qquad Q = T^3 + Y. \tag{1.41}$$

We may use this to simplify the expression to the $Z-$boson as well. Defining $T^{\pm} = \sigma^{\pm} = \frac{\sigma^1 \pm i\sigma^2}{2}$, we may now write the covariant derivative after EW Symmetry Breaking (EWSB), in the mass basis,

$$\mathcal{D}_\mu = \partial_\mu - ig_s G^a_\mu t^a - i\frac{g}{\sqrt{2}}\left(W^+_\mu T^+ + W^-_\mu T^-\right) - i\frac{e}{s_W c_W} Z_\mu (T^3 - s^2_W Q) - ieA_\mu Q. \tag{1.42}$$

This couples to the Higgs as in eq. 1.35, and to fermions as,

$$\mathcal{L}^{f,\text{ gauge}} = i\bar{\psi}_L \mathcal{D}_\mu \gamma^\mu \psi_L + i\bar{\psi}_R \mathcal{D}_\mu \gamma^\mu \psi_R. \tag{1.43}$$

1.2.5 Fermion Masses

We may now study the couplings of fermions to the Higgs doublets. Whereas previously with no Higgs doublet, inserting a mass term breaks gauge invariance we may now couple to the Higgs doublet which carries $SU(2)_L$ and $U(1)_Y$. For a single generation of charged leptons, we may write down a general coupling to the Higgs boson,

$$\mathcal{L}^{e,\Phi} = -\left(y^0_e \bar{L}_L \Phi e^0_R + y^{0*}_e \bar{e}^0_R \Phi^\dagger L_L\right), \tag{1.44}$$

where the second term is the hermitian conjugate of the first, L is the lepton doublet, Φ is the Higgs doublet and y_e is the complex Yukawa coupling. This may first be made real by a rotation of the field. Writing y^0_e as a real part with phase, $y^0_e = y_e e^{i\phi_{y_e}}$, and a field rotation $e^0_R \to e^{-i\phi_{y_e}} e_R$, then

$$y^0_e e^0_R = y_e e^{i\phi_{y_e}} e^0_R \to y_e e^{i\phi_{y_e}} e^{-i\phi_{y_e}} e_R = y_e e_R, \tag{1.45}$$

$$\implies \mathcal{L}^{e,\Phi} = -\left(y_e \bar{L}_L \Phi e_R + y_e \bar{e}_R \Phi^\dagger L_L\right). \tag{1.46}$$

In unitary gauge and using Weyl notation, this finds

$$\mathcal{L}^{e,\Phi} = -\frac{y_e(v+h)}{\sqrt{2}}(\bar{e}_R e_L + \bar{e_L} e_R), \tag{1.47}$$

which corresponds to an interaction term with the Higgs field, and a mass term for the charged lepton,

$$m_e = \frac{y_e v}{\sqrt{2}}. \tag{1.48}$$

We will now briefly consider the analogous scenario but with a single quark generation. Since the charged lepton appears in the $T^3 = -1/2$ piece of the L doublet, it is clear to see how the mass

is generated. For down quarks this is exactly analogous, but for up quarks there is a subtlety. We are required to construct a doublet where the vev appears in the upper term. This can be done in $SU(2)$ as we may take the $\bar{\mathbf{2}}$ representation, which transforms in the same was as the $\mathbf{2}$ [4]. Explicitly, we construct the object,

$$\tilde{\Phi} \equiv i\sigma^2\Phi^* = i\begin{pmatrix} 0 & -i \\ i & 0 \end{pmatrix}\begin{pmatrix} \phi^{0*} \\ -\phi^- \end{pmatrix}, \tag{1.49}$$

$$\tilde{\Phi}|_{\text{Unitary}} = \begin{pmatrix} (v+h)/\sqrt{2} \\ 0 \end{pmatrix}. \tag{1.50}$$

We may then couple the up-type quarks (after rotating away the complex Yukawa phase), as

$$-\mathcal{L}^{u,\Phi} = y_u \bar{u}_R \tilde{\Phi}^\dagger Q_L + y_u \bar{Q}_L \tilde{\Phi} u_R. \tag{1.51}$$

In the SM, we have three generations of quarks, and so the Yukawa couplings become 3×3 complex matrices. For the quarks before any field rotations, in the flavour basis, in unitary gauge,

$$-\mathcal{L}^{q,\Phi} = \frac{v}{\sqrt{2}}\begin{pmatrix} \bar{u}^0 & \bar{c}^0 & \bar{t}^0 \end{pmatrix}_R Y_u^0 \begin{pmatrix} u^0 \\ c^0 \\ t^0 \end{pmatrix}_L + \frac{v}{\sqrt{2}}\begin{pmatrix} \bar{d}^0 & \bar{s}^0 & \bar{b}^0 \end{pmatrix}_R Y_d^0 \begin{pmatrix} d^0 \\ s^0 \\ b^0 \end{pmatrix}_L + h.c.. \tag{1.52}$$

We may diagonalise this Yukawa matrix by a "bi-unitary" transformation to guarantee real, positive eigenvalues. Defining $\bar{\psi}^0_{u,R} = \begin{pmatrix} \bar{u}^0 & \bar{c}^0 & \bar{t}^0 \end{pmatrix}_R$, and similarly for the RH, down-type, and unconjugated fields, we make the field rotations

$$\psi^0_{u,R} = U_{u,R}\,\psi_{u,R}, \quad \psi^0_{u,L} = U_{u,L}\,\psi_{u,L}, \quad \psi^0_{d,R} = U_{d,R}\,\psi_{d,R}, \quad \psi^0_{d,L} = U_{d,L}\,\psi_{d,L}, \tag{1.53}$$

which are defined such that [5]

$$U^\dagger_{u,R} Y^0_u U_{u,L} = Y_u = \text{diag}(y_u,\ y_c,\ y_t), \quad U^\dagger_{d,R} Y^0_d U_{d,L} = Y_d = \text{diag}(y_d,\ y_s,\ y_b), \tag{1.54}$$

[4] This is not the case in $SU(3)$ (or $SU(N \geq 3)$), where the $\mathbf{3}$ and $\bar{\mathbf{3}}$ do not transform in the same way. If the Higgs mechanism were based on triplet $SU(3)$ interactions, with fermion triplets transforming, then one sector of the fermions would remain massless, unlike the $SU(2)$ case where both up and down type quarks gain mass. This is because of the group theory result that in $SU(2)$ we have $\mathbf{2}\times\bar{\mathbf{2}} = \mathbf{2}\times\mathbf{2} = \mathbf{3}+\mathbf{1}$. Whereas in $SU(3)$, $\mathbf{3}\times\mathbf{3} = \mathbf{6}+\bar{\mathbf{3}}$ and $\mathbf{3}\times\bar{\mathbf{3}} = \mathbf{8}+\mathbf{1}$. We require singlet pieces in the Lagrangian, so we could not perform the same trick with a Higgs triplet of $SU(3)$ as Higgs doublet in $SU(2)$.

[5] We prove here that any complex, square matrix, Y, may be diagonalised to have real, positive eigenvalues via bi-unitary matrices, $U^\dagger_R$ and U_L here. Given the form $D = U^\dagger_R Y U_L$, we construct two Hermitian matrices $H_L = Y^\dagger Y$, and $H_R = YY^\dagger$. A Hermitian matrix may be diagonalised by a single unitary matrix, by $U^\dagger_L H_L U_L = U^\dagger_R H_R U_R = H^{\text{diag}} = \text{diag}(|y_1|^2,\ |y_2|^2,\ |y_3|^2)$. Now $D^\dagger D = H^{\text{diag}}$, so $D = \text{diag}(y_1,\ y_2,\ y_3)$. Note there are cases where this procedure apparently fails, such as when $D^\dagger D = \mathbb{1}$, however in these cases the matrix D is already diagonal up to permutations of the rows, which is allowed by the theory.

where y_i are positive, real entries. As with the charged lepton example, $m_f = \frac{vy_f}{\sqrt{2}}$. This rotation into the mass basis causes flavour changing charged currents, through the $W-$boson, but no Flavour Changing Neutral Currents (FCNCs). We write the gauge-quark interactions from eq. 1.43 in the flavour basis, and then mass basis,

$$\mathcal{L}^{q,(W,Z)} = \bar{\psi}^0_{u,L}\frac{g\cdot\mathbb{1}}{\sqrt{2}}W^+_\mu\gamma^\mu\psi^0_{d,L} + h.c. + \left[\bar{\psi}^0_{u,L}(g_{dZ}\cdot\mathbb{1})Z_\mu\gamma^\mu\psi^0_{u,L} + \bar{\psi}^0_{d,L}(g_{uZ}\cdot\mathbb{1})Z_\mu\gamma^\mu\psi^0_{d,L} + (L\leftrightarrow R)\right], \tag{1.55}$$

$$= \bar{\psi}_{u,L}\frac{U^\dagger_{u,L}(g\cdot\mathbb{1})U_{d,L}}{\sqrt{2}}W^+_\mu\gamma^\mu\psi_{d,L} + h.c. \tag{1.56}$$

$$+ \left[\bar{\psi}_{u,L}U^\dagger_{u,L}(g_{dZ}\cdot\mathbb{1})U_{u,L}Z_\mu\gamma^\mu\psi_{u,L} + \bar{\psi}_{d,L}U^\dagger_{d,L}(g_{uZ}\cdot\mathbb{1})U_{d,L}Z_\mu\gamma^\mu\psi_{d,L} + (L\leftrightarrow R)\right], \tag{1.57}$$

where g_{qZ} parametrises the interaction strength between the up and down type quarks with the Z, and we have written explicitly that the coupling multiplies a unit matrix. In the flavour basis the couplings are diagonal, there are no mixed terms. For the Z interactions, the couplings are of the form $U^\dagger U = \mathbb{1}$, and hence after rotating into the mass basis, these couplings are still flavour conserving. This is referred to as the Glashow–Iliopoulos–Maiani (GIM) mechanism. For the W interactions, the object

$$U^\dagger_{u,L}U_{d,L} \equiv U^{\text{CKM}}, \tag{1.58}$$

is non-diagonal and so there will be flavour changing interactions in W-quark interactions. These are parametrised by the unitary [6] Cabibbo–Kobayashi–Maskawa (CKM) matrix. There is an analogous mixing matrix in the lepton sector, derived in the same way as the CKM but with no RH neutrinos, called the Pontecorvo-Maki-Nakagawa-Sakata (PMNS) matrix. We change notation slightly, that whilst charged fermions in the flavour basis are written with a superscript zero, such as $e^0,\ \mu^0,\ \tau^0$, and the mass basis without the superscript, $e,\ \mu,\ \tau$, we now write neutrinos in flavour basis without the superscript zero, $\nu_e,\ \nu_\mu,\ \nu_\tau$ and in the mass basis with numbered elements $\nu_1,\ \nu_2,\ \nu_3$. The reason for this inconsistency will become apparent later as eases notation in other areas of neutrino physics. We now present the analogue to the CKM matrix in the lepton sector, the PMNS [7] matrix, which rotates the neutrinos in the flavour basis into the mass basis,

$$\begin{pmatrix}\nu_e\\ \nu_\mu\\ \nu_\tau\end{pmatrix}_L = U^{\text{PMNS}}\begin{pmatrix}\nu_1\\ \nu_2\\ \nu_3\end{pmatrix}_L. \tag{1.59}$$

Both the CKM and PMNS matrices may be described in terms of just four parameters, three angles and a complex phase. This parameter counting may be determined in the following way. To begin with there are 9 complex entries in the 3×3 matrix (18 real parameters). The matrices are

[6] $(U^\dagger_{u,L}U_{d,L})^\dagger(U^\dagger_{u,L}U_{d,L}) = \mathbb{1}$.
[7] Also known as MNS, or MNSP.

unitary, which sets 9 constraints from $U_{ij}^{\dagger}U_{jk} = \delta_{ik}$, which reduces the number of free parameters to 9 (made up of 6 phases and 3 angles). [8]

In addition, 5 further phases may be removed by phase rotations on the fermions. [9] This leaves three angles, and one phase which causes CP violation for both the CKM and PMNS matrices. The final matrix may be parametrised by

$$\begin{pmatrix} c_{12}c_{13} & s_{12}c_{13} & s_{13}e^{-i\delta} \\ -s_{12}c_{23} - c_{12}s_{13}s_{23}e^{i\delta} & c_{12}c_{23} - s_{12}s_{13}s_{23}e^{i\delta} & c_{13}s_{23} \\ s_{12}s_{23} - c_{12}s_{13}c_{23}e^{i\delta} & -c_{12}s_{23} - s_{12}s_{13}c_{23}e^{i\delta} & c_{13}c_{23} \end{pmatrix}, \tag{1.60}$$

where $\delta \equiv \delta_{CP}$ is the CP violating phase in each sector (quark and lepton) and $s_{13} = \sin\theta_{13}$, etc. with (very) different angles for quarks and leptons.

To conclude our discussion on the SM, the predictions of this theory have matched experimental observations remarkably well, but there are still some unanswered questions. It is to these that we devote the remainder of this thesis. We begin with introductions on some of the main problems in BSM physics.

1.3 Neutrino Masses

In the SM, LH neutrinos are massless and have no RH partners. We observe, however, that from neutrino oscillation experiments that they have small non-zero masses. The absolute scale of these masses has not been directly measured, but is constrained by cosmological data to be $\lesssim \mathcal{O}(1)$ eV. What is measured precisely by oscillation experiments is the squared mass differences between the three neutrino mass species, in addition to the three mixing angles defined in Eq. 1.60 which parametrise the mixing between the flavour and mass basis. So far the Mass Ordering (MO), of the three states has also not been measured, and results in two possibilities which are discussed in figure 1.2. Further to the MO, the CP violating phase has not yet been directly measured, but in both cases there are hints. The experimentally observed masses and mixing angles are written later in this thesis, in table 5.6.

There are many possibilities for BSM theories which generate these observed masses. One such interesting idea generates masses without needed to introduce any RH partners. This is the "type-II see-saw mechanism", which introduces a new $SU(2)_L$ triplet Higgs field. Here the

[8] Since we may write a unitary matrix in terms of a Hermitian matrix as $U = e^{iH}$, and since a Hermitian matrix has real diagonals, and complex upper triangle, one show there are $N(N-1)/2$ angles and $N(N+1)/2$ phases, hence for a 3×3 unitary matrix, of the 9 real parameters, there are 6 phases and 3 angles

[9] For example, we can write entries of the CKM in terms of a real part and phase, so what appears in the Lagrangian are terms like $(\bar{u}_L e^{i\phi_{ud}} U_{ud} d_L)$. We may then make rotations on the fermion fields to fix this. By setting $u_L \to e^{-i\phi_{ud}} u_L$ then the $(1,1)$ entry of the CKM is made real. Importantly, this phase in the up field does not appear in any other terms in the Lagrangian, as the up quark appears in the combination $\bar{u}_L u_L$ which cancels this phase. We may similarly go through other elements, such as $s_L \to e^{i(\phi_{us} - \phi_{ud})}$ fixing U_{us}, taking care to cancel the new u_L phase. Similarly we may fix U_{ub} with b_L and U_{cd} with c_L. Now U_{cs} and U_{cb} cannot be fixed, but we may fix U_{td} with t. The remaining two terms U_{ts} and U_{tb} also cannot be fixed. We note that no further piece could be helped by any rephasing on d_L, and we removed 5 phases in total.

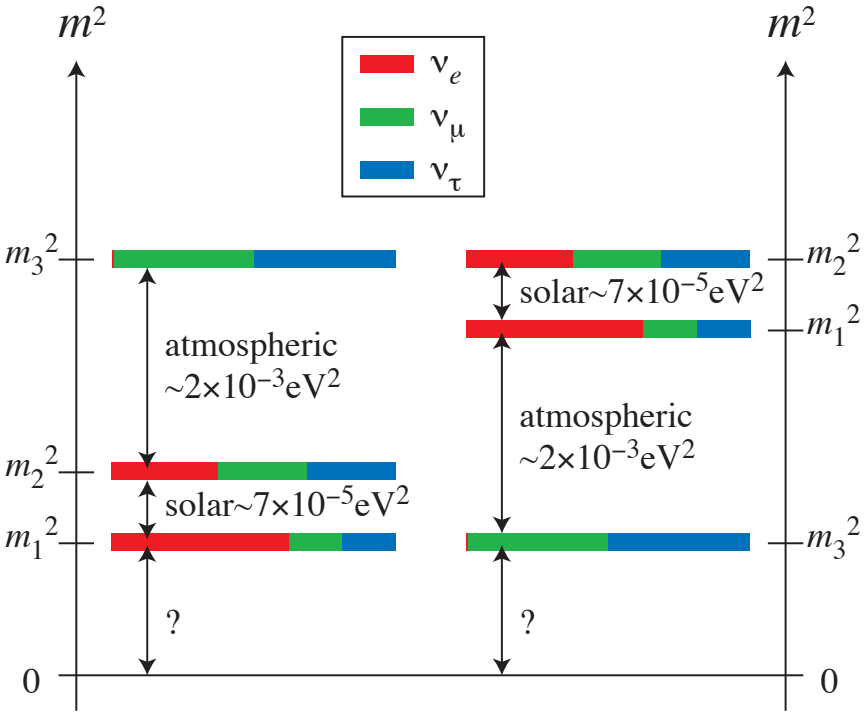

Figure 1.2: (Figure taken from reference [6]). The probability that a particular neutrino mass state ν_i with mass m_i contains a particular charged lepton mass basis state $(\nu_e, \nu_\mu, \nu_\tau)$ is represented by colours. The left and right panels of the figure are referred to as normal or inverted mass squared ordering, respectively, referred to as NO or IO. The value of the lightest neutrino mass is presently unknown.

$SU(2)$ product of the two lepton doublets with a triplet is a singlet, and so we allow a mass term of the form (schematically) $m_\nu \nu_L \nu_L$. This possibility precludes the assumption that there must exist any RH partners to the LH neutrinos, and so we may not simply assert there must exist such RH pieces, in addition to the SM, due to the presence of neutrino masses.

1.3.1 Type-I See-Saw

In this thesis, we consider the implications of introducing RH neutrinos, which offer perhaps a simpler and more natural explanation of neutrino masses compared to other models. For concreteness, we will add three generations [10] of RH neutrinos, which are singlets under the SM gauge group. This will generate a usual Dirac mass term after SSB for the neutrinos,

$$\mathcal{L}_D = -\bar{\nu}_R m^\nu_{LR} \nu_L + \text{h.c.}. \tag{1.61}$$

[10] Though, we note that models exist which may explain data with just two families, or more than three, but for an embedding into $SO(10)$ which we will discuss later, or for gauging $U(1)_{B-L}$, one requires exactly three species to match the number of LH generations.

Whilst inserting fermion mass terms was forbidden by gauge invariance for fermions charged under the SM gauge group, for the RH neutrinos there is no such prevention by symmetry, and so one must also include, in this extension, an unprotected Majorana mass term,

$$\mathcal{L}_M = -\frac{1}{2}\bar{\nu}_R M_{RR} (\nu_R)^c + \text{h.c.}. \tag{1.62}$$

Where ψ^c, is the CP-conjugate of ψ. We note that this mass term M_{RR} will break the global $B-L$ symmetry, since through a mass insertion we may change lepton number by two units. Breaking a symmetry in this way, through the use of a mass term is referred to as "soft" symmetry breaking, so-called since it appears as a mass term, rather than in an interaction which would generate a "hard" scattering process. As this mass, M_{RR}, is unprotected, it is typically set to be very high scales (such as the GUT $\sim 10^{16}$ GeV or Planck $\sim 10^{19}$ GeV), if not fixed by a dynamical scale such as in a gauged $B-L$ model. We write down these two mass terms together, as a mass matrix,

$$\mathcal{L}^\nu_m = \mathcal{L}_M + \mathcal{L}_D = -\frac{1}{2}(\bar{\nu_L}\bar{\nu^c_R}) \begin{pmatrix} 0 & m^T_{LR} \\ m_{LR} & M^T_{RR} \end{pmatrix} \begin{pmatrix} \nu^c_L \\ \nu_R \end{pmatrix} + \text{h.c.}. \tag{1.63}$$

Noting we have used the relation $\bar{\psi_1}^c M \psi^c_2 = \bar{\psi}_2 M^T \psi_1$, which is true for any two fermions (and also note this is a scalar quantity, rather than a matrix), and matrix M, providing $[M, \gamma^\mu] = 0$, which will be true if the indices on M are for neutrino flavour, rather than spinor based.

We wish to diagonalise[11] this matrix as we are interested in the physical masses of our observed neutrino states. We can do this by defining a new set of fields

$$\begin{pmatrix} (\nu_L^{\text{light}})^c \\ \nu_R^{\text{heavy}} \end{pmatrix} \equiv U \begin{pmatrix} \nu^c_L \\ \nu_R \end{pmatrix}, \tag{1.64}$$

$$\begin{pmatrix} \bar{\nu_L}^{\text{light}} & (\bar{\nu_R}^{\text{heavy}})^c \end{pmatrix} = \begin{pmatrix} \bar{\nu_L} & \bar{\nu^c_R} \end{pmatrix} U^\dagger. \tag{1.65}$$

Noting that the charge conjugation and "bar" operations only apply to the spinorial indices, rather than the matrix indices we see here. (ie there is no such operation as $\bar{U}$, nor U^c). We choose the unitary matrix to diagonalise our neutrino mass matrix,

$$U^\dagger \begin{pmatrix} 0 & m^T_{LR} \\ m_{LR} & M^T_{RR} \end{pmatrix} U = \begin{pmatrix} m_{LL} & 0 \\ 0 & m_{RR} \end{pmatrix}. \tag{1.66}$$

So, we may rewrite our neutrino mass Lagrangian as

$$\mathcal{L}^\nu_m = -\frac{1}{2} \begin{pmatrix} \bar{\nu_L}^{\text{light}} & (\bar{\nu_R}^{\text{heavy}})^c \end{pmatrix} \begin{pmatrix} m_{LL} & 0 \\ 0 & m_{RR} \end{pmatrix} \begin{pmatrix} (\nu_L^{\text{light}})^c \\ \nu_R^{\text{heavy}} \end{pmatrix} + \text{h.c.}. \tag{1.67}$$

[11] Because this mass matrix is symmetric, it is diagonalisable under $U^T M^{sym} U = M^{diag}$, on contrast to the traditional $U^\dagger M U = M^{diag}$, though this is not relevant for this derivation

Where in the large $M_{RR} \gg m_{LR}$ limit we find

$$m_{LL} = \frac{-m_{LR}^T m_{LR}}{M_{RR}^T}, \tag{1.68}$$

$$m_{RR} = M_{RR}^T. \tag{1.69}$$

If we take $m_{LR} \sim 100\text{GeV}$ and $M_{RR} \sim 10^{16}\text{GeV}$, then our physical, light neutrino mass state (ie solar neutrinos) will have a mass like $m_{LL} \equiv m_{LR} M_{RR}^{-1} m_{LR} \sim 10^{-3}\text{eV}$, which is very reasonable.

1.3.2 Inverse See-Saw

Another see-saw model, though less minimal is to add 3 SM singlet fermions, "S_2" in addition to the RH neutrinos. This is motivated, for example, by $B-L$ models, as done in [7], where we follow their notation (why we use S_2 rather than S). The Lagrangian for neutrino masses in this model appear like:

$$\mathcal{L}_m^\nu = \bar{\nu}_L m_D \nu_R + \bar{\nu}_R^c M_N S_2 + \text{h.c.}. \tag{1.70}$$

In the basis $\{\nu_L^c, \nu_R, S_2\}$, the 9×9 neutrino mass matrix has the form

$$\begin{pmatrix} \bar{\nu}_L & \bar{\nu}_R^c & \bar{S}_2{}^c \end{pmatrix} \begin{pmatrix} 0 & m_D & 0 \\ m_D^T & 0 & M_N \\ 0 & M_N^T & \mu_s \end{pmatrix} \begin{pmatrix} \nu_L^c \\ \nu_R \\ S_2 \end{pmatrix}. \tag{1.71}$$

Which diagonalises to

$$\begin{pmatrix} -\sqrt{M_N^2 + m_D^2} & 0 & 0 \\ 0 & \dfrac{m_D \mu_s m_D^T}{M_N M_N^T} & 0 \\ 0 & 0 & \sqrt{M_N^2 + m_D^2} \end{pmatrix}. \tag{1.72}$$

Thus one may have light neutrino masses $\mathcal{O}(\text{eV})$ from the central term and $\mathcal{O}(\text{TeV})$ scale heavy masses as favoured by the $B-L$ model, assuming values of $m_D \simeq 100$ GeV, $M_N \simeq 1$ TeV and $\mu_s \simeq 1$ KeV. The physical neutrino states are given in terms of ν_L^c, ν_R, and S_2 as follows:

$$\nu_l = \nu_L^c + a_1 \nu_R + a_2 S_2, \tag{1.73}$$

$$\nu_H = a_3 \nu_L^c + \alpha \nu_R - \alpha S_2, \tag{1.74}$$

$$\nu_{H'} = \alpha \nu_R + \alpha S_2, \tag{1.75}$$

where now ν_l refers to the light state and $\nu_{H,H'}$ are the two degenerate heavy mass states. Given the mass values above, one finds $a_{1,2} \sim m_D/(M_N\sqrt{2 + 2m_D/M_N}) \sim 0.05$, $a_3 \sim m_D/M_N \sim 0.1$ and $\alpha \sim \sin \pi/4$. The smallness of μ is natural in the t'Hooft sense, as the symmetry enhances as $\mu \to 0$, though there is no dynamical understanding of this smallness.

1.3.3 Linear See-Saw

The linear see-saw is similar to the inverse see-saw case, but now with a small element in the (1,3) component, rather than (3,3):

$$\begin{pmatrix} 0 & m_D & \epsilon \\ m_D^T & 0 & M_\chi \\ \epsilon^T & M_\chi^T & 0 \end{pmatrix}. \tag{1.76}$$

Each element here corresponds to a 3×3 block. Solving this in block diagonal form, assuming $\epsilon \ll m_d \ll M_\chi$, one finds

$$\begin{pmatrix} M_\chi + m_D^2 M_\chi^{-1} & 0 & 0 \\ 0 & -(M_\chi + m_D^2 M_\chi^{-1}) & 0 \\ 0 & 0 & -\epsilon \frac{m_D^T}{M_\chi} \end{pmatrix}. \tag{1.77}$$

So the light and heavy physical masses are

$$M_{\nu_L} = -\epsilon \frac{m_D^T}{M_\chi} + \text{h.c.}, \tag{1.78}$$

$$M_{N_1} \sim M_{N_2} \sim M_\chi + m_D^2 M_\chi^{-1} + \text{h.c.}. \tag{1.79}$$

Here we have the light neutrinos as observed in oscillation experiments and $M_{N_{1,2}}$ are the heavier neutral fermions. The smallness of ϵ may allow for a low (TeV) scale M_χ, which is a fundamental feature of all low-scale see-saw mechanisms. We see that M_{ν_l} is linear in m_D, which is proportional to the Yukawa couplings, hence the name "linear" see-saw.

1.4 Supersymmetry

SUSY is the unique space-time extension of the Poincaré group. This has interesting applications to more formal physics, such as string theory, supergravity (SUGRA), meta-stability of the vacuum, inflation and scattering amplitudes, but low-scale (ie near EW) supersymmetric theories also have phenomenological applications. It has been one of the great interests of recent years in HEP to find low scale evidence of this theory, but so far there are no hints. There are many appealing features which address problems in the SM from low-scale SUSY, but perhaps none more compelling than a solution to the "hierarchy problem". So far we have only discussed the SM with tree level physics, but a problem arises when we consider quantum corrections to the Higgs boson mass parameter, μ. A full derivation is done in appendix A, but simply write the result here. With a Lagrangian $\mathcal{L} \supset -\lambda H \bar{f} f$, a self energy diagram with fermion loop yields a correction

$$\Delta m_H^2 = -N_c \frac{|\lambda_F|^2}{8\pi^2} \Lambda_{UV}^2 + \ldots, \tag{1.80}$$

and for a complex scalar S with mass m_S with Lagrangian term $-\lambda_S|H|^2|S|^2$, there is the mass correction,

$$\Delta m_H^2 = \frac{\lambda_S}{16\pi^2}\left[\Lambda_{UV}^2 - 2m_S^2\ln(\Lambda_{UV}/m_S) + \ldots\right], \tag{1.81}$$

where N_c is the number of colours of a fermion, and Λ_{UV} is an ultraviolet momentum cut-off used to regulate the loop integral. This should be interpreted as an energy scale at which new physics alters the high-energy behaviour of the theory. This is generally thought to be the GUT scale at which point the gauge groups unify $\sim \mathcal{O}(10^{16}$ GeV), or certainly at the Planck scale, $\sim \mathcal{O}(10^{19}$ GeV), where quantum gravity effects should be considered. Further to the problems associated with a Λ_{UV}, even using dimensional regularization, the counter term to the Higgs mass parameter μ has pieces proportional to m_S^2. For any large m_S content, such as appearing in GUTs, or even for any heavy vector-like fermions F with masses m_F not from a Higgs coupling (but coupling to the Higgs at two-loop order, through gauge interactions), then the bare Higgs mass will have to be extremely finely tuned such that these large counter-terms cancel. In the GUT scenario, this leads to a Fine-Tuning (FT) of $M_{GUT}^2/M_{EW}^2 \sim 1$ part in 10^{28}. This large degree of FT is known as the Hierarchy problem. This problem is fundamentally with the μ parameter of the Higgs potential, and so extends not just to the mass of the physical scalar Higgs, but is also intimately related to the vev, from $v = \frac{\sqrt{\mu^2}}{\lambda}$. Since $\lambda \lesssim 1$ for perturbativity, taking orders of magnitude $v \sim \mu$. So, unrelated to the tuning due to high mass new content is the question of why gravity is so much weaker than the other forces, i.e. why is $v|_{246\text{ GeV}} << M_{Pl}|_{10^{19}\text{ GeV}}$?

There are numerous solutions to the Hierarchy problem, such as suggesting the observed 125 GeV state is not a fundamental scalar but composite, or that one should only consider effective field theory approach and so the cut-off scale is much lower, or even that this amount of FT is acceptable (the anthropic principle). The final approach we will discuss is to notice that the scalar and fermion corrections to the Higgs mass come with opposite signs, due to Bose-Einstein statistics. To cancel the contributions from each fermion, there exists a scalar partner. Likewise to cancel any scalar contribution, there is a new fermionic partner. This involves the imposition of a symmetry between fermions and bosons, called a supersymmetry.

We may introduce an operator Q and $Q^\dagger$ that generate such transformations,

$$Q\,|\text{Boson}\rangle = |\text{Fermion}\rangle\,, \qquad Q\,|\text{Fermion}\rangle = |\text{Boson}\rangle\,. \tag{1.82}$$

Further details of the algebra associated with these operators (SUSY algebra) will not be discussed here. With this new symmetry between fermions and bosons, the irreducible representations of the SUSY algebra are supermultiplets, which contain equal numbers of fermionic and bosonic degrees of freedom, and combining a Weyl fermion and complex scalar field is a chiral supermultiplet.

We will now discuss the MSSM. Chiral supermultiplets embed the SM fermions and their scalar, spin-0 counterparts (prefixed with an "s-" for scalar), the sfermions. The gauge fields of the SM are placed in gauge (or vector) supermultiplets, with their spin 1/2 partners (suffixed

with "-ino"), the gauginos. The Higgs is also placed in a chiral supermultiplet with its spin 1/2 superpartner the Higgsino. All SUSY partners must have the same quantum numbers as their counterparts, and in the limit of unbroken SUSY, also the same masses. Since we do not observe any partners at the same mass as the usual particle content, then SUSY must be broken in some way. Since we are interested in solving the hierarchy problem, we expect the scale of this breaking to happen at low energies. As with the global $B-L$ softly broken with a mass term M_{RR}, we may break the SUSY by inserting "soft" mass terms for the sfermions, by hand [12].

Supersymmetric theories may be described in terms of their superpotential, W. The Lagrangian may be reconstructed from this in the following way. A SUSY model with several chiral supermultiplets, ψ_i has a non-gauge, interacting Lagrangian given by

$$\mathcal{L}^{\text{int}} = -\frac{1}{2}W^{ij}\psi_i\psi_j + W^i F_i + \text{h.c.}, \tag{1.83}$$

where the holomorphic [13] superpotential W derives the W^i and W^{ij} terms as

$$W^i = \frac{\partial W}{\partial \phi_i}, \qquad W^{ij} = \frac{\partial^2 W}{\partial \phi_i \partial \phi_j}. \tag{1.84}$$

The auxiliary fields F_i and their conjugates are defined from

$$F_i = -W_i^*, \qquad F^{*i} = -W^i. \tag{1.85}$$

The SUSY gauge interactions are made from

$$D^a = -g(\phi^* T^a \phi), \tag{1.86}$$

where T^a are the relevant generators of the gauge group. Finally, the scalar potential is recovered from

$$V(\phi, \phi^*) = F^{*k}F_k + \frac{1}{2}\sum_a D^a D_a = W^k W_k^* + \frac{1}{2}\sum_a g_a^2(\phi^* T^a \phi)^2. \tag{1.87}$$

The superpotential for the MSSM is

$$W_{\text{MSSM}} = \bar{u}\mathbf{y_u}QH_u - \bar{d}\mathbf{y_d}QH_d - \bar{e}\mathbf{y_e}LH_d + \mu H_u H_d, \tag{1.88}$$

where the objects $\{H_u,\ H_d,\ Q,\ L,\ \bar{u},\ \bar{d},\ \bar{e}\}$ are the chiral superfields which correspond to the chiral supermultiplets in table 1.2 and we have suppressed all gauge and family indices. The left and RH pieces of the quarks and leptons are separate two component Weyl spinors which transform differently under the SM gauge group. We use a tilde ($\tilde{}$) to denote superpartners

[12] We also note inserting soft masses is also works as an 'effective theory' for other forms of SUSY breaking, such as spontaneous.

[13] The holomorphicity condition enforces that a complex function $f(z)$ does not depending on the conjugate, z^*, i.e. that $\frac{\partial f}{\partial z^*} = 0$. In this case we require W^{ij} does not contain ϕ^{*k} for the Lagrangian to be invariant under SUSY transformations, which we do not detail here.

of the SM particles, and subscript to differentiate which Weyl fermion it is a partner of (the sfermions are scalars and so have helicity 0). The necessity for two Higgs chiral supermultiplets is twofold, firstly since the Higgsinos (the fermion superpartner to the Higgs boson) would produce a chiral (gauge) anomaly, so one requires one chiral supermultiplet with $Y = +1/2$ and one with $Y = -1/2$ to cancel this. Secondly related to the holomorphicity condition. A term like $\bar{u}QH_u$ could not be replaced by $\bar{u}QH_d^*$ and likewise $\bar{d}QH_d$ could not be replaced by $\bar{d}QH_u^*$. The μ parameter sets the Higgsino masses, in addition to other observed SM masses, and requires a value close (within an order of magnitude) to the EW scale. This is considered unnatural as this dimensionful parameter could take any value; this is known as the μ problem, and less minimal model, such as the Next-to Minimal Supersymmetric Standard Model (NMSSM) seek to address this. The two Higgs doublet fields are part of the type-II 2 Higgs doublet Model (2HDM), and so relate the two vevs by

$$v_u^2 + v_d^2 = v|_{174\ \mathrm{GeV}}{}^2, \tag{1.89}$$

$$\tan\beta = \frac{v_u}{v_d}. \tag{1.90}$$

We will now briefly discuss some of the more phenomenological consequences of the MSSM. Firstly, with the additional field content, there is unification of forces. The extra particle content in loops modify the three beta functions so that unlike in the SM where the forces almost unify, as can be seen in the upper figure of 1.3, in the MSSM the couplings meet exactly, implying unification, as in the lower image of 1.3. In addition there are several DM candidates. By assuming R-parity conservation, this prevents the Lightest SUSY Particle (LSP) from decaying, and hence it is stable. In the MSSM the lightest neutralino (superpartner to the gauge and Higgs fields) is a good candidate. When presented with all constraints from the LHC, in addition to requiring the correct DM relic density, the parameter space for an MSSM DM candidate is vastly reduced. Finally, the MSSM does not address the issues of neutrino masses, beyond allowing for a SUSY embedding of a seesaw model. These two issues call for further, non-minimal extensions, which we will address in great detail in chapters 2 and 3.

1.5 Grand Unified Theories

Unification of forces as been an overwhelmingly successful guiding principle in physics for centuries. With Maxwell's unification of electricity and magnetism into electromagnetism in 1865, and years later with unification of EM and the weak force into the EW, the notion that nuanced behaviour may be described in terms of laws with a great deal of symmetry has lead to great success. There are several striking features of the SM which beg for a greater symmetry which will unify for forces. Firstly, that the SM may be unified at all. The gauge group $SU(3)\times SU(2)\times U(1)$ is suggestively able to be embedded in larger gauge groups, where all fermions may be accounted for in the representations and no further fermions arise which spoil anomaly cancellation. Given a particular gauge group and fermionic content, it is not the case that such a theory is unifiable

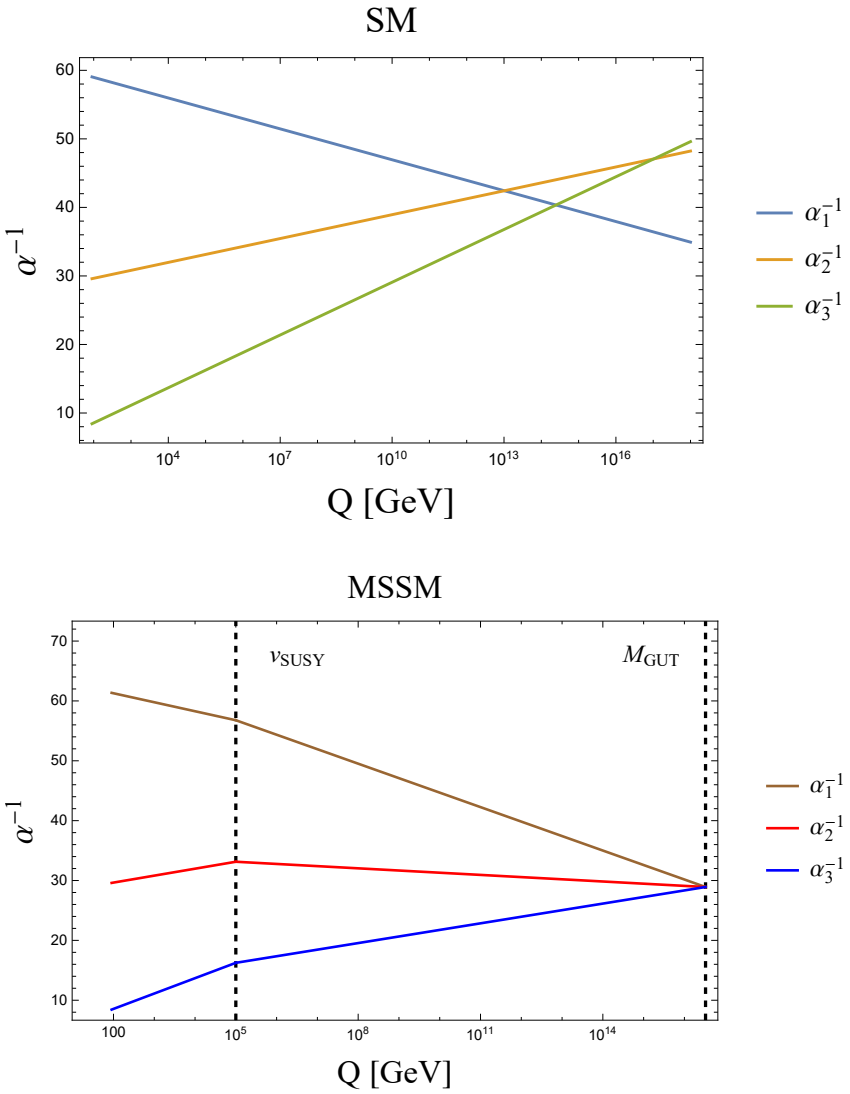

Figure 1.3: The upper panel shows the running couplings in the SM (at one loop) and the lower panel shows the running couplings in the MSSM, given a a SUSY scale $v_{\text{SUSY}} = 10^5$ GeV, and a determined GUT scale of $M_{\text{GUT}} = 3.3 \times 10^{16}$ GeV.

whatsoever. In addition, the running of the SM gauge couplings appear to almost unify (i.e. meet at the same coupling value). Adding in certain extra particle content, such as in the MSSM, will lead to all three groups unifying.

There are numerous choices for the GUT gauge group, but we will focus on $SU(5)$, the Pati-Salam (PS) group $SU(4)_C \times SU(2)_L \times SU(2)_R$, and $SO(10)$.

1.5.1 $SU(5)$

The gauge group $SU(5)$ is rank 4, with $5^2 - 1 = 24$ gauge bosons which transform in the **24** adjoint representation. The fermions (more difficult to accommodate in a given QFT) nicely fit

Names		spin 0	spin 1/2	$SU(3)_C$, $SU(2)_L$, $U(1)_Y$
squarks, quarks	Q	$(\widetilde{u}_L \;\; \widetilde{d}_L)$	$(u_L \;\; d_L)$	$(\mathbf{3}, \mathbf{2}, \frac{1}{6})$
($\times$3 families)	$\overline{u}$	$\widetilde{u}^*_R$	$u^\dagger_R$	$(\overline{\mathbf{3}}, \mathbf{1}, -\frac{2}{3})$
	$\overline{d}$	$\widetilde{d}^*_R$	$d^\dagger_R$	$(\overline{\mathbf{3}}, \mathbf{1}, \frac{1}{3})$
sleptons, leptons	L	$(\widetilde{\nu} \;\; \widetilde{e}_L)$	$(\nu \;\; e_L)$	$(\mathbf{1}, \mathbf{2}, -\frac{1}{2})$
($\times$3 families)	$\overline{e}$	$\widetilde{e}^*_R$	$e^\dagger_R$	$(\mathbf{1}, \mathbf{1}, 1)$
Higgs, Higgsinos	H_u	$(H^+_u \;\; H^0_u)$	$(\widetilde{H}^+_u \;\; \widetilde{H}^0_u)$	$(\mathbf{1}, \mathbf{2}, +\frac{1}{2})$
	H_d	$(H^0_d \;\; H^-_d)$	$(\widetilde{H}^0_d \;\; \widetilde{H}^-_d)$	$(\mathbf{1}, \mathbf{2}, -\frac{1}{2})$

Table 1.2: Chiral supermultiplets in the MSSM. The spin-0 fields are complex scalars, and the spin-1/2 fields are LH two-component Weyl fermions.

into the $F = \overline{\mathbf{5}}$ and $T = \mathbf{10}$, where (for one family)

$$F = \begin{pmatrix} d^c_r \\ d^c_b \\ d^c_g \\ e^- \\ -\nu_e \end{pmatrix}_L , \qquad T = \begin{pmatrix} 0 & u^c_g & -u^c_b & u_r & d_r \\ . & 0 & u^c_r & u_b & d_b \\ . & . & 0 & u_g & d_g \\ . & . & . & 0 & e^c \\ . & . & . & . & 0 \end{pmatrix}_L . \tag{1.91}$$

The subscripts represent the three quark colours (r, g, b) and superscript c is represents the CP conjugated fermions. These assignments in the F and T may be derived from the requirement of both F and T being invariant under the SM gauge group (for example the sum of electric charges in F and T are zero), this can be seen from

$$\overline{\mathbf{5}} = d^c(\overline{\mathbf{3}}, \mathbf{1}, 1/3) \oplus L(\mathbf{1}, \overline{\mathbf{2}}, -1/2), \tag{1.92}$$

$$\mathbf{10} = u^c(\overline{\mathbf{3}}, \mathbf{1}, -2/3) \oplus Q(\mathbf{3}, \mathbf{2}, 1/6) \oplus e^c(\mathbf{1}, \mathbf{1}, 1). \tag{1.93}$$

RH neutrinos may not be embedded here, and must be added separately as singlets of $SU(5)$. The breaking $SU(5) \to SU(3)_C \times SU(2)_L \times U(1)_Y$ is done by the Higgs multiplets in the **24** representation developing a VEV. The usual EW doublets appear from the $SU(5)$ multiplets $H_{\mathbf{5}}$ and $H_{\overline{\mathbf{5}}}$, but this requires a colour triplet to remain heavy (as it is not observed by experiment). This is known as the doublet-triplet splitting problem. The Yukawa couplings to these Higgses take the form (for one family),

$$\mathcal{L}^{SU(5),\,\text{Yuk}} = y_u H_{\mathbf{5}i} T_{jk} T_{lm} \epsilon^{ijklm} + y_\nu H_{\mathbf{5}i} F^i \nu^c + y_d H^i_{\overline{\mathbf{5}}} T_{ij} F^j, \tag{1.94}$$

where ϵ^{ijklm} is the totally antisymmetric tensor with $i, j, j, k, l = 1, \ldots, 5$. These generate the Yukawa terms for the SM content,

$$\mathcal{L}^{SU(5),\text{ Yuk, SM}} = y_u H_u Q u^c + y_\nu H_u L \nu^c + y_d (H_d Q d^c + H_d e^c L). \tag{1.95}$$

At the GUT scale the Yukawa couplings for d and e are equal (meaning an electron and down quark share the same mass at high scale). Extending this argument to the other families finds the relation

$$Y_d = Y_e^T. \tag{1.96}$$

Which works well for the third generation (i.e. at GUT scale $m_\tau = m_b$), however for the first two generations this fails. Georgi and Jarlskog [8] proposed the $(2, 2)$ entry of the Yukawa matrices may be given by

$$\mathcal{L}^{SU(5),\text{ Yuk, } d_{22}} = (Y_d)_{22} H_{\overline{\mathbf{45}}} T_2 F_2, \tag{1.97}$$

where now the down type Higgs doublet H_d is a mixture of the EW doublets in $H_{\overline{\mathbf{5}}}$ and $H_{\overline{\mathbf{45}}}$. In terms of SM fields, this term finds

$$\mathcal{L}^{SU(5),\text{ Yuk, SM } d_{22}} = (Y_d)_{22} (H_d Q_2 d_2^c - 3 H_d e_2^c L_2), \tag{1.98}$$

where the factor -3 on the lepton piece is a Clebsch-Gordan (CG) coefficient. Placing a zero element in the $(1, 1)$ piece of the Yukawa matrix predicts the following relations between charged lepton and down quark masses at GUT scale,

$$y_b = y_\tau, \quad y_s = \frac{y_\mu}{3}, \quad y_d = 3 y_e, \tag{1.99}$$

which previously worked as a successful model for observed quark masses. In recent times, with new quark mass data from lattice QCD results, [9], alternative fermion mass ratios are preferred, such as [10]

$$\frac{y_\tau}{y_b} = -\frac{3}{2}, \quad \frac{y_\mu}{y_s} = \frac{9}{2}. \tag{1.100}$$

1.5.2 Pati-Salam $SU(4)_C \times SU(2)_L \times SU(2)_R$

Prior to the suggestion of $SU(5)$ as the unifying group, Pati and Salam were the first to propose a unification of the SM gauge group [11] based on the gauge group [14]

$$G_{PS} \equiv SU(4)_C \times SU(2)_L \times SU(2)_R, \tag{1.101}$$

[14] The $SU(4)_C$ group is also referred to in literature as $SU(4)_{PS}$ referring to Pati and Salam.

where the leptons act as the fourth colour and the assignment is left-right symmetric. The LH and RH fermions transform (respectively) under G_{PS} as

$$\psi_i(4,2,1) = \begin{pmatrix} u_r & u_b & u_g & \nu \\ d_r & d_b & d_g & e^- \end{pmatrix}_i , \tag{1.102}$$

$$\psi_i^c(\bar{4},1,\bar{2}) = \begin{pmatrix} u_r^c & u_b^c & u_g^c & \nu^c \\ d_r^c & d_b^c & d_g^c & e^c \end{pmatrix}_i , \tag{1.103}$$

where again ψ_i^c are the CP conjugated RH fermions (so they become LH) and $i = 1 \ldots 3$ is the family index. Unlike in $SU(5)$ the RH neutrinos are predicted as part of the gauge multiplets, gaining masses via the seesaw mechanism as desired. The Higgs fields are contained in the following representations,

$$h(1,\bar{2},2) = \begin{pmatrix} {H_u}^+ & {H_d}^0 \\ {H_u}^0 & {H_d}^- \end{pmatrix}, \tag{1.104}$$

where the light Higgs doublets are again given by H_d and H_u. Unlike $SU(5)$, there is no splitting problem here, as the heavy Higgses are contained in different representations,

$$H(4,1,2) = \begin{pmatrix} u_H^R & u_H^B & u_H^G & \nu_H \\ d_H^R & d_H^B & d_H^G & e_H^- \end{pmatrix}, \tag{1.105}$$

$$\bar{H}(\bar{4},1,\bar{2}) = \begin{pmatrix} \bar{d}_H^R & \bar{d}_H^B & \bar{d}_H^G & e_H^+ \\ \bar{u}_H^R & \bar{u}_H^B & \bar{u}_H^G & \bar{\nu}_H \end{pmatrix}, \tag{1.106}$$

and develop vevs at the GUT scale, $\langle v_H \rangle \sim \langle \bar{v}_H \rangle \sim M_{GUT}$, which breaks G_{PS} to the SM gauge group,

$$SU(4)_C \times SU(2)_L \times SU(2)_R \to SU(3)_C \times SU(2)_L \times U(1)_Y . \tag{1.107}$$

This may be done through intermediate breaking steps, where

$$SU(4)_C \to SU(3)_C \times U(1)_{B-L}, \tag{1.108}$$

$$SU(2)_R \to U(1)_R, \tag{1.109}$$

and then

$$U(1)_R \times U(1)_{B-L} \to U(1)_Y , \tag{1.110}$$

where $B - L$ refers to baryon minus lepton number and R represents a charge given to RH fermions (analogously to how $SU(2)_L$ is assigned for LH pieces). The hypercharge is then related to the R and $B - L$ quantum numbers through $Y = T_R^3 + \frac{B-L}{2}$, and hence electric charge

from $Q = T_L^3 + T_R^3 + \frac{B-L}{2}$. This is a remarkable formula, that the hypercharges of the SM may be predicted in terms of two new quantum numbers, which were already accidental (global) symmetries of the model. The breaking scale of this $U(1)_{B-L}$ will fix the scale of the RH neutrino masses, $M_R \sim v_{B-L}$. The Yukawa couplings for all fermions take the simple form

$$\mathcal{L}^{PS,\text{ Yuk}} = y_{ij} h \psi_i \psi_j^c, \tag{1.111}$$

which at low energies reproduces the couplings for the SM fields,

$$\mathcal{L}^{PS,\text{ Yuk, SM}} = y_{ij}(H_u Q_i u_j^c + H_u L_i \nu_j^c + H_d Q_i d_j^c + H_d L_i e_j^c). \tag{1.112}$$

which predicts the same Yukawa coupling for all SM fields at GUT scale,

$$Y_d = Y_u = Y_e = Y_\nu, \tag{1.113}$$

which does not match the usual SUSY RGE Yukawas at GUT scale. These relations may be fixed following similar procedures to the $SU(5)$ case, by including CG coefficients through suitable model building. The Majorana mass term for the RH neutrinos can be written in terms of non-renormalisable operators,

$$\mathcal{L}^{M_R} = \frac{\lambda_{ij}}{\Lambda} \bar{H}\bar{H}\psi_i^c \psi_j^c \to \frac{\lambda_{ij}}{\Lambda} \langle \bar{\nu}_H \rangle^2 \nu_i^c \nu_j^c \equiv M_R^{ij} \nu_i^c \nu_j^c, \tag{1.114}$$

where λ may be of the order of the Planck scale.

1.5.3 $SO(10)$

The final GUT group we will consider is $SO(10)$, which may break to the SM via the PS group, as well as $SU(5)$. It is rank 5 (compared to rank 4 for $SU(5)$), and has $2\left(\frac{10}{2}\right)^2 - \frac{10}{2} = 45$ gauge bosons which transform as the **45** adjoint representation. One complete family of SM fermions fits nicely in a single **16** spinor representation, which includes the RH neutrinos. We will briefly discuss some relevant group theory to motivate this (as the theory of $SO(N)$ is not as common as $SU(N)$ to most phenomenologists). To begin, $SO(3)$ is locally isomorphic to $SU(2)$, and has a **2** spinor representation which can be written as a single set of Pauli matrices with eigenstates $|\pm\rangle \equiv |\pm\frac{1}{2}\rangle$. We can write the **4** of $SO(5)$ as the product of two Pauli matrices with eigenstates $|\pm\pm\rangle$. Similarly to $SO(3) \cong SU(2)$, we see that $SO(6)$ is isomorphic to $SU(4)$, and has two complex spinor representations where $\mathbf{4}+\overline{\mathbf{4}}$ may be written as the product of three Pauli matrices with eigenstates $|\pm\pm\pm\rangle$, where the **4** corresponds to an odd number of $|-\rangle$ eigenstates, and the $\overline{\mathbf{4}}$ to the states with an even number of $|-\rangle$. $SO(6) \cong SU(4)$ has an $SU(3)$ subgroup where the **4** decomposes to a $\mathbf{1}+\mathbf{3}$ where the singlet is identified as $|---\rangle$ and the triplet as the remaining $|++-\rangle$, $|+-+\rangle$, $|-++\rangle$, which are all permutations of requiring an odd number of $|-\rangle$ states. The **4** state is similarly identified by exchanging $(- \leftrightarrow +)$. The GUT group $SO(10)$ has subgroup $SO(6) \times SO(4)$, where we identify the $SO(6)$ with the PS group, $SO(6) \cong SU(4)_C$,

and then $SO(4)$ with the Left-Right symmetric group, $SO(4) \cong SU(2)_L \times SU(2)_R$. In figure 1.4, taken from [12], we show the components of the **16** spinor for each quark, where the first three components correspond to the PS colour group (i.e. the first three $|---, \ldots\rangle$ is a colour singlet) and the last two dictate (schematically) whether the particle resides in an $SU(2)_L$ or $SU(2)_R$ doublet,

$$SU(2)_L : \ \mathbf{2} \sim \begin{pmatrix} |-+\rangle \\ |+-\rangle \end{pmatrix}, \qquad SU(2)_R : \ \mathbf{2} \sim \begin{pmatrix} |--\rangle \\ |++\rangle \end{pmatrix}. \tag{1.115}$$

So one possible breaking direction is

$$SO(10) \to SU(4)_C \times SU(2)_L \times SU(2)_R, \tag{1.116}$$

with

$$\mathbf{16} \to (\mathbf{4}, \mathbf{2}, \mathbf{1}) \oplus (\overline{\mathbf{4}}, \mathbf{1}, \overline{\mathbf{2}}). \tag{1.117}$$

One is not forced to go through PS though. By changing the vevs of Higgses, another possible symmetry breaking direction is,

$$SO(10) \to SU(5) \times U(1)_X, \tag{1.118}$$

with

$$\mathbf{16} \to \overline{\mathbf{5}}_{-3} \oplus \mathbf{10}_1 \oplus \mathbf{1}_5, \tag{1.119}$$

$$\mathbf{10} \to \mathbf{5}_{-2} \oplus \overline{\mathbf{5}}_2. \tag{1.120}$$

In terms of Yukawa couplings, to decide which representation the Higgs should reside in, we will take the Kronecker product of two fermion spinors, and find representations which multiply with this product to make a singlet. Since

$$\mathbf{16} \otimes \mathbf{16} = \mathbf{10} \oplus \mathbf{126} \oplus \mathbf{120}. \tag{1.121}$$

Then the Higgs can reside in the **10**, **126**, **120** representations, since all of $\mathbf{10} \times \mathbf{10}$, $\mathbf{126} \times \mathbf{126}$, $\mathbf{120} \times \mathbf{120}$ will produce a singlet. It is preferred to place the Higgses in a **10** as it is the smallest representation (to reduce doublet, N-plet splitting), and the **126** is preferred for neutrino masses as it is symmetric. The singlet term will look like

$$\mathcal{L}^{SO(10),\ \mathrm{Yuk}} = y_{ij} h \psi_i \psi_j, \tag{1.122}$$

where $i, j = 1, \ldots, 3$ are family indices. For the SM fields at low energy, this finds

$$\mathcal{L}^{SO(10),\ \mathrm{Yuk,\ SM}} = y_{ij}(H_u Q_i u_j^c + H_u L_i \nu_j^c + H_d Q_i d_j^c + H_d L_i e_j^c), \tag{1.123}$$

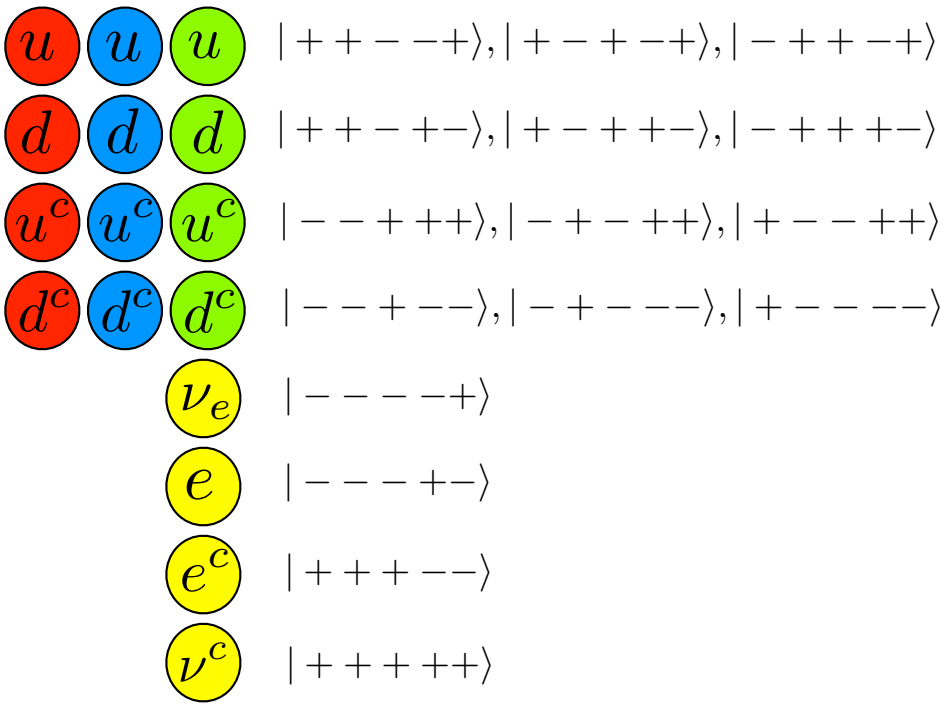

Figure 1.4: (Taken from [12]). A complete family of LH quarks and leptons (where RH fermions are CP conjugated) forms a single **16** spinor representation of $SO(10)$, including the RHN (CP conjugated as ν^c). The notation $|\pm\pm\pm\pm\pm\rangle$ labels the components of the spinor, in terms of a direct product of five Pauli matrices with eigenstates $|\pm\rangle$, respectively, with the constraint that there must be an even number of $|-\rangle$ eigenstates. The embedding of the SM gauge group is such that the first three components of $|\pm\pm\pm\pm\pm\rangle$ is associated $SU(3)_C$, while the last two components are associated with the $SU(2)_L \times U(1)_Y$ gauge group.

where y_{ij} is a symmetric matrix. As with the PS model, the initial prediction is that the Yukawa couplings for all fermions are equal, at the GUT scale,

$$Y_d = Y_u = Y_e = Y_\nu, \tag{1.124}$$

which may be fixed using CG relations as done in [13]. Again, the RH Majorana masses M_R may be generated from the non-renormalisable operators,

$$\frac{\lambda_{ij}}{\Lambda}\bar{H}\bar{H}\psi_i\psi_j \to \frac{\lambda_{ij}}{\Lambda}\langle\bar{\nu}_H\rangle^2\nu_i^c\nu_j^c \equiv M_R^{ij}\nu_i^c\nu_j^c, \tag{1.125}$$

where Λ may be of order the Planck scale, and $\bar{H}$ are Higgs in the $\overline{\mathbf{16}}$ representation, and their RH component may gain a vev, breaking $SO(10)$ to $SU(5)$ at the GUT scale.

Chapter 2

Supersymmetric Extension of the $U(1)_{B-L}$ Model: Naturalness

2.1 Non-SUSY $B - L$

Before discussing the SUSY version of the $B - L$ model, we will briefly discuss the non-SUSY version [14, 15]. In the SM, at Lagrangian level, there is an accidental baryon, B, and lepton, L symmetry. Since there are three quarks in a baryon, we assign up and down type quarks a baryon number $B(q) = 1/3$, and assign leptons a lepton number $L(l) = L(\nu) = 1$, else they are zero, $B(l) = B(\nu) = L(q) = 0$. Writing down all allowed Lagrangian terms in the SM, one finds that every term conserve these two quantities. When considering non-perturbative effects (such as sphaleron processes, which we will not discuss), it is the difference between baryon and lepton number, which is conserved as a global symmetry, $U(1)^{\text{global}}_{B-L}$. There has been a great deal of success in the SM being guided by the principle of gauge symmetries, so it is worth considering the implications if this global symmetry were promoted to a gauge form, $U(1)_{B-L}$ (where in our notation, the absence of a superscript "global" implies it is a gauge symmetry).

The $U(1)_{B-L}$ gauge group appears in several GUT extensions as mentioned in the introduction, such as $SU(3)_C \times SU(2)_L \times U(1)_R \times U(1)_{B-L}$ from $SO(10)$, but can be viewed as a different model in its own right. One may begin with the SM gauge group, and then promote $B - L$ to a gauge symmetry,

$$G_{B-L} = SU(3)_C \times SU(2)_L \times U(1)_Y \times U(1)_{B-L}. \tag{2.1}$$

This has several consequences. Firstly, to cancel chiral anomalies, one must introduce three SM singlet fermions, with $U(1)_{B-L}$ charge $+1$. These fermions have the same behaviour as, and thus we identify them to be, the three RH neutrinos. An unbroken gauge symmetry will have massless gauge bosons which mediate the force, such as the gluons in the strong force. Since we do not observe such mediators of $B - L$ in nature, then the group must be broken at some scale. To break the $B - L$ symmetry, one may introduce an extra complex scalar, a $B - L$ Higgs, which we denote with η, and proceed with spontaneous symmetry breaking, analogously to how

$SU(2)_L \times U(1)_Y$ is broken in the SM. This will also generate a massive gauge boson, a Z' and finally the RH neutrinos will gain a Majorana mass term through a coupling with η. All three mass scales: $\{m_\eta,\ m_{Z'},\ M_R\}$, are dependent on the dimensionful vev (breaking scale) v_{BL} of the $U(1)_{B-L}$. In addition, the scalar mass is also dependent on the potential term λ_{BL}, the Z' boson on the gauge coupling g_{BL} and the RH neutrino mass on the Yukawa coupling y_N. For a "natural" theory, we expect that these three parameters are order unity $\lambda \sim g_{BL} \sim y_N \sim 1$, and so (at least to a good approximation) one expects the three new mass scales of the theory to be near the breaking scale. As with the SM, on a theoretical level this breaking scale can be anywhere up to the Planck scale, and is only guided by experimental observation. From the measurement of $\lesssim O(0.1)$ eV neutrino masses [1], then one may determine this breaking scale from requiring a natural Dirac coupling $y_D \sim 1$ using the type-I seesaw, $v_{BL} \sim 10^{16}$ GeV, but taking the Dirac coupling to be more similar to that of the electron, $y_e = 10^{-6}$ would find $v_{BL} \sim 1$ TeV. This model has many interesting features and has been well studied, but we will devote the remainder of the next two chapters to the supersymmetric version of this theory. In this brief discussion we have neglected many features, including Gauge-Kinetic Mixing (GKM), for which a full description may be found in appendix C.3.

2.2 Introduction

Low scale SUSY is motivated by solving two major flaws of the SM: the gauge hierarchy and DM problems.

In the SM, the hierarchy problem stems from the fact that a very unnatural FT is required to keep the Higgs mass at an acceptable value for current data. SUSY provides an elegant solution to this. However, SUSY must be broken at a high scale, hence some FT is reintroduced at some level. In the MSSM, with universal soft SUSY breaking terms, a heavy spectrum is required to give large radiative corrections to the SM-like Higgs mass and account for the recently measured value of 125 GeV at the LHC. Thus naturalness becomes seriously challenged in the MSSM by well established experimental conditions.

Furthermore, the alluring hints of DM existence are serious indications for new BSM physics. Due to R-parity conservation, the LSP in the MSSM, the lightest neutralino, is stable and thus is a good candidate for DM. However, in the constrained MSSM (CMSSM) framework, in which universal boundary conditions are imposed at the GUT scale, the extra Higgs bosons of the MSSM are beyond the reach of the LHC experiments, while the lightest CP-even Higgs boson is reserved as the SM-like one. Such heavy Higgs bosons result in large FT at the EW scale. In addition, the strict bound on the gluino mass ($m_{\tilde{g}} \leq 1.9$ TeV [16]) causes heavy EW –inos (bino and wino) at low scale, since the gaugino masses are also set universal at the GUT scale. Besides, the null results from direct searches for SUSY particles lead to a heavy mass spectrum. The ensuing EW sector, in particular, severely raises the required FT leading to the correct scale

[1] This is an oversimplification of the current bound on the sum of neutrino masses.

for EW Symmetry Breaking (EWSB). Even though it is not possible to exclude the CMSSM completely, such a heavy spectrum brings poor agreement with various precision observables [17]. Detailed discussions of the FT issue in the CMSSM framework can be found in [18].

Besides the LHC ones, the latest measurements for DM also provide strict constraints for the MSSM regardless of imposing universal boundary conditions at the GUT scale or otherwise. The latest results from, e.g., the LUX collaboration [19] have a strong impact especially for light DM candidates. A low FT condition requires the higgsino-like LSP neutralino to have a large cross-section with nuclei, since the relevant scattering processes happen through the Yukawa interactions, so that LUX results exclude such solutions. Indeed, only a bino-like LSP neutralino can more or less survive, since its corresponding scattering cross-section is instead low [20]. However, the relic abundance of the bino is usually much larger than the ranges allowed by the current Wilkinson Microwave Anisotropy Probe (WMAP) and Planck results [21, 22].

Quite apart from the aforementioned two problems of the SM, it should be recalled that non-vanishing neutrino masses are presently some of the most important evidence for BSM physics. Massive neutrinos are not present in the SM. However, a simple extension of it, based on the gauge group $SU(3)_C \times SU(2)_L \times U(1)_Y \times U(1)_{B-L}$, can account for current experimental results of light neutrino masses and their large mixing [23–33]. Within the $B-L$ Supersymmetric Standard Model (BLSSM), the SUSY version of such a scenario, which inherits the same beneficial features of the MSSM in connection with SUSY dynamics, it has been emphasised that the scale of $B-L$ symmetry breaking is related to the SUSY breaking one and both occur in the TeV region [34–39]. Therefore, several testable signals of the BLSSM are predicted for the current experiments at the LHC [40–51].

In addition, the BLSSM provides new candidates for DM different from those of the MSSM. In particular, there are two kinds of neutralinos, corresponding to the gaugino of $U(1)_{B-L}$ and the $B-L$ Higgsinos. Also a RH sneutrino, in a particular region of parameter space, may be a plausible candidate for DM. We also consider the scenario where the extra $B-L$ neutralinos can be cold DM states. We then examine the thermal relic abundance of these particles and discuss the constraints imposed on the BLSSM parameter space from the negative results of their direct detection. We argue that, unlike the MSSM, the BLSSM offers one with significant parameter space satisfying all available experimental constraints. This may be at the expense of high FT, if Z' is quite heavy and soft SUSY breaking terms are universal. Nevertheless, for what we will eventually verify to be a small increase in FT with respect to the MSSM, we will gain in the BLSSM a more varied DM sector and much better compliance with relic and (in)direct detection data.

In the build-up to this DM phenomenology, we analyse the naturalness problem in the BLSSM and compare its performance in this respect against that of the MSSM. In the latter, the weak scale (M_Z) depends on the soft SUSY breaking terms through the Renormalisation Group Equa-

tions (RGEs) and the EW minimisation conditions, which can be expressed as

$$\frac{1}{2}M_Z^2 = \frac{m_{H_d}^2 - m_{H_u}^2 \tan^2\beta}{\tan^2\beta - 1} - \mu^2. \tag{2.2}$$

Therefore, a possible measure of FT is defined as [52]

$$\Delta(M_Z^2, a) = \left| \frac{a}{M_Z^2} \frac{\partial M_Z^2}{\partial a} \right|, \tag{2.3}$$

where a stands for the GUT scale parameters (e.g., $m_0, m_{1/2}, A_0$, etc.) or low scale parameters (e.g., $M_1, M_2, M_3, m_{\tilde{q}}, m_{\tilde{\ell}}$, etc.). In order for SUSY to stabilise the weak scale, $\Delta \equiv \text{Max}\left(\Delta(M_Z^2, a)\right)$ should be less than $\mathcal{O}(100)$. However, as the scale of SUSY breaking is increased, the EW one becomes highly fine-tuned. As intimated, in the BLSSM, both the weak and $B-L$ scales are related to soft SUSY breaking terms and, in addition to Eq. (2.2), which is slightly modified by the presence of the gauge mixing $\tilde{g}$, we also have, in the same limit $\tilde{g} \simeq 0$,

$$\frac{1}{2}M_{Z'}^2 = \frac{m_{\eta_1}^2 \tan^2\beta' - m_{\eta_2}^2}{1 - \tan^2\beta'} - \mu'^{\,2}, \tag{2.4}$$

where $\eta_{1,2}$ are scalar bosons, with $\langle \eta_{1,2} \rangle = v'_{1,2}$ that break the $B-L$ symmetry spontaneously, and $\tan\beta' = v'_1/v'_2$. The bound on $M_{Z'}$, due to negative searches at the Large Electron-Positron Collider (LEP), is given by $M_{Z'}/g_{BL} > 6$ TeV [53]. As we will see in section 2.5, we fix the value of $M_{Z'} = 4$ TeV, which satisfies all constraints from the LHC and LEP2. Furthermore, LHC constraints from the Drell-Yan (DY) process also exist, which force the $B-L$ Z' mass to be in the few TeV region. This indicates that $m_{\eta_{1,2}}$ and μ' are of order TeV. Therefore, in the scenario of universal soft SUSY breaking terms of the BLSSM, a heavy $M_{Z'}$ implies higher soft terms, hence the estimation of the FT is expected to be worse than in the MSSM. At this point, it is worth mentioning that the Z' gauge boson in the BLSSM can have a large decay width, thus potentially evading LEP and LHC constraints, which are based on the assumption of a narrow decay width, hence on Z' decays into SM particles and additional neutrinos only. While this has been proven to be possible in a non-unified version of the BLSSM, wherein the aforementioned limits can be relaxed and $M_{Z'}$ can be of order one TeV [48, 49], it remains to be seen whether a similar phenomenology can occur in the unified version of it which we are going to deal with here.

2.3 The $B-L$ Supersymmetric Standard Model

In this section, we briefly review the BLSSM with an emphasis on its salient features with respect to the MSSM. Even though its gauge group seems like a simple extension of the MSSM gauge group with a gauged $U(1)_{B-L}$ (hereafter, $B-L$ symmetry), it significantly enriches the particle content, which drastically changes the low scale phenomena. First of all, the anomaly cancellation

in the BLSSM requires three singlet fields; the most natural candidates in the BLSSM framework are the three RH neutrino fields. We may implement the SUSY seesaw mechanisms, where non-zero neutrino masses and mixings consistent with experimental data [54] are achieved. In addition, $R-$parity, which is assumed in the MSSM to avoid fast proton decay, can be linked to the $U(1)_{B-L}$ gauge group and it can be preserved if the $B-L$ symmetry is broken spontaneously [55], as is the case in the BLSSM studied here.

Spontaneous breaking of the $B-L$ symmetry can be realised in a similar way to the Higgs mechanism. That is, one can introduce two scalar fields, denoted as $\eta_{1,2}$. These fields should carry non-zero $B-L$ charges to break the $B-L$ symmetry and they are preferably singlets under the MSSM gauge group so as not to spoil EWSB. Thus, the Superpotential in the BLSSM can be written as

$$\begin{aligned} W &= \mu H_u H_d + Y_u^{ij} Q_i H_u u_j^c + Y_d^{ij} Q_i H_d d_j^c + Y_e^{ij} L_i H_d e_j^c \\ &+ Y_\nu^{ij} L_i H_u N_i^c + Y_N^{ij} N_i^c N_j^c \eta_1 + \mu' \eta_1 \eta_2, \end{aligned} \tag{2.5}$$

where the first line represents the MSSM Superpotential using the standard notation for (s)particles while the second line includes the terms associated with the RH neutrinos, N_i^cs, plus the singlet Higgs fields η_1 and η_2. The $B-L$ symmetry requires η_1 and η_2 to carry -2 and $+2$ charges under $B-L$ transformations, respectively. The presence of the N_i^c terms makes it possible to have Yukawa interaction terms for the neutrinos, denoted by Y_ν. Finally, μ' stands for the bilinear mixing term between the singlet Higgs fields.

In addition to the RH neutrinos and the singlet Higgs fields, the BLSSM also introduces a gauge field (B') and its gaugino ($\tilde{B}'$) associated with the gauged $B-L$ symmetry, so that the appropriate Soft SUSY-Breaking (SSB) Lagrangian can be written as

$$\begin{aligned} -\mathcal{L}_{\rm SSB}^{\rm BLSSM} &= -\mathcal{L}_{\rm SSB}^{\rm MSSM} + m_{\tilde{N}^c}^2 |\tilde{N}^c|^2 + m_{\eta_1}^2 |\eta_1|^2 + m_{\eta_2}^2 |\eta_2|^2 + A_\nu \tilde{L} H_u \tilde{N}^c + A_N \tilde{N}^c \tilde{N}^c \eta_1 \\ &+ \frac{1}{2} M_{B'} \tilde{B}' \tilde{B}' + M_{BB'} \tilde{B} \tilde{B}' + B(\mu' \eta_1 \eta_2 + \text{h.c.}). \end{aligned} \tag{2.6}$$

Note that, in contrast to its non-SUSY version, the BLSSM does not allow mixing between the doublet and singlet Higgs fields through the Superpotential and SSB Lagrangian. Therefore, the scalar potential for these can be written separately and their mass matrices can be diagonalised independently. The scalar potential for the singlet Higgs fields can be derived as

$$V(\eta_1, \eta_2) = \mu_1'^2 |\eta_1|^2 + \mu_2'^2 |\eta_2|^2 - \mu_3' (\eta_1 \eta_2 + \text{h.c.}) + \frac{1}{2} g_{BL}^2 (|\eta_1|^2 - |\eta_2|^2)^2 \tag{2.7}$$

and the minimisation of this potential yields Eq. (2.4). Despite the non-mixing Superpotential and SSB Lagrangian, one can implement mixing between the two abelian gauge fields via $-\chi B_{\mu\nu}^{B-L} B^{Y,\mu\nu}$, where $B_{\mu\nu}^a$ is the field strength tensor of a $U(1)$ gauge field, with $a = (Y,\ B-L)$, the hypercharge and $B-L$ charge, respectively. The gauge kinetic mixing can be rotated away

from the kinetic Lagrangian and the covariant derivative takes a non-canonical form [42]

$$D_\mu = \partial_\mu + \ldots . + (\tilde{g}\, Y + g'\,(B-L))B'_\mu, \tag{2.8}$$

where $\tilde{g}$ describes the kinetic mixing in place of χ. Even though $\tilde{g}$ is set to zero at the GUT scale, it can be generated at the low scale through the RGEs [56]. In this basis, one finds

$$M_Z^2 \simeq \frac{1}{4}(g_1^2+g_2^2)v^2, \qquad M_{Z'}^2 \simeq g_{BL}^2 v'^2 + \frac{1}{4}\tilde{g}^2 v^2, \tag{2.9}$$

where $v = \sqrt{v_u^2+v_d^2} \simeq 246$ GeV and $v' = \sqrt{v_1'^2+v_2'^2}$ with the Vacuum Expectation Values (VEVs) of the Higgs fields given by $\langle \mathrm{Re} H^0_{u,d}\rangle = v_{u,d}/\sqrt{2}$ and $\langle \mathrm{Re}\ \eta_{1,2}\rangle = v'_{1,2}/\sqrt{2}$. It is worth mentioning that the mixing angle between Z and Z' is given by

$$\tan 2\theta' \simeq \frac{2\tilde{g}\sqrt{g_1^2+g_2^2}}{\tilde{g}^2+16(\frac{v'}{v})^2 g_{BL}^2 - g_2^2 - g_1^2}. \tag{2.10}$$

The minimisation conditions of the BLSSM scalar potential at tree-level lead to the following relations [42]:

$$v'_1\left(m_{\eta_1}^2+|\mu'|^2+\frac{1}{4}\tilde{g}g_{BL}(v_d^2-v_u^2)+\frac{1}{2}g_{BL}^2(v_1'^2-v_2'^2)\right) - v'_2 B\mu' = 0, \tag{2.11}$$

$$v'_2\left(m_{\eta_2}^2+|\mu'|^2+\frac{1}{4}\tilde{g}g_{BL}(v_u^2-v_d^2)+\frac{1}{2}g_{BL}^2(v_2'^2-v_1'^2)\right) - v'_1 B\mu' = 0. \tag{2.12}$$

From these equations, one can determine $|\mu'|^2$ and $B\mu'$ in terms of other soft SUSY breaking terms. (Note that, with $\tilde{g}=0$, the expression of $|\mu'|^2$ takes the form of Eq. (2.4).) Breaking the EW and $B-L$ symmetries naturally shapes a Type-I seesaw mechanism for the six neutrino states of the model. The effective lepton flavour violating scale is dynamically generated and identified with the $B-L$ one. The resulting 6×6 mass matrix will include these two different breaking scales in two separated 3×3 blocks. The singlet Higgsino VEVs are responsible for the Majorana block in the subspace of RH neutrinos whereas EWSB determines the left-right neutrino mixing of a Dirac type. Hierarchies between the two scales, with the Majorana scale much larger than the Dirac one, is the origin of the Type-I seesaw mechanism. As a consequence of the additional neutral states $\tilde{B}', \tilde{\eta}_1$ and $\tilde{\eta}_2$, the corresponding neutralino mass matrix is extended to a 7×7 one given by

$$\mathcal{M}_7(\tilde{B},\ \tilde{W}^3,\ \tilde{H}_1^0,\ \tilde{H}_2^0,\ \tilde{B}',\ \tilde{\eta}_1,\ \tilde{\eta}_2) \equiv \begin{pmatrix} \mathcal{M}_4 & \mathcal{O} \\ \mathcal{O}^T & \mathcal{M}_3 \end{pmatrix}, \tag{2.13}$$

where $\mathcal{M}_4$ is the MSSM-type neutralino mass matrix and $\mathcal{M}_3$ is the additional 3×3 neutralino

mass matrix, which is given by

$$\mathcal{M}_3 = \begin{pmatrix} M_{B'} & -g_{BL}v_1' & g_{BL}v_2' \\ -g_{BL}v_1' & 0 & -\mu' \\ g_{BL}v_2' & -\mu' & 0 \end{pmatrix}. \tag{2.14}$$

In addition, the off-diagonal matrix $\mathcal{O}$ is given by

$$\mathcal{O} = \begin{pmatrix} M_{BB'} & 0 & 0 \\ 0 & 0 & 0 \\ -\frac{1}{2}\tilde{g}v_d & 0 & 0 \\ \frac{1}{2}\tilde{g}v_u & 0 & 0 \end{pmatrix}. \tag{2.15}$$

(Note that the off-diagonal matrix elements vanish identically if $\tilde{g} = 0$ and $M_{BB'} = 0$). One can then diagonalise the real matrix $\mathcal{M}_7$ with a symmetric mixing matrix V such that

$$V\mathcal{M}_7V^T = \text{diag}(m_{\tilde{\chi}_k^0}), \quad k = 1, \ldots, 7. \tag{2.16}$$

In these conditions, the LSP has the following decomposition

$$\tilde{\chi}_1^0 = V_{11}\tilde{B} + V_{12}\tilde{W}^3 + V_{13}\tilde{H}_d^0 + V_{14}\tilde{H}_u^0 + V_{15}\tilde{B}' + V_{16}\tilde{\eta}_1 + V_{17}\tilde{\eta}_2. \tag{2.17}$$

If the LSP is then considered as a candidate for DM, each species in the above equation, if dominant, leads to its own phenomenology that can possibly be distinguished in direct detection experiments. For example, to achieve the correct relic density of Bino-like DM is challenging, since its abundance is usually so high over the fundamental parameter space that one needs to identify several annihilation and/or coannihilation channels to reduce its density down to the WMAP [21] or Planck [22] measurements. Since this DM state interacts through the hypercharge, its scattering with nuclei has a very low cross section. Conversely, the largest cross section in DM scattering can be obtained when DM is Higgsino-like, since it interacts with the quarks through the Yukawa interactions. Since the BLSSM sector offers significant interference in the neutralino sector, this may also drastically change the DM kinematics. In contrast to a Bino, the $\tilde{B}'-$ino interacts more strongly depending on the $B-L$ gauge coupling. Despite the severe mass bound on the Z', there is no specific bound on $m_{\tilde{B}'}$, so that it can be even as low as 100 GeV [57]. In this context, one can expect the LSP neutralino to be mostly formed by $\tilde{B}'$ and its cross section in its scattering with nuclei can be very large, in contrast to the Bino case. In addition to $\tilde{B}'$, the LSP neutralino can be formed by the singlet Higgsinos (also dubbed Bileptinos due to their $L = \pm 2$ lepton charge). In this case, it is challenging for their abundance to be compatible with the experimental results. The reduction through the coannihilation channels involving SUSY

particles arises from the gauge kinetic mixing, which is restricted to be moderate. If its mass is nearly degenerate with that of the $\tilde{B}'$ state, they can significantly coannihilate. Also, a singlet Higgsino yields low cross section in DM scattering experiments. Besides the neutralinos, one can also consider the sneutrino as a DM candidate, when it is the LSP. In this case, the extended sector of the BLSSM involves twelve states coming from the Superpartners of the left- and the RH neutrinos. In a Charge and Parity (CP)-conserving framework the states entering the sneutrino mixing matrix can be expressed by separating their scalar and pseudo-scalar components

$$\tilde{\nu}_i = \frac{\sigma_{Li} + i\phi_{Li}}{\sqrt{2}}, \quad \tilde{N}_i = \frac{\sigma_{Ri} + i\phi_{Ri}}{\sqrt{2}}. \tag{2.18}$$

The breaking of $B-L$ generates an effective mass term through $Y_N^{ij} N_i^c N_j^c \eta_1$ causing a mass splitting between the CP-even and CP-odd sector. Therefore, in terms of Eq. (2.18), the corresponding 12×12 mass matrix is reduced to two different 6×6 blocks

$$\mathcal{M}^{2\,\sigma}(\sigma_L, \sigma_R) \equiv \begin{pmatrix} \mathcal{M}^{2\,\sigma}_{LL} & \mathcal{M}^{2\,\sigma}_{LR} \\ \mathcal{M}^{2\,\sigma\,T}_{LR} & \mathcal{M}^{2\,\sigma}_{RR} \end{pmatrix}, \quad \mathcal{M}^{2\,\phi}(\phi_L, \phi_R) \equiv \begin{pmatrix} \mathcal{M}^{2\,\phi}_{LL} & \mathcal{M}^{2\,\phi}_{LR} \\ \mathcal{M}^{2\,\phi\,T}_{LR} & \mathcal{M}^{2\,\phi}_{RR} \end{pmatrix}. \tag{2.19}$$

Such differences between CP-even and CP-odd sectors do not involve the left components with $\mathcal{M}^{\sigma}_{LL}$ and $\mathcal{M}^{\phi}_{LL}$ described by the common form $\mathcal{M}^{2}_{LL}$

$$\mathcal{M}^{2}_{LL}{}^{i,j} \equiv \frac{\delta^{i,j}}{8}\left(\left(g_1^2 + g_2^2 + \tilde{g}\,(g_{BL} + \tilde{g})\right)\delta_H + (g_{BL} + \tilde{g})\,\delta_\eta\right) + \frac{1}{2} v_u^2 \left(Y_\nu^T Y_\nu\right)^{i,j} + m_l^{2\,i,j}, \tag{2.20}$$

where we have introduced $\delta_\eta = v_1'^2 - v_2'^2$ and $\delta_H = v_d^2 - v_u^2$. For the submatrices $\mathcal{M}^{2\sigma}_{RR}$ and $\mathcal{M}^{2\,\phi}_{RR}$ we have instead

$$\begin{aligned} \mathcal{M}^{2}_{RR}{}^{i,j} &\equiv -\frac{\delta^{i,j}}{8} g_{BL}\,(\tilde{g}\delta_H + 2 g_{BL}\delta_\eta) + \frac{1}{2} v_u^2 \left(Y_\nu Y_\nu^T\right)^{i,j} + m^{2}_{\tilde{N}}{}^{i,j} + 2\, v_1'^2 \left(Y_N^2\right)^{i,j} \\ &\mp \sqrt{2}\left(v_2'\,\mu' Y_N^{i,j} - v_1'\, A_N^{i,j}\right) \end{aligned} \tag{2.21}$$

while the left-right sneutrino mixing is ruled by the matrices

$$\mathcal{M}^{2}_{LR}{}^{i,j} \equiv \frac{1}{2}\left(-\sqrt{2}\, v_d \mu Y_\nu^{i,j} + v_u \sqrt{2}\, A_\nu^{i,j} \pm 2 v_u\, v_1'\, \left(Y_N Y_\nu\right)^{i,j}\right), \tag{2.22}$$

with upper(lower) signs corresponding to CP-even(odd) cases. The parameter Y_ν and the corresponding trilinear term A_ν determine the mixing between the left and right components. In our setup, Y_ν is negligible and can safely be set to zero already at the GUT scale, as it is the case also for the boundary condition of A_ν. The resulting 12×12 sneutrino mass matrix is consequently unable to mix the RH and RH components as the CP-even and CP-odd parts of a sneutrino state will be completely determined by assigning its CP value and the chirality of its Supersymmetric

partner.

2.4 Renormalisation Group Equations

The presence of an extra Abelian gauge group introduces a distinctive feature, the gauge kinetic mixing, through a renormalisable and gauge invariant operator $\chi B^{\mu\nu} B'_{\mu\nu}$ of the two Abelian field strengths. Moreover, off-diagonal soft breaking terms for the Abelian gaugino masses are also allowed. This effect is completely novel with respect to the MSSM or other Supersymmetric models in which only a single $U(1)$ factor is considered. If the two Abelian gauge factors emerge from the breaking of a simple gauge group, the kinetic mixing is absent at that scale. For this reason, arguing that the BLSSM could be embedded into a wider GUT scenario (the matter content of the BLSSM, which includes three generations of RH neutrinos, nicely fits into the 16-D spinorial representation of $SO(10)$), we require the vanishing of the kinetic mixing at the GUT scale. As we stated above, we nevertheless end up with a non-zero kinetic mixing at low scales affecting the Z' interactions as well as the Higgs and the neutralino sectors [42].

Instead of working with a non-canonical kinetic Lagrangian in which the kinetic mixing χ appears, it is more practical to introduce a non-diagonal gauge covariant derivative with a diagonal kinetic Lagrangian. The two approaches are related by a gauge field redefinition and are completely equivalent. In this basis the covariant derivative of the Abelian fields takes the form $\mathcal{D}_\mu = \partial_\mu - iQ^T G A_\mu$, where Q is the vector of the Abelian charges, A is the vector of the Abelian gauge fields and G is the Abelian gauge coupling matrix with non-zero off-diagonal elements. The matrix G can be recast into a triangular form with an orthogonal transformation $G \to GO^T$ [58]. With this parametrisation, the three independent parameters of G are explicitly manifest and correspond to the Abelian couplings, g_1, g_{BL} and $\tilde{g}$, describing, respectively, the hypercharge interactions, the extra $B-L$ ones and the gauge kinetic mixing. Differently from the MSSM case, the Abelian gaugino mass term is replaced by a symmetric matrix with a non-zero mixed mass term $M_{BB'}$ between the B and B' gauginos. Coherently with our high energy unified embedding, we choose $M_{BB'} = 0$ at the GUT scale. Notice that the Abelian gaugino mass matrix M is affected by the same rotation O and in the basis in which G is triangular and M transforms through $M \to OMO^T$.

We have performed an RGE study of the BLSSM assuming gauge coupling unification and minimal Super-Gravity (mSUGRA) boundary conditions at the GUT scale. This scenario considerably constrains the parameter space connecting different sectors which are usually independent in non-unified scenarios. In particular, the two main scales describing BSM physics, the scale of SUSY and $B-L$ breaking, are linked by the RGEs. In a non-SUSY model, the $B-L$ symmetry breaking scale is arbitrary and can be placed anywhere between TeV and GUT energies. However, within a SUSY scenario, the radiative symmetry breaking approach can also be applied to $B-L$ symmetry breaking. This mechanism was studied for the first time in [35]. As discussed in detail herein, radiative $B-L$ symmetry breaking requires $m_{\eta_1} \neq m_{\eta_2}$ at the low scale. This requirement relates then the $B-L$ symmetry breaking scale to the SUSY one, since $m_{\eta_{1,2}}$ are

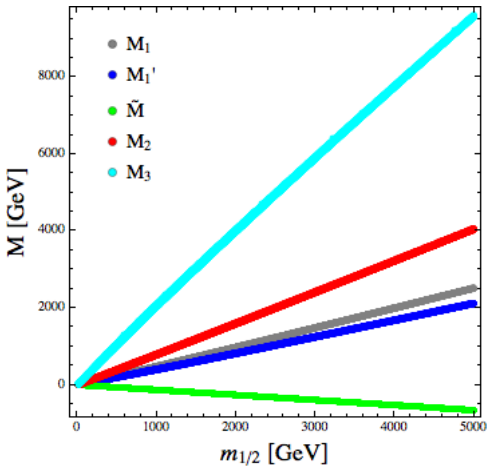

Figure 2.1: Gaugino masses at the SUSY scale as a function of the GUT $m_{1/2}$ mass. Here, both gauge coupling and soft mass unification have been assumed.

SSB masses for the relevant Higgs fields denoted by η_i.

The two-loop RGEs have been computed with SARAH [59] and fed into SPheno [60] which has been used for the spectrum computation and for the numerical analysis of the model. Here we show the one-loop β functions of the gauge couplings highlighting the appearance of the kinetic mixing contributions

$$\begin{aligned}
\beta_{g_1}^{(1)} &= \frac{33}{5} g_1^3, \\
\beta_{g_{BL}}^{(1)} &= \frac{3}{5} g_{BL} \left(15 g_{BL}^2 + 4\sqrt{10} g_{BL}\, \tilde{g} + 11 \tilde{g}^2\right), \\
\beta_{\tilde{g}}^{(1)} &= \frac{3}{5} \tilde{g} \left(15 g_{BL}^2 + 4\sqrt{10} g_{BL}\, \tilde{g} + 11 \tilde{g}^2\right) + \frac{12\sqrt{10}}{5} g_1^2 g_{BL}, \\
\beta_{g_2}^{(1)} &= g_2^3, \\
\beta_{g_3}^{(1)} &= -3 g_3^3,
\end{aligned} \tag{2.23}$$

where we have adopted the GUT normalisations $\sqrt{3/5}$ and $\sqrt{3/2}$, respectively, for the $U(1)_Y$ and $U(1)_{B-L}$ gauge groups. At one-loop level the expressions of the β functions of g_1, g_2 and g_3 are the same as those of the MSSM with differences appearing at two-loop order only. Notice that the term responsible for the reintroduction of a non-vanishing mixing coupling $\tilde{g}$ along the RGE running, even if absent at some given scale, is the last term in $\beta_{\tilde{g}}^{(1)}$. We recall again that the kinetic mixing is a peculiar feature of Abelian extensions of the SM and their Supersymmetric versions, admissible only between two or more $U(1)$ gauge groups.

Assuming gauge coupling unification at the GUT scale, the RGE analysis provides the results $\tilde{g} \simeq -0.144$ and $g_{BL} \simeq 0.55$ with $M_{\rm GUT} \simeq 10^{16}$ GeV, which are controlled by the leading one-loop β functions given in Eq. (2.23). The spread of points around these central values, less than 1% for g_{BL} and 5% for $\tilde{g}$, is only due to higher-order corrections, namely two-loop running and threshold corrections.

The running of the gaugino masses is directly linked to that of the gauge couplings. In the Abelian sector and at one-loop, the Abelian gaugino mass matrix M evolves with

$$\beta_M = MG^T Q^2 G + G^T Q^2 GM = MG^{-1}\beta_G + G^{-1}\beta_G M, \tag{2.24}$$

where $Q = \sum_p Q_p Q_p^T$, with Q_p the vector of the Abelian charges of the p particle. Exploiting the structure of the β functions of the gaugino masses, a simple relation is obtained, $M_i/m_{1/2} = g_i^2/g_{\rm GUT}^2$, for non-Abelian masses at one-loop order. In the Abelian sector, due to the presence of the mixing, the previous equation is replaced by a matrix relation. Indeed, from the product $GM^{-1}G^T$, which remains constant along the RGE evolution, one finds the Abelian gaugino mass matrix $M/m_{1/2} = G^T G/g_{\rm GUT}^2$. We show in Fig. 2.1 the dependence of the gaugino masses as a function of the GUT gaugino mass $m_{1/2}$. The hierarchy is obviously controlled by the size of the gauge couplings at low scale.

The gaugino masses M_1, M_1' and $\tilde{M}$ are obtained from $M_B, M_{B'}$ and $M_{BB'}$ through the transformation OMO^T. The coefficients $\sigma_{1,2}$ are defined as

$$\begin{aligned}
\sigma_1 &= m_{H_d}^2 - m_{H_u}^2 - {\rm tr}(m_d^2) - {\rm tr}(m_e^2) + {\rm tr}(m_l^2) - {\rm tr}(m_q^2) + 2{\rm tr}(m_u^2), \\
\sigma_2 &= 2m_{\eta_1}^2 - 2m_{\eta_2}^2 + {\rm tr}(m_d^2) - {\rm tr}(m_e^2) + 2{\rm tr}(m_l^2) - 2{\rm tr}(m_q^2) + {\rm tr}(m_u^2) - {\rm tr}(m_{\nu_R}^2)
\end{aligned} \tag{2.25}$$

and are found to be RGE invariant combinations of the soft SUSY masses. Assuming unification conditions at the GUT scale, $\sigma_{1,2}$ remain zero along all the RGE evolution. As $\beta_{m_{\eta_2}^2}$ is only characterised by negative contributions proportional to the Abelian gaugino masses, the corresponding soft mass $m_{\eta_2}^2$ will increase and remain positive during the run from the GUT to the EW scale. The same feature is shared by $m_{H_d}^2$ except for some particular values of the gaugino and soft scalar masses at the GUT scale for which the Y_b Yukawa coupling contribution (of the b-quark) to $\beta_{m_{\eta_2}^2}$ is not negligible. The spontaneous symmetry breaking of EW and B-L, requiring negative $m_{H_u}^2$ and $m_{\eta_1}^2$, can be realised radiatively, which is a nice feature in both MSSM and BLSSM. Namely, even though there is no spontaneous symmetry breaking at a high scale, the large top-quark Yukawa coupling Y_t and its trilinear soft term A_t can drive $m_{H_u}^2$ negative through its RGE evolution, which triggers spontaneous EWSB. Similarly, a sufficiently large neutrino Yukawa coupling Y_N and corresponding trilinear soft term A_n turn $m_{\eta_1}^2$ negative in its RGE evolution and break the $B-L$ symmetry spontaneously.

In general only one of the three components of the diagonal Y_N matrix is required to be large in order to realise the spontaneous symmetry breaking of the extra Abelian symmetry, thus providing a heavy and two possible lighter heavy-neutrino states. Notice also that the elements of the low scale values of the Y_N matrix cannot be taken arbitrary large otherwise a Landau pole is hit before the GUT scale. A close inspection of the one-loop β function of the heavy-neutrino Yukawa coupling

$$\beta_{Y_N} = 8Y_N Y_N^* Y_N + 2{\rm tr}(Y_N Y_N^*) Y_N - \frac{9}{2} {g_{BL}}^2 Y_N, \tag{2.26}$$

where we have neglected the negligible contribution of the light-neutrino Yukawa coupling Y_ν, shows that $Y_N \gtrsim 0.5$ spoils indeed the perturbativity of the model at the GUT scale or below.

2.5 Collider and Dark Matter Constraints

To investigate the viability of the BLSSM parameter space, with mSUGRA boundary conditions, we have challenged its potential signatures against two sets of experimental constraints. To the first set belong different bounds coming from collider probes which have been used in building the scan procedure. These form a varied set of requirements affecting our choice of the Z' benchmark mass as well as the character of the acceptable low-scale particle spectrum. As already stated, stringent constraints come from LEP2 data via EW Precision Observables (EWPOs) and from Run 2 of the LHC through a signal-to-background analysis using Poisson statistics to extract a 95% Confidence Level (CL) bound in the di-lepton channel. The CL has been extracted at the LHC with $\sqrt{s} = 13$ TeV and $\mathcal{L} = 13.3$ fb^{-1}, updating the analysis presented in [61]. We have taken into account the Z' signal and its interference with the SM background and included efficiency and acceptance for both the electron and muon channels as described in [62]. Such studies affect the extended gauge sector $(\tilde{g}, g_{BL}, M_{Z'})$ in a way that, in all safety, allow us to select the value $M_{Z'} = 4$ TeV for all magnitudes of gauge couplings and Z' total width (in the range 30–45 GeV) met in the RGE evolution. Notice that the BLSSM supplied with unification conditions at the GUT scale provides a very narrow Z' width with a $\Gamma_{Z'}/M_{Z'}$ ratio reaching 1% at most. Thus, this is unlike the results of [48, 49], which were indeed obtained without any universality conditions. Such a Z' mass value completes the independent parameters that feed our scan and which in turn provides a BLSSM low-energy spectrum. We now impose the exclusion bounds coming from LEP, Tevatron and LHC linked to the negative searches of scalar degrees of freedom and to the correct reproduction of the measured Higgs signal strength around 125 GeV. More precisely, from our scan it is possible to extract the masses and the Branching Ratios (BRs) of all the (neutral and charged) scalars plus their effective couplings to SM fermions and bosons. This information is then processed into HiggsBounds (HB) [63–66] which, considering all the available collider searches, expresses whether a parameter point has been excluded at 95% CL or not.

This analysis removes a considerable number of acceptable points, among those with successful EW and $U(1)_{B-L}$ symmetry breaking, as obtained from the GUT parameters scan. Over such points, the compatibility fit of the generated Higgs signal strengths with the ones measured at LHC is taken into account by HiggsSignals (HS) [67], which provides the corresponding χ^2. By asking for a 2σ interval around the minimum χ^2 generated, we obtain a further constraint over the parameter space investigated. The strongest sparticle bounds which may affect our generated SUSY spectra come from the mass limits on the chargino and stau sectors, which must be more massive than ≈100 GeV [68]. However, for our generated sparticles, we are safe from this limit.

The second set of bounds that we considered emerges from the probe of DM signatures which are a common and natural product of many SUSY models. Among these, the BLSSM stands

out for both theoretical and phenomenological reasons that make the study of its DM aspects particularly worthwhile. The presence of a gauged $B-L$ symmetry, being broken by the scalar fields η_1 and η_2, as they are charged under $B-L$ [36], provides a local origin to the discrete $R-$symmetry that is usually imposed ad-hoc to prevent fast proton decay. Consequently, the BLSSM embeds the stability of the LSP through its gauge structure, as it does for the produced DM density.

From the phenomenological side, the BLSSM, like the MSSM, has the neutralino as a possible cold DM candidate. The presence of additional neutral degrees of freedom drastically changes its properties with respect to the corresponding MSSM ones, which is mostly Bino in GUT constrained models, possibly giving the necessary degrees of freedom to accommodate the measured DM evidences. Moreover, the BLSSM also envisages a scalar LSP in its spectrum, generated by the superpartners of the six Majorana neutrinos, which may also be the origin of a cold DM relic.

For every possible low energy spectrum obtained, the LSP provided by the BLSSM will participate in the early thermodynamical evolution of the universe. After an initial regime of thermal equilibrium with the SM particles, decoupling takes place once the DM annihilation rate becomes slower than the Universe expansion. This process would result in the relic density lasting until now. Consequently, a crucial test of the cosmological viability of the BLSSM is enforced by requiring the relic abundance generated not to overclose the Universe by exceeding the measured current value of the DM relic density

$$\Omega h^2 = 0.1187 \pm 0.0017 \text{ (stat)} \pm 0.0120 \text{ (syst)} \tag{2.27}$$

as measured by the Planck Collaboration [22].

The requirement to reproduce the measured relic density would finally highlight the region of the parameter space where the model is able to solve the DM puzzle. The computation of the DM abundance is achieved by solving the evolution numerically with `MicrOMEGAs` [69, 70], which collects the amplitudes for all the annihilation, as well as coannihilation, processes. Another source of constraints, which cannot be neglected due to the recent increase in precision reached by the LUX collaboration [19, 71], is linked to the direct searches intended to detect DM signatures coming from DM scatterings with nuclei. We have tested the BLSSM spectrum against the challenging upper limit on the Spin Independent (SI) component of the LSP-nucleus scattering. The zeptobarn order of magnitude, reached in the recent upgrade of the DM-nucleus cross section bound, will have an interesting interplay with the parameter space analysed to test the surviving ability of the BLSSM against stringent exclusions.

The DM scenarios provided represent a peculiar signature of the model, with characteristic degrees of freedom playing a key role in drawing a rich DM texture. As already stated, the BLSSM has two candidates for cold DM as it is possible to have, other than the neutralino, also a heavy stable sneutrino. The extended neutral sector, consequence of the inclusion of an extra $B-L$ gauge factor, enlarges the neutralino components with three new states (two coming from Bileptinos and one from BLino) as seen in Eq. (2.17). To study the behaviour of the neutralinos

we may consider the following classification

$V_{11}^2 > 0.5$	Bino-like,
$V_{12}^2 > 0.5$	Wino-like,
$V_{13}^2 + V_{14}^2 > 0.5$	Higgsino-like,
$V_{15}^2 > 0.5$	BLino-like,
$V_{16}^2 + V_{17}^2 > 0.5$	Bileptino-like,
Neither of the previous cases	Mixed.

In this scheme the nature of the neutralino is identified with the interaction eigenstate that makes up for more than half of its content.

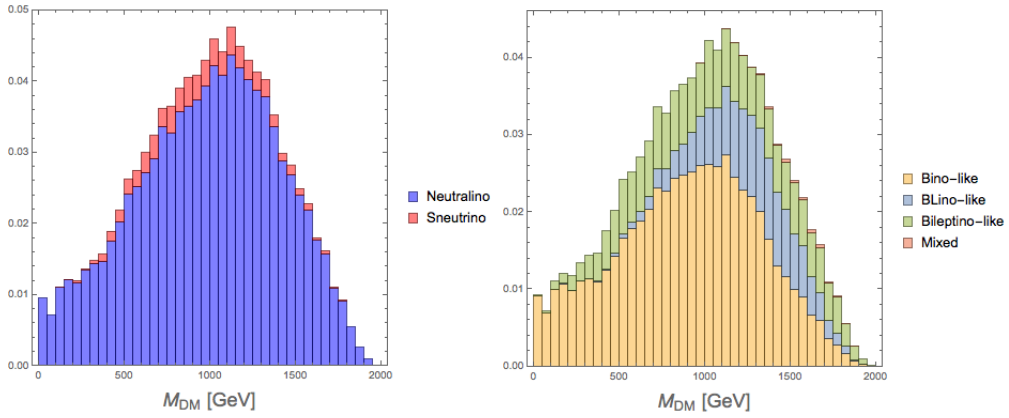

Figure 2.2: (a) The normalised distribution of the neutralino and sneutrino types found in our scan. (b) The normalised distribution of the different types of LSP found in our scan. The histograms are stacked.

For all the points generated in our scan, in agreement with the constraints from Higgs searches, the LSP will, in the majority of cases, results in a fermionic DM candidate with mass below 2 TeV, see Fig. 2.2(a). The sneutrino will instead be a subdominant option over our entire set of points. It is interesting to explore the composition of the sneutrino LSP written in terms of CP eigenstates and left-right parts. This is relevant to appreciate the chances to survive the direct detection probes of DM, with a LH sneutrino having a dangerously enhanced scattering rate against nuclei [72] due to Z mediation. Fig. 2.3 indicates that only sneutrinos above ~ 2 TeV may have a large left handed component. However, we will see only sneutrinos lighter than this limit will compete against the neutralino as a possible LSP. So, the LSP sneutrino in our constrained BLSSM will always be a RH sneutrino. Following the previous classification, a Bino-like neutralino will be more common to encounter as the BLSSM favourite LSP, but, as typical features of the model, also states of BLino and Bileptino nature are often met, see Fig. 2.2(b). Notably, no Higgsino-like neutralino are found while the Wino possibility is a most rare one, which requires very tuned conditions over the parameter space to be produced in a sizeable

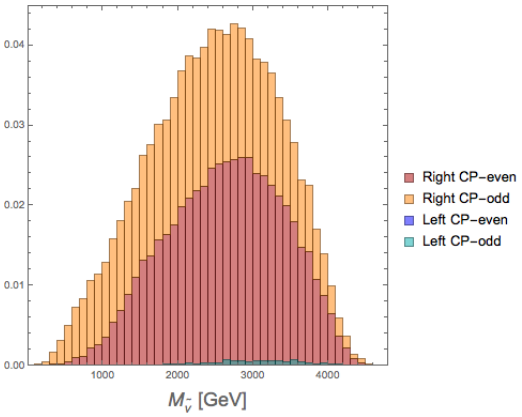

Figure 2.3: Composition of the lightest sneutrino for the set of points in agreement with the constraints from HB and HS. Histogram is of stacked type with normalised heights.

amount. Given our uniform treatment over the boundary conditions, we will not consider this case though.

2.6 Fine-Tuning Measures

We introduce measures of FT in this section to compare BLSSM and MSSM in respect of naturalness. FT is not a physical observable, but it is rather an indication for an unknown mechanism, which is missing in the model under concern. Its quantitative values, then, can be interpreted as the effectiveness of the missing mechanisms over the low scale results. In this context, the model may cover most of the whole BSM physics, when FT is small.

There are many alternatives for a quantitative measure of FT [52, 73–86], which are commonly based on the change in the Z-boson mass. Its measure (denoted by Δ) equals the largest of these changes defined as [87, 88]

$$\Delta = \text{Max}\left|\frac{\partial \ln v^2}{\partial \ln a_i}\right| = \text{Max}\left|\frac{a_i}{v^2}\frac{\partial v^2}{\partial a_i}\right| = \text{Max}\left|\frac{a_i}{M_Z^2}\frac{\partial M_Z^2}{\partial a_i}\right|. \tag{2.28}$$

When viewing a parameter space, a particular point has a low FT if the Z mass does not largely change when deviating from its position. A natural model will, therefore, possess large regions of viable parameter space with low FT values. Having this feature in a particular model will make it more attractive a prospect. Our goal here is to find allowed regions of parameter space for the BLSSM with a similar (or better) level of FT to the MSSM, so the models may be of comparable naturalness. We apply this same measure in two different scenarios (high- and low-scale parameters) for both the MSSM and BLSSM. We will proceed by explaining the procedure for the two models. We compute the minimisation conditions, or tadpole equations, and solve them to find a relation for the Z-mass and SUSY-scale parameters. At this point, we have two choices: to use these SUSY-scale parameters or to relate these to high-scale (GUT) ones and use those. For the GUT-FT, we treat loop corrections as dependent on the EW VEV, as done in [89],

which will eventually reduce the FT value by up to a factor of ~ 2. For the SUSY-FT case, we use the approximation that loop factors are independent of the other parameters, e.g., the Higgs masses (m_{H_u} and m_{H_d}). Notice, in fact, that this approximation has been widely used in the literature [18, 86, 90–97], hence we have adopted it here too. However, what is important in this work is not the comparison of the two FT methods, but rather for each one of these the difference between the two SUSY models at hand. With this in mind, we begin first by discussing the high and low scale scenarios for the MSSM, and proceed to extend this discussion to the BLSSM.

For the GUT-FT in the MSSM, our high-scale parameters are: the unification masses for scalars (m_0) and gauginos ($m_{1/2}$), the universal trilinear coupling (A_0), the μ parameter and the quadratic soft SUSY term ($B\mu$),

$$a_i = \left\{m_0,\ m_{1/2},\ A_0,\ \mu,\ B\mu\right\}. \tag{2.29}$$

In order to calculate this FT measure for a particular spectrum point, the high scale parameters are altered slightly and a new SUSY spectrum is calculated using the two-loop RGEs to run from GUT to SUSY scale. These new (modified) SUSY-scale parameters (eg m_{H_d}) are used to solve the tadpole equations and calculate a new M_Z. Practically, this computation is implemented in the `SPheno` program [60] and performed automatically for each spectrum point.

The GUT-FT will compare the naturalness at high scale, but two models with similar measures here may have large differences at the SUSY-scale. To test whether the BLSSM and MSSM have a similar FT at both GUT and SUSY-scale, we will consider a low-scale FT. To do this, we begin with the relation for the Z-mass and SUSY-scale parameters,

$$\frac{1}{2}M_Z^2 = \frac{(m_{H_d}^2 + \Sigma_d) - (m_{H_u}^2 + \Sigma_u)\tan^2\beta}{\tan^2\beta - 1} - \mu^2, \tag{2.30}$$

where

$$\Sigma_{u,d} = \frac{\partial \Delta V}{\partial v_{u,d}^2}. \tag{2.31}$$

Unlike in the GUT-FT case, we treat the loop corrections as independent of the EW VEV, as in [86]. If we substitute this expression into Eq. (2.28) and use the low-scale parameters $a_i = \{m_{H_d}^2$, $m_{H_u}^2$, μ^2, Σ_u, $\Sigma_d\}$, one will find [86]

$$\Delta_{\rm SUSY} \equiv {\rm Max}(C_i)/(M_Z^2/2)\ , \tag{2.32}$$

where

$$C_i = \begin{cases} C_{H_u} = \left|m_{H_u}^2 \dfrac{\tan^2\beta}{(\tan^2\beta - 1)}\right|\ , \quad C_{H_d} = \left|m_{H_d}^2 \dfrac{1}{(\tan^2\beta - 1)}\right|, \\ \\ C_\mu = \left|\mu^2\right|, \quad C_{\Sigma_u} = \left|\Sigma_u \dfrac{\tan^2\beta}{(\tan^2\beta - 1)}\right|, \quad C_{\Sigma_d} = \left|\Sigma_d \dfrac{1}{(\tan^2\beta - 1)}\right|. \end{cases} \tag{2.33}$$

We now turn to the BLSSM. For the GUT-FT, we follow the same universal parameters as the MSSM, but with two additional terms, relating to the μ' parameter and the corresponding quadratic soft SUSY term, $B\mu'$, so that all of our high scale terms are:

$$a_i = \left\{m_0,\ m_{1/2},\ A_0,\ \mu,\ B\mu,\ \mu',\ B\mu'\right\}. \tag{2.34}$$

We may also follow our previous procedure to find a SUSY-scale FT (SUSY-FT) for the BLSSM. By minimising the scalar potential, we find (at loop level),

$$\frac{Mz^2}{2} = \frac{1}{X}\left(\frac{m_{H_d}^2 + \Sigma_d}{(\tan^2(\beta)-1)} - \frac{(m_{H_u}^2 + \Sigma_u)\tan^2(\beta)}{(\tan^2(\beta)-1)} + \frac{\tilde{g}M_{Z'}^2 Y}{4g_{BL}} - \mu^2\right), \tag{2.35}$$

where

$$X = 1 + \frac{\tilde{g}^2}{(g_1^2+g_2^2)} + \frac{\tilde{g}^3 Y}{2g_{BL}(g_1^2+g_2^2)}, \tag{2.36}$$

and

$$Y = \frac{\cos(2\beta')}{\cos(2\beta)} = \frac{\left(\tan^2\beta+1\right)\left(1-\tan^2\beta'\right)}{\left(1-\tan^2\beta\right)\left(\tan^2\beta'+1\right)} \tag{2.37}$$

In the limit of no gauge kinetic mixing ($\tilde{g}\to 0$), this equation reproduces the MSSM minimised potential of Eq. (2.30). Our SUSY-FT parameters for the BLSSM are thus

$$C_i = \begin{cases} C_{H_u} = \left|\dfrac{m_{H_u}^2}{X}\dfrac{\tan^2\beta}{(\tan^2\beta-1)}\right|, C_{H_d} = \left|\dfrac{m_{H_d}^2}{X}\dfrac{1}{(\tan^2\beta-1)}\right|, C_{\Sigma_d} = \left|\dfrac{\Sigma_d}{X}\dfrac{1}{(\tan^2\beta-1)}\right| \\ C_{\Sigma_u} = \left|\dfrac{\Sigma_u}{X}\dfrac{\tan^2\beta}{(\tan^2\beta-1)}\right|,\ C_\mu = \left|\dfrac{\mu^2}{X}\right|,\ C_{Z'} = \left|M_{Z'}^2\dfrac{\tilde{g}Y}{4g_{BL}X}\right|. \end{cases} \tag{2.38}$$

These equations resemble those of the MSSM SUSY-FT, but now with a factor of $1/X$. In addition, we have a contribution from the Z' mass and BLSSM loop factors. Considering the heavy mass bound on $M_{Z'}$, its contribution could be expected much larger than the other terms in Eq. (2.35), which would worsen the required FT at the low scale. However, a significantly large $M_{Z'}$ severely constrains the VEVs of the singlet Higgs fields as $\tan\beta' \sim 1$ [42] and, hence, Y yields a very stringent suppression in $C_{Z'}$. Note that, even though the trilinear A-terms are not included in determining the FT, their effects can be counted in the SSB masses in Eq. (2.38), whose values include also the loop corrections.

If the required FT measure is quantified in terms of the GUT scale parameters, as done for the MSSM in [87], such as $m_0, m_{1/2}, A_0, \mu, B\mu, \mu', B\mu'$, one can investigate which parameter is most frequently responsible for determining FT. Since the value of FT is taken to be equal to the maximum contribution out of all parameters, for a given SUSY spectrum only one parameter will determine the FT.

Fig. 2.4 displays the FT contributions of the fundamental parameters of the MSSM and

BLSSM. For each of our SUSY spectrum points which survive the HB/HS constraints, we count the number of times each parameter determines the FT. This has been done for both MSSM and BLSSM points, then the vertical axis is rescaled so the sum of counts is 1.

The dominating term in both cases is from the μ term, which is fixed (along with $B\mu$) by requiring EWSB. The next largest contribution to the FT measure arises from the gaugino sector, whose masses are parametrised via $m_{1/2}$. This can be understood with the heavy gluino mass bound [**gluino**] and its large loop contribution to realise the 125 GeV Higgs boson. The BLSSM sector is also effective in the FT in terms of μ' and $B\mu'$. There is a very small dependence on A_0 as discussed previously, and approximately no dependence on m_0 or $B\mu$ in either case.

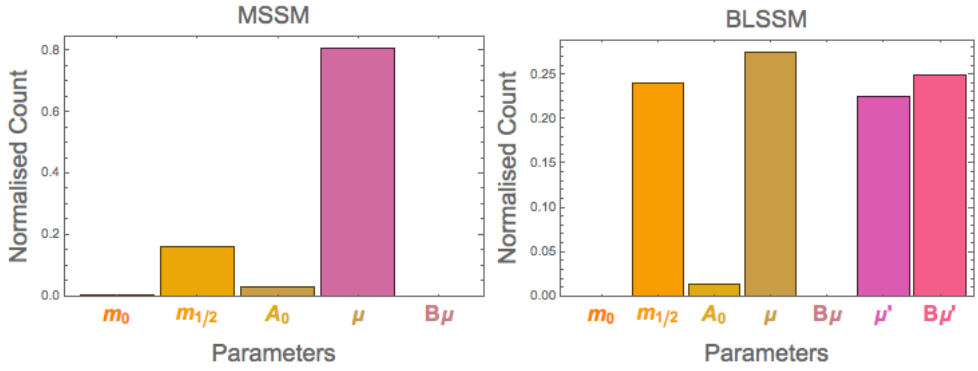

Figure 2.4: Histogram for GUT-FT parameters for MSSM (left) and BLSSM (right), counting the number of spectrum points each parameter determines the FT value, and normalised so the sum of counts is unity.

Fig. 2.5 uses the same method as figure 2.4, counting the frequency each parameter determines the FT, but now for SUSY-scale parameters. Both the MSSM and BLSSM are dominated by the μ's FT, with a small contribution from m_{H_u} and also a slight dependence on $M_{Z'}$ for the BLSSM. Considering this, what will affect the FT between the BLSSM and MSSM will be a combination of how large the factor X is and the largeness of μ in both models. This value will

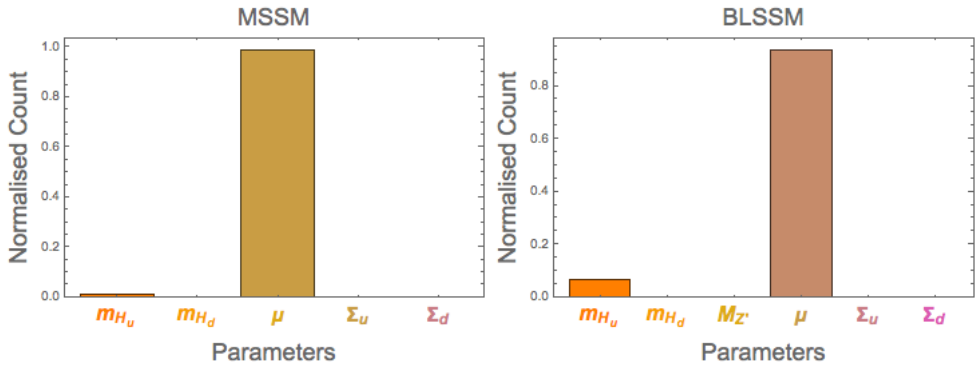

Figure 2.5: Histogram for SUSY-FT parameters for MSSM (left) and BLSSM (right), counting the number of spectrum points each parameter determines the FT value, and normalised so the sum of counts is unity.

not be identical, as there is an additional factor of $\frac{M_{Z'}(\tilde{g}Y)}{4g_{BL}}$ in the BLSSM minimisation equation.

2.7 Results

We will now compare the FT obtained in the BLSSM and MSSM scenarios, for our two FT measures. We will begin by explaining the interval ranges of our data, then we will discuss the SUSY-scale and GUT-scale FTs and which parameters are most responsible for their values. This will be done for both the BLSSM and MSSM, though the same parameters in both models are usually responsible for the largeness of FT. Then we will compare the GUT-FT and SUSY-FT for both the BLSSM and MSSM in the plane (m_0, $m_{1/2}$), as is commonly done.

The scan performed to obtain this data has been done by SPheno with all points being passed through HB and HS. We have scanned over the range $[0, 5]$ TeV in both m_0 and $m_{1/2}$, $\tan\beta$ in $[0, 60]$, A_0 in $[-15, 15]$ TeV, which are common universal parameters for both the MSSM and the BLSSM, while for the BLSSM we also required $\tan\beta'$ in the interval $[0, 2]$ with neutrino Yukawa couplings $Y^{(1,1)}$, $Y^{(2,2)}$, $Y^{(3,3)}$ in $[0, 1]$. The $M_{Z'}$ value has been fixed to 4 TeV as discussed in Section 2.5. We will now compare the FT for both the MSSM and BLSSM, using both low- and high-scale parameters.

We begin by presenting a measure of how the SUSY-FT parameter varies with μ in the BLSSM. Fig. 2.6 displays how the SUSY FT parameter, Δ_{SUSY} varies with μ. The FT measure is equal to the maximum contribution from any of the SUSY parameters, but here we see all data points centred on the curve. The tightness of this line (very few points that lie above or below the μ line) shows that very rarely are the other (m_{h_u}, m_{h_d}, Σ_u, Σ_d) parameters ever responsible for the FT. This behaviour is expected, as one can see from the histogram plot of SUSY parameters, see Fig. 2.5. The corresponding plot for the MSSM looks very similar and so is not shown. The behaviour is almost identical, as is expected from the MSSM version of the histogram discussed in section 2.6, where the μ parameter dominates the FT.

Now, we turn our attention to considering loop contributions in the SUSY-scale FT. By treating the loop factors as independent parameters which contribute to FT, we may observe their contributions. Fig. 2.7 presents the contribution to FT from Σ_u and Σ_d whilst varying μ. Immediately, one can compare the typical FT values with that of the overall FT as in Fig. 2.6 and see that the loop contributions will never be the dominant contribution for the FT. There is some growth with μ, but for any given value, the contribution from μ itself is 10 times larger. Since only the maximum contribution of any C_i parameter is taken, we find that treating the tadpole loop contributions as independent of the VEV causes the one-loop FT to look much the same as at tree-level. Once again, this behaviour is mimicked in the MSSM, where the VEV independent tadpole loop corrections are also dwarfed by μ's FT.

Penultimately, before we turn to our final comparison of FT, we will discuss the dominant parameters in the GUT-FT sector. Fig. 2.8 shows how the GUT-FT depends on $m_{1/2}$. There is a proportionality with $m_{1/2}$, favouring lower values for a better FT, but the points are not tightly constrained, unlike in SUSY-FT. The upward spread of points indicates that other parameters

in addition to $m_{1/2}$ affect the FT. This is expected from the histogram in Fig. 2.4, where no one single parameter always determines FT, but rather a more even mix.

Finally, we will consider how the FT changes in the plane of (m_0, $m_{1/2}$). These parameters have been chosen as they dominantly characterise the behaviour of the model itself at the GUT scale. The μ parameter that dominates FT is determined by the minimisation conditions, which may be written as functions of m_0 and $m_{1/2}$. We colour the points with their FT values in four intervals, namely: red for FT > 5000, green for $1000 <$ FT < 5000, orange for $500 <$ FT < 1000 and blue (the least finely-tuned points) for FT < 500. The same set of points is used to compare the GUT-FT and the SUSY-FT (there is only a recolouring of these data points between left and right hand side) for the BLSSM and MSSM. The overall picture is similar for all four cases and it is immediately clear that the FT is comparable between the BLSSM and the MSSM. There is a difference in the distribution of points between the MSSM and BLSSM, where there seem to be no viable points until $m_0 \sim 1$TeV in the latter. This is due to the requirement of a Z' mass consistent with current constraints (see Section 2.5). Moreover, due to the tadpole equation given in Eq. (2.4) relating $M_{Z'}$ to the soft-masses $m_{\eta_{1,2}}$, which are functions of m_0, notice that a larger $M_{Z'}$ leads to a larger m_0. All four graphs have a similar FT distribution, where a low $m_{1/2}$ is favoured and which manifests an approximate independence of m_0. Indeed, $m_{1/2}$ is mostly responsible for the FT rather than m_0 (see Fig. 2.4). Since there is a little dependence on m_0, we expect to see an increasing FT as $m_{1/2}$ increases, as can be seen in all four cases. When comparing the BLSSM and MSSM GUT-FT, the two pictures are very similar, with a slightly better FT in the MSSM, though the less fine tuned (blue) points appear about the same mass of $m_{1/2} \approx 2$ TeV. This behaviour is very similar when comparing the SUSY-FT between BLSSM and MSSM, where the pictures (up to the distribution of points) are very similar, with a slight dependence on m_0, where larger values are favoured. Lastly, we compare the GUT-FT and SUSY-FT for each of the models. In the BLSSM we find a more concentrated region of less fine-tuned points at higher m_0. Both measures show a strong dependence on $m_{1/2}$. In the MSSM, we again find this dependence, but not the increase in density of less-finely tuned points as in the BLSSM. To conclude the discussion on FT, we find that the overall FT is very comparable between the BLSSM and MSSM. Though the GUT-parameter measure is similar in both pictures, with the MSSM as slightly less finely tuned, the BLSSM has a larger density of less-finely-tuned points when considering SUSY-parameters.

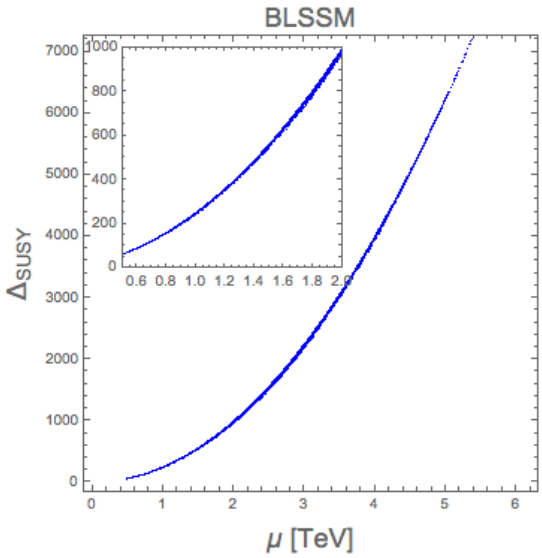

Figure 2.6: (a) The SUSY-FT, Δ_{SUSY} vs μ plotted for BLSSM spectrum points. As one expects from figure 2.5, there is a strong dependence of the overall FT, Δ_{SUSY} with the μ parameter; as for nearly every spectrum point, C_μ is the largest of all C parameters.

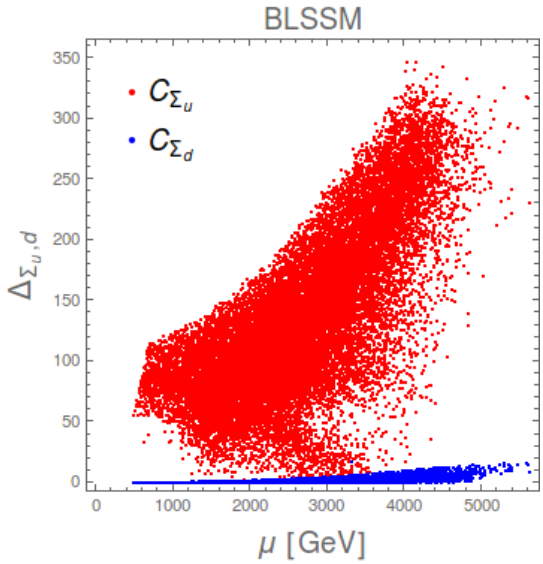

Figure 2.7: Strength of loop factors, $\Sigma_{u,d}$, appearing in Eq. (2.38) as a function of μ plotted for BLSSM spectrum points. This may be compared to the overall FT value, appearing in Fig. 2.6, and one can see the loop factors contributions are never dominant and so loop corrections do not affect the SUSY-FT.

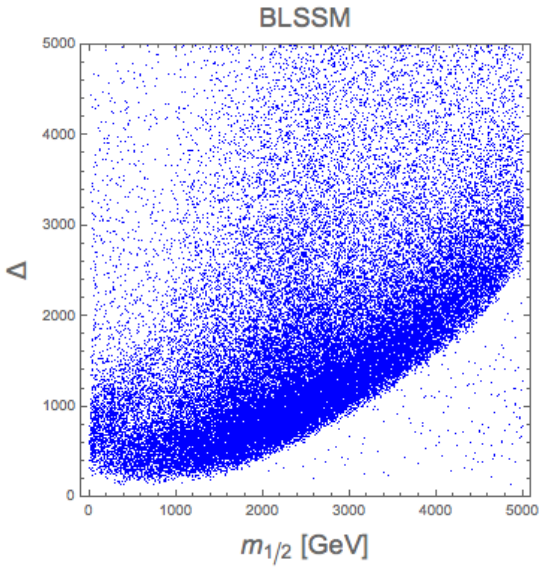

Figure 2.8: GUT-FT plotted against $m_{1/2}$ for BLSSM spectrum points. There is a strong dependence for the GUT-FT with the $m_{1/2}$ parameter, although the wide upward spread indicates other parameters may also be the dominant FT contribution.

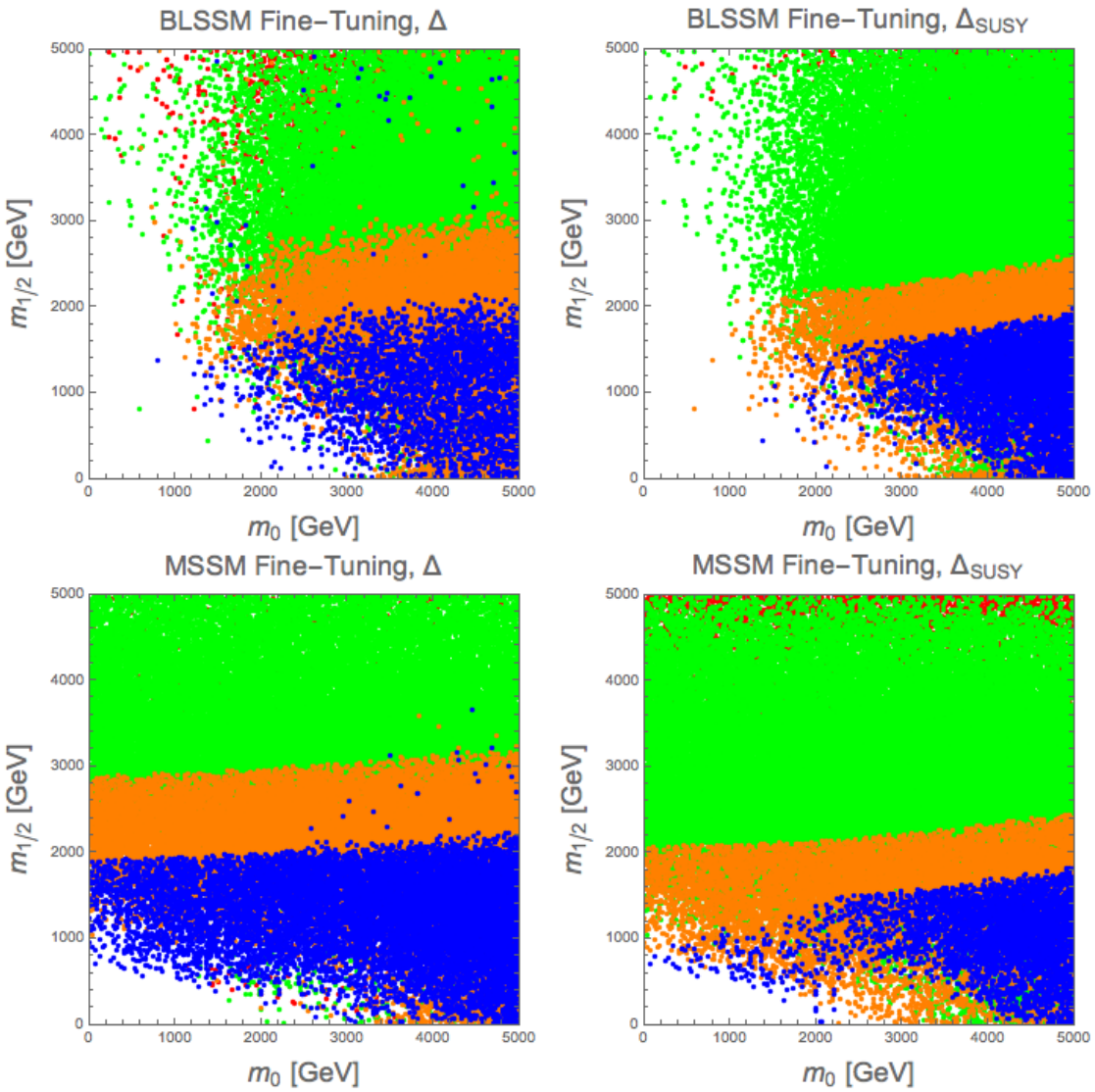

Figure 2.9: FT in the plane of unification of scalar, gaugino masses for BLSSM and MSSM for both GUT-parameters (Δ) and EW parameters ($\Delta_{\rm EW}$). The FT is indicated by the colour of the dots: blue for FT $<$ 500; Orange for 500 $<$ FT $<$ 1000; Green for 1000 $<$ FT $<$ 5000; and Red for FT $>$ 5000.

We now turn to considering the DM sectors of both models. We will see that once cosmological and direct detection bounds are imposed on the DM candidates, the BLSSM parameter space is far less constrained than the MSSM one, although at the cost of an increased GUT-FT.

For each generated spectrum, the LSP must comply with the cosmological and direct detection bounds of Section 2.5. The relic density in respect to the mass of the LSP ($M_{\rm DM}$) is plotted in Fig. 2.10(a). The relic is overabundant for the large part of points surviving the screening from collider constraints. Without specifying initial conditions, as those igniting a favourable coannihilation, our scan reveals multiple extended areas with relic densities close to zero. Interestingly, the BLSSM successfully accommodates values within the allowed interval in Eq. (2.27), with all

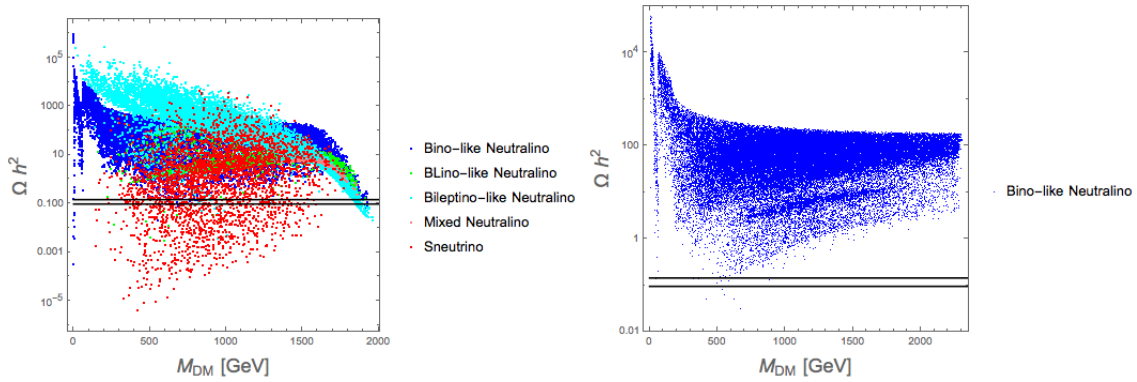

Figure 2.10: (a) Relic density vs LSP mass for the BLSSM. (b) Relic density vs LSP mass for the MSSM. In both plots the horizontal lines identify the 2σ region around the current central value of Ωh^2.

LSP species. The corresponding distributions in Fig. 2.10(a) have recognisable shapes, which point to different areas where a given LSP is more likely to cross the experimentally allowed interval. Neutralinos may be found mostly, but not entirely, at large $M_{\rm DM}$ values. Sneutrinos appear in a cloud, with low relic density values around the centre of our mass span. The sneutrino option stands out as a very promising one, compensating its low rate of production as a LSP with a milder value of the relic with respect to the neutralino.

The extended particle spectrum of the BLSSM yields a more varied nature of the LSP, with more numerous combinations of DM annihilation diagrams, and can play a significant role in dramatically changing the response of the model to the cosmological data, in comparison to the much constrained MSSM. This is well manifested by the relic density computed in the MSSM, as shown in Fig. 2.10(b). From here, it is obvious how the BLSSM offers a variety of solutions to saturate the relic abundance compatible with the constraints, whether taken at 2σ from the central value measured by experiment or as an absolute upper limit, precluded to the MSSM. In the former, different DM incarnations (Bino-, BLino-, Bileptino-like and mixed neutralino, alongside the sneutrino) can comply with experimental evidence over a $M_{\rm DM}$ interval which extends up to 2 TeV or so, while in the MSSM case solutions can only be found for much lighter LSP masses and limitedly to one nature (the usual Bino-like neutralino). Together with the limit on the cosmological relic produced at decoupling by the candidate DM particle, we challenge the constrained BLSSM against the negative search for Weakly Interactive Massive Particle (WIMP) nuclear recoils by the LUX experiment.

The 2016 results of the LUX collaboration have seen the upper bound on the cross section decreasing by a factor of four in the three years of exposure. Such constraining analyses are still ongoing and will interestingly become a threat or a confirmation of the WIMP hypothesis in future years. From Fig. 2.11 we notice how the BLSSM with the parameter space investigated largely survives such tight limits. We impose the modified constraint [98]:

$$\sigma_{SI} < \xi \sigma_{SI}^{LUX} \tag{2.39}$$

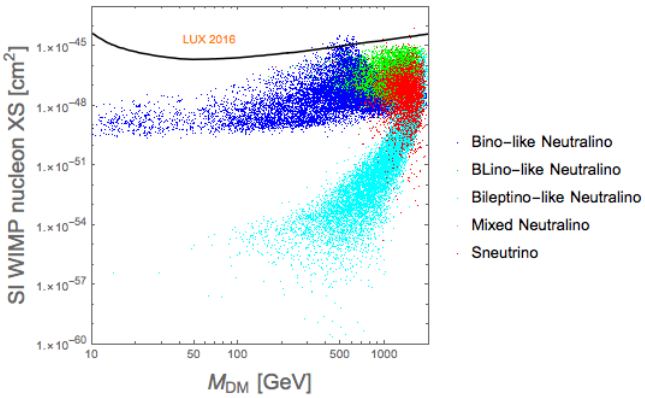

Figure 2.11: Spin-independent WIMP-nucleus scattering cross section generated in our scan against the upper bounds from 2016 run of the LUX experiment.

where

$$\xi = \begin{cases} 1 & \text{if } \ 0.1168 < \Omega h^2 < 0.1208 \ , \\ \dfrac{0.1188}{\Omega h^2} & \text{if } \ \Omega h^2 < 0.1168 \ . \end{cases} \tag{2.40}$$

This accounts for the LUX experimental search assuming the DM has the correct relic density. The effect is to weaken constraints for low relic density points. The LUX bounds have just started touching the BLSSM parameter space, so the next improvements of direct DM searches will continue to further probe BLSSM's parameter space. Even without accounting for this "low relic-density" effect, the picture is still similar. For the MSSM, the SI bounds look identical to the BLSSM, but with a Bino-like neutralino only.

2.8 Chapter Summary

While several studies of the SUSY version of the $B-L$ model, BLSSM for short, exist for its low energy phenomenology and predict distinctive experimental signatures, very little had been said about the theoretical degree of FT required in this scenario in order to produce them. Alternatively, these studies fail to escape current experimental constraints coming from EWPOs, collider and cosmological data. We have addressed these issues in the first part of this chapter, by adopting a suitable FT measure amongst those available in literature and expressed it in terms of the low energy spectra of the MSSM and BLSSM as well as of the (high-scale) universal parameters of the two models. The latter, for the MSSM, include: masses for scalars and gauginos, trilinear coupling, Higgsino mass and the quadratic soft SUSY term. In the BLSSM, we have all of these parameters plus two additional ones, the BLino mass and another quadratic soft SUSY term. The low and high energy spectra in the two SUSY scenarios can be related by RGEs, which we have computed numerically at two-loop level.

We have found that the level of FT required in the BLSSM is somewhat higher than in the MSSM when computed at the GUT scale in presence of all available experimental constraints,

but those connected to DM searches, and this is primarily driven by the requirement of a large Z' mass, of order 4 TeV or higher, which in turn corresponds to somewhat different acceptable values for the scalar and fermionic unification masses, which partially reflect in different low energy spectra potentially accessible at the LHC. However, when the FT is computed at the SUSY scale, the pull now originating from all available experimental constraints, chiefly the DM ones, destabilises the MSSM more than the BLSSM, as the latter appears more natural, well reflecting a much lower level of tension against data existing in the latter with respect to the former.

Furthermore, we have examined the response to the relic density constraints of the non-minimal SUSY scenario, wherein the extra $B-L$ neutralinos (three extra neutral fermions, i.e., a $U(1)_{B-L}$ gaugino $\widetilde{B}'$ and two extra Higgsinos $\widetilde{\eta}$) can be cold DM candidates. As well known, taking the lightest neutralino in the MSSM as the sole possible DM candidate implies severe constraints on the parameter space of this scenario. Indeed, in the case of universal soft-breaking terms, the MSSM is almost ruled out by combining collider, astrophysics and rare decay constraints. Therefore, it is important to explore very well motivated extensions of the MSSM, such as the BLSSM, that provide new DM candidates that may account for the relic density with no conflict with other phenomenological constraints.

After an extensive study in this direction, we have concluded that the extended particle spectrum of the BLSSM, in turn translating into a more varied nature of the LSP as well as a more numerous combination of DM annihilation diagrams, can play a significant role in dramatically changing the ability of SUSY to adapt to cosmological data, in comparison to the much constrained MSSM. In fact, the BLSSM offers a variety of solutions to the relic abundance constraint, whether taken at 2σ from the central value measured by experiment or as an absolute upper limit, which are unavailable in the MSSM. Alongside the usual Bino- (and possibly sneutrino), also BLino- and Bileptino-like as well as mixed neutralino can comply with experimental evidence over an $M_{\rm DM}$ interval which extends up to 2 TeV or so, while in the MSSM case solutions can only be found for much lighter LSP masses (~ 500 GeV) and limited to the standard Bino-like neutralino.

Chapter 3

Supersymmetric Extension of the $U(1)_{B-L}$ Model: Dark Matter

3.1 Introduction

In the previous chapter, we introduced possible dark matter candidates from the BLSSM and calculated FT metrics in comparison to the CMSSM. [1] In this chapter, we investigate the feasibility of the RH sneutrino LSP as a suitable DM candidate within the BLSSM framework, which embeds a Type-I seesaw mechanism for the neutrino masses. In this case though, realising that consistency with relic density of such a DM candidate is difficult due to the tiny Yukawa couplings ($Y_\nu \lesssim 10^{-6}$) involved [99], one may be tempted to conclude that its observation would be difficult. This perception may be further reinforced by the fact, even though the RH sneutrino can interact with the Z boson through the gauge kinetic mixing between $U(1)_Y$ and $U(1)_{B-L}$, such an interaction is strongly suppressed by the heavy mass bound on the gauge boson associated with the $(B-L)$ symmetry (the aforementioned Z'). These difficulties can however be overcome by identifying some new DM annihilation channels, which we will discuss below, in which the specific $(B-L)$ sector plays a crucial role. In this case then, one may even attempt to extract evidence of such new DM dynamics which can be tested, if not at present, in near future experiments, both collider and astrophysical ones.

3.2 RH Sneutrinos in the BLSSM

We now consider the RH sneutrino sector in the BLSSM model. With a TeV scale BLSSM with Type-I seesaw and very small neutrino Yukawa coupling, $Y_\nu \lesssim \mathcal{O}(10^{-6})$, the sneutrino mass matrix, in the basis $(\tilde{\nu}_L, \tilde{\nu}_L^*, \tilde{\nu}_R, \tilde{\nu}_R^*)$, is approximately given by a 2×2 block diagonal matrix, where the element 11 of this matrix is given by the diagonal LH sneutrino mass matrix and the

[1] The C refers to "constrained", which means using unified input parameters.

element 22 represents the RH sneutrino mass matrix, M_{RR}, defined as [100]

$$M^2_{RR} = \begin{pmatrix} M^2_{\tilde{N}} + m^2_{\tilde{N}} + m^2_D + \frac{1}{2}M^2_{Z'}\cos 2\beta' & M_N(A_N - \mu' \cot\beta') \\ M_N(A_N - \mu' \cot\beta') & M^2_{\tilde{N}} + m^2_{\tilde{N}} + m^2_D + \frac{1}{2}M^2_{Z'}\cos 2\beta' \end{pmatrix}. \quad (3.1)$$

It is notable that a large mixing between the RH sneutrinos and RH antisneutrinos is quite plausible, since it is given in terms of large Yukawa couplings, $Y_N \sim \mathcal{O}(1)$. Therefore, $\tilde{\nu}_R, \tilde{\nu}^*_R$ are not the mass eigenstates. The mass splitting and mixing between the RH sneutrino $\tilde{\nu}_R$ and RH antisneutrino $\tilde{\nu}^*_R$ are a result of the induced $\Delta L = 2$ lepton number violating term $M_N N^c N^c$. One can show that the mass eigenvalues of RH sneutrinos are given by [44, 101]

$$m^2_{\tilde{\nu}_\mp} = M^2_{\tilde{N}} + m^2_{\tilde{N}} + m^2_D + \frac{1}{2}M^2_{Z'}\cos 2\beta' \mp \Delta m^2_{\tilde{\nu}_R}, \quad (3.2)$$

where $\Delta m^2_{\tilde{\nu}_R} = \left| M_N(A_N - \mu' \cot\beta') \right|$ and the mass eigenstates $\tilde{\nu}_\mp$ are defined in terms of $\tilde{\nu}_R, \tilde{\nu}^*_R$ as follows:

$$\tilde{\nu}_- = \frac{-i}{2}\left(e^{i\phi/2}\tilde{\nu}_R - e^{-i\phi/2}\tilde{\nu}^*_R\right), \quad (3.3)$$

$$\tilde{\nu}_+ = \frac{1}{2}\left(e^{i\phi/2}\tilde{\nu}_R + e^{-i\phi/2}\tilde{\nu}^*_R\right), \quad (3.4)$$

where ϕ is the phase of the off-diagonal element of M_{RR}, i.e., $\phi = \arg(M_N(A_N - \mu' \cot\beta'))$. In case of real soft SUSY breaking terms, one finds $\phi = 0$ or $\phi = \pi$, depending on the relative sign of A_N and μ'. In the former case, we see that $\tilde{\nu}_-(\phi = 0) = \mathrm{I}(\tilde{\nu}_R) \equiv \tilde{\nu}^{\mathrm{I}}_1$, so the lightest state is an imaginary sneutrino with $m_{\tilde{\nu}^{\mathrm{I}}_1} = m_{\tilde{\nu}_-}$ and the real type, $\mathrm{R}(\tilde{\nu}_R) \equiv \tilde{\nu}^{\mathrm{R}}_1$, has a larger mass $m_{\tilde{\nu}^{\mathrm{R}}_1} = m_{\tilde{\nu}_+}$. The other possibility is $\phi = \pi$, where now $\tilde{\nu}_-(\phi = \pi) = \tilde{\nu}^{\mathrm{R}}_1$ is the lightest state with $m_{\tilde{\nu}^{\mathrm{R}}_1} = m_{\tilde{\nu}_-}$ and $\tilde{\nu}^{\mathrm{I}}_R$ is heavier with $m_{\tilde{\nu}^{\mathrm{I}}_R} = m_{\tilde{\nu}_+}$.

Before we consider the effect this will have on spectrum points in parameter space, we must first discuss how we obtain our numerical results. In this work, we have used the spectra for RH sneutrino LSP candidates in the BLSSM, previously obtained in [1], and discussed in the previous chapter, where the exact details of the numerical results are discussed in great detail, though we summarise them here. We have used the SARAH [59] and SPheno [60] programs, considering a complete universal scenario where the gauge couplings all unify at GUT scale, and evolve at two-loop order to low scale. We have scanned over the range $[0, 5]$ TeV in both m_0 and $m_{1/2}$, $\tan\beta$ in $[0, 60]$, A_0 in $[-15, 15]$ TeV, $\tan\beta'$ in the interval $[0, 2]$ with neutrino Yukawa couplings $Y^{(1,1)}$, $Y^{(2,2)}$, $Y^{(3,3)}$ in $[0, 1]$. The $M_{Z'}$ value has been fixed to 4 TeV to comply with dedicated $U(1)_{B-L}$ searches, such as in [49, 61, 102, 103]. In particular, 95% CL bound has been extracted in the di-lepton channel at the LHC with $\sqrt{s} = 13$ TeV and $\mathcal{L} = 40\,\mathrm{fb}^{-1}$ luminosity. The Z' signal and its interference with the SM background have been properly taken into account as well as the efficiency and acceptance factors as illustrated in [62]. The Z' values of the gauge couplings, $g_{BL} \simeq 0.55$ and $\tilde{g} \simeq -0.144$, have been obtained from an RGE analysis assuming unification

at the GUT scale [1]. The spectra are then processed into HB [63–66] which, considering all the available collider searches, expresses whether a parameter point has been excluded at 95% CL or not. Finally, the compatibility fit of the generated Higgs signal strengths with the ones measured at LHC is taken into account by HS [67], which provides the corresponding χ^2. By asking for a 2σ interval around the minimum χ^2 generated, we obtain a further constraint over the parameter space investigated. After these conditions are satisfied, we then enforce that all spectra satisfy the SUSY mass bounds for gluinos, staus, neutralinos, charginos and stops [104]. It is worth noting, at this point, that fixing $M_{Z'} = 4$ TeV enforces a heavy SUSY spectrum, so enforcing masses greater than SUSY search bounds is not in general more constraining than the enforcement of Higgs data. We would also like to stress that the additional content of the BLSSM compared to the MSSM will not act to enhance the production rate of any simplified model searches, so it is reasonable to use these limits; though they do not greatly remove many spectrum points after all other constraints are imposed. Finally, for the work in this chapter, we isolate the RH sneutrino LSP candidate points generated by this scan which comply with all our constraints.

One can now see the behaviour of the mass difference, $\Delta m^2_{\tilde{\nu}_R}$, on the sneutrino mass, applied to our scan, in Fig. 3.1. When the mass difference is positive, $\phi = 0$ and so the $\tilde{\nu}_1^{\rm I}$ acquires the lightest mass $m_{\tilde{\nu}_-}$. In the case of a negative mass difference ($\phi = \pi$), one has a $\tilde{\nu}_1^{\rm R}$ LSP, with mass $m_{\tilde{\nu}_-}$. In general, one finds that $M_N(A_N - \mu' \cot\beta')$ tends to be positive and so there are many more CP-odd sneutrino LSPs than CP-even ones (by a factor of ~ 10).

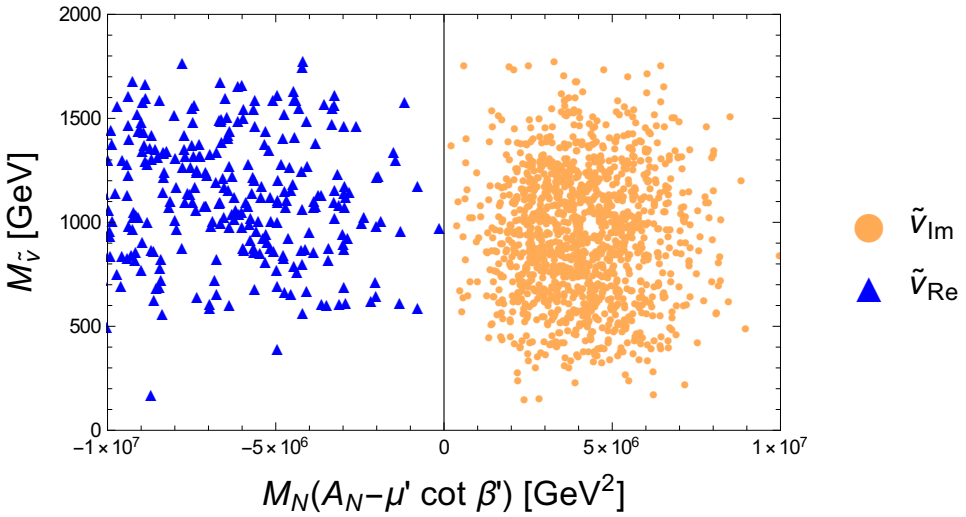

Figure 3.1: Masses of real and imaginary RH sneutrino LSP candidates are plotted against the mass difference of the two eigenstates, $M_N(\mu' \cot\beta' - A_N)$.

Now, we briefly describe the relevant interactions of sneutrino DM, for $\tilde{\nu}_R^{\rm I}$ and $\tilde{\nu}_R^{\rm R}$ LSPs. The relic abundance of the sneutrino DM is a direct consequence of the strength of these interactions, in addition to revealing what signatures this DM candidate may provide. The main interactions which contribute to the annihilations of the sneutrino DM are given by four-point interaction $\left(\tilde{\nu}_1^{\rm (R,I)}\tilde{\nu}_1^{\rm (R,I)} \to h_i h_j\right)$ and processes mediated by the CP-even Higgs sector

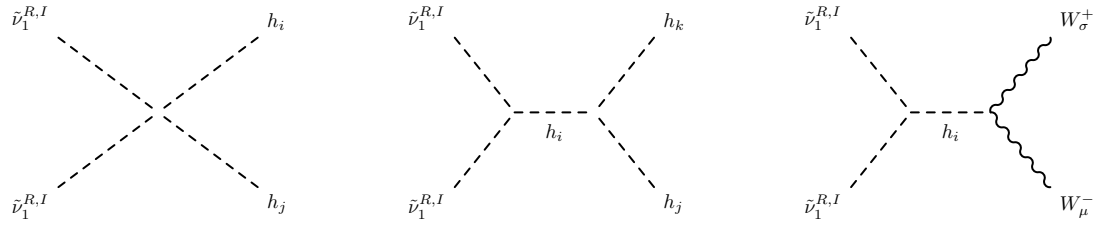

Figure 3.2: Feynman diagrams of the dominant interaction terms of two real or two imaginary RH sneutrinos.

$\left(\tilde{\nu}_1^{(\mathrm{R,I})}\tilde{\nu}_1^{(\mathrm{R,I})} \to h_i \to h_i h_j \text{ or } W^+W^-\right)$, as shown in Fig. 3.2. With $Y_\nu \ll 1$, the Lagrangian of these interactions can be written as follows:

$$\begin{aligned}
\mathcal{L} \quad \supset i\Bigg\{ & \left(\tilde{\nu}_1^{\mathrm{R,I}}\right)^2 h_i \textstyle\sum_{a=1}^{3} (Z_{13+a}^{(\mathrm{R,I})})^2 \Big[\frac{g_B^2}{2}\Big(v_\eta Z_{i3}^H - v_{\bar{\eta}} Z_{i4}^H\Big) \pm \sqrt{2}\Big(Z_{i4}^H \mu_\eta Y_{x,aa} - Z_{i3}^H T_{x,aa}\Big) - 4 v_\eta Z_{i3}^H Y_{x,aa}^2\Big] \\
& + \left(\tilde{\nu}_1^{\mathrm{R,I}}\right)^2 h_i h_j \textstyle\sum_{a=1}^{3} (Z_{13+a}^{(\mathrm{R,I})})^2 \Big[\frac{g_B^2}{2}\Big(Z_{i3}^H Z_{j3}^H - Z_{i4}^H Z_{j4}^H\Big) + \frac{g_B g_{YB}}{4}\Big(Z_{i1}^H Z_{j1}^H - Z_{i2}^H Z_{j2}^H\Big) - 4 Z_{i3}^H Z_{j3}^H Y_{x,aa}^2\Big] \\
& + (h_i h_j h_k)\, g_B^2 \Big[v_\eta\Big(-3 Z_{i3}^H Z_{j3}^H Z_{k3}^H + Z_{i3}^H Z_{j4}^H Z_{k4}^H + Z_{i4}^H Z_{j3}^H Z_{k4}^H + Z_{i4}^H Z_{j4}^H Z_{k3}^H\Big) \\
& + v_{\bar{\eta}}\Big(Z_{i3}^H Z_{j3}^H Z_{k4}^H + Z_{i3}^H Z_{j4}^H Z_{k3}^H + Z_{i4}^H Z_{j3}^H Z_{k3}^H - 3 Z_{i4}^H Z_{j4}^H Z_{k4}^H\Big)\Big] \\
& + h_i W_\mu^- W_\sigma^+ \tfrac{g_2^2}{2}\Big(v_d Z_{i1}^H + v_u Z_{i2}^H\Big)\Big(g^{\sigma\mu}\Big)\Bigg\},
\end{aligned} \tag{3.5}$$

where h_i is one of the four mixed CP-even Higgs mass eigenstates [46] (h_1 is the lightest SM-like Higgs, h_2 is the light $(B-L)$-like Higgs, h_3 is the heavy MSSM-like Higgs and h_4 is the heavy $(B-L)$-like state). These states are all mixed and the matrix which diagonalises the Higgs mass matrix is written as Z^H. There are four Higgs VEVs, corresponding to the MSSM H_u and H_d doublets and the BLSSM η and $\bar{\eta}$ singlets, written as $(v_u,\ v_d,\ v_\eta,\ v_{\bar{\eta}})$, respectively. The diagonalising mass matrices for the CP-even and CP-odd sneutrinos are denoted by $Z^{(\mathrm{R,I})}$ while the $Y_{x,aa}$'s are the Yukawa couplings for the RH neutrinos, which are assumed to be diagonal along with the trilinear couplings, the $T_{x,aa}$'s. The gauge couplings g_B and g_{YB} will be rotated, along with the (unseen) g_{YY} and g_{BY} couplings, to become the physical g_1, g_{BL} and $\tilde{g}$ couplings.

3.3 Annihilation Cross Section and DM Relic Abundance

The two CP-eigenstate RH sneutrinos, $\tilde{\nu}_1^{\mathrm{I}}$ and $\tilde{\nu}_1^{\mathrm{R}}$, produce different phenomena in respect of the cross sections of their annihilation channels, which may yield detectable consequences in cosmological measurements. The DM is annihilating at low (thermal) energies, so the final product masses must be $\lesssim 2M_{\tilde{\nu}}$. As indicated by the interaction terms in (3.5), the highest cross section channel (for both CP-even and -odd) is $\tilde{\nu}\tilde{\nu} \to h'h'$[2], as long as $M_{h'} < M_{\tilde{\nu}}$. If this is not the case then the next highest cross section channel is $\tilde{\nu}\tilde{\nu} \to W^+W^-$. One is also allowed decays

[2]For ease of notation, hereafter, we identify $h' \equiv h_2$.

to ZZ, with a cross section approximately half that of W^+W^-, but this contribution will be neglected for the remainder of the thesis. We find that other channels have small contributions to the total annihilation cross section in comparison to these two. So, what separates the phenomena of the real and imaginary sneutrinos is then simply the mass relation between h' and $\tilde{\nu}$. If $M_{\tilde{\nu}} > M_{h'}$, the annihilation cross section will be dominated by the $h'h'$ production and, if not, then W^+W^-. In order to determine which mass is larger, and hence the phenomenology of a given state, we must consider the dependence of the mass splitting relation (3.2) on the trilinear coupling A_0. This initial input parameter will determine the properties of our sneutrino LSP at the low scale. For $A_0 \lesssim 0$, this mass splitting will favour a lower mass CP-even sneutrino and hence LSP, while for $A_0 \gtrsim 0$ we find CP-odd LSPs. The exact details are discussed previously, in Section 3.2, but one finds this general trend, as seen in Fig. 3.3.

Now, we turn to how the lightest $(B-L)$ Higgs is affected by the trilinear coupling,

$$M_{h'} = \frac{1}{2}\Big[(m_{A'}^2 + M_{Z'}^2) - \sqrt{(m_{A'}^2 + M_{Z'}^2)^2 - 4m_{A'}^2 M_{Z'}^2 \cos^2 2\beta'}\,\Big], \tag{3.6}$$

where $m_{A'}^2$ is the mass of the $(B-L)$ CP-odd Higgs,

$$m_{A'} = \frac{2B_{\mu'}}{\sin 2\beta'}, \tag{3.7}$$

and $B_{\mu'}$ is determined by the $B-L$ minimisation condition,

$$B_{\mu'} = \frac{1}{4}\left[-2g_{BL}^2 v'^2 \cos 2\beta' + 2m_{\chi_1}^2 - 2m_{\chi_2}^2 + \tilde{g} g_{BL} v^2 \cos 2\beta\right] \tan 2\beta'. \tag{3.8}$$

At low scale, $m_{\chi_{1,2}}^2$ depends on A_0 (due to the RGE running from GUT scale to EW scale). This directly affects $B_{\mu'}$ and also $\tan\beta'$ and hence induces an A_0 dependence on $m_{A'}$ and also $M_{h'}$. Fig. 3.3 displays this relation and we see that, for large positive A_0 values, a wide range of $M_{h'}$ masses are allowed ($\sim 100 - 2000$ GeV) whereas, for $A_0 \lesssim 0$, lower $M_{h'}$ values are favoured, with the largest density of points over the interval $\sim 100 - 500$ GeV.

Combining this trend with larger mass scales for CP-even sneutrinos, as seen in Fig. 3.1, provides us with two general cases based on the GUT parameters. Firstly, A_0 is negative, the sneutrino LSP is CP-even, with $m_{\tilde{\nu}} \gtrsim 500$ GeV and $M_{h'} \lesssim 500$ GeV, hence, in general, $m_{\tilde{\nu}} > M_{h'}$. The other possibility is that A_0 is positive, here, the sneutrino LSP is CP-odd and both masses are similar, $100 \lesssim m_{\tilde{\nu}}, M_{h'} \lesssim 2000$ GeV. Further, there are cases where $m_{\tilde{\nu}}$ is larger and also $M_{h'}$ is larger. This behaviour is reflected in Fig. 3.4, where the histogram counts the number of spectrum points where the annihilation channels $h'h'$, W^-W^+ or something else have the largest cross section of annihilation. The different spectrum points are coloured according to the value of their normalised annihilation cross section for a particular channel (e.g., $\sigma(\tilde{\nu}\tilde{\nu} \to h'h')/\sigma(\tilde{\nu}\tilde{\nu} \to X)$, for any combination of particles X). As mentioned, the CP-even case has many more parameter points with $m_{\tilde{\nu}} > M_{h'}$, hence a larger number of our spectra have the largest annihilation into $h'h'$. The CP-odd case has a larger number of points in our parameter

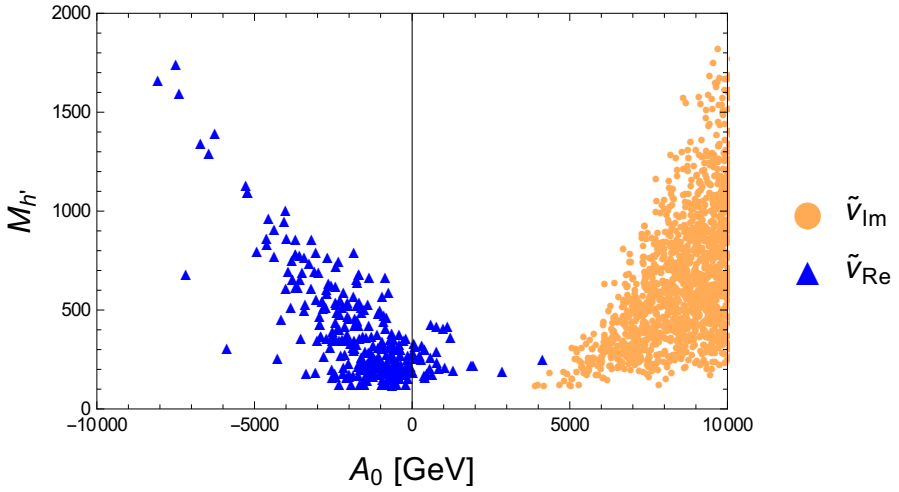

Figure 3.3: Mass of lightest $(B-L)$-like Higgs versus the GUT parameter A_0, for CP-even sneutrino LSPs (red) and CP-odd sneutrino LSPs (blue).

space with the largest cross section of annihilation into W^+W^-. A particular point in parameter space will have a specified cross section into W^+W^-, which will strongly affect the ability to detect that scenario via indirect detection, as we detail in the next section. If nature realises a given point in parameter space, it may be the case that this is detectable via indirect detection methods in the near future as we detail next section.

However, further to this we may make comments regarding the parameter space as a whole. Firstly, we see general differences between the CP-even and CP-odd scenarios, which are directly a consequence of the initial GUT conditions, especially the value of the trilinear coupling A_0; for which we choose a wide range of positive and negative values (-15TeV$< A_0 <$15 TeV). Choosing this positive and scanning over our parameter space (detailed in section 3.2), one will find the majority of the sneutrino-LSP points will be CP-odd and for many of these, where $m_{\tilde{\nu}} < M_{h'}$, they will annihilate most strongly into W^+W^-, which can lead to a detectable signal. So one may make the point that positive A_0 values will generally lead to larger direct detection signals. We emphasise here, though, that we are not saying a particular scenario is more likely realised in nature, but rather one may observe interesting features of our choice of parameter space.

These annihilation cross sections will be what determine the relic abundance of the sneutrinos. In this work we consider a standard cosmological scenario, where the DM particles were in thermal equilibrium with the SM ones in the early Universe and decoupled when the temperature fell below their relativistic energy. The relic density of our sneutrino species is written as [105]:

$$\Omega h^2_{\tilde{\nu}_1^{\mathrm{R,I}}} = \frac{2.1\times 10^{-27}\mathrm{cm}^3\mathrm{s}^{-1}}{\langle \sigma^{\mathrm{ann}}_{\tilde{\nu}_1^{\mathrm{R,I}}} v\rangle}\left(\frac{x_F}{20}\right)\left(\frac{100}{g_*(T_F)}\right)^{\frac{1}{2}}, \tag{3.9}$$

where $\langle \sigma^{\mathrm{ann}}_{\tilde{\nu}_1^{\mathrm{R,I}}} v\rangle$ is a thermal average for the total cross section of annihilation to SM objects multiplied by the relative sneutrino velocity, T_F is the freeze out temperature, $x_F \equiv m_{\tilde{\nu}_1^{\mathrm{R,I}}}/T_F \simeq$

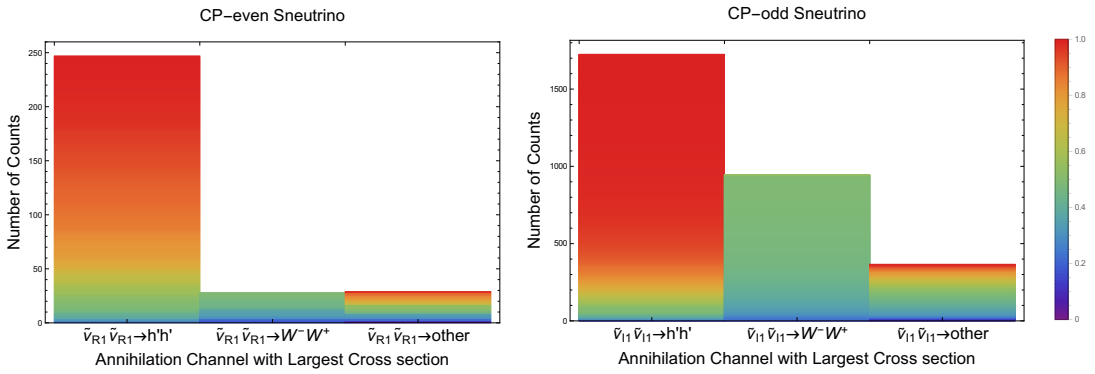

Figure 3.4: Histogram counting the number of spectrum points with the largest annihilation cross section being in either the $h'h'$, W^+W^- or other channel. This has been done for spectrum points which have a CP-odd (left) or CP-even (right) sneutrino LSP. Each count is also coloured by the normalised cross section (so that the sum of annihilation cross section channels for a given point is unity), where a red coloured point means the given annihilation channel has a larger cross section.

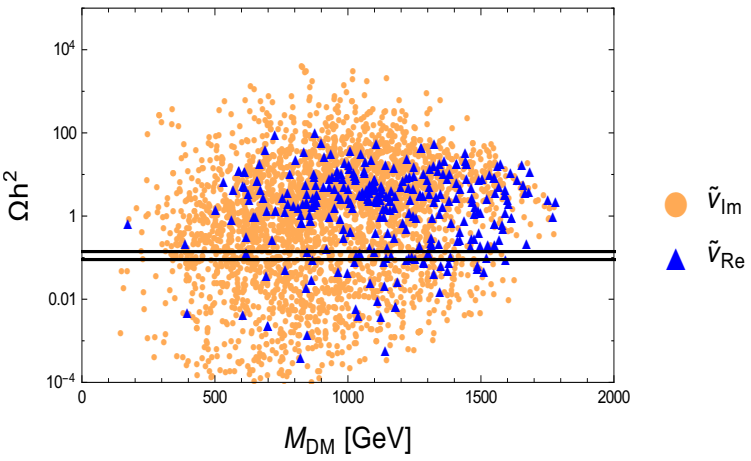

Figure 3.5: Relic density of CP-even and CP-odd sneutrinos versus their mass in GeV, where horizontal lines correspond to the Planck limits for the relic abundance.

$\mathcal{O}(20)$ and $g_*(T_F) \simeq \mathcal{O}(100)$ is the number of degrees of freedom at freeze-out.

Fig. 3.5 shows the thermal relic abundance for sneutrinos. This has been computed by micrOMEGAs [69, 70] and one can see that both CP-even and CP-odd candidates are allowed by current limits of $0.09 < \Omega h^2 < 0.14$, which is the 2σ allowed region by the Planck collaboration [22]. These points also satisfy the HB/HS [65, 67] constraints (that the lightest CP-even Higgs must be SM-like and subject to negative Higgs searches), in addition to SUSY mass bounds for gluinos, staus, neutralinos, charginos and stops [104].

3.4 Indirect Detection

When the sneutrino contribute to the observed or a part of DM abundance, its annihilation to SM particles produces an energetic spectrum of SM particles which has chances of being measured in DM indirect detection experiments. In this section, we will focus on the photon spectrum, produced as secondaries when sneutrino DM annihilates to SM final states. We will analyse the impact of FermiLAT searches from dwarf spheroidal galaxies (dSphs) and the galactic center in order to constrain and understand the future potential to explore sneutrino DM. The annihilation of sneutrinos in astrophysical objects with DM density $\rho_{\rm DM}$ yields a $\gamma-$ray flux which is given by

$$\frac{d\Phi}{dE_\gamma} = \left(\frac{1}{4\pi}\frac{\langle\sigma v\rangle}{2m_{\rm DM}^2}\frac{dN_\gamma}{dE_\gamma}\right) \times \left(\int_{\Delta\Omega}\int_{l.o.s.} \rho_{\rm DM}^2\, dl d\Omega'\right), \tag{3.10}$$

where it is possible to separate a particle-dependent part, as the cross section $\langle\sigma v\rangle$ and the differential distribution dN_γ/dE_γ, from the astrophysical term involving the integration of $\rho_{\rm DM}$ over the line-of-sight (l.o.s) and the solid angle $\Delta\Omega$. The differential distribution dN_γ/dE_γ is the photon energy spectrum per annihilation. In our scenario we will focus on the W^+W^- channel, which yields photons primarily through the decay of charged and neutral pions produced from hadronization, but also from decays to charged fermions which propagate and emit photons from inverse Compton scattering. This shape will be derived in our work by micrOMEGAs, but in general this distribution takes the form [106]

$$\frac{dN_\gamma}{dx} = \frac{m_{\rm DM} dN_\gamma}{dE_\gamma}\frac{a}{x^{1.5}}e^{-bx}, \tag{3.11}$$

where $x = E_\gamma/m_{\rm DM}$, and in ref. [106] the coefficients $a = 0.73$, $b = 7.8$ are calculated by matching the coefficients to a continuum spectrum result calculated through PYTHIA [107].

The last term, dubbed J-factor, depends on the particular $\gamma-$ray source where the DM annihilation takes place. The FermiLAT experiment has searched for $\gamma-$rays production with a sensitivity in the energy range from 20 MeV to $\sim$ 300 GeV. Now, dSphs of the Milky Way, which are expected to have a sizable DM content, have a J-factor of 10^{19} GeV^2 cm^{-5} and a small non-thermal $\gamma-$ray background. These features make their observation particularly suitable in constraining $\langle\sigma v\rangle$ and we challenge the BLSSM sneutrino predicition against the bounds coming from 6 years of observation over 15 dSphs [108]. Consistently with the result of the previous section that, by far, the main *charged* annihilation channel is represented by W^+W^-, we have checked that also the biggest constraint is provided in the same channel[3]. In Fig. 3.6, we plot the sneutrino annihilation cross section in the W^+W^- channel. We denote the two populations of sneutrino DM candidates namely, CP-odd and CP-even, with two different colours and compare the thermal cross section prediction with the existing bounds form dSphs (solid line). We also

[3]We notice that, when the DM candidate is not fully responsible for the measured relic density, the cross section has been rescaled by an appropriate factor as shown in [98].

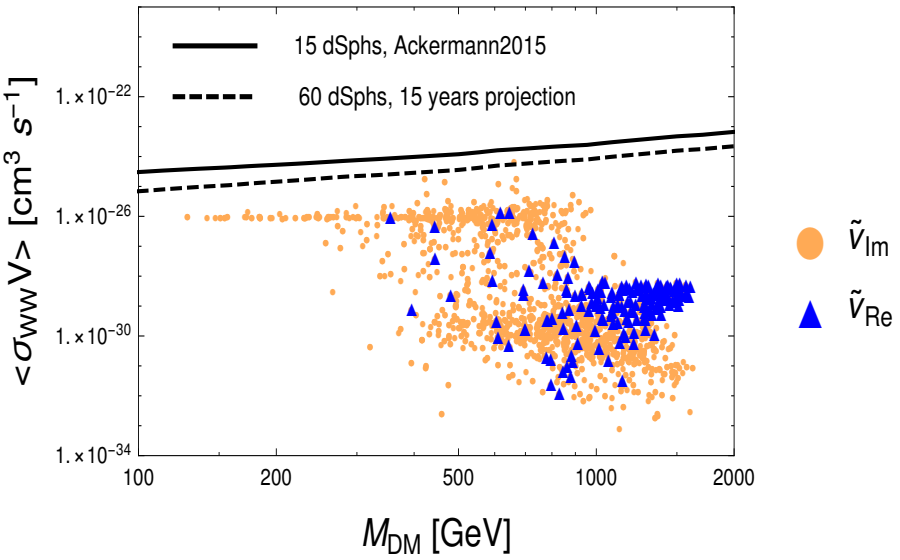

Figure 3.6: Thermal cross section for DM DM $\to W^+W^-$ annihilation as predicted by theory as a function of the DM mass, for CP-even (blue) and CP-odd (orange) sneutrinos. Also shown are the FermiLAT limit from dSphs at present (solid black) and as projection for 15 years from now (dashed black). All points obey the relic density upper limit, for which rescaling, where necessary, has been applied.

show the projection from 15 years of observation of 60 dSphs sample. While some CP-odd sneutrino candidates can be tested with future FermiLAT searches, the constraining power for CP-even candidates is far weaker. Most of the parameter space of this model though remains safely allowed from existing and also future searches. It is imperative to note that the constraining power of FermiLAT for sneutrino DM is weaker in our scenarios because of underabundant DM component. Moreover, our scan reveals the existence of a section of the GUT-constrained parameter space amenable to investigation in future searches, here represented by the single point above the dashed line. Finally, we see a line of points with a similar cross section of $\sim 10^{-26}$ cm^3 s^{-1} which can be explained as follows. When the sneutrino mass is larger then the $B-L$ Higgs mass, $m_{\tilde{\nu}} > m_{h_2}$, the sneutrinos will largely decay into two $B-L$ Higgses preferentially via the four point coupling in eq. 3.5. Otherwise they will decay via h_i mostly into either $h_i h_j$ or WW. Since the sneutrinos couple most strongly to the $B-L$ Higgs, usually the h_2 is the mediator, and the mixing into two SM-like Higgses is small, as a direct coupling is forbidden in the superpotential. It is then the mixed, gauge coupling h_2WW which becomes strongest and so light sneutrinos will largely annihilate into WW, whereas when $m_{\tilde{\nu}} > h_2$, they will preferably annihilate to h_2h_2, and so σ_{WW} is small. The reason for such a compressed line is then due to the logarithmic nature of the plot, where small differences in the couplings appear suppressed compared to the 10 orders of magnitude which the figure spans.

In a second attempt to confront our model with the FermiLAT observations, we turn to the galactic center and compute the differential γ-ray flux due to snuetrino annihilation at the center of the Milky Way. The differential distributions for the gamma spectrum as computed in (3.10)

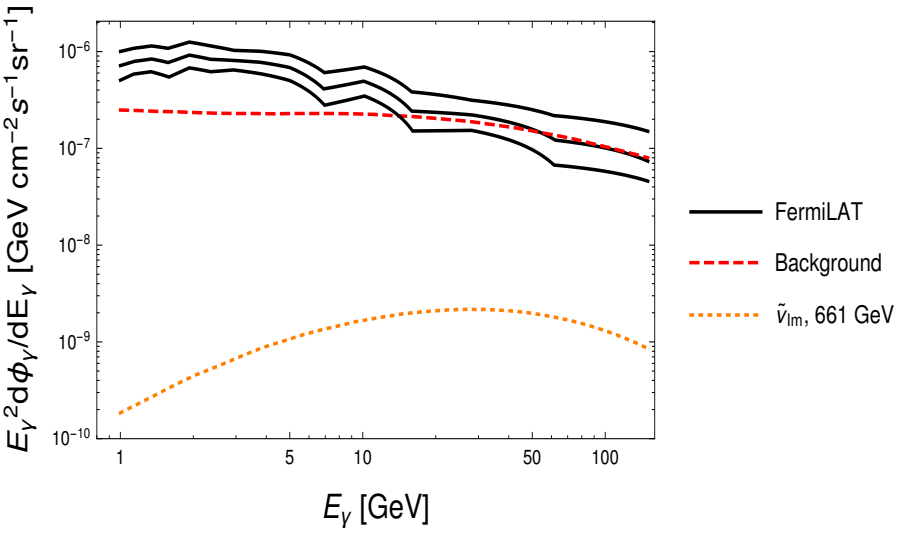

Figure 3.7: Differential flux of γ-ray secondary radiation induced by DM DM $\to W^+W^-$ annihilation as a function of the photon energy, with fixed DM mass, for our benchmark CP-odd sneutrino (orange). The corresponding distribution for the background is also given (red). The FermiLAT present data (with error) are in black. The sneutrino point considered is compliant with the relic density constraint taken as an upper limit.

is itself also a subject of dedicated analyses and experimental searches based on FermiLAT data. The flux detected has therefore two components, of signal (SIG) and background (BG),

$$\frac{d\Phi_\gamma}{dE_\gamma} = \frac{d\Phi_\gamma^{\rm BG}}{dE_\gamma} + \frac{d\Phi_\gamma^{\rm SIG}}{dE_\gamma} \tag{3.12}$$

and we computed the signal flux ($d\Phi_\gamma^{\rm SIG}/dE_\gamma$) for the case of the sneutrino corresponding to the largest annihilation cross section in our scan. We notice, as shown in Fig. 3.7, how for our benchmark point of mass of 661 GeV and $\langle\sigma_{WW}\rangle \simeq 7\times10^{-25}$ cm^3 s^{-1} the signal is far below the large background (given by $\frac{d\Phi_\gamma^{\rm BG}}{dE_\gamma}$). Hence, our prediction for FermiLAT is that to a possible detection of a signal in the integrated flux measurement it would not correspond a γ-ray spectrum significantly distorted from the background shape, at least not in the current experimental run. However, as the FermiLAT data sample will increase, more and more of the spectrum will be accessible at larger energies, where a characteristic signal shape may eventually emerge.

When this will happen, it will be interesting to understand whether such a shape may enable one to distinguish between a fermionic DM hypothesis and a CP-even or -odd one (and possibly between the latter two). With this in mind, we compare the shape of the differential γ-ray flux from CP-even, CP-odd sneutrino and neutralino DM candidates in Fig. 3.8. Here, we plot the normalised flux distribution allowing us to make comparison between the three candidates independently of the size of their annihilation cross sections and relic density. The three chosen points have very similar mass, hence also determining similar end points in the spectrum. While the CP-even and CP-odd sneutrinos have a very similar shape, the neutralino one is very different,

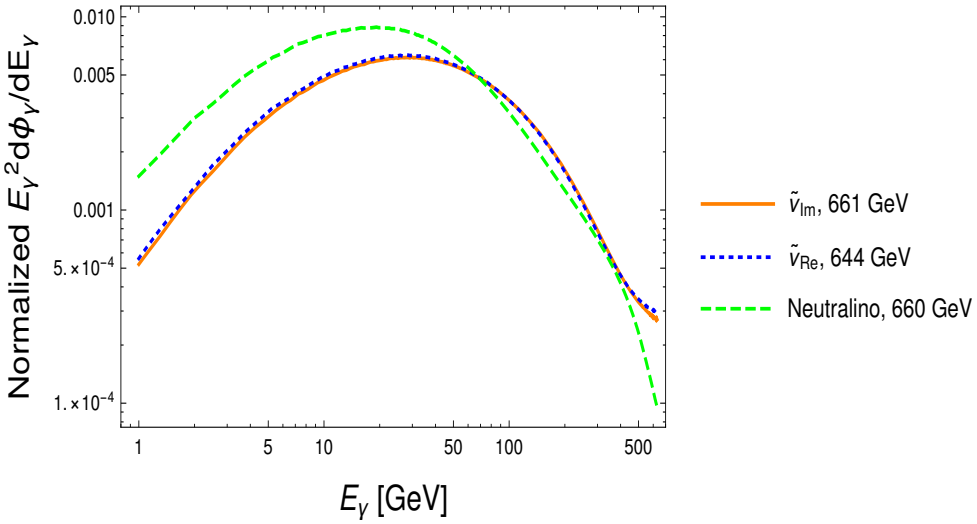

Figure 3.8: Differential flux of γ-ray secondary radiation induced by DM DM $\to W^+W^-$ scatterings as a function of the photon energy, with fixed DM mass, for our benchmark CP-even (blue) and CP-odd (orange) sneutrinos. The corresponding distribution for a neutralino is also given for comparison (green). Normalisation is the same for all curves.

this result allowing us to speculate on the possibility of extracting the DM spin via indirect detection experiments. It should however be noted that a more complete analysis, taking into account various theoretical and experimental uncertainties, must be carried out in order to make a more concrete statement in this direction. Nonetheless, we find this result to be important, as it may actually be testable via data expected to be collected in the years to come.

3.5 LHC Signatures

In this section we discuss the possibility of characterising the sneutrino DM at the LHC by qualitatively describing some of the most interesting signatures provided by the BLSSM.

Since the LSP sneutrino is mostly RH, it carries no $SU(2)_L$ quantum numbers and hence may only interact with the MSSM-like states via mixing with the LH sneutrinos. This is highly suppressed, being proportional to the very small Dirac Yukawa coupling for the LH neutrinos. As such, searches in the neutral or charged DY processes, mediated respectively by the SM Z and $W^\pm$ gauge bosons, are hopeless. In contrast, the largest couplings of the RH sneutrinos are with the typical $(B-L)$ degrees of freedom, among the others, the Z' and heavy bi-leptonic scalars. In particular, as required by CP conservation, the Z' couples to $\tilde{\nu}^{\rm R}$ (CP-even) and $\tilde{\nu}^{\rm I}$ (CP-odd), where one of the two is the LSP and the other can be the Next-to-LSP (NLSP), while the heavy CP-even Higgses can couple to two LSPs. Hence, for the case of *direct* DM production at the LHC, one can attempt relying upon $pp \to Z' \to \tilde{\nu}_{\rm LSP}\tilde{\nu}_{\rm NLSP}$, with the decay of the NLSP to the LSP via $\tilde{\nu}_{\rm NSLP} \to \tilde{\nu}_{LSP}Z^{(*)}$ providing a di-lepton (plus missing transverse energy) signature through a SM Z boson decay, unlike the heavy Higgs mediated process, which, since the final

state is made up by LSP pairs, is invisible and can only be accessed through mono-jet, -photon, etc. searches. In searching for these direct DM signals, we have scanned over several benchmark CP-even and CP-odd sneutrino LSPs and used MadGraph [109] for the computation of the LHC cross sections. In detail, we have computed the inclusive cross section for $pp \to \tilde{\nu}_1^{\rm I}\tilde{\nu}_i^{\rm R}$, where $\tilde{\nu}_1^{\rm I}$ is the LSP and allowed for the production of any other CP-even sneutrinos ($i = 1, \ldots, 6$) alongside it. We also have explored the $pp \to \tilde{\nu}_1^{\rm R}\tilde{\nu}_i^{\rm I}$ channel in which the LSP is represented by the CP-even component of the lightest sneutrino. These cross sections are totally dominated by the s-channel exchange of a Z', i.e., $pp \to Z' \to \tilde{\nu}_1^{\rm I}\tilde{\nu}_i^{\rm R}, \tilde{\nu}_1^{\rm R}\tilde{\nu}_i^{\rm I}$, and found to be $\sigma \simeq 0.025$ fb at most for both the CP charges of the LSP. It is unsurprising that this cross section is so small, as we are forced to have a heavy Z' to comply with current LHC search limits ($M_{Z'} \gtrsim 4$ TeV). As this cross section is so small, it would be difficult to observe any signal here without a much higher luminosity than at present.

Another intriguing possibility to search for LSP states though is to do so *indirectly*, e.g., via slepton $\tilde{l}$ pair production. The corresponding cross section may lay in the ~ 0.1 fb range. When the slepton mass is light enough, the $\tilde{l} \to W^{\pm}\tilde{\nu}_{\rm LSP}$ channel is the only available decay mode despite its width being suppressed by the smallness of the Dirac Yukawa coupling, yiedling a di-lepton signature. Alternatively, if kinematically allowed, one can have $\tilde{l} \to \tilde{\chi}^0 l$ with $\tilde{\chi}^0 \to \nu_h\tilde{\nu}_{\rm LSP}$, where ν_h is the heavy neutrino. The latter will mainly undergo $\nu_h \to W^{\pm}l^{\mp}$ or $\nu_h \to Z\nu_l$ decay, thus providing fully or semi-leptonic signatures (again, accompanied by missing transverse energy). Other interesting DM signatures may arise from squark pair production for which the cross sections can reach several fb's. In this case, e.g., one can exploit the decay chain $\tilde{t} \to \tilde{\chi}^0 t$, which can occur with a BR $\sim 80\%$ if the $\tilde{t}$ is the lightest squark, where $\tilde{\chi}^0 \to \nu_h\tilde{\nu}_{\rm LSP}$, as discussed above. Here, one would have a variety of jet plus multi-lepton final states recoiling against missing transverse energy.

3.6 Chapter Summary

The BLSSM provides a preferential DM candidate which is notably different from the MSSM neutralino. The former is a spin-0 boson (specifically, a CP-even or CP-odd sneutrino) and the latter a spin-1/2 fermion (specifically, a neutralino). While in a previous chapter we had assessed that sneutrino DM affords the BLSSM with an amount of parameter space comparatively much larger than the one of the MSSM offering neutralino DM, both compliant with WMAP/Planck and LUX constraints, here, we have shown that signals of sneutrino DM are, on the one hand, just below the current sensitivity of FermiLAT and, on the other hand, within reach of it in the next 15 years of foreseen data taking, unlike the neutralino case. Furthermore, we have illustrated that, once a DM signal is established by such an experiment as an excess in the integrated photon flux for some DM mass, there exists scope in establishing the (pseudo)scalar nature of sneutrino DM by studying the differential photon flux in energy, as its shape is notably different from the one pertaining to (fermionic) neutralino DM. However, there exists no possibility in this experiment to separate with differential data the CP-even from the CP-odd sneutrino hypothesis,

although their integrated rates are significantly different, with a predominance of relic CP-odd states over CP-even ones. This phenomenology is enabled by the fact that one of the dominant DM annihilation channels in the case of the BLSSM has charged particles in the final state, notably $W^{\pm}$ boson pairs, as already noted in such a previous publication of ours. In fact, it is the copious γ-ray emission from the charged gauge boson pair that puts FermiLAT in the position of exploring signals of sneutrino DM, unlike the MSSM, wherein the annihilation channel of neutralino DM into $W^{\pm}$ pairs is negligible. Intriguingly, the favourite BLSSM candidate for DM is also potentially accessible at the LHC over the same time scale, 15 years or so. In fact, Run 2 and 3 data from the CERN machine may be able access a series of signatures, involving multi-lepton final states, with and without jets, alongside the expected missing transverse energy. In fact, also customary mono-jet, -photon, etc. searches may eventually develop sensitivity to the BLSSM candidate for DM.

Altogether, we should like to conclude by mentioning that the DM sector of the BLSSM has very distinctive features with respect to those specific to the prevalent SUSY description, i.e., the MSSM, that can be eventually established in both DM indirect detection experiments and at the LHC. In constrast, we do not expect (nor we have investigated here) the possibility of differences in case of DM direct searches, as potential BLSSM mediators, a Z' or additional heavy Higgs states, are either too heavy or too weakly coupled to nuclear constituents, respectively, to play any significant role. We therefore advocate more thorough investigations of DM phenomenology in this non-minimal SUSY scenario, which is beyond the scope of this chapter.

Chapter 4

Hints of Unification at the LHC

Having now studied carefully some of the phenomenological consequences of the BLSSM, in this chapter we look at an aspect not carefully studied previously: distinguishing models with similar signatures at the LHC. Both in the non-SUSY and SUSY version of the BLSSM, one of the strongest signals one might see first is from the Z' in breaking the $U(1)_{B-L}$. As mentioned previously, there is a difference between the model of $SO(10)$ broken to $SU(3)_C \times SU(2)_L \times U(1)_R \times U(1)_{B-L}$ and the usual $SU(3)_C \times SU(2)_L \times U(1)_Y \times U(1)_{B-L}$. In this chapter, we explore these differences and attempt to discriminate the two scenarios at the LHC.

4.1 Introduction

$SO(10)$ GUTs are very attractive since they predict RH neutrinos and make neutrino mass inevitable. SUSY allows for a single step unification of the gauge couplings. Being a rank 5 gauge group, $SO(10)$ also naturally accommodates an additional Z' gauge boson, which may have a mass at the TeV scale within the range of the LHC. Such Z' models are attractive since, apart from the three RH neutrinos, they do not require any new exotic particles to make the theory anomaly free.

There are two main symmetry breaking patterns of $SO(10)$ leading to the SM gauge group. Firstly there is the $SU(5)$ embedding,

$$SO(10) \to SU(5) \times U(1)_\chi \to SU(3)_C \times SU(2)_L \times U(1)_Y \times U(1)_\chi, \tag{4.1}$$

where the $U(1)_\chi$ is broken at the TeV scale, yielding a massive Z'_χ. For recent examples of models based on such a Z'_χ, see e.g. [110].

Secondly there is the PS gauge group embedding,

$$SO(10) \to SU(4)_{PS} \times SU(2)_L \times SU(2)_R \tag{4.2}$$

The PS colour group $SU(4)_{PS}$ may be broken to $SU(3)_C \times U(1)_{B-L}$, leading to the left-right symmetric model gauge group. The $SU(2)_R$ group may be broken to the gauge group $U(1)_R$

associated with the diagonal generator T_{3R}. It is thus possible to break $SO(10)$ in a single step at the GUT scale without reducing the rank,

$$SO(10) \to SU(3)_C \times SU(2)_L \times U(1)_R \times U(1)_{B-L} \tag{4.3}$$

The resulting gauge group in Eq.4.3 does not predict any new charged currents and is not very tightly constrained phenomenologically. It may therefore survive down to the TeV scale before being broken to the SM gauge group, leading to the prediction of a massive Z'_{BLR}, accessible to the LHC.

In this chapter we shall focus on $SO(10)$ broken at the GUT scale in a single step, as in Eq.4.3. In order to allow for gauge coupling unification we shall assume SUSY which is broken close to the TeV scale, but at a high enough scale to enable the superpartners to have evaded detection at the LHC. We shall be interested in the Z'_{BLR} which emerges when the Abelian subgroup $U(1)_R \times U(1)_{B-L}$ is broken down to the SM hypercharge gauge group $U(1)_Y$ near the TeV scale (for brevity we refer to this scenario as the BLR model). We study the discovery prospects of such a Z'_{BLR} at the LHC, its possible decay mode into Higgs bosons, and the expected forward-backward asymmetry, comparing the predictions to the well studied $B-L$ model based on $U(1)_Y \times U(1)_{B-L}$ [35, 36, 40, 100, 111]. We comment on the $U(1)_Y \times U(1)_\chi$ model [112, 113] below.

The Abelian gauge group $U(1)_R \times U(1)_{B-L}$ has quite a long history in the literature as reviewed in [113, 114]. It was recently realised that SUSY $SO(10)$ models which break down to this gauge group may allow for a new type of seesaw model, namely the linear seesaw model [115, 116]. Subsequently, the phenomenology of the SUSY $U(1)_R \times U(1)_{B-L}$ model has been studied in a number of works [43, 117–122]. Indeed it has been demonstrated that the Abelian BLR gauge group $U(1)_R \times U(1)_{B-L}$ is equivalent to $U(1)_Y \times U(1)_\chi$ (arising from the breaking chain in Eq.4.1) by a basis transformation and furthermore that this equivalence is preserved under RGE running, when kinetic mixing is consistently taken into account [122]. Therefore the physics of the TeV scale Z'_{BLR} considered here should be identical to that of the Z'_χ [122].

We emphasise that there are several new aspects of our study including: the statistical significance of producing a Z'_{BLR} at the LHC including finite width and interference effects (the LHC uses a narrow width approximation); the study of Higgs final states in the $U(1)_{B-L} \times U(1)_R$ model; and the study of forward-backward asymmetry at the High-Luminosity (HL) LHC as a discriminator between the $U(1)_R \times U(1)_{B-L}$ model (or equivalently the $U(1)_Y \times U(1)_\chi$ model) and the usual Z'_{BL} based on $U(1)_Y \times U(1)_{B-L}$, i.e. the commonly studied $B-L$ model [35, 36, 40, 100, 111].

4.2 Model

We shall not consider the high energy $SO(10)$ breaking here, so the starting point of the considered model is to assume that, below the GUT scale, we have the gauge group as on the RH side of

Eq.4.3, namely,

$$SU(3)_C \times SU(2)_L \times U(1)_R \times U(1)_{B-L} \tag{4.4}$$

Note that in this basis the hypercharge gauge group $U(1)_Y$ of the SM is not explicitly present, instead it is "unified" into $U(1)_R \times U(1)_{B-L}$. Note that, although the Abelian factors are equivalent to the $U(1)_Y \times U(1)_\chi$ model by a basis transformation, we shall work in the $U(1)_R \times U(1)_{B-L}$ basis. In order to allow gauge coupling unification we need SUSY, but we shall assume it is broken above the Z'_{BLR} mass scale so that SUSY particles are not present in the decays of the Z'_{BLR}. Note that such SUSY decays have been considered extensively in [43, 117–122].

At the Z'_{BLR} mass scale (typically a few TeV), hypercharge emerges from the breaking,

$$U(1)_R \times U(1)_{B-L} \to U(1)_Y \tag{4.5}$$

where the hypercharge generator is identified as

$$Y = T_{3R} + T_{B-L}, \tag{4.6}$$

where

$$T_{B-L} = (B - L)/2. \tag{4.7}$$

The symmetry breaking in Eq.4.5 requires two Higgs superfields $\chi_{1,2}$ whose scalar components develop Vacuum Expectation Values (VEVs) which carry non-zero T_{3R} and opposite T_{B-L} so that they are neutral under hypercharge. If they arise from an $SU(2)_R$ doublet then this fixes their charges to be $T_{3R} = \pm 1/2$ and hence $T_{B-L} = \mp 1/2$. Two of them with opposite quantum numbers are required by SUSY to cancel anomalies (and for holomorphicity). They must be singlets under both $SU(3)_C$ and $SU(2)_L$ in order to preserve these gauge groups.

Finally, at the EW scale we have the usual SM breaking

$$SU(2)_L \times U(1)_Y \to U(1)_Q, \tag{4.8}$$

where the electric charge generator is identified as

$$Q = T_{3L} + Y. \tag{4.9}$$

As in usual SUSY models, the EW symmetry breaking is accomplished by two Higgs doublets $H_{u,d}$ of $SU(2)_L$ which have $B - L = 0$. If the two Higgs doublets of $SU(2)_L$ were embedded into a single $SU(2)_R$ doublet, then we expect that $H_{u,d}$ will have $T_{3R} = \pm 1/2$, respectively. In addition, in order to accomplish neutrino masses via the linear seesaw model, we need to add three complete singlet superfields S, as discussed in the appendix C. The particle content of the model (henceforth denoted as BLR) is then summarised in Tab. 4.1.

Particle	T_{3L}	T_{3R}	T_{B-L}	T_χ	$Y = T_{3R} + T_{B-L}$	$Q = T_{3L} + Y$
$\begin{pmatrix} u \\ d \end{pmatrix}_L$	+1/2	0	+1/6	+1/4	+1/6	+2/3
	-1/2	0	+1/6	+1/4	+1/6	-1/3
u_R	0	+1/2	+1/6	-1/4	+2/3	+2/3
d_R	0	-1/2	+1/6	+3/4	-1/3	-1/3
$\begin{pmatrix} \nu_e \\ e^- \end{pmatrix}_L$	+1/2	0	-1/2	-3/4	-1/2	0
	-1/2	0	-1/2	-3/4	-1/2	-1
ν_R	0	+1/2	-1/2	-5/4	0	0
e_R	0	-1/2	-1/2	-1/4	-1	-1
χ_R^1	0	-1/2	+1/2	+5/4	0	0
χ_R^2	0	+1/2	-1/2	-5/4	0	0
S	0	0	0	0	0	0
$H \begin{cases} H_u = \begin{pmatrix} \phi_u^+ \\ \phi_u^0 \end{pmatrix}_L \\ H_d = \begin{pmatrix} \phi_d^0 \\ \phi_d^- \end{pmatrix}_L \end{cases}$	+1/2	+1/2	0	-1/2	+1/2	+1
	-1/2	+1/2	0	-1/2	+1/2	0
	+1/2	-1/2	0	+1/2	-1/2	0
	-1/2	-1/2	0	+1/2	-1/2	-1

Table 4.1: The particle content and generators of the $SU(3)_C \times SU(2)_L \times U(1)_R \times U(1)_{B-L}$ model.

4.3 Z' Couplings to Fermions

In this work, numerically, we use the SARAH program [59] to determine the vector and axial couplings of the fermions with the Z'_{BLR}. This includes the full impact of GKM as done in [119, 122]. Considering this effect in full leads to $\sim \mathcal{O}(1)\%$ differences in vector and axial couplings. In this section, for simplicity, we neglect the impact of GKM but stress that all implications are considered in our final results.

We begin by examining the low energy breaking of the gauge group in Eq.4.5. The coupling of a fermion f to the $U(1)_R$ and $U(1)_{B-L}$ fields are obtained from

$$-\mathcal{L}_{\rm BLR} = \bar{f}\gamma^\mu \left(g_R T_{3R} W^3_{\mu R} + g_{BL} T_{B-L} B^{BL}_\mu\right) f, \tag{4.10}$$

where $T_{B-L} = \frac{B-L}{2}$.

After symmetry breaking, these two fields will mix to become the SM massless hypercharge gauge boson, B_μ, and a massive Z'_μ (corresponding to the Z'_{BLR}),

$$\begin{pmatrix} B^{BL}_\mu \\ W^3_{\mu R} \end{pmatrix} = \begin{pmatrix} \cos\theta_{BL} & -\sin\theta_{BL} \\ \sin\theta_{BL} & \cos\theta_{BL} \end{pmatrix} \begin{pmatrix} B_\mu \\ Z'_\mu \end{pmatrix}. \tag{4.11}$$

So, the Z'_{BLR} has the following coupling to fermions:

$$-\mathcal{L}^{Z'}_{\rm BLR} = Z'_\mu \bar{f}\gamma^\mu \left(g_R \cos\theta_{BL} T_{3R} - g_{BL} \sin\theta_{BL} T_{B-L}\right) f. \tag{4.12}$$

Since

$$g_R \sin\theta_{BL} = g_{BL} \cos\theta_{BL} = g_Y, \tag{4.13}$$

we may rewrite the Z' couplings of the BLR model in a more compact form,

$$\begin{aligned} -\mathcal{L}^{Z'}_{\rm BLR} &= Z'_\mu \bar{f}\gamma^\mu g_Y Q_{LR} f, \\ Q_{LR} &\equiv \left(\cot\theta_{BL} T_{3R} - \tan\theta_{BL} T_{B-L}\right), \quad \tan\theta_{BL} = g_{BL}/g_R. \end{aligned} \tag{4.14}$$

We shall be interested in comparing the Z' couplings in the BLR model above to those in related models where the SM gauge group (including hypercharge) is augmented by an Abelian gauge group $U(1)'$, identified with the generator T_{BL}, resulting in the Z' couplings

$$-\mathcal{L}^{Z'}_{BL} = Z'_\mu \bar{f}\gamma^\mu g_{BL} T_{B-L} f, \tag{4.15}$$

which may be compared to the BLR couplings in Eq.4.14. We shall find to one-loop the non-GUT

Model	ϵ_L^u	ϵ_R^u	ϵ_L^d	ϵ_R^d	ϵ_L^e	ϵ_R^e	ϵ_L^ν	ϵ_R^ν
T_{3R}	0	1/2	0	−1/2	0	−1/2	0	1/2
T_{B-L}	1/6	1/6	1/6	1/6	−1/2	−1/2	−1/2	−1/2

Table 4.2: Chiral couplings for the $U(1)_R$ and $U(1)_{B-L}$ models.

Model	g_V^u	g_A^u	g_V^d	g_A^d	g_V^e	g_A^e	g_V^ν	g_A^ν
T_{3R}	1/2	−1/2	−1/2	1/2	−1/2	1/2	0	0
T_{B-L}	1/3	0	1/3	0	−1	0	−1/2	−1/2

Table 4.3: Vector and axial couplings for the $U(1)_R$ and $U(1)_{B-L}$ models. Note that we have integrated out the RH neutrinos[2] in calculating g_V^ν and g_A^ν.

normalised couplings (i.e., in the conventions of this section)[1]:

$$g_R = 0.448, \quad g_{BL} = 0.459. \tag{4.16}$$

In general the Z'_{BLR} couples to a fermion f which may be either left- or RH and the above couplings sum over both chiral components of all the fermions. For analysing the couplings of different models it is useful to decompose the couplings into either left-chiral or right-chiral components, leading to the vector and axial couplings in the BLR model as follows

$$-\mathcal{L}^{Z'}_{\rm BLR} = g_Y Z'_\mu \bar{f}\gamma^\mu(\epsilon_L^f P_L + \epsilon_R^f P_R)f = g_Y Z'_\mu \bar{f}\gamma^\mu \frac{1}{2}\left(g_V^f - g_A^f\gamma^5\right) f, \tag{4.17}$$

where $P_{R,L} = (1 \pm \gamma_5)/2$ and the vector/axial couplings are defined as $g_{V/A}^f = \epsilon_L^f \pm e_R^f$. Similar decompositions can be made for the Z' couplings of the other models in Eq.4.15. Tab. 4.2 shows the chiral couplings for the relevant generators T_R and $T_{B-L} = (B-L)/2$. Tab. 4.3 shows the vector and axial couplings obtained for the two different models.

4.4 Z' Couplings to Higgs Bosons

In this section we shall ignore the Z'_{BLR} decays into bosons arising from χ_R^1 and χ_R^2. The χ_R^1 and χ_R^2 bosonic sector contains four degrees of freedom, two scalars plus two pseudoscalars, where one of the pseudoscalars is eaten by the Z'_{BLR}, to leave two CP even scalars plus one CP odd pseudoscalar in the physical spectrum. If the soft SUSY breaking masses associated with χ_R^1

[1]Including GUT normalisation, $\sqrt{3/2}g_{BL} = 0.563$. We also find the mixed couplings, related to GKM, $g_{R,BL} \sim g_{BL,R} \sim 0.01$.

[2]In the linear seesaw, the heavy neutrino mass is approx $M_N \sim \tilde{F}v_R$, see Eq.C.1 in appendix A for the definition of $\tilde{F}$ while v_R is the BLR breaking scale. We will see that the mass of the Z' is approximately $M_{Z'} \sim \frac{1}{2}\sqrt{\left(\frac{3}{2}g_{B-L}^2 + g_R^2\right)}v_R$. We thus prevent heavy neutrino decays ($2M_N > M_{Z'}$) through the requirement that the free Yukawa coupling be large enough, $\tilde{F} > \sqrt{\left(\frac{3}{2}g_{B-L}^2 + g_R^2\right)} \sim 0.2$.

Vertex	$g_{Z'S_1S_2}$
$Z'h^0A^0$	$\frac{g_R \cos\theta_{B-L}\cos(\beta-\alpha)}{2}$
$Z'H^0A^0$	$\frac{-g_R \cos\theta_{B-L}\sin(\beta-\alpha)}{2}$
$Z'H^+H^-$	$-i\frac{g_R \cos\theta_{B-L}}{2}$

Table 4.4: The coupling of the BLR Z' to the physical 2HDM mass states. The Feynman rule for the vertex is given by $(g_{Z'S_1S_2})(p-p')_\mu$, where p, p' are the momenta of the two scalars towards the vertex.

and χ_R^2 are very large, then we would expect the physical CP odd pseudoscalar to become very heavy. Since the Z'_{BLR} must decay into a scalar plus a pseudoscalar (assuming that CP and angular momentum are conserved) then this would imply that none of the bosons arising from χ_R^1 and χ_R^2 would be kinematically accessible in Z'_{BLR} decays.

Under the above assumption of large soft masses for χ_R^1 and χ_R^2, we shall discuss the Z'_{BLR} coupling to the Higgs bosons arising from H_u and H_d only, which are assumed to have smaller soft masses. To investigate the Z' coupling to what is essentially a 2HDM sector, we begin with the Lagrangian term with the covariant derivative

$$\mathcal{L}_{Z',\text{scalars}} = (D_\mu\Phi_1)^\dagger(D_\mu\Phi_1) + (D_\mu\tilde{\Phi}_2)^\dagger(D_\mu\tilde{\Phi}_2) \tag{4.18}$$

with

$$D_\mu = \partial_\mu - i\frac{g_Y}{s_{BL}c_{BL}}(T_{3R} - s_{BL}^2\frac{Y}{2}), \tag{4.19}$$

where $\cos(\theta_{B-L}) \equiv c_{BL}$ and $\sin(\theta_{B-L}) \equiv s_{BL}$. Our two Higgs doublets are

$$\Phi_1 = \begin{pmatrix} \phi_1^+ \\ (v_1 + h_1 + ia_1)/\sqrt{2} \end{pmatrix}, \quad \tilde{\Phi}_2 = i\sigma_2\Phi_2^* = \begin{pmatrix} \phi_2^+ \\ (-v_2 - h_2 + ia_2)/\sqrt{2} \end{pmatrix} \tag{4.20}$$

and we rotate the fields to the physical basis as in the standard 2HDM procedure,

$$\Phi_1^R = \begin{pmatrix} G^+ \\ (h^0 s_{\beta\alpha} + H^0 c_{\beta\alpha} + v_{SM} + iG^0)/\sqrt{2} \end{pmatrix}, \quad \tilde{\Phi}_2^R = \begin{pmatrix} H^+ \\ (-h^0 c_{\beta\alpha} + H^0 s_{\beta\alpha} + iA^0)/\sqrt{2} \end{pmatrix}, \tag{4.21}$$

where we defined the standard 2HDM rotation angles $\cos(\alpha-\beta) \equiv c_{\alpha\beta}$ and $\sin(\alpha-\beta) \equiv s_{\alpha\beta}$. We extract the physical couplings for our Z'_{BLR} to the $h^0, H^0, H^\pm, A^0$ in Tab. 4.4.

We find the partial widths by using the general expression for a Z' decaying into two spinless

bosons of unequal masses M_1 and M_2, with coupling $g_{Z'S_1S_2}$ (read off from Tab. 4.4),

$$\Gamma(Z'_{BLR} \to S_1 S_2) = \frac{1}{48\pi}\frac{1}{M^3_{Z'}} g^2_{Z'S_1S_2}\left(M^4_{Z'} + M^4_1 + M^4_2 - 2\left(M^2_2 M^2_{Z'} + M^2_1 M^2_{Z'} + M^2_1 M^2_2\right)\right). \tag{4.22}$$

For a discussion of the Z'_{BL} coupling to the scalar sector in the $U(1)_{B-L}$ model see e.g. [43].

4.5 Renormalisation Group Equations

We now turn to the RGEs at one-loop. These RGEs will determine the $U(1)_R$ and $U(1)_{B-L}$ coupling constants and will also predict a value of the SM hypercharge coupling constant, given measured results of α_2 and α_3. We begin by using the SM β-function coefficients $b_2^{\rm SM} = -19/6$ and $b_3^{\rm SM} = -7$ for the $SU(2)_L$ and $SU(3)_c$ groups, respectively. We perform the running from M_Z up to our BLR breaking scale, which we denoted by v_R. From the scale $v_R < Q < v_{\rm SUSY}$, these two β-function coefficients are unchanged, as none of the additional BLR particle content has quantum numbers under these two groups. Then, at $v_{\rm SUSY} < Q < M_{\rm GUT}$, we introduce the SUSY partners and the β-function coefficients are modified to $b_2^{\rm SUSY} = +1$ and $b_3^{\rm SUSY} = -3$. These are the familiar MSSM β-function coefficients. The strong and weak coupling constants are run until they intersect, which determines $Q = M_{\rm GUT}$ and $\alpha_{\rm GUT} \equiv \alpha_2(M_{\rm GUT}) = \alpha_3(M_{\rm GUT})$. We now run our $U(1)_{B-L}$ and $U(1)_R$ coupling constants down from this GUT scale.

As we have two $U(1)$ groups, they undergo GKM. We begin with the β-function coefficients $b_{BL}^{\rm BLR,SUSY} = 27/4$, $b_R^{\rm BLR,SUSY} = 15/2$ and a mixed term $b_{R,B-L}^{\rm BLR,SUSY} = -\sqrt{3/8}$, including a GUT normalisation term of $3/8$ on the $U(1)_{B-L}$ and hence $\sqrt{3/8}$ on the $(U(1)_{B-L}\times U(1)_R)$ coefficient. Rotating the couplings into the upper triangular physical basis [58], and following the procedure of [123], we find the following β-functions for the GUT normalised couplings[3]

$$\frac{dg_R}{dt} = \frac{1}{(4\pi)^2}\frac{15 g_R^3}{2}, \tag{4.23}$$

$$\frac{d\tilde{g}}{dt} = \frac{1}{(4\pi)^2}\left[\left(\frac{27}{4}g^2_{BL} - \sqrt{\frac{3}{2}}g_{BL}\tilde{g} + \frac{15}{2}\tilde{g}^2\right)\tilde{g} + \left(-\sqrt{\frac{3}{2}}g_{BL} + 15\tilde{g}\right)g_R^2\right], \tag{4.24}$$

$$\frac{dg_{BL}}{dt} = \frac{1}{(4\pi)^2}\left(\frac{27}{4}g^2_{BL} - \sqrt{\frac{3}{2}}g_{BL}\tilde{g} + \frac{15}{2}\tilde{g}^2\right)g_{BL}. \tag{4.25}$$

At the GUT scale, we set $\tilde{g} = 0$ and allow it to run to non-zero values at low scale. Fig. 4.1 shows the running of the $U(1)_R$ and $U(1)_{B-L}$ groups both with (solid line) and without (dashed line) including the GKM procedure. One can see immediately that these two lines lie on top of one another, meaning the effect of the GKM is negligible. The α_R has an entirely negligible change and one can see a zoomed plot of the shift in the α_{BL} coefficient, which changes by $\mathcal{O}(0.1\%)$.

[3]The couplings in this section are GUT normalised, while those in earlier sections are the non-GUT normalised couplings We have chosen the same nomenclature for both normalisations, being careful to specify which normalisation we are using.

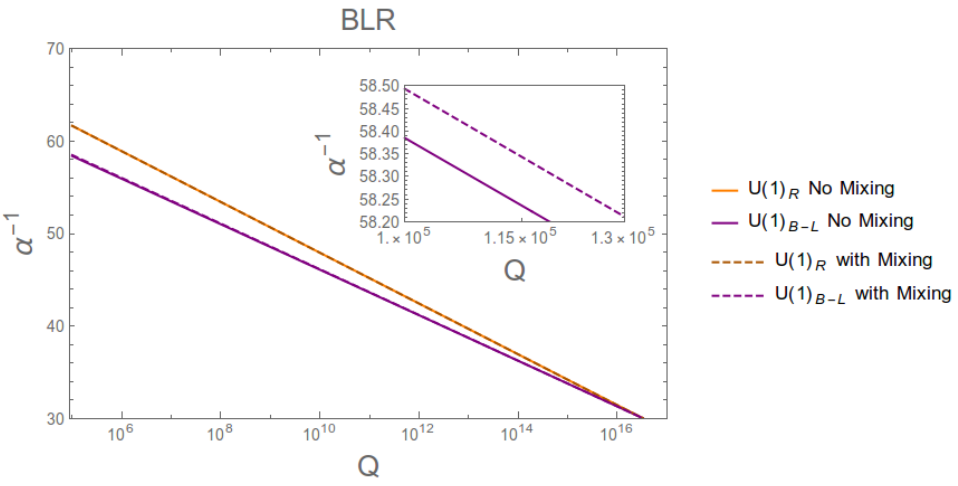

Figure 4.1: Comparison of RGE evolution with (solid lines) and without (dashed lines) gauge-kinetic mixing from GUT to SUSY scale. The $U(1)_R$ evolution is unchanged, whereas the $U(1)_{B-L}$ is modified slightly. A zoomed in plot of this modification is shown.

At the low (TeV) scale, one finds a negligible mixing coupling term $\tilde{g} \approx 10^{-2}$, nevertheless we include this correction in our numerical work.

We include GKM from the SUSY scale to the $U(1)_R \times U(1)_{B-L}$ breaking scale, v_R. From $v_R < Q < v_{\rm SUSY}$, decoupling the SUSY particles, the β-function coefficients change to $b_{BL}^{\rm BLR} = 17/4$, $b_R^{\rm BLR} = 13/3$ and a mixed term $b_{R,B-L}^{\rm BLR,SUSY} = b_{B-L,R}^{\rm BLR,SUSY} = -1/\sqrt{24}$. We summarise these beta function coefficients and their meaning in appendix C.1. At v_R these two coupling values determine the (GUT normalised) hypercharge coupling,

$$\alpha_1^{-1} = \frac{3}{5}\alpha_R^{-1} + \frac{2}{5}\alpha_{BL}^{-1}. \tag{4.26}$$

From this scale, α_1 is run further down from v_R to M_Z, with the SM β-function coefficient $b_1^{\rm SM} = 41/10$. The BLR breaking scale has been chosen such that the VEV and coupling values at this point correspond to a Z' with a statistical significance $\leq 2\sigma$, which is seen later to be 3750 GeV. Using this Z' mass, the v_R VEV is determined from the formula[4] [119] in the limit $\tilde{g} = 0$,

$$M_{Z'}^2 = \frac{1}{4}\left(\frac{3}{2}g_{B-L}^2 + g_R^2\right)v_R^2 + \frac{\frac{1}{4}g_R^4 v^2}{(3/2)g_{B-L}^2 + g_R^2} \approx \frac{1}{4}\left(\frac{3}{2}g_{B-L}^2 + g_R^2\right)v_R^2, \tag{4.27}$$

where $\sqrt{(3/2)}g_{B-L} = 0.563$, as seen in Eq.4.16, and $M_{Z'} = 3750$ GeV leads to $v_R = 10328$ GeV.

The upper panel of Fig. 4.2 shows the running couplings of the BLR model, setting $v_R = 10328$ GeV and $v_{\rm SUSY} = 10^5$ GeV. Using our one-loop RGEs, we predict a value for the SM hypercharge coupling as $\alpha_Y(M_Z) = \frac{3}{5}\alpha_1(M_Z) = 1/102.44$, which we may compare to the experimentally

[4]The factor of 3/2 in Eq.4.27 multiplying g_{B-L}^2 comes from the 3/8 GUT normalisation factor times a factor of 4 in going from $B-L$ to $(B-L)/2$. This is responsible for the GUT scale prediction $\tan\theta_{BL} = g_{BL}/g_R = \sqrt{3/2}$ in terms of the non-GUT normalised couplings in Eq.4.14.

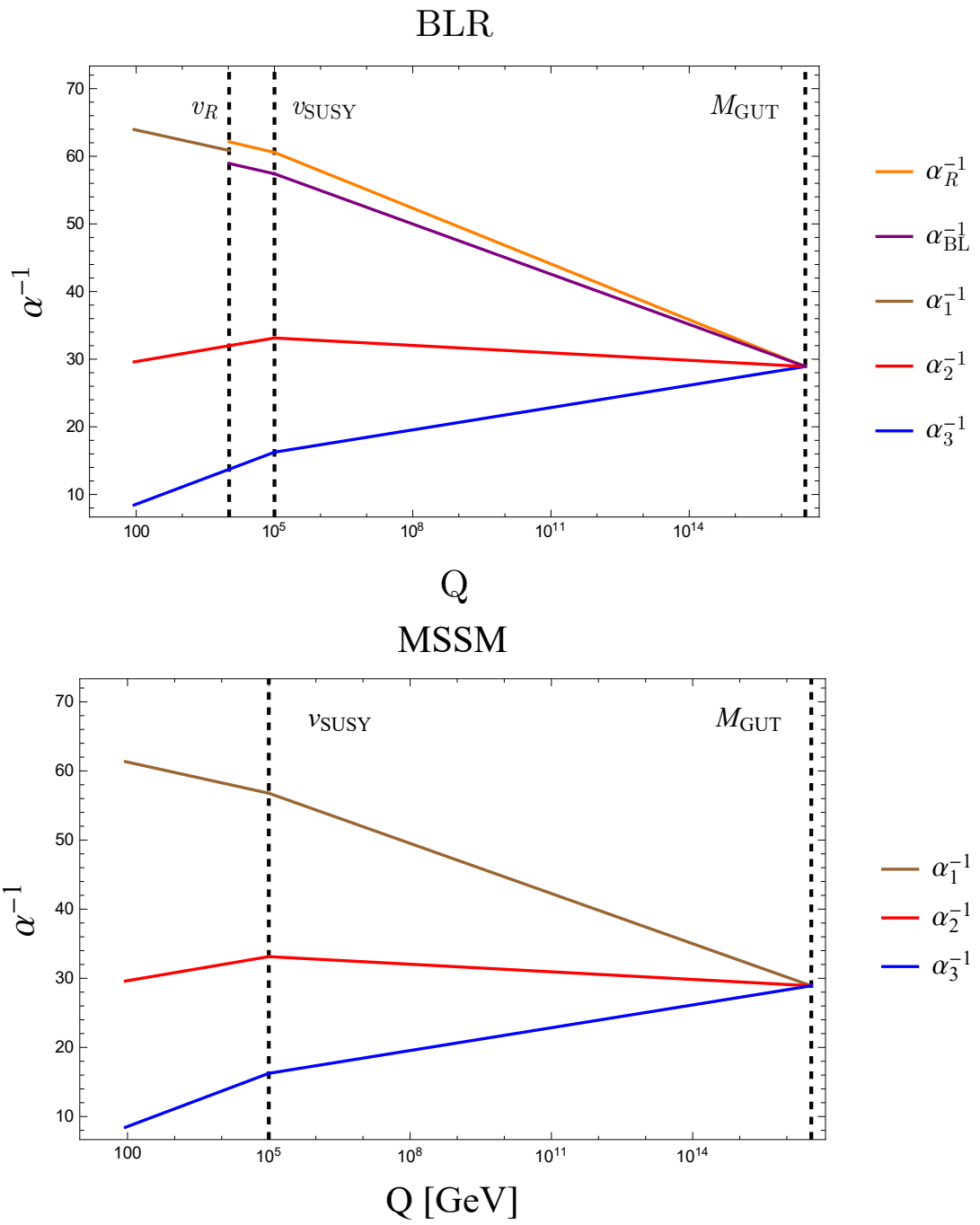

Figure 4.2: The upper panel shows the running couplings in the BLR model, with $v_R = 11660$ GeV, which corresponds to $M_{Z'} = 3750$ GeV and $v_{\rm SUSY} = 10^5$ GeV. The GUT scale is determined to be $M_{\rm GUT} = 3.30 \times 10^{16}$ GeV. The lower panel shows the running couplings in the MSSM.

determined value of $\alpha_Y^{\rm exp} = \dfrac{\alpha_{EM}}{1-\sin^2\theta_W} = 1/98.39$ [104]. The difference between the two values may be partly accounted for by our procedure of running up the best fit experimental values of α_2 and α_3 at M_Z to determine $M_{\rm GUT}$ and $\alpha_{\rm GUT}$ at the point where they meet, then running all the gauge couplings from this point down to low energies. This procedure, though convenient for the BLR model where the hypercharge gauge coupling is not defined above v_R, does not take into account the experimental error in $\alpha_3^{\rm exp}$ in the prediction for $\alpha_Y^{\rm exp}$. Another source of error is the fact that we do not consider either two loop RGEs or threshold effects, both of which are beyond the scope of this chapter. Using our one loop results, we determine the values of the couplings in Eq.4.16, which refer to the non-GUT normalised couplings.

For comparison, the lower panel of Fig. 4.2 shows the MSSM at one-loop running couplings, again assuming $v_{\rm SUSY} = 10^5$ GeV. In this case the analogous procedure to that used in the BLR model yields a prediction for the SM hypercharge coupling of $\alpha_Y^{\rm MSSM}(M_Z) = 1/102.25$.

4.6 Results

4.6.1 Preliminaries

In this section, we review the LHC results specific to the BLR model in DY processes as well as in final states including Higgs bosons. We do so in two separate subsections to follow. In the case of DY studies, we also compare the BLR results to those of the $U(1)_{B-L}$ scenario. Throughout our analysis we assume the aforementioned heavy SUSY scale, thereby preventing decays of the Z' into sparticles. However, we consider the possibility that the 2HDM-like Higgs states of the BLR models are lighter than the Z', which may therefore decay into them via the couplings in Tab. 4.4. Further, notice that Z' decays into non-MSSM-like Higgs states can be heavily suppressed in comparison, in virtue of the fact that the additional CP-odd state not giving mass to the Z' can be made arbitrarily heavy (as previously explained), a setup which we assume here, so that we refrain from accounting for these decay patterns. Finally, recall that heavy neutrino decays are prevented here in the light of footnote 2 and that they have already been studied in, e.g., [45] (for the $B-L$ case), from where it is clear that they have little Z' diagnostic power. In contrast, we aim at making the point that the Higgs decays we study below can eventually be used for this purpose.

We use standard 2HDM notation, such that h^0 and H^0 are the CP-even Higgs mass states (with the lighter h^0 being the discovered SM-like one), A^0 the CP-odd one and $H^\pm$ the charged ones.

Tab. 4.5 summarises the numerical values of the vector and axial couplings of the Z' to fermions for the $B-L$ and BLR models. For each scenario we have defined new vector and axial couplings with the gauge coupling absorbed:

$$-\mathcal{L}^{Z'} = Z'_\mu \bar{f}\gamma^\mu \frac{1}{2}(\bar{g}_V^f - \bar{g}_A^f\gamma^5)f, \tag{4.28}$$

Model	Gauge Coupling	$\bar{g}_V^u$	$\bar{g}_A^u$	$\bar{g}_V^d$	$\bar{g}_A^d$	$\bar{g}_V^e$	$\bar{g}_A^e$	$\bar{g}_V^\nu$	$\bar{g}_A^\nu$
$B-L$	g_{BL}=0.592	0.197	0	0.197	0	-0.592	0	-0.296	-0.296
BLR	See Eq.4.16	-0.0103	-0.135	-0.279	0.135	0.300	0.135	0.217	0.217

Table 4.5: Numerical values of the vector and axial couplings for the $U(1)_{B-L}$ and $U(1)_{B-L} \times U(1)_R$ models. Note that we have decoupled the RH neutrinos in calculating g_V^ν and g_A^ν.

which may be compared to Eq. 4.17. For the $U(1)_{B-L}$ model the calculation of $\bar{g}_{V,A}^f$ in Tab. 4.5 uses the gauge coupling constants shown there multiplied by the vector and axial couplings given previously in Tab. 4.3. For the BLR model, the new numerical vector and axial couplings are derived including the full effects of GKM using SARAH (as a function of the mixed couplings $g_{BL,R}$, $g_{R,BL}$ and the rotation matrix which diagonalises the neutral gauge boson mass matrices), but may be approximated analytically neglecting GKM using Eqs. 4.14, 4.17 as

$$\bar{g}_{V,A}^f(\text{BLR}) \approx g_Y \left[(\cot\theta_{BL}) g_{V,A}^f(R) - (\tan\theta_{BL}) g_{V,A}^f(BL) \right] \tag{4.29}$$

in terms of the vector and axial couplings $g_{V,A}^f(R)$ and $g_{V,A}^f(BL)$ for the T_{3R} and T_{B-L} models as written in Tab. 4.3. The non-GUT normalised gauge couplings for the BLR model in Eq.4.29 and Tab. 4.5 come from the RGE analysis leading to Eq.4.16. The values of the non-GUT normalised gauge couplings g_{BL} and g_χ for the $B-L$ and χ models in Tab. 4.5 were taken from the low energy parametrisation in [113] rather than an RGE analysis, which would require us to specify the corresponding high energy models, which we do not wish to do here, bearing in mind that the $B-L$ model does not emerge from $SO(10)$. If some other value of g_{BL} were used instead, then the vector and axial couplings for the $B-L$ model in Tab. 4.5 would be straightforwardly rescaled.

Many qualitative features of the results can be understood by examining the fermion couplings in Tab. 4.5, for example, the vector nature of the $B-L$ couplings.

4.6.2 Drell-Yan

The most promising channel to search for and profile a Z' boson at the LHC in the BLR model is DY production and decay, namely, $pp \to \gamma, Z, Z' \to e^+e^-$ and $\mu^+\mu^-$. Fig. 4.3 illustrates the current LHC reach (assuming 30 fb^{-1} of integrated luminosity at 13 TeV), highlighting that a Z' of BLR origin with a mass of 3750 GeV is allowed by data, as its statistical significance $\alpha \equiv \frac{|S|}{\sqrt{|S+B|}}$ is less than 2 in the entire mass range over which the signal $|S|$ could manifest itself over the background $|B|$. Notice that, here and in the following, our signal is given by the (modulus of the) cross section of $pp \to \gamma, Z, Z' \to e^+e^-$ and $\mu^+\mu^-$ minus that of $pp \to \gamma, Z \to e^+e^-$ and $\mu^+\mu^-$ (thereby including interference effects between Z' and γ, Z), the latter being the (irreducible) background[5]. This very same Z' boson will, however, become accessible by the end

[5]Notice that, for the Z' mass ranges currently allowed by experiment, other (reducible) backgrounds can be neglected.

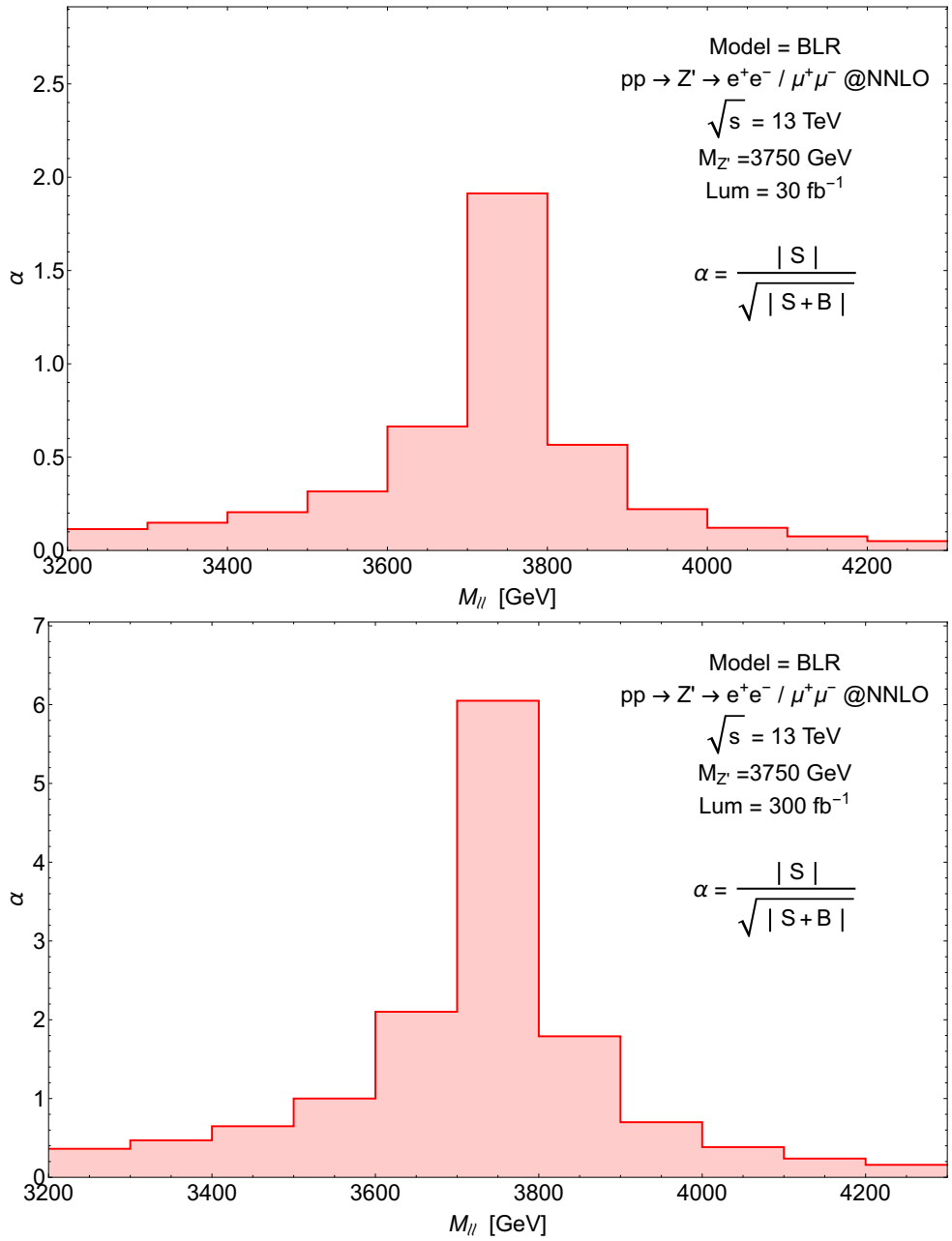

Figure 4.3: Statistical significance for producing a Z' decaying into e^+e^- and $\mu^+\mu^-$ in the BLR model at integrated luminosities of (a) $L = 30$ fb^{-1} and (b) 300 fb^{-1}. The number of events obtained at these luminosities for $pp \to Z'$ is 74 in case (a) and 737 in case (b).

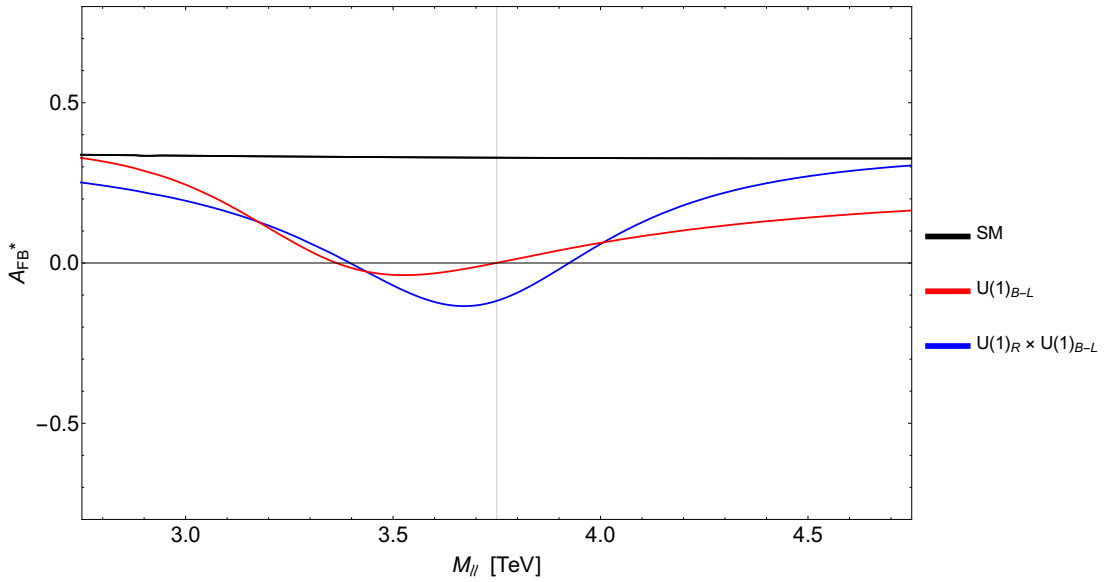

Figure 4.4: The theoretical predictions of the leptonic forward-backward asymmetry at the LHC $A^*_{\rm FB}$ in the presence of a Z' decaying into e^+e^- and $\mu^+\mu^-$ for the $U(1)_Y \times U(1)_{B-L}$ (red) and $U(1)_R \times U(1)_{B-L}$ (blue) models. We have taken $M_{Z'} = 3750$ GeV. The SM (black) result is also given for comparison.

of Run 2 of the LHC, as illustrated in Fig. 4.3, where (assuming 300 fb^{-1} of integrated luminosity at 13 TeV) values of α in excess of 5 are found near the peak region[6].

Once such a Z' signal is established, it will be necessary to diagnose it, i.e., to assess to which model it belongs. A useful variable in this respect is the (reconstructed) Forward-Backward Asymmetry ($A^*_{\rm FB}$) of the DY cross section. We use here the definition adopted in Ref. [125], see Sect. 3 therein, with no cut on the the di-lepton rapidity (see also Refs. [126, 127]). Fig. 4.4 shows the shape of this observable at the LHC, for $\sqrt{s} = 13$ TeV and $M_{Z'} = 3750$ GeV, as it would appear in the Z' peak region of the di-lepton invariant mass distribution for the BLR model as well as the $U(1)_{B-L}$ scenario. The shape emerging from the BLR case is notably different from the one of the companion $SO(10)$ model[7].

In order to quantify whether the LHC will be able to differentiate these two models, from one another or the SM, one must include the statistical error in the formulation of $A^*_{\rm FB}$ [126]:

$$\delta A_{\rm FB} = \sqrt{\frac{1 - A^2_{\rm FB}}{N}}. \tag{4.30}$$

[6]In performing this exercise, we have used the program described in Refs. [48, 49] for the $U(1)_{B-L}$ case suitably adapted to the BLR one. In particular, our implementation accounts for Z' width and interference (with SM di-lepton production) effects, which tend to reduce somewhat the sensitivity of the LHC experiments. Needless to say, when these are neglected, we are able to reproduce results obtained by the LHC collaborations [62, 124] with percent accuracy, for the corresponding choice of couplings (which differ somewhat from those used in the present chapter). This is why our limits for Z' masses differ from those quoted by the LHC.

[7]As intimated, recall that the Z' couplings to leptons in the $U(1)_{B-L}$ case are purely vectorial, so that non-zero values of $A^*_{\rm FB}$ are due in this case to interference effects.

In Fig. 4.5 we include this error in a binned version of Fig. 4.4, which overlays the $U(1)_{B-L}$ and BLR models, for a luminosity of 3000 fb^{-1} corresponding to the final result for the High-Luminosity LHC (HL-LHC) run [128]. The purple region is the overlap of errors between the two models. One can see that there are areas where the errors do not overlap and, by looking at the entire invariant mass distribution, a detailed statistical analysis may in principle differentiate between these two models at this luminosity, although we leave this task to the experimental collaborations. The shape of the errors here strongly depends on the number of events, N, which depends on the differential cross sections for the two models. The $U(1)_{B-L}$ model has a wider resonance, and so at larger invariant masses there are more Z' events produced and hence a smaller AFB error, $\delta A^*_{\rm FB}$.

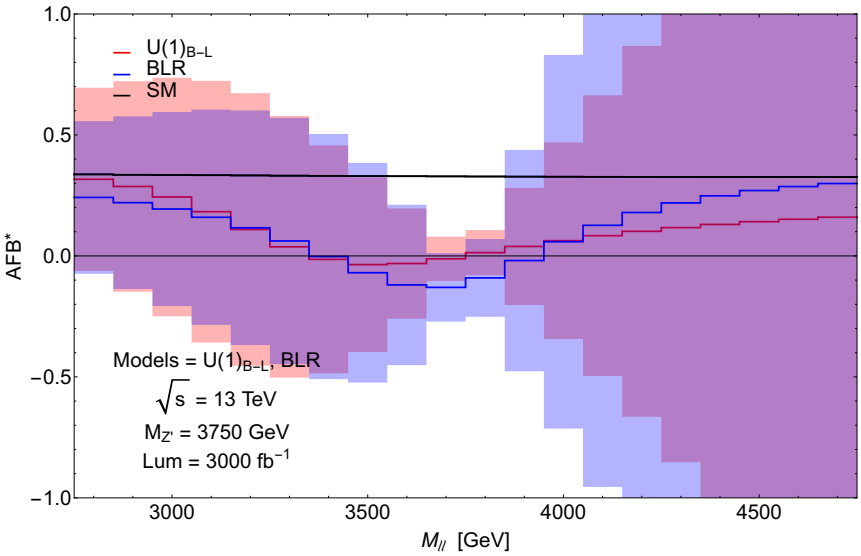

Figure 4.5: The $A^*_{\rm FB}$ spectrum of the DY cross section in the presence of a Z' of mass $M_{Z'} = 3750$ GeV. The figure we shows the BLR model prediction for $A^*_{\rm FB}$ (in blue) and its error (shaded in light blue) as well as the $U(1)_{B-L}$ prediction for $A^*_{\rm FB}$ (in red) and its error (shaded in light red) as a function of the dilepton invariant mass. The purple region is the overlap of errors between the two models. Here, $L = 3000$ fb^{-1}.

4.6.3 Higgs Final States

An alternative way of singling out the BLR nature of a Z' signal established via DY studies would be by pursuing the isolation of its exotic decays, i.e., into non-SM objects. Under the enforced assumption of heavy neutrinos, additional CP-odd Higgs boson and all sparticles being (much) heavier than the Z', the latter would include those into all possible MSSM-like (pseudo)scalar states pertaining to the Higgs sector of the BLR model, which, as discussed while commenting Tab. 4.1, is notably different from those of the $U(1)_{B-L}$ scenario. In particular, in presence of CP conservation, the following decay channels would be allowed in the BLR framework: $Z' \to A^0 h^0$, $A^0 H^0$ and $H^+ H^-$. These are presented for the usual Z' benchmark, assuming $\cos(\beta - \alpha) = 0.1$ (so as to comply with LHC data from Higgs studies), in Fig. 4.6, for representative values of

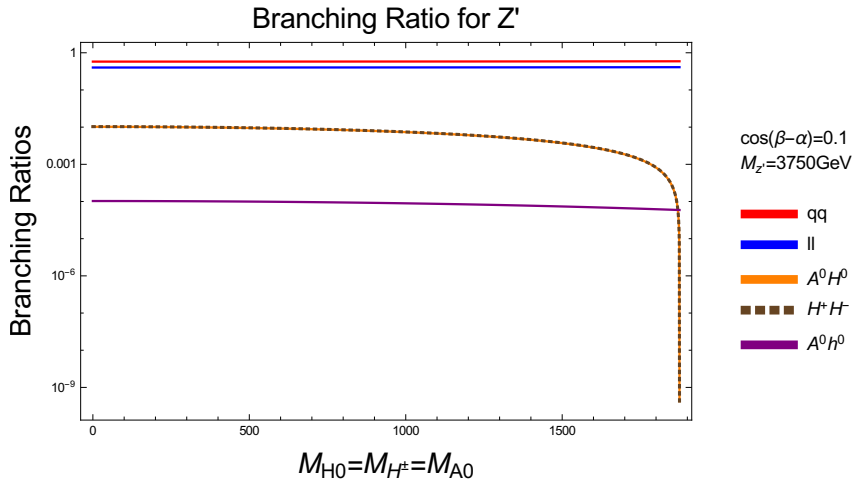

Figure 4.6: BRs of a Z' in the BLR model as a function of degenerate A_0, H^0 and $H^\pm$ masses. Here, $M_{Z'} = 3750$ GeV and $\cos(\beta - \alpha) = 0.1$.

the Higgs boson masses. While the corresponding BRs are always subleading (of $\mathcal{O}(10^{-4})$ to $\mathcal{O}(10^{-2})$) with respect to those of the decays into SM fermions, the (on-shell) Z' cross section is 2.46 fb. For $M_{H^\pm} \approx 500$ GeV, we see branching ratios of order 10^{-2}, which leads to a production cross section of $\sigma(pp \to Z' \to \{A^0H^0, H^+H^-,\ A^0h^0\}) \sim \mathcal{O}(0.01)$ fb. We may compare this to the cross section for pair production in generic 2HDMs (ie not via this Z'), which has been studied extensively, such as in ref. [129]. In this reference, the full NLO calculation has been performed for several benchmarks in 2HDM models. We see that production cross sections can vary by up to an order of magnitude depending on the exact 2HDM scenario, but broadly we find for $200 \lesssim M_{H_i} \lesssim 500$ GeV, where $H_i = \{M_{H^0},\ M_{A^0},\ M_{H^\pm}\}$, cross sections of

$$\begin{aligned} \sigma(gg \to \{A^0H^0,\ H^+H^-\}) \approx \sigma(q\bar{q} \to \{A^0H^0,\ H^+H^-\}) \sim \mathcal{O}(1) \text{ fb}, \\ \sigma(gg \to A^0h^0) \sim \mathcal{O}(10) \text{ fb}. \end{aligned} \tag{4.31}$$

For a larger mass scenario, with similar masses for all extended Higgses of $M_{H^0} \approx M_{A^0} \approx M_{H^\pm} \sim 700$ GeV, we find smaller cross sections of

$$\begin{aligned} \sigma(q\bar{q} \to \{A^0H^0,\ H^+H^-\}) \sim \mathcal{O}(0.1) \text{ fb}, \\ \sigma(gg \to A^0h^0) \sim \mathcal{O}(1) \text{ fb}, \end{aligned} \tag{4.32}$$

where we have omitted modes with small cross sections. The cross sections written above are generally much larger than our scenario, so one will likely see a signal directly in these channels before any detection via the Z' decay.

4.7 Chapter Summary

$SO(10)$ GUTs have the remarkable property that they predict RH neutrinos, making neutrino mass inevitable. $SO(10)$ is also a rank 5 gauge group, which implies that any rank preserving GUT breaking sector will lead to an extra Abelian factor in the low energy effective theory, which protects RH neutrinos from gaining mass. If the rank is broken at the TeV scale, then there will be a Z' and massive RH neutrinos possibly observable at the LHC.

We have considered $SO(10)$ motivated Z' models. In particular we have focussed on the breaking pattern in Eq. 4.3, where the final breaking scale in Eq. 4.5, of the $U(1)_R \times U(1)_{B-L}$ Abelian subgroup into the hypercharge $U(1)_Y$ of the SM, may be around the TeV scale without spoiling gauge unification, within the accuracy of our one-loop analysis. The SUSY version of the $U(1)_R \times U(1)_{B-L}$ (BLR) model permits a linear seesaw mechanism for neutrino mass generation.

After defining the BLR model particle content and giving the relevant Z'_{BLR} and Higgs couplings, we have focussed on the discovery prospects of the Z'_{BLR} at the LHC, its decay into Higgs states, and the forward-backward asymmetry as a diagnostic for discriminating it from the Z'_{BL} of the $U(1)_Y \times U(1)_{B-L}$ model. It is noteworthy that the Z'_{BL} of the $B-L$ model has purely vector couplings to quarks and leptons, making the forward-backward asymmetry a powerful discriminator, as we have discussed. In general, we have set out to test whether such models can be disentangled at past (like LEP/Stanford Linear Collider (SLC)) and present (like LHC) machines, assuming that the SUSY scale is higher than the Z'_{BLR} mass.

Having determined the parameters of the BLR model to one-loop accuracy at the TeV scale, we have examined the feasibility of the LHC to extract a Z'_{BLR} signal. We have shown that Z'_{BLR} mass values just below the current sensitivity of the LHC can easily be accessed by the end of Run 2 in standard DY searches exploiting electron and muon final states. Furthermore, we have made a detailed investigation of $A^*_{\rm FB}$ (i.e., the reconstructed forward-backward asymmetry) of these di-lepton final states and shown that it may be possible to distinguish the Z'_{BLR} of the $U(1)_R \times U(1)_{B-L}$ from the Z'_{BL} of the $U(1)_Y \times U(1)_{B-L}$ case, assuming HL-LHC luminosities. This is probably the main new result of this chapter.

We have also considered the Z'_{BLR} decays into MSSM-like Higgs bosons, which would include $Z'_{BLR} \to A^0 h^0$, $A^0 H^0$ and $H^+ H^-$, but excluding possible decays into χ^1_R and χ^2_R bosons which we assume to be too heavy to be produced. While the Higgs decay rates are always small, from percent to fraction of permille level, compared to those into SM leptons and quarks, HL-LHC luminosities should render the extraction of all of these signals feasible. Though such decays are often neglected in the literature, they provide an additional Higgs production mechanism, possibly the dominant mechanism on the Z'_{BLR} resonance at an e^+e^- collider, and a crucial test of the gauge structure of the model in the 2HDM versions of the models that SUSY demands.

Chapter 5

Modular Symmetry with Natural Lepton Masses

The models we have discussed until now have all featured massive neutrinos, but these have not been the main focus. In this chapter we will change direction and put the prediction of neutrino masses and mixing at the forefront.

5.1 Overview of Modular Symmetry

Over the next two chapters, we will concern ourselves with the framework of modular symmetry. These are a class of supersymmetric models which predict lepton masses and mixing angles similarly to the usual discrete symmetry flavour models, but with this role now being played by modular invariance. For a given modular level, N, the matter supermultiplets transform under representations of the discrete group Γ_N. The Yukawa couplings are modular forms and the flavour symmetry breaking is solely from a single complex parameter, the modulus τ. The usual models studied in the literature are the special case where the modular forms are constant functions which collapses the whole construction to a supersymmetric flavour model invariant under Γ_N. This framework can be extremely predictive, where all neutrino mass ratios, lepton mixing angles and Dirac and Majorana phases can be determined in a model with just two parameters, the real and complex part of τ. Modular invariance has a long history in both string and field theories. Target space modular invariance has been studied after the discovery that the spectrum of a closed string when compactified on a circle of radius R is invariant under the modular transformation $\tau \to -1/\tau$. There have been many studies subsequently in numerous areas, such as orbifold compactification [130–138], orientifold compactifications of Type II strings [139–145] and magnetised extra dimensions [146, 147]. Modular invariant SUSY string theories have been analysed in the late 80s [148, 149] for both global and local SUSY. In field theory constructions, modular invariance has been involved in flavour problem model building [150–156], and finally duality and modular invariance has been suggested as the underlying properties of the quantum Hall effect [157–165].

5.2 Introduction

Masses and mixing angles of elementary fermions are known with good precision and in the last few years the progress in the lepton sector has been particularly impressive, with neutrino squared mass differences and mixing angles that are attaining or approaching percent-level precision. Despite such an advance on the experimental side, the fundamental principle, if any, ruling this important aspect of fundamental interactions has remained elusive. In recent times a lot of attention has been focused on neutrinos, since the relatively mild mass hierarchy and the large mixing angles discovered through neutrino oscillations have not matched the expectations based on the knowledge of the quark sector. Neutrinos led to a change of perspective, particularly relevant when we look at the flavour puzzle in the light of a unified theory, where leptons and quarks loose their individuality.

One of the few tools we have to address the flavour puzzle is the one based on flavour symmetries, which, however, comes with its own drawbacks. Flavour symmetries cannot be exact symmetries [166] and Yukawa couplings are usually expressed as a power series in the symmetry breaking terms, with many independent free variables, to the detriment of predictability. In addition, such an approach typically makes use of several symmetry breaking parameters, with specific orientation in flavour space, considerably complicating the construction. Finally, the most popular flavour symmetries of the lepton sector constrain only mixing angles and phases, leaving fermion masses essentially undetermined [12, 167–173].

Recently, modular invariance has been invoked as candidate flavour symmetry [174]. In its simplest implementation a unique complex field, the modulus, acts as symmetry breaking parameter, thus simplifying the vacuum alignment problem. Modular invariance, in the limit of exact SUSY, completely determines the Yukawa couplings, to any order of the expansion in powers of the modulus. Moreover, neutrino masses, mixing angles and phases are all related to each other and, in minimal models, depend only on a few parameters. The formalism has been extended to consistently include CP transformations [175] [1] and it can involve several moduli [149, 178]. The idea that Yukawa couplings are determined by a set of moduli is clearly not new, and has been naturally realized in the context of string theory [130–134], in D-brane compactification [139–145], in magnetized extra dimensions [146, 147, 179], and in orbifold compactification [135–138]. Modular invariance has also been incorporated in early flavour models [150–154]. However, the main advantage of the recent approach is that it can be implemented in a bottom-up perspective, relying on the group transformation properties of modular forms of given weight and level.

Several models of lepton masses and mixing angles have been built at level 2 [180, 181], 3 [174, 182–185], 4 [186–188] and 5 [189, 190]. Extensions to quarks [191, 192] and to grand unified theories [193, 194] have also been proposed. In most of the existing constructions, there is a unique symmetry breaking parameter: the modulus itself. While this scenario is certainly

[1] The interplay between CP and modular invariance in string theory have been discussed in Ref. [155, 156] and especially in Ref. [176, 177] where a unified picture of flavour, CP and modular invariance has been analyzed from a string theory perspective.

appealing since it minimizes the symmetry breaking sector, it does not yet provide a convincing explanation of the charged lepton masses. The mass hierarchy is achieved by hand by introducing one parameter for each charged lepton species. This can be intuitively understood by recognizing that the dependence of modular forms on the modulus is nearly exponential and small neutrino mass hierarchies and large mixing angles require a modulus with small imaginary part, which is inadequate to generate the large hierarchies observed among electron, muon and tau masses. This may indicate that the charged lepton sector requires a different description, perhaps in terms of more moduli, a natural possibility in string theory.

In the present work we explore alternative descriptions of the charged lepton sector in a modular invariant framework. We test the dependence of charged lepton masses on an additional set of fields by including in the symmetry breaking sector both the modulus and ordinary flavons, chiral multiplets invariant under gauge transformations carrying non-trivial representations of the finite modular groups and non-trivial weights, to guarantee consistence with invariance under the full modular group. This has been done at level 3 in Ref. [182] and at level 5 in Ref. [190]. We will extend the investigation to level 4 and extend the possibilities studied so far al level 5. At level 4 the charged lepton Yukawa couplings are tailored to depend only on the flavons, with the hope of reproducing charged lepton masses with parameters similar in size, at least at the level of order of magnitudes. We will let RH charged leptons be responsible for the observed mass hierarchy, by assigning them different modular weights compensated by growing powers of the flavons, much as in Ref. [152–154]. At level 5 we will take a more radical departure from the existing constructions and we will assign the RH charged leptons to an irreducible triplet of Γ_5, to treat them more closely to their LH partners. In our models only the neutrino sector depends non-trivially on the modulus. As done in Ref. [182], we will not attempt to dynamically select the vacuum configurations in the symmetry breaking sector. We have no compelling indications so far that Nature follows a dynamical principle to set the cosmological constant or the EW scale. We thus treat the VEVs as free parameters, to be varied to match the experimental data.

The models are built aiming at minimizing the number of free parameters. So far few predictive models use four independent parameters to describe neutrino masses, mixing angles and phases and a variety of models achieve that with five free parameters, including real and imaginary part of the modulus. As we will see the models we have been able to construct make use of at least five parameters and can be considered next-to-minimal. In our attempts we have also incorporated CP invariance, to be spontaneously broken by the modulus and by the flavons. We present realistic examples where neutrino masse are described both in terms of the Weinberg operator and via the type I seesaw mechanism.

Our chapter is organized as follows. In section 2 we briefly review the formalism of modular invariant supersymmetric theories applied to the lepton sector and we will describe our models. In section 3 we present the data, describe our fit and we show the results of the fit and the predictions of the models. Finally in 4 we draw our conclusion.

5.3 The Models

We brefly review the formalism of modular invariant supersymmetric theories [148, 149]. The models analyzed here are supersymmetric and gauge invariant under SU(3)×SU(2)×U(1). We are mainly interested to the Yukawa interactions, described by the action:

$$\mathcal{S} = \int d^4x d^2\theta d^2\bar{\theta}\ K(\Phi, \bar{\Phi}) + \int d^4x d^2\theta\ w(\Phi) + h.c. \quad , \tag{5.1}$$

where $K(\Phi, \bar{\Phi})$, the Kähler potential, is a real gauge-invariant function of the chiral superfields Φ and their conjugates and $w(\Phi)$, the superpotential, is a holomorphic gauge-invariant function of the chiral superfields Φ. The chiral superfields $\Phi = (\tau, \varphi^{(I)})$ include the modulus τ, a dimensionless chiral supermultiplet, and the remaining chiral supermultiplets, $\varphi^{(I)}$. Under the modular group Γ the modulus transforms as

$$\tau \to \gamma\tau \equiv \frac{a\tau + b}{c\tau + d} \quad , \tag{5.2}$$

with a, b, c and d integers satisfying $ad - bc = 1$. The modular group Γ is an infinite discrete group, generated by the elements S and T satisfying $S^2 = (ST)^3 = 1$. They act as

$$\tau \to -\frac{1}{\tau} \qquad (S) \qquad\qquad \tau \to \tau + 1 \qquad (T) \quad . \tag{5.3}$$

The transformation properties of $\varphi^{(I)}$ are fully specified by the data $(k_I, N, \rho^{(I)})$, where k_I (the weight) is a real number, N (the level) is an integer and $\rho^{(I)}$ is a unitary representation of the quotient group $\Gamma_N = \Gamma/\Gamma(N)$. $\Gamma(N)$ is a principal congruence subgroup of Γ and the level N can be kept fixed in the construction. The multiplets $\varphi^{(I)}$ transform as

$$\varphi^{(I)} \to (c\tau + d)^{k_I} \rho^{(I)}(\gamma)\varphi^{(I)} \quad . \tag{5.4}$$

We choose a minimal form of the Kahler potential, invariant under Eqs. (5.2, 5.4) up to Kahler transformations:

$$K(\Phi, \bar{\Phi}) = -h \log(-i\tau + i\bar{\tau}) + \sum_I (-i\tau + i\bar{\tau})^{-k_I} |\varphi^{(I)}|^2 \quad , \tag{5.5}$$

where h is a positive constant. Concerning the superpotential $w(\Phi)$, its expansion in power series of the supermultiplets $\varphi^{(I)}$ reads:

$$w(\Phi) = \sum_n Y_{I_1 \ldots I_n}(\tau)\ \varphi^{(I_1)} \ldots \varphi^{(I_n)} \quad . \tag{5.6}$$

For the n-th order term to be modular invariant the functions $Y_{I_1...I_n}(\tau)$ should be modular forms of weight $k_Y(n)$ and level N, transforming in the representation ρ of Γ_N:

$$Y_{I_1...I_n}(\gamma\tau) = (c\tau + d)^{k_Y(n)}\rho(\gamma)\ Y_{I_1...I_n}(\tau) \quad , \tag{5.7}$$

satisfying the conditions:

1. The weight $k_Y(n)$ should compensate the overall weight of the product $\varphi^{(I_1)}...\varphi^{(I_n)}$:

$$k_Y(n) + k_{I_1} + ... + k_{I_n} = 0 \quad . \tag{5.8}$$

2. The product $\rho \times \rho^{I_1} \times ... \times \rho^{I_n}$ contains an invariant singlet.

The above requirement is very restrictive. Indeed, for each level N and for each even non-negative weight k, there is only a finite number of linearly independent modular forms [2]. They span the linear space $\mathcal{M}_k(\Gamma(N))$. Forms with vanishing weight are constant, that is independent from τ. We will analyze models with $N = 4$ and 5. The dimension of $\mathcal{M}_k(\Gamma(4))$ is $2k+1$, while $\mathcal{M}_k(\Gamma(5))$ has dimension $5k+1$. Modular forms of weight 2 generate the whole ring of modular forms. The five independent modular forms of level 4 and weight 2 have been constructed in Ref. [186]. They decompose as $\mathbf{2} + \mathbf{3'}$ under the finite group $\Gamma_4 \equiv S_4$. The eleven independent modular forms of level 5 and weight 2 have been constructed in Ref. [189] and [190]. They decompose as $\mathbf{3} + \mathbf{3'} + \mathbf{5}$ under $\Gamma_5 \equiv A_5$. In Appendix D.1 and D.2 we list them.

The chiral multiplets $\varphi^{(I)}$ comprise three generations of lepton singlets E^c and doublets L, the Higgses $H_{u,d}$, and gauge invariant flavons φ. We will consider both the case where neutrino masses arise through the Weinberg operator and the case where neutrinos get their masses through the seesaw mechanism. In the latter framework also three generations of gauge singlets N^c are included. In our conventions both the modulus τ and the flavon φ are dimensionless fields. The correct dimensions can be recovered by an appropriate rescaling.

Invariance under CP can be incorporated in a consistent way [175] by requiring:

$$\tau \xrightarrow{CP} -\tau^* \quad , \tag{5.9}$$

up to a modular transformation. On the chiral multiplets $\varphi^{(I)}$ a CP transformation acts as

$$\varphi^{(I)} \xrightarrow{CP} X_{(I)}[\varphi^{(I)}]^* \quad , \tag{5.10}$$

where $X_{(I)}$ is a matrix satisfying the consistency conditions:

$$X_{(I)}[\rho^{(I)}(\gamma)]^* X_{(I)}^{-1} = \rho^{(I)}(\gamma') \quad , \qquad (\gamma, \gamma') \in \Gamma \quad . \tag{5.11}$$

In a basis where all the matrices $\rho^{(I)}(\gamma)$ are symmetric, these conditions are always solved by

[2] Recently modular forms of general integer weights and their transformation properties under the double covering of finite modular groups have been analyzed in Ref. [195].

$X_{(I)} = \mathbb{1}$. This is the case of our choice of basis at level 5. At level 4 our basis does not enjoy this property and a non-canonical solution for $X_{(I)}$ is listed in Appendix A.

5.3.1 Level 4 Models

The group Γ_4 has order 24 and is isomorphic to S_4. Its irreducible representations are $\mathbf{1}$, $\mathbf{1'}$, $\mathbf{2}$, $\mathbf{3}$ and $\mathbf{3'}$. It is generated by two elements S and T satisfying the relations $S^2 = (ST)^3 = T^4 = \mathbb{1}$. In Appendix D.1 we detail the explicit form of the generators for the irreducible representations and the relevant CG coefficients used in this chapter. The particle content, weights and representations of our models are shown in Tab. 5.1.

	E_1^c	E_2^c	E_3^c	N^c	L	$H_{u,d}$	φ	φ'
$\Gamma_4 \equiv S_4$	$\mathbf{1}$	$\mathbf{1}$	$\mathbf{1}$	$\mathbf{3}$	$\mathbf{3}$	$\mathbf{1}$	$\mathbf{3}$	$\mathbf{1'}$
k_I (`Seesaw`)	$k-3k_\varphi$	$k-2k_\varphi$	$k-k_\varphi$	k	$-k$	0	k_φ	$k_{\varphi'}$
k_I (`Weinberg`)	$-k-3k_\varphi$	$-k-2k_\varphi$	$-k-k_\varphi$	$-$	k	0	k_φ	$k_{\varphi'}$

Table 5.1: Chiral supermultiplets, transformation properties and weights. Weights for E_i^c and L depend on whether neutrinos get their masses from the seesaw mechanism or from the Weinberg operator. A possible choice leading to the superpotential given in the text is $k = -5/3$, $k_{\varphi'} = +4/3$ and $k_\varphi = +3/2$. As a consequence, the neutrino sector depends only on φ' and the charged lepton sector depends only on φ.

With the above assignment the superpotential reads

$$w = w_h + w_e + w_\nu \quad , \tag{5.12}$$

where w_h, w_e, w_ν describe the Higgs sector, the charged lepton sector and the neutrino sector, respectively. Since the Higgs sector plays no role in our discussion, we neglect w_h. We set $H_u = H_d = 1$ in the superpotential, but we keep track of the correct dimension of the operators.

In the neutrino sector w_ν depends on the mass generation mechanism. When neutrino masses originate from the Weinberg operator we have:

$$w_\nu = -\frac{1}{\Lambda}\left[(\varphi' LL\ Y_{\mathbf{2}})_1 + \xi(\varphi' LL\ Y_{\mathbf{3'}})_1\right] \quad , \tag{5.13}$$

where Λ stands for the scale associated to lepton number violation, $(...)_r$ denotes the r representation of Γ_4 and ξ is a free parameter. When light neutrinos get their masses from the seesaw mechanism, the terms of w_ν bilinear in the matter multiplets L and N^c read

$$w_\nu = -y_0(N^c L)_1 + \Lambda\left[(\varphi' N^c N^c\ Y_{\mathbf{2}})_1 + \xi(\varphi' N^c N^c\ Y_{\mathbf{3'}})_1\right] + ... \tag{5.14}$$

Dots denote terms containing three or more powers of the matter fields, having no impact on

our analysis. A truly minimal model would involve a single invariant in the neutrino sector. For instance, a suitable assignement of weights can allow the unique term $w_\nu = -(LL\ Y_{\mathbf{2}})_1/\Lambda$ (Weinberg) or $w_\nu = -(N^c N^c\ Y_{\mathbf{2}})_1 \Lambda$ (seesaw). We have studied these possibilities, but we found no viable choice of parameters which may reproduce data.

At energies below the mass scale Λ for both models we have, in a matrix notation:

$$w_\nu = -\frac{1}{\Lambda} L^T \mathcal{W} L + ... \quad , \tag{5.15}$$

where $\mathcal{W}$ denotes a matrix in generation space depending on the 5 independent level 4 and weight +2 modular forms $Y_i(\tau)$ ($i = 1, ..., 5$). We list these results in table 5.2, where the VEV of φ' has been absorbed in Λ, Y_i stands for $Y_i(\tau)$, and the indices W, S distinguish neutrino masses originating from the Weinberg operator or from the seesaw mechanism.

`Weinberg`,	$\mathcal{W}_W = \begin{pmatrix} 0 & Y_1 & -Y_2 \\ Y_1 & -Y_2 & 0 \\ -Y_2 & 0 & Y_1 \end{pmatrix} + \xi \begin{pmatrix} 2Y_3 & -Y_5 & -Y_4 \\ -Y_5 & 2Y_4 & -Y_3 \\ -Y_4 & -Y_3 & 2Y_5 \end{pmatrix}$
`Seesaw`,	$\mathcal{W}_S = \frac{y_0^2}{2} \begin{pmatrix} 1 & 0 & 0 \\ 0 & 0 & 1 \\ 0 & 1 & 0 \end{pmatrix} \mathcal{W}_W^{-1} \begin{pmatrix} 1 & 0 & 0 \\ 0 & 0 & 1 \\ 0 & 1 & 0 \end{pmatrix}$

Table 5.2: Relevant matrices in the neutrino sector of the superpotential in Γ_4 models.

The light neutrino mass matrix m_ν is

$$m_\nu = \mathcal{W} \frac{v^2}{\Lambda} \sin^2 \hat{\beta} \quad , \tag{5.16}$$

where $\tan \hat{\beta}$ is the ratio of VEVs, $\langle H_u \rangle \,/\, \langle H_d \rangle$. So far, the results in the neutrino sector would not vary had we instead defined N^c and L to transform as a **3'**, rather than a **3** under Γ_4. However, the following discussion in the charged lepton sector requires the properties as defined in Tab. 5.1. The superpotential w_e for the charged lepton sector reads:

$$w_e = -aE_1^c (L\ \varphi^3)_1 - a' E_1^c (L\ \varphi^3)'_1 - bE_2^c (L\ \varphi^2)_1 - cE_3^c (L\ \varphi)_1 \equiv -E^{cT} \mathcal{Y}_e L \quad . \tag{5.17}$$

In the last equality we use a vector notation and

$$\mathcal{Y}_e = \begin{pmatrix} a(\varphi_2^3 - 2\varphi_1^3 + \varphi_3^3) & 3a(\varphi_1\varphi_2^2 - \varphi_2\varphi_3^2) & -3a(\varphi_2^2\varphi_3 - \varphi_1\varphi_3^2) \\ +a'(\varphi_1^3 + 2\varphi_1\varphi_2\varphi_3) & +a'(\varphi_1^2\varphi_3 + 2\varphi_2\varphi_3^2) & +a'(\varphi_1^2\varphi_2 + 2\varphi_2^2\varphi_3) \\ b(\varphi_1^2 - \varphi_2\varphi_3) & b(\varphi_2^2 - \varphi_1\varphi_3) & b(-\varphi_1\varphi_2 + \varphi_3^2) \\ c\varphi_1 & c\varphi_3 & c\varphi_2 \end{pmatrix} \quad . \tag{5.18}$$

There are two independent Γ_4 invariants that can be built out of L and φ^3, hence the two independent parameters a and a'. The dependence on the flavon supermultiplet φ is fixed by the weight assignment. There is no dependence on the modulus τ, since the bilinears $(E_1^c L, E_2^c L, E_3^c L)$ have weight $(-3k_\varphi, -2k_\varphi, -k_\varphi)$. Taking, for instance, $k_\varphi = +3/2$, these weights cannot be matched by modular forms. The charged lepton mass matrix m_e reads

$$m_e = \mathcal{Y}_e \frac{v}{\sqrt{2}} \cos\hat{\beta} \quad . \tag{5.19}$$

Notice that if the flavon φ is aligned along the $(0, \varphi_2, 0)$ direction, $\mathcal{Y}_e$ is diagonal and the charged lepton masses are given by:

$$m_e = \frac{a}{\sqrt{2}} v\varphi_2^3 \cos\hat{\beta} \quad , \qquad m_\mu = \frac{b}{\sqrt{2}} v\varphi_2^2 \cos\hat{\beta} \quad , \qquad m_\tau = \frac{c}{\sqrt{2}} v\varphi_2 \cos\hat{\beta} \quad . \tag{5.20}$$

Hence, a mass hierarchy can be generated by $|\varphi_2| < 1$, even with a, b and c of the same order.

In our numerical analysis we will treat the modulus τ and the VEV of φ as free parameters. Beyond that, the parameters controlling lepton masses and mixing angles are the overall scale Λ and the five dimensionless constants ξ, a, a', b and c. Without loss of generality, we can require a, a', b and c to be real, since their phases are always unphysical. On the contrary, the phase of ξ cannot be removed by a field redefinition. We will consider two options, either requiring the theory to be invariant under CP at the Lagrangian level, or not. In the former case, using the CP transformation given in Appendix A, we find that ξ should be real and CP can be spontaneously broken by the VEVs of τ and/or φ. In the latter case, we will treat ξ as a complex free parameter. The dependence on $\tan\hat{\beta}$ can be absorbed into the above parameters and will not be explicitly shown when reporting numerical values.

5.3.2 Level 5 Models

The irreducible representations of the group $\Gamma_5 \equiv A_5$ are **1**, **3**, **3′**, **4** and **5**. Its generators are S and T, satisfying $S^2 = (ST)^3 = T^5 = \mathbb{1}$. In appendix D.2 we specify the explicit form of the generators for each representation, together with the relevant Clebsh-Gordan coefficients. Here, we construct modular-invariant models in which all leptons are collected into **3** or **3′** multiplets of A_5, containing the three generations of each type of field. We take the neutrino sector to be

minimal, it should only depend on the modulus τ and an overall scale. Modular forms will not appear in the charged-lepton sector, which instead will contain two extra flavons. In table 5.3, we show the assignments of representations and weights that we consider.

	E^c	N^c	L	$H_{u,d}$	φ	χ
$\Gamma_5 \equiv A_5$	ρ_L	ρ_N	ρ_L	1	ρ_L	1
k_I	$-3-k_L$	k_N	k_L	0	3/2	3/2

	ρ_N	ρ_L	k_N	k_L
`Weinberg`	–	$\mathbf{3}$	–	-1
	–	$\mathbf{3'}$	–	-1
`Seesaw`	$\mathbf{3}$	$\mathbf{3}$	-1	1
	$\mathbf{3'}$	$\mathbf{3'}$	-1	1
	$\mathbf{3}$	$\mathbf{3'}$	0	-2
	$\mathbf{3'}$	$\mathbf{3}$	0	-2

Table 5.3: Chiral supermultiplets, transformation properties and weights for the level-5 models.

Setting $H_u = H_d = 1$, the neutrino sector w_ν of the superpotential is, depending on the choice Weinberg vs. Seesaw and ($\rho_L = \rho_N$) vs. ($\rho_L \neq \rho_N$):

$$w_\nu = \begin{cases} -\frac{1}{\Lambda}(LL\,Y_5)_1 & \texttt{Weinberg} \\ -y_0(N^cL)_1 + \Lambda(N^cN^c\,Y_{\mathbf{5}})_1 & \texttt{Seesaw},\ \rho_L = \rho_N \\ -y_0(N^cL\,Y_{\mathbf{5}})_1 + \Lambda(N^cN^c)_1 & \texttt{Seesaw},\ \rho_L \neq \rho_N \end{cases} \tag{5.21}$$

The case of $\rho_L \sim \rho_N \sim 3$ has been studied in detail in Ref. [196] and so not discussed here.

Below the energy scale Λ, w_ν can always be written as

$$w_\nu = -\frac{1}{\Lambda} L^T \mathcal{W} L, \tag{5.22}$$

with $\mathcal{W}$ a 3×3 matrix, whose explicit form for each case can be read from table 5.4, using the equation $\mathcal{W} = \frac{y_0^2}{2}\,\mathcal{Y}_\nu^T \mathcal{W}_W^{-1} \mathcal{Y}_\nu$ for the seesaw case. The light neutrino mass matrix m_ν can be obtained from $\mathcal{W}$ as in Eq. 5.16.

The charged-lepton sector w_e of the superpotential is

$$w_e = \alpha(E^cL)_{\mathbf{1}}\chi^2 + \beta(E^cL)_{\mathbf{3}}\chi\varphi + \gamma(E^cL)_{\mathbf{5}}(\varphi^2)_{\mathbf{5}} + \delta(E^cL)_{\mathbf{1}}(\varphi^2)_{\mathbf{1}} \equiv -E^{cT}\mathcal{Y}_e L \quad . \tag{5.23}$$

In what follows we set the flavons to their vevs and denote them by χ, φ_i. We absorb $\chi \neq 0$, $\varphi_1 \neq 0$ and the Lagrangian parameter δ into α, β, γ, φ_2 and φ_3. Once this is done, the matrix

Weinberg, $\rho_L = \mathbf{3}$ $k_L = -1$	$\mathcal{W} = \begin{pmatrix} 2Y_1 & -\sqrt{3}Y_5 & -\sqrt{3}Y_2 \\ -\sqrt{3}Y_5 & \sqrt{6}Y_4 & -Y_1 \\ -\sqrt{3}Y_2 & -Y_1 & \sqrt{6}Y_3 \end{pmatrix}$
Weinberg, $\rho_L = \mathbf{3'}$ $k_L = -1$	$\mathcal{W} = \begin{pmatrix} 2Y_1 & -\sqrt{3}Y_4 & -\sqrt{3}Y_3 \\ -\sqrt{3}Y_4 & \sqrt{6}Y_2 & -Y_1 \\ -\sqrt{3}Y_3 & -Y_1 & \sqrt{6}Y_5 \end{pmatrix}$
Seesaw, $\rho_L = \rho_N = \mathbf{3}$ $k_L = 1,\ k_N = -1$	$\mathcal{W}_W = \begin{pmatrix} 2Y_1 & -\sqrt{3}Y_5 & -\sqrt{3}Y_2 \\ -\sqrt{3}Y_5 & \sqrt{6}Y_4 & -Y_1 \\ -\sqrt{3}Y_2 & -Y_1 & \sqrt{6}Y_3 \end{pmatrix}$, $\mathcal{Y}_\nu = \begin{pmatrix} 1 & 0 & 0 \\ 0 & 0 & 1 \\ 0 & 1 & 0 \end{pmatrix}$
Seesaw, $\rho_L = \rho_N = \mathbf{3'}$ $k_L = 1,\ k_N = -1$	$\mathcal{W}_W = \begin{pmatrix} 2Y_1 & -\sqrt{3}Y_4 & -\sqrt{3}Y_3 \\ -\sqrt{3}Y_4 & \sqrt{6}Y_2 & -Y_1 \\ -\sqrt{3}Y_3 & -Y_1 & \sqrt{6}Y_5 \end{pmatrix}$, $\mathcal{Y}_\nu = \begin{pmatrix} 1 & 0 & 0 \\ 0 & 0 & 1 \\ 0 & 1 & 0 \end{pmatrix}$
Seesaw, $\rho_L = 3, \rho_N = \mathbf{3'}$ $k_L = -2,\ k_N = 0$	$\mathcal{W}_W = \begin{pmatrix} 1 & 0 & 0 \\ 0 & 0 & 1 \\ 0 & 1 & 0 \end{pmatrix}$, $\mathcal{Y}_\nu = \begin{pmatrix} \sqrt{3}Y_1 & Y_5 & Y_2 \\ Y_4 & -\sqrt{2}Y_3 & -\sqrt{2}Y_5 \\ Y_3 & -\sqrt{2}Y_2 & -\sqrt{2}Y_4 \end{pmatrix}$
Seesaw, $\rho_L = 3', \rho_N = \mathbf{3}$ $k_L = -2,\ k_N = 0$	$\mathcal{W}_W = \begin{pmatrix} 1 & 0 & 0 \\ 0 & 0 & 1 \\ 0 & 1 & 0 \end{pmatrix}$, $\mathcal{Y}_\nu = \begin{pmatrix} \sqrt{3}Y_1 & Y_4 & Y_3 \\ Y_5 & -\sqrt{2}Y_3 & -\sqrt{2}Y_2 \\ Y_2 & -\sqrt{2}Y_5 & -\sqrt{2}Y_4 \end{pmatrix}$

Table 5.4: Relevant matrices in the neutrino sector of the superpotential in Γ_5 models.

$\mathcal{Y}_e$ takes the form

$$\mathcal{Y}_e = \begin{pmatrix} \alpha + 4\gamma(1-\varphi_2\varphi_3) & (\beta+6\gamma)\varphi_3 & (-\beta+6\gamma)\varphi_2 \\ (-\beta+6\gamma)\varphi_3 & 6\gamma\varphi_3^2 & \alpha+\beta-2\gamma(1-\varphi_2\varphi_3) \\ (\beta+6\gamma)\varphi_2 & \alpha-\beta-2\gamma(1-\varphi_2\varphi_3) & 6\gamma\varphi_2^2 \end{pmatrix} \quad . \tag{5.24}$$

The charged lepton mass matrix m_e has the same form as in Eq. (5.19), $m_e = \mathcal{Y}_e v \cos\hat{\beta}/\sqrt{2}$. Setting $\varphi_2 = \varphi_3 = 0$ and switching the last two rows gives a diagonal m_e, with eigenvalues

$$m_a = (\alpha+4\gamma)\frac{v}{\sqrt{2}}\cos\hat{\beta} \quad , \qquad m_b = (\alpha-\beta-2\gamma)\frac{v}{\sqrt{2}}\cos\hat{\beta} \quad , \qquad m_c = (\alpha+\beta-2\gamma)\frac{v}{\sqrt{2}}\cos\hat{\beta} \quad . \tag{5.25}$$

As for the Γ_4 case, we treat τ and the VEVs $\varphi_{2,3}$ as parameters to be freely varied in our fit. The remaining parameters are the overall scale Λ and the dimensionless constants α, β and γ.

By enforcing CP conservation, the latter three are required to be real. The dependence on $\tan\hat{\beta}$ can be absorbed into these parameters.

5.4 Results

In this section we identify which scenarios we analyse, state the experimental data used and report the results of a chi-square analysis with the predictions of the models. In table 5.5, we list the seven scenarios which reproduce the data well, with a reasonable $\chi^2_{\text{min, red}}$ and minimum number of parameters. We will present results only for these scenarios, omitting those presenting a high $\chi^2_{\text{min, red}}$ or a large number of parameters. We identify the different cases with a code referring to the modular level $\Gamma_4 \equiv S_4$ or $\Gamma_5 \equiv A_5$ "4 (5)"; Weinberg or Seesaw "W (S)"; CP conserving or violating "C (V)". For the A_5 Weinberg scenario, we add the transformation property of the lepton triplet, whether this transforms as a **3**, or **3'** "3 (3p)".

We present the results in this section for which τ is not restricted to be in the fundamental domain, $|\text{Re}(\tau)| \leq 1/2$, $|\tau| \geq 1$. However, in appendix D.3 we also include a full list of modular transformations to the set of input parameters which transforms τ into the fundamental region, as well as the explicit numerical values for these transformed parameters, which will yield the same set of physical observables. In this main text we list the non-fundamental region input parameters to avoid confusion stemming from spurious additional imaginary parameters which are just an artefact of a basis transformation.

Model	Operator	CP conservation	Charged Lepton sector	Case Identifier
S_4	Weinberg	~~CP~~	Diagonal	4WV
S_4	Seesaw	~~CP~~	Diagonal	4SV
S_4	Weinberg	CP	Modified	4WC
S_4	Seesaw	CP	Modified	4SC
A_5	Weinberg, $\rho_L = \mathbf{3}$	CP	Modified	5WC3
A_5	Weinberg, $\rho_L = \mathbf{3'}$	CP	Modified	5WC3p
A_5	Seesaw, $\rho_L = \mathbf{3}$, $\rho_N = \mathbf{3'}$, $\text{Im}(\varphi_{2,3}) = 0$	CP	Modified	5SC

Table 5.5: A list of the seven scenarios presented with good fits to data.

5.4.1 Fit to Leptonic Data

In Tab. 5.6, we list the experimental data and errors we use to calculate our pulls and $\chi^2_{\text{min, red}}$ values. For the Yukawa couplings, we use the renomalised values at m_Z scale, as detailed in Ref. [197]. For the neutrino oscillation data, we use the most recent results from the NuFit collboration, Ref. [198]. For the calculation of our $\chi^2_{\text{min,red}}$, we assume the conservative estimate of gaussian errors, unless explicitly stated otherwise. Even though current data seem to prefer

normal to inverted neutrino MO, we do not weight this option in our χ^2 function.

We show our results for all the considered Γ_4 and Γ_5 cases in the three tables contained in Tab. 5.7 and 5.8 respectively. For each case we present the point in parameter space which minimises the χ^2, as a result of a numerical minimisation procedure. In the first table, one finds the predictions and, in parentheses, pulls to the six observed neutrino parameters: the two mass squared differences, $\Delta m^2_{21},\ \Delta m^2_{3l}$ (where the latter refers to $\Delta m^2_{32} > 0$ for NO and $\Delta m^2_{31} < 0$ for IO), three PMNS angles, $\theta_{12},\ \theta_{13},\ \theta_{23}$, and CP violating phase, δ; as well as the final $\chi^2_{\text{min, red}}$. In the second table, we list the predictions for each scenario for the: three individual neutrino masses, $m_1,\ m_2,\ m_3$; Majorana phases $\alpha_{21},\ \alpha_{31}$; neutrinoless double beta decay parameter, m_{ee}; and MO. In the third table we specify the input parameters used to generate the best fit point discussed. In neither Γ_4, nor Γ_5 do we present the pulls from the Yukawa of the charged lepton sector, as we find sufficient freedom for every considered case to reproduce the observed values with negligible pulls ($\Delta\chi^2 < 0.01$).

$y_e(m_Z)$	$2.794745(16) \times 10^{-6}$
$y_\mu(m_Z)$	$5.899863(19) \times 10^{-4}$
$y_\tau(m_Z)$	$1.002950(91) \times 10^{-2}$

	IO	NO
$\frac{\Delta m^2_{21}}{10^{-5}\ \text{eV}^2}$	7.39(21)	7.39(21)
$\frac{\Delta m^2_{3\ell}}{10^{-3}\ \text{eV}^2}$	$-2.512(33)$	$+2.525(32)$
$\sin^2\theta_{12}$	0.310(13)	0.310(13)
$\sin^2\theta_{13}$	0.02263(66)	0.02240(66)
$\sin^2\theta_{23}$	0.582(17)	0.582(17)
δ/π	1.56(15)	1.21(19)

Table 5.6: Left panel: charged lepton Yukawa couplings renormalized at the m_Z scale, from Ref. [197]. Right panel: neutrino oscillation data, from Ref. [198]. The squared mass difference $\Delta m^2_{3\ell}$ is equal to Δm^2_{31} for normal ordering and Δm^2_{32} for inverted ordering. Errors, shown in brackets, are the average of positive and negative 1σ deviations. The χ^2 function is not gaussian along the $\sin^2\theta_{23}$ direction and our definition overestimates the error.

5.4.2 Numerical Results at Level 4

To minimize the number of effective parameters, we first analyze the case of diagonal charged lepton sector. This can be realized by fixing the VEV of the flavon φ along the direction $(0, \varphi_2, 0)$. All terms depending on a' drop. The remaining input parameters a, b and c, can be fixed to exactly reproduce the charged lepton masses:

$$(a, b, c) = \frac{\sqrt{2}}{v \cos\beta} \left(\frac{m_e}{\varphi_2^3}, \frac{m_\mu}{\varphi_2^2}, \frac{m_\tau}{\varphi_2} \right) \quad . \tag{5.26}$$

Due to the hierarchical pattern in powers of the VEV, these input parameters may be all of similar order by fixing, for example, $|\varphi_2| = 1/100$, which leads to

$$a \cos\beta \simeq 2.8, \qquad b \cos\beta \simeq 5.9, \qquad c \cos\beta \simeq 1. \tag{5.27}$$

We are left with 3 Lagrangian parameters, $(\Lambda, \mathtt{Re}(\xi), \mathtt{Im}(\xi))$ and the (complex) modulus VEV τ. Choosing the neutrino mass generated by the Weinberg operator (denoted case "4WV"), we get a good agreement between the model and the data by the parameter choice shown in Tab. 5.7, with a $\chi^2_{\text{min, red}} \sim 0.6$. We also present results for the same scenario, but now with neutrino mass generated by a type-I seesaw (denoted case "4SV"), with a $\chi^2_{\text{min, red}} \sim 1.1$.

We may further reduce the number of free parameters by imposing that the Lagrangian be CP conserving. This amounts, in our basis, to requiring real Lagrangian parameters, i.e. $\text{Im}(\xi) = 0$. We found no feasible solutions with this further restriction keeping the charged lepton sector diagonal as before. Thus we relax this requirement and at the same we set $a' = 0$. Though a' is a legitimate parameter of our model, we can safely neglect it in the limit of nearly diagonal charged lepton sector. Indeed, in such a limit, the contribution to lepton mixing is dominated by the elements of $\mathcal{Y}_e$ below the diagonal, controlled by the parameters b and c. We find a good fit to data allowing small perturbations (in units of φ_2) of $\text{Im}(\varphi_1) = -\text{Im}(\varphi_3) \neq 0$. Along this particular direction CP is spontaneously broken, see Appendix A, and the charged lepton sector contributes to the physical phases of the PMNS matrix. However, the main motivation for choosing such a direction is to show that it is possible to achieve a good agreement with the data by turning on a minimum number of extra parameters. We present our results for this scenario for both the Weinberg case (denoted "4WC"), with $\chi^2_{\text{min, red}} \sim 3.2$ and the seesaw case (denoted "4SC"), with $\chi^2_{\text{min, red}} \sim 0.3$. In both CP conserving and violating scenarios, neutrino masses from the Weinberg operator have inverted ordering, while those coming from the seesaw mechanism are normal ordered.

In our setup we were unable to describe both the neutrino masses and the mixing matrix with fewer than five parameters. On the other hand the overall results and predictions are quite stable with respect to the details of the model. The quality of the fit is quite similar in all cases analysed and the results mainly depend on the choice between the Weinberg operator and the seesaw mechanism. In both cases the neutrino mass spectrum is nearly degenerate and

	value (pull)						
Case	$\Delta m^2_{21} \cdot 10^5$ eV^{-2}	$\Delta m^2_{3l} \cdot 10^3$ eV^{-2}	$\sin^2\theta_{12}$	$\sin^2\theta_{13}$	$\sin^2\theta_{23}$	δ/π	$\chi^2_{\text{min, red}}$
$4WV$	7.39 (0)	-2.517 (-0.2)	0.310 (+0.0)	0.02262 (-0.0)	0.583 (+0.1)	1.68 (+0.8)	0.6
$4SV$	7.39 (0)	2.527 (+0.1)	0.310 (+0.0)	0.02241 (+0.0)	0.580 (-0.1)	1.40 (+1.0)	1.1
$4WC$	7.39 (0)	-2.512 (-0.0)	0.310 (+0.0)	0.02264 (+0.0)	0.580 (-0.1)	1.83 (+1.8)	3.2
$4SC$	7.39 (0)	2.526 (+0.0)	0.317 (+0.5)	0.02237 (-0.1)	0.580 (-0.1)	1.25 (+0.2)	0.3

	value						
Case	$m_1 \cdot 10^2$ eV^{-2}	$m_2 \cdot 10^2$ eV^{-2}	$m_3 \cdot 10^2$ eV^{-2}	α_{21}/π	α_{31}/π	$m_{ee} \cdot 10^2$ eV^{-1}	MO
$4WV$	6.56	6.61	4.31	0.21	1.76	6.18	IO
$4SV$	4.23	4.32	6.57	0.22	0.54	4.01	NO
$4WC$	6.33	6.39	3.96	1.88	1.69	6.20	IO
$4SC$	4.26	4.35	6.59	0.11	0.30	4.25	NO

	Input parameters								
Case	Re(τ)	Im(τ)	Re(ξ)	Im(ξ)	Im(φ_3)=-Im(φ_1)	a	b	c	$1/\Lambda$ (eV^{-1})
$4WV$	1.155	0.9797	-2.536	-0.07654	-	2.795	5.900	1.003	0.007395
$4SV$	0.8436	0.9968	-2.600	0.1151	-	2.795	5.900	1.003	0.7672
$4WC$	2.530	0.5380	-0.1063	-	-0.001063	2.647	5.899	0.9918	0.003799
$4SC$	2.506	0.5905	-2.595	-	0.001081	2.642	5.899	0.9914	1.301

Table 5.7: Results of the fit to lepton data for the Γ_4 models. In the top panel, best values and pulls for the observables used in the fit. Also the minimum χ^2 is shown. In the middle table, predictions of the models: neutrino masses, phases and parameter m_{ee} relevant for neutrinoless double beta decay. In the bottom panel input parameters at the minimum of the χ^2 function. We have fixed $\varphi_2 = 0.01$ for all four cases. To simplify the notation, the factors $\cos\hat{\beta}$ and $1/\sin^2\hat{\beta}$ have been omitted from a, b, c and Λ, respectively.

the lightest neutrino mass is around 40 meV. When we adopt the Weinberg operator (seesaw mechanism) m_{ee} is close to 60 (40) meV. A normally ordered spectrum (corresponding to the seesaw mechanism) predicting a relatively high m_{ee} parameter seems a common feature to most of the models enjoying modular invariance and providing a good fit to the data. The neutrino masses in our model are slightly heavier than those of the level 4 models studied in Ref. [186, 187].

5.4.3 Numerical Results at Level 5

We now turn to the models at level 5. Unlike in level 4, all the examples listed here produce a CP conserving Lagrangian. In our basis, this requirement is that all Lagrangian parameters be real. The charged lepton masses are essentially controlled by α, β, γ, while neutrino masses and mixing angles are mainly governed by Λ, τ and φ. We fix $\varphi_1 = 1$ and, to reduce the number of parameters, we restrict the two VEVs of (φ_2, φ_3) to real values. Neutrino properties are thus described by a total of five parameters and CP violating phases are entirely due to the neutrino sector, since CP is preserved by a real φ VEV. Here again this choice is mainly dictated by the desire to match the data using a small number of parameters.

As we can see from Tab. 5.8, we get the best agreement with data when neutrino masses come from the Weinberg operator, with $\rho_L \sim \mathbf{3}$ (denoted case "5WC3"), for which we get a $\chi^2_{\text{min, red}} \sim 1.1$. The τ value is very close to the border of the fundamental region (see also Tab. D.2 in Appendix C), where CP is conserved. This result strongly supports the indication that, in a CP invariant model, even a tiny departure from the region of moduli space where CP is preserved can cause large observable CP-violating effects [175]. We also notice that all the components of the multiplet φ are of the same order, indicating that the charged lepton mass matrix is far from the diagonal form, related to $\varphi \propto (1, 0, 0)$. This is a new feature, since in the level 4 models discussed here and in the level 3 model of Ref. [182], the contribution to the lepton mixing of the charged lepton mass matrix (depending on ordinary flavons) is small. The model predicts $m_{ee} \approx 27$ meV. The MO is inverted, as in all previous cases dealing with the Weinberg operator. An exception is provided by the other Weinberg case at level 5 in which $\rho_L \sim \mathbf{3'}$ (denoted "5WC3p"), which predicts normal ordering at the price of a considerably worse $\chi^2_{\text{min, red}} \sim 12.6$. The largest pulls are the one in δ, which deviates by more than 3σ and by $\sin^2\theta_{13}$, about 1σ below the current best value.

We have also explored this model in a seesaw scenario, in which $\rho_L \sim \mathbf{3}$, $\rho_N \sim \mathbf{3'}$ (denoted "5SC"). The agreement with data is not excellent and our estimate of the $\chi^2_{\text{min, red}}$ is 11.1. The main contributions to the $\chi^2_{\text{min, red}}$ come from δ, which deviates by more than 2σ and by $\sin^2\theta_{23}$, about 2σ below the current best value. For $\sin^2\theta_{23} \simeq 0.45$ we do not use the nominal pull, since the error is non-gaussian. We assess the contribution to the $\chi^2_{\text{min, red}}$ directly using the results from NuFit. The neutrino mass spectrum has normal ordering. Specific to the seesaw realization are the prediction of θ_{23} in the first octant and of a vanishing m_1. The latter result has no counterpart in any model based on modular invariance so far investigated. The presence of a vanishing eigenvalue is independent from the choice of the modular parameter τ and is due to the fact that the determinant of the combination $\mathcal{Y}_\nu^T \mathcal{W}_W^{-1} \mathcal{Y}_\nu$ vanishes identically for the chosen representations. Though we do not have a full analytic proof of such behavior, we have checked it by means a q-expansion of the modular forms Y_i $(i = 1, ..., 5)$: the determinant is proportional to a power of q that grows with the order at which we stop the q-expansion of Y_i. The vanishing of the determinant probably reflects one of the many algebraic identities involving lowest weight modular forms. As a consequence $m_{ee} \approx 1.3$ meV is rather small.

	value (pull)						
Case	$\Delta m^2_{21} \cdot 10^5$ eV^{-2}	$\Delta m^2_{3l} \cdot 10^3$ eV^{-2}	$\sin^2\theta_{12}$	$\sin^2\theta_{13}$	$\sin^2\theta_{23}$	δ/π	$\chi^2_{\text{min, red}}$
$5WC3$	7.39 (0)	-2.512 (+0.0)	0.312 (+0.1)	0.02260 (-0.0)	0.592 (+0.6)	1.69 (+0.9)	1.1
$5WC3p$	7.39 (0)	2.525 (+0.0)	0.309 (-0.1)	0.0217 (-1.2)	0.586 (+0.3)	0.57 (-3.3)	12.6
$5SC$	7.39 (0)	2.522 (-0.1)	0.292 (-1.4)	0.0228 (+0.5)	0.449 (-2.0*)	1.63 (+2.2)	11.1*

	value						
Case	$m_1 \cdot 10^2$ eV^{-2}	$m_2 \cdot 10^2$ eV^{-2}	$m_3 \cdot 10^2$ eV^{-2}	α_{21}/π	α_{31}/π	$m_{ee} \cdot 10^2$ eV^{-1}	MO
$5WC3$	4.94	5.01	0.0942	0.70	0.94	2.7	IO
$5WC3p$	2.82	2.95	5.76	0.38	0.26	2.3	NO
Case	$m_1 \cdot 10^2$ eV^{-2}	$m_2 \cdot 10^2$ eV^{-2}	$m_3 \cdot 10^2$ eV^{-2}	$(\alpha_{21} - \alpha_{31})/\pi$		$m_{ee} \cdot 10^2$ eV^{-1}	MO
$5SC$	0	0.860	5.02	1.68		0.13	NO

	Input parameters									
Case	Re(τ)	Im(τ)	Re(φ_2)	Im(φ_2)	Re(φ_3)	Im(φ_3)	$\alpha \cdot 10^3$	$\beta \cdot 10^3$	$\gamma \cdot 10^3$	$1/\Lambda$ (eV^{-1})
$5WC3$	-0.01882	0.9929	0.4260	-	0.8030	-	3.018	3.927	-0.4484	0.008180
$5WC3p$	-0.09033	0.2190	0.4244	-	0.01694	-	3.259	4.311	-0.8036	0.0006303
$5SC$	-0.3615	0.2412	0.04759	-	0.3731	-	3.368	4.411	-0.8126	0.0001639

Table 5.8: Results of the fit to lepton data for the A_5 models. For the $5SC$ case, the predicted lightest neutrino mass is $m_1 = 0$ and so only one physical Majorana phase exists, which appears in the combination $(\alpha_{21} - \alpha_{31})$ in neutrinoless double beta decay and hence we report only this combination. We have fixed $\varphi_1 = 1$ for all three cases. *Actual NuFit 4.0 error on $\sin^2\theta_{23}$ measurement (for NO) used, rather than assumed Gaussian error. To simplify the notation, the factors $\cos\hat{\beta}$ and $1/\sin^2\hat{\beta}$ have been omitted from α, β, γ and Λ, respectively.

In all these cases we find that the spread of the parameters α, β, γ is less than one order of magnitude, much less than the one among the charged lepton masses. This statement requires a specification since, from the matrix of charged lepton Yukawa couplings, eq. (5.24), for α, β, γ of the same order and generic VEVs φ_i ($i = 1, 2, 3$), there is no evident preferred pattern of eigenvalues. Indeed, though the best fit values of α, β, γ are of the same order, some amount of tuning is needed to correctly reproduce the masses. This can be appreciated from eq. (5.25), the unrealistic case of diagonal $\mathcal{Y}_e$. Indeed, close to our best fit point, the combinations $\alpha + 4\gamma$, $\alpha - \beta - 2\gamma$ and $\alpha + \beta - 2\gamma$ are of order 1, 0.01 and 10 respectively, revealing a hidden conspiracy of the input parameters. Our approach and the related results significantly differ from those of

refs. [189, 190] where several modular invariant models at level 5 have been analysed, under the assumption that the charged lepton sector be always diagonal [189] or diagonal when depending on ordinary flavons [190]. We have also looked for a better agreement with data in the seesaw case by relaxing the requirement of a real (φ_2, φ_3). At the price of more parameters, we obtain an better fit to data, though we do not present this example explicitly.

5.5 Chapter Summary

Modular invariance has been proven to offer a promising framework to describe lepton masses and mixing angles. In minimal models masses, mixing angles and phases are all predicted in terms of the modulus in addition to a few free parameters. Despite these nice features, neutrinos and charged leptons typically require different realizations to reproduce the sizeable hierarchy among electron, muon and tau masses. In most of the existing models RH leptons are assign to singlets of the modular group to allow a sufficient number of free parameters, tuned to match the charged lepton masses. We think that this aspect might indicate the need for a different description, perhaps in terms of other moduli than the one controlling the neutrino sector. In a simple-minded approach, not aiming at a fundamental description but rather to test the ground for a more extensive analysis, we have explored alternative realisations of the charged lepton sector in modular invariant models at levels 4 and 5.

At level 4 we have shown that it is possible to ascribe the charged lepton mass hierarchy to the weight difference in the right handed sector, similar to what occurs in Froggatt-Nielsen (FN) models, wherein the role of the weights is played by the charges. At level 5 we have assigned both RH and LH leptons to irreducible triplets of the finite modular group Γ_5. Moreover we have shown that also at level 5 the three parameters required to describe charged lepton masses can be almost within the same order of magnitude, though requiring some degree of tuning. In all models considered here we do not need a strong hierarchy at the level of Lagrangian parameters to reproduce charged lepton masses.

We built several models along these lines, analysing neutrino masses coming either from the Weinberg operator or from a type I seesaw, and we have selected seven scenarios which produce a reasonable fit to data, four of them at level 4 and three at level 5. We looked for minimal realisations, in terms of the lowest possible number of free parameters. Among them we also count the vacuum expectation values of both modulus and flavons, which we varied in order to maximise the agreement with the data. Three parameters are in a one-to-one relation with the charged lepton masses. Besides them, all of our scenarios make use of five parameters, always including an overall scale Λ, and real and imaginary parts of τ. In these cases we get four predictions: the absolute neutrino mass scale and all CP violating phases, which allow one to pin down the value of m_{ee}, relevant to neutrinoless double beta decay. So far few models based on modular invariance perform better, managing to fit the neutrino data with four free parameters. In all cases analysed at level 5 and in two cases at level 4 we demanded that the Lagrangian be CP conserving. A common feature of level 4 and 5 scenarios is that inverted ordering for

neutrino masses is predicted when adopting the Weinberg operator and normal ordering when making use of type I seesaw, with a single exception whose $\chi^2_{\text{min, red}}$ is not particularly good. At level 4 the overall results and predictions are quite stable with respect to the details of the model, only depending on the choice between the Weinberg operator and the seesaw mechanism. In both cases the neutrino mass spectrum is nearly degenerate and the lightest neutrino mass is around 40 meV. At level 5 we get an excellent $\chi^2_{\text{min, red}}$ only when considering neutrino masses generated by the Weinberg operator, predicting inverted MO. In the seesaw scenario a good fit requires the introduction of additional parameters. Remarkably we find that our seesaw models at level 5 predict a massless neutrino.

A weak point of our construction is the correct vacuum selection. We have not attempted to dynamically select the vacuum configurations in the symmetry breaking sector, while our results, relying on ordinary flavons besides the modular parameter, require a specific vacuum alignment. We have treated the VEVs as free parameters, to be varied to match the experimental data. The VEV pattern suggested by data is peculiar and points to a nontrivial vacuum selection mechanism, where such an elucidation goes beyond the scope of this chapter. We do not consider our results conclusive and we think that there is still a considerable room to improve the characterization of the charged lepton sector. Nevertheless, by exploring some nonstandard possibilities, we hope to have provided some new element for the identification of a basic framework.

Chapter 6

Modular Symmetry with Natural Fermion Masses

In the previous chapter, we studied models of neutrino masses in the framework of modular symmetry. In particular, we focused on models in which the charged lepton masses were described by natural parameters. In this chapter, we will consider a further step in this direction, and describe all fermion (both lepton and quark) masses using natural parameters in the framework of modular symmetry.

6.1 Introduction

The origin of the three families of quarks and leptons and their extreme range of masses remains a mystery of particle physics. According to the SM, quarks and leptons come in complete families that interact identically with the gauge forces, leading to a remarkably successful quantitative theory describing practically all data at the quantum level. The various quark and lepton masses are described by having different interaction strengths with the Higgs doublet, also leading to quark mixing and charge-parity (CP) violating transitions involving strange, bottom and charm quarks. However, the SM provides no understanding of the pattern of quark and lepton masses, quark mixing or CP violation.

The discovery of neutrino mass and mixing makes the flavour puzzle hard to ignore, with the fermion mass hierarchy now spanning at least 12 orders of magnitude, from the neutrino to the top quark. However, it is not only the fermion mass hierarchy that is unsettling. There are now 28 free parameters in a Majorana-extended SM, of which 22 are associated with flavour, surely too many for a fundamental theory of nature. While the quark mixing angles are small, the lepton sector has two large mixing angles θ_{12}, θ_{23} and one small mixing angle θ_{13} which is of the same order of magnitude as the quark Cabibbo mixing angle [199].

One early attempt to understand the quark and lepton mass hierarchies is the FN mechanism [200]. This approach assumes an additional $U(1)_{FN}$ symmetry under which the quarks and leptons carry various charges and a cut-off scale M_{FN} is associated with the breaking of the

$U(1)_{FN}$ symmetry. In the SM the top quark mass of 173 GeV is given by a Yukawa coupling times the Higgs vacuum expectation value of 246 GeV divided by the square root of two. This implies a top quark Yukawa coupling close to unity. From this point of view, the top quark mass is not at all puzzling - it is the other fermion masses associated with much smaller Yukawa couplings that require explanation. According to FN, the fermions are assigned various $U(1)_{FN}$ charges and small Yukawa couplings are forbidden at the renormalisable level due to the $U(1)_{FN}$ symmetry. The symmetry is broken by the vacuum expectation value of a new "flavon" field θ, where θ is a neutral scalar under the SM but carries one unit of $U(1)_{FN}$ charge. Small effective Yukawa couplings then originate from non-renormalisable contact operators where the fermion charges are compensated by powers of θ, leading to suppression by powers of the small ratio $\langle\theta\rangle/M_{fl}$ (where M_{fl} acts as a cut-off scale of the contact interaction).

To account for family replication and to address the question of large lepton mixing, theorists have explored a larger non-Abelian family symmetry, $SU(3)_{fl}$ [201], where the three families are analogous to the three quark colours in quantum chromodynamics (QCD). Many other examples have been proposed based on subgroups of $SU(3)_{fl}$, including non-abelian discrete flavour symmetry (for reviews see e.g. [6, 12, 167, 168, 170, 171, 202]). Moreover, the leptonic CP violation phases can be predicted and the precisely measured quark CKM mixing matrix can be accommodated if the discrete flavour symmetry is combined with generalized CP symmetry [203–206]. However the main drawback of all such approaches that the flavour symmetry must be broken down to different subgroups in the neutrino and charged lepton sectors at low energy and this requires flavon fields to obtain vacuum expectation values (VEVs) along specific directions in order to reproduce phenomenologically viable lepton mixing angles. As a consequence, the scalar potential of discrete flavour symmetry models is rather elaborate, and auxiliary abelian symmetries are usually needed to forbid dangerous operators.

Recently, modular symmetry has been suggested as the origin of flavour symmetry, with neutrino masses as complex analytic functions called modular forms [174]. The starting point of this novel idea is that non-Abelian discrete family symmetries may arise from superstring theory in compactified extra dimensions, as a finite subgroup of the modular symmetry of such theories (i.e. the symmetry associated with the non-unique choice of basis vectors spanning a given extra-dimensional lattice). It follows that the 4D effective Lagrangian must respect modular symmetry. This implies that Yukawa couplings may be modular forms. So if the leptons transform as triplets under some finite modular symmetry, then the Yukawa couplings must transform nontrivially under the modular symmetry and they are modular forms which are holomorphic functions of a complex modulus field τ [174]. At a stroke, this removes the need for flavon fields and ad hoc vacuum alignments to break the family symmetry, and potentially greatly simplifies the particle content of the theory. Moreover, all higher-dimensional operators in the superpotential are completely determined by modular invariance if SUSY is exact. Models with modular flavour symmetry can be highly predictive; the neutrino masses and mixing parameters can be predicted in terms of few input parameters, although the predictive power of this framework may be reduced by the Kähler potential which is less constrained by modular symmetry [207].

The finite modular groups $\Gamma_2 \cong S_3$ [180, 181, 194, 208], $\Gamma_3 \cong A_4$ [174, 180–185, 191, 209, 210], $\Gamma_4 \cong S_4$ [4, 186, 187, 210, 211] and $\Gamma_5 \cong A_5$ [4, 189, 190] have been considered. For example, simple A_4 modular models can reproduce the measured neutrino masses and mixing angles[174, 183, 185]. The quark masses and mixing angles may also be included together with leptons in an A_4 modular invariant model [192]. The modular invariance approach has been extended to include odd weight modular forms which can be decomposed into irreducible representations of the the homogeneous finite modular group Γ'_N [195], and the modular symmetry $\Gamma'_3 \cong T'$ has been discussed, including the new possibility of texture zeroes [212]. Also modular symmetry may be combined with generalized CP symmetry, where the modulus transforms as $\tau \to -\tau^*$ under the CP transformation [155, 175, 176, 213, 214]. The formalism of the single modulus has been generalized to the case of a direct product of multiple moduli [178, 188], which is motivated by the additional extra dimensions in superstring theory, assuming toroidal compactification. Indeed, from a top-down perspective, modular symmetry naturally appears in string constructions [176, 177, 179, 215, 216].

It has been realised that, if the VEV of the modulus τ takes some special value, a residual subgroup of the finite modular symmetry group Γ_N would be preserved. The phenomenological implications of the residual modular symmetry have been discussed in the context of modular A_4 [184, 210], S_4 [187, 210] and A_5 [189] symmetries. If the modular symmetry is broken down to a residual Z_3 (or Z_5) subgroup in charged lepton sector and to a Z_2 subgroup in the neutrino sector, the trimaximal TM1 and TM2 mixing patterns can be obtained [184, 187].

In this chapter, we show how fermion mass hierarchies can be reproduced in the framework of modular symmetry. The mechanism is analogous to the FN mechanism, but without requiring any Abelian symmetry to be introduced, nor any SM singlet flavon to break it. The modular weights of fermion fields play the role of FN charges, and a SM singlet field ϕ with non-zero modular weight (called a "weighton") plays the role of a flavon. We illustrate the mechanism with modular level 3 (A_4) models of quark and lepton (including neutrino) masses and mixing, using a single modulus field τ and where the charged fermion mass hierarchies originate from a single weighton ϕ. We discuss two such viable models in some detail, both numerically and analytically, showing how both fermion mass and mixing hierarchies emerge from the modular symmetry. The class of modular level 3 (with even weight modular forms) examples of the mechanism we present here is by no means exhaustive; the new mechanism may be be applied to other levels and choices of weights, and to models with any number of moduli fields and weightons.

We also remark that the approach here differs from an early work based on $U(1)_{FN}$ broken by a flavon θ, where all fields carried both FN charge and modular weight [154]. In our approach, the Yukawa couplings are modular forms, which means that the modular weights do not have to sum to zero, and are triplets under the A_4 modular symmetry, which constrains the rows of the Yukawa matrices. We also emphasise that we do not have any $U(1)_{FN}$ symmetry, nor any flavon θ to break such a symmetry. Our weighton ϕ is an A_4 singlet which does not break any flavour symmetry and is therefore not a flavon.

6.2 Modular Symmetry

The modular group $\overline{\Gamma}$ is the group of linear fraction transformations which acts on the complex modulus τ in the upper half complex plane as follow,

$$\tau \to \gamma\tau = \frac{a\tau+b}{c\tau+d}, \quad \text{with} \quad a,b,c,d \in \mathbb{Z}, \quad ad-bc=1, \quad \text{Im}\,\tau > 0\,. \tag{6.1}$$

We note that the map

$$\frac{a\tau+b}{c\tau+d} \mapsto \begin{pmatrix} a & b \\ c & d \end{pmatrix} \tag{6.2}$$

is an isomorphism from the modular group to the projective matrix group $PSL(2,\mathbb{Z}) \cong SL(2,\mathbb{Z})/\{\pm I\}$, where $SL(2,\mathbb{Z})$ is the group of two-by-two matrices with integer entries and determinant equal to one.

The modular group $\overline{\Gamma}$ can be generated by two generators S and T

$$S : \tau \mapsto -\frac{1}{\tau}, \qquad T : \tau \mapsto \tau + 1\,, \tag{6.3}$$

which are represented by the following two matrices of $PSL(2,\mathbb{Z})$,

$$S = \begin{pmatrix} 0 & 1 \\ -1 & 0 \end{pmatrix}, \qquad T = \begin{pmatrix} 1 & 1 \\ 0 & 1 \end{pmatrix}\,. \tag{6.4}$$

We can check that the generators S and T obey the relations,

$$S^2 = (ST)^3 = (TS)^3 = 1\,. \tag{6.5}$$

The principal congruence subgroup of level N is the subgroup

$$\Gamma(N) = \left\{ \begin{pmatrix} a & b \\ c & d \end{pmatrix} \in SL(2,\mathbb{Z}),\ b = c = 0\,(\text{mod N}), a = d = 1\,(\text{mod N}) \right\}\,, \tag{6.6}$$

which is an infinite normal subgroup of $SL(2,\mathbb{Z})$. It is easy to see that T^N is an element of $\Gamma(N)$. The projective principal congruence subgroup is defined as $\overline{\Gamma}(N) = \Gamma(N)/\{\pm I\}$ for $N = 1, 2$. For the values of $N \geq 3$, we have $\overline{\Gamma}(N) = \Gamma(N)$ because $\Gamma(N)$ doesn't contain the element $-I$. The quotient group $\Gamma_N \equiv \overline{\Gamma}/\overline{\Gamma}(N)$ is the finite modular group, and it can be obtained by further imposing the condition $T^N = 1$ besides those in Eq. (6.5).

A crucial element of the modular invariance approach is the modular form $f(\tau)$ of weight k and level N. The modular form $f(\tau)$ is a holomorphic function of the complex modulus τ and it

is required to transform under the action of $\overline{\Gamma}(N)$ as follows,

$$f\left(\frac{a\tau+b}{c\tau+d}\right)=(c\tau+d)^k f(\tau) \quad \text{for} \quad \forall \begin{pmatrix} a & b \\ c & d \end{pmatrix} \in \overline{\Gamma}(N)\,. \tag{6.7}$$

The modular forms of weight k and level N span a linear space of finite dimension. It is always possible to choose a basis in this linear space such that the modular forms can be arranged into some modular multiplets $f_{\mathbf{r}} \equiv (f_1(\tau), f_2(\tau), ...)^T$ which transform as irreducible representation $\mathbf{r}$ of the finite modular group Γ_N for even k [174, 195], i.e.

$$f_{\mathbf{r}}(\gamma\tau)=(c\tau+d)^k \rho_{\mathbf{r}}(\gamma) f_{\mathbf{r}}(\tau) \quad \text{for} \quad \forall\, \gamma \in \overline{\Gamma}\,, \tag{6.8}$$

where γ is the representative element of the coset $\gamma\overline{\Gamma}(N)$ in Γ_N, and $\rho_{\mathbf{r}}(\gamma)$ is the representation matrix of the element γ in the irreducible representation $\mathbf{r}$.

The superpotential $W(\Phi_I, \tau)$ can be expanded in power series of the supermultiplets Φ_I,

$$W(\Phi_I,\tau)=\sum_n Y_{I_1...I_n}(\tau)\ \Phi_{I_1}...\Phi_{I_n}\,, \tag{6.9}$$

where $Y_{I_1...I_n}$ is a modular multiplet of weight k_Y and it transforms in the representation ρ_Y of Γ_N,

$$\begin{aligned} &\tau \to \gamma\tau = \frac{a\tau+b}{c\tau+d}\,, \\ &Y(\tau) \to Y(\gamma\tau) = (c\tau+d)^{k_Y}\rho_Y(\gamma) Y(\tau)\,. \end{aligned} \tag{6.10}$$

The requirement of modular invariance of the superpotential implies

$$k_Y = k_{I_1} + ... + k_{I_n}, \qquad \rho_Y \otimes \rho_{I_1} \otimes \ldots \otimes \rho_{I_n} \ni \mathbf{1}\,. \tag{6.11}$$

where the supermultiplet Φ_{I_1} is assumed to transform in a representation ρ_{I_1} of Γ_N, with a modular weight $-k_{I_1}$, and so on for the other supermultiplets.

6.3 Modular Forms of $\Gamma_3 \cong A_4$ (Level 3)

The modular group $\Gamma(3)$ has been extensively studied in the literature [174, 180–184, 191, 209, 210]. In the present work we shall adopt the same convention as [174, 185, 210]. The finite modular group Γ_3 is isomorphic to A_4 which is the symmetry group of the tetrahedron. It contains twelve elements and it is the smallest non-abelian finite group which admits an irreducible three-dimensional representation. The A_4 group has three one-dimensional representations $\mathbf{1}$, $\mathbf{1}'$, $\mathbf{1}''$

and a three-dimensional representation **3**. In the singlet representations, we have

$$\begin{aligned} &\mathbf{1}: \quad S=1, \qquad T=1\,, \\ &\mathbf{1}': \quad S=1, \qquad T=\omega^2\,, \\ &\mathbf{1}'': \quad S=1, \qquad T=\omega\,. \end{aligned} \tag{6.12}$$

For the representation **3**, we will choose a basis in which the generator T is diagonal. The explicit forms of S and T are

$$S=\frac{1}{3}\begin{pmatrix} -1 & 2 & 2 \\ 2 & -1 & 2 \\ 2 & 2 & -1 \end{pmatrix}, \qquad T=\begin{pmatrix} 1 & 0 & 0 \\ 0 & \omega^2 & 0 \\ 0 & 0 & \omega \end{pmatrix}, \tag{6.13}$$

with $\omega=e^{2\pi i/3}=-1/2+i\sqrt{3}/2$. The basic multiplication rule is

$$\mathbf{3}\otimes\mathbf{3}=\mathbf{1}\oplus\mathbf{1}'\oplus\mathbf{1}''\oplus\mathbf{3}_S\oplus\mathbf{3}_A\,, \tag{6.14}$$

where the subscripts S and A denotes symmetric and antisymmetric combinations respectively. If we have two triplets $\alpha=(\alpha_1,\alpha_2,\alpha_3)\sim\mathbf{3}$ and $\beta=(\beta_1,\beta_2,\beta_3)\sim\mathbf{3}$, we can obtain the following irreducible representations from their product,

$$\begin{aligned} &(\alpha\beta)_{\mathbf{1}}=\alpha_1\beta_1+\alpha_2\beta_3+\alpha_3\beta_2\,, \\ &(\alpha\beta)_{\mathbf{1}'}=\alpha_3\beta_3+\alpha_1\beta_2+\alpha_2\beta_1\,, \\ &(\alpha\beta)_{\mathbf{1}''}=\alpha_2\beta_2+\alpha_1\beta_3+\alpha_3\beta_1\,, \\ &(\alpha\beta)_{\mathbf{3}_S}=(2\alpha_1\beta_1-\alpha_2\beta_3-\alpha_3\beta_2, 2\alpha_3\beta_3-\alpha_1\beta_2-\alpha_2\beta_1, 2\alpha_2\beta_2-\alpha_1\beta_3-\alpha_3\beta_1)\,, \\ &(\alpha\beta)_{\mathbf{3}_A}=(\alpha_2\beta_3-\alpha_3\beta_2, \alpha_1\beta_2-\alpha_2\beta_1, \alpha_3\beta_1-\alpha_1\beta_3)\,. \end{aligned} \tag{6.15}$$

The linear space of the modular forms of integral weight k and level $N=3$ has dimension $k+1$ [174]. The modular space $\mathcal{M}_{2k}(\Gamma(3))$ can be constructed from the Dedekind eta-function $\eta(\tau)$ which is defined as

$$\eta(\tau)=q^{1/24}\prod_{n=1}^{\infty}(1-q^n), \qquad q=e^{2\pi i\tau}\,. \tag{6.16}$$

The Dedekind eta-function $\eta(\tau)$ satisfies the following identities

$$\eta(\tau+1)=e^{i\pi/12}\eta(\tau), \qquad \eta(-1/\tau)=\sqrt{-i\tau}\;\eta(\tau)\,. \tag{6.17}$$

There are only three linearly independent modular forms of weight 2 and level 3, which are denoted as $Y_i(\tau)$ with $i=1,2,3$. We can arrange the three modular functions into a vector $Y^{(2)}_{\mathbf{3}}=(Y_1,Y_2,Y_3)^T$ transforming as a triplet **3** of A_4. The modular forms Y_i can be expressed in

terms of $\eta(\tau)$ and its derivative as follow [174]:

$$\begin{aligned}
Y_1(\tau) &= \frac{i}{2\pi}\left[\frac{\eta'(\tau/3)}{\eta(\tau/3)}+\frac{\eta'((\tau+1)/3)}{\eta((\tau+1)/3)}+\frac{\eta'((\tau+2)/3)}{\eta((\tau+2)/3)}-\frac{27\eta'(3\tau)}{\eta(3\tau)}\right], \\
Y_2(\tau) &= \frac{-i}{\pi}\left[\frac{\eta'(\tau/3)}{\eta(\tau/3)}+\omega^2\frac{\eta'((\tau+1)/3)}{\eta((\tau+1)/3)}+\omega\frac{\eta'((\tau+2)/3)}{\eta((\tau+2)/3)}\right], \\
Y_3(\tau) &= \frac{-i}{\pi}\left[\frac{\eta'(\tau/3)}{\eta(\tau/3)}+\omega\frac{\eta'((\tau+1)/3)}{\eta((\tau+1)/3)}+\omega^2\frac{\eta'((\tau+2)/3)}{\eta((\tau+2)/3)}\right].
\end{aligned} \tag{6.18}$$

The q-expansions of the triplet modular forms $Y^{(2)}_{\mathbf{3}}$ are given by

$$Y^{(2)}_{\mathbf{3}} = \begin{pmatrix} Y_1(\tau) \\ Y_2(\tau) \\ Y_3(\tau) \end{pmatrix} = \begin{pmatrix} 1+12q+36q^2+12q^3+84q^4+72q^5+\ldots \\ -6q^{1/3}(1+7q+8q^2+18q^3+14q^4+\ldots) \\ -18q^{2/3}(1+2q+5q^2+4q^3+8q^4+\ldots) \end{pmatrix}. \tag{6.19}$$

They satisfy the constraint [174]

$$(Y^{(2)}_{\mathbf{3}}Y^{(2)}_{\mathbf{3}})_{\mathbf{1}''} \equiv Y_2^2+2Y_1Y_3 = 0\,. \tag{6.20}$$

Multiplets of higher weight modular forms can be constructed from the tensor products of $Y^{(2)}_{\mathbf{3}}$.

Using the A_4 contraction $\mathbf{3}\otimes\mathbf{3} = \mathbf{1}\oplus\mathbf{1}'\oplus\mathbf{1}''\oplus\mathbf{3}_S\oplus\mathbf{3}_A$, we can obtain five independent weight 4 modular forms,

$$\begin{aligned}
&Y^{(4)}_{\mathbf{1}} = Y_1^2+2Y_2Y_3 \sim \mathbf{1}, \\
&Y^{(4)}_{\mathbf{1}'} = Y_3^2+2Y_1Y_2 \sim \mathbf{1}', \\
&Y^{(4)}_{\mathbf{3}} = \begin{pmatrix} Y^{(4)}_1 \\ Y^{(4)}_2 \\ Y^{(4)}_3 \end{pmatrix} = \begin{pmatrix} Y_1^2-Y_2Y_3 \\ Y_3^2-Y_1Y_2 \\ Y_2^2-Y_1Y_3 \end{pmatrix} \sim \mathbf{3}\,.
\end{aligned} \tag{6.21}$$

Similarly there are seven modular forms of weight 6, which can be decomposed as $\mathbf{1}\oplus\mathbf{3}\oplus\mathbf{3}$

	L	e^c_3	e^c_2	e^c_1	N^c	$H_{u,d}$
A_4	$\mathbf{3}$	$\mathbf{1'}$	$\mathbf{1''}$	$\mathbf{1}$	$\mathbf{3}$	$\mathbf{1}$
k_I	1	1	1	1	1	0

Table 6.1: The Feruglio model of leptons, where each supermultiplet has a modular weight $-k_I$.

under A_4 [174],

$$\begin{aligned} Y^{(6)}_{\mathbf{1}} &= Y_1^3 + Y_2^3 + Y_3^3 - 3Y_1Y_2Y_3 \sim \mathbf{1}\,, \\ Y^{(6)}_{\mathbf{3},I} &= \begin{pmatrix} Y^{(6)}_{1,I} \\ Y^{(6)}_{2,I} \\ Y^{(6)}_{3,I} \end{pmatrix} = \begin{pmatrix} Y_1^3 + 2Y_1Y_2Y_3 \\ Y_1^2Y_2 + 2Y_2^2Y_3 \\ Y_1^2Y_3 + 2Y_3^2Y_2 \end{pmatrix}\,, \\ Y^{(6)}_{\mathbf{3},II} &= \begin{pmatrix} Y^{(6)}_{1,II} \\ Y^{(6)}_{2,II} \\ Y^{(6)}_{3,II} \end{pmatrix} = \begin{pmatrix} Y_3^3 + 2Y_1Y_2Y_3 \\ Y_3^2Y_1 + 2Y_1^2Y_2 \\ Y_3^2Y_2 + 2Y_2^2Y_1 \end{pmatrix}\,. \end{aligned} \tag{6.22}$$

It has been realised that, if the VEV of the modulus τ takes some special value, a residual subgroup of the finite modular symmetry group Γ_3 would be preserved. Thus, the fixed points $\tau_S = i$, $\tau_{ST} = (-1+i\sqrt{3})/2$, $\tau_{TS} = (1+i\sqrt{3})/2$, $\tau_T = i\infty$ in the fundamental domain are invariant under modular transformations, and there are many other examples in the upper half complex plane [210]. For example, $\tau_T = i\infty$ implies $Y^{(2)}_{\mathbf{3}} \propto (1,0,0)^T$, $Y^{(4)}_{\mathbf{3}} \propto (1,0,0)^T$, $Y^{(6)}_{\mathbf{3},I} \propto (1,0,0)^T$, $Y^{(6)}_{\mathbf{3},II} \propto (0,0,0)^T$.

6.4 Models with $\Gamma_3 \cong A_4$ (Level 3)

6.4.1 The Feruglio Model of Leptons

In this subsection we review an example of a model of lepton masses and mixing based on A_4 modular symmetry, first introduced as example 3 in [174] and later reanalysed in the light of current data in [185]. In this example, there is no flavon field other than the modulus τ. The Higgs doublets H_u and H_d are assumed to transform as $\mathbf{1}$ under A_4 and their modular weights k_{H_u,H_d} are vanishing. The neutrino masses are assumed arise from the type I seesaw mechanism. In this example [174], the three generations of LH lepton doublets $L \equiv (L_1, L_2, L_3)^T$ and of the CP conjugated RH neutrino $N^c \equiv (N^c_1, N^c_2, N^c_3)^T$ are organised into two triplets $\mathbf{3}$ of A_4 with modular weights denoted as k_L and k_N, which will be fixed to take the values of unity shown in Table 6.1.

When the three CP conjugated RH charged leptons $e^c_{3,2,1}$ are assigned to three different singlets $\mathbf{1'}$, $\mathbf{1''}$ and $\mathbf{1}$ of A_4 as in previous works [174, 180–184, 191], their modular weights could

be identical, which will be fixed to take the values of unity as shown in Table 6.1, and only the lowest weight modular form $Y_{\mathbf{3}}^{(2)}$ is necessary in the minimal model.

Then the superpotential for the charged lepton masses takes the form

$$\begin{aligned} W_e &= \alpha e_1^c (L Y_{\mathbf{3}}^{(2)})_{\mathbf{1}} H_d + \beta e_2^c (L Y_{\mathbf{3}}^{(2)})_{\mathbf{1}'} H_d + \gamma e_3^c (L Y_{\mathbf{3}}^{(2)})_{\mathbf{1}''} H_d \\ &= \alpha e_1^c (L_1 Y_1 + L_2 Y_3 + L_3 Y_2) H_d + \beta e_2^c (L_3 Y_3 + L_1 Y_2 + L_2 Y_1) H_d \\ &\quad + \gamma e_3^c (L_2 Y_2 + L_3 Y_1 + L_1 Y_3) H_d \,. \end{aligned} \tag{6.23}$$

The invariance of W_e under modular transformations implies the following relations for the weights,

$$\begin{cases} k_{e_1} + k_L = 2 \,, \\ k_{e_2} + k_L = 2 \,, \\ k_{e_3} + k_L = 2 \,, \end{cases} \tag{6.24}$$

which implies

$$k_{e_1} = k_{e_2} = k_{e_3} = 2 - k_L \,, \tag{6.25}$$

where all values are fixed to be unity as shown in Table 6.1. This is exactly the case considered in the literature [174, 180–184, 191]. We can straightforwardly read out the charged lepton Yukawa matrix

$$Y_e = \begin{pmatrix} \alpha\, Y_1 & \alpha\, Y_3 & \alpha\, Y_2 \\ \beta Y_2 & \beta Y_1 & \beta Y_3 \\ \gamma Y_3 & \gamma Y_2 & \gamma Y_1 \end{pmatrix} \tag{6.26}$$

For example, $\tau_T = i\infty$ implies $Y_{\mathbf{3}}^{(2)} \propto (1,0,0)^T$, leads to a diagonal charged lepton Yukawa matrix with $m_e : m_\mu : m_\tau = \alpha : \beta : \gamma$. The charged lepton mass hierarchies are accounted for in the Feruglio model by tuning the parameters to be $\alpha \ll \beta \ll \gamma$.

If neutrino masses are generated through the type-I seesaw mechanism, for the triplet assignments of both RH neutrinos N^c and LH lepton doublets L, the most general form of the superpotential in the neutrino sector is

$$W_\nu = g \left(N^c L H_u f_N(Y)\right)_{\mathbf{1}} + \Lambda \left(N^c N^c f_M(Y)\right)_{\mathbf{1}} \,, \tag{6.27}$$

where $f_N(Y)$ and $f_M(Y)$ are generic functions of the modular forms $Y(\tau)$. Motivated by the principle of minimality, we consider the following example: $f_N(Y) \propto Y_{\mathbf{3}}^{(2)}$ and $f_M(Y) \propto Y_{\mathbf{3}}^{(2)}$,

which implies,

$$\begin{aligned}
W_\nu &= g_1((N^c\,L)_{\mathbf{3}_S}Y^{(2)}_{\mathbf{3}})_{\mathbf{1}}H_u + g_2((N^c\,L)_{\mathbf{3}_A}Y^{(2)}_{\mathbf{3}})_{\mathbf{1}}H_u + \Lambda((N^cN^c)_{\mathbf{3_S}}\,Y^{(2)}_{\mathbf{3}})_{\mathbf{1}} \\
&= g_1\big[(2N^c_1L_1 - N^c_2L_3 - N^c_3L_2)Y_1 + (2N^c_3L_3 - N^c_1L_2 - N^c_2L_1)Y_3 \\
&\quad + (2N^c_2L_2 - N^c_3L_1 - N^c_1L_3)Y_2\big]H_u + g_2\big[(N^c_2L_3 - N^c_3L_2)Y_1 + (N^c_1L_2 - N^c_2L_1)Y_3 \\
&\quad + (N^c_3L_1 - N^c_1L_3)Y_2\big]H_u + 2\Lambda\big[(N^c_1N^c_1 - N^c_2N^c_3)Y_1 + (N^c_3N^c_3 - N^c_1N^c_2)Y_3 \\
&\quad + (N^c_2N^c_2 - N^c_1N^c_3)Y_2\big]\,. \qquad (6.28)
\end{aligned}$$

The modular weights of N^c and L correspond to $k_L = k_N = 1$ as shown in Table 6.1.

We find M_D and M_N take the following form

$$M_N = \begin{pmatrix} 2Y_1 & -Y_3 & -Y_2 \\ -Y_3 & 2Y_2 & -Y_1 \\ -Y_2 & -Y_1 & 2Y_3 \end{pmatrix}\Lambda\,,$$

$$M_D = \begin{pmatrix} 2g_1Y_1 & (-g_1+g_2)Y_3 & (-g_1-g_2)Y_2 \\ (-g_1-g_2)Y_3 & 2g_1Y_2 & (-g_1+g_2)Y_1 \\ (-g_1+g_2)Y_2 & (-g_1-g_2)Y_1 & 2g_1Y_3 \end{pmatrix}v_u\,. \qquad (6.29)$$

The light neutrino mass matrix is given by the seesaw formula,

$$M_\nu \;=\; -M_D^T M_N^{-1} M_D\,. \qquad (6.30)$$

This is the original Feruglio model introduced as example 3 in [174], corresponding to the case of $\mathcal{D}_{10}$ in [185], giving an excellent fit to current experimental data. The best fit (allowed range) of the modulus for $\mathcal{D}_{10}$ in [185] is: $\mathrm{Re}\,\langle\tau\rangle = 0.0386(0.0307 \sim 0.1175)$, $\mathrm{Im}\,\langle\tau\rangle = 2.230(1.996 \sim 2.50)$, which approximates the fixed point case $\tau_T = i\infty$, since the real part is much less than the imaginary part.

6.4.2 A Natural Model of Charged Leptons

In this subsection we show how Feruglio's A_4 modular model of charged leptons can be recast in natural form by introducing a single weighton. The neutrino sector will remain unchanged to leading order. The resulting model of leptons shown in Table 6.2 now involves a single "weighton" ϕ which is defined to be a SM and A_4 singlet field with $k_\phi = 1$ (i.e. weight -1). We show how such a model can generate a natural charged lepton mass hierarchy. In the next subsection we extend the idea to the quark sector, thereby explaining all charged fermion masses naturally.

The three RH charged leptons $e^c_{3,2,1}$ are assigned to three different singlets $\mathbf{1'}$, $\mathbf{1''}$ and $\mathbf{1}$ of A_4 as before but now their their modular weights are not identical, and correspond to $k_{e^c_{3,2,1}} = 0, -1, -3$

	L	e^c_3	e^c_2	e^c_1	N^c	$H_{u,d}$	ϕ
A_4	$\mathbf{3}$	$\mathbf{1'}$	$\mathbf{1''}$	$\mathbf{1}$	$\mathbf{3}$	$\mathbf{1}$	$\mathbf{1}$
k_I	1	0	-1	-3	1	0	1

Table 6.2: A natural A_4 model of leptons with a weighton ϕ. Note that each supermultiplet has a modular weight $-k_I$.

(i.e. weights $0, 1, 3$) such that powers of ϕ with $k_\phi = 1$ are required compensate the terms in the previous model, with the combinations $e^c_3\phi, e^c_2\phi^2, e^c_1\phi^4$ each having combined weights of unity as before. The weighton ϕ is assumed to develop a vacuum expectation value (vev) so that the corresponding terms are suppressed by powers of

$$\tilde{\phi} \equiv \frac{\langle\phi\rangle}{M_{fl}}, \tag{6.31}$$

where M_{fl} is a dimensionful cut-off flavour scale. This generates the charged lepton mass hierarchy naturally, with $m_{\tau,\mu,e} \propto \tilde{\phi}, \tilde{\phi}^2, \tilde{\phi}^4$, with only the lowest weight modular form $Y^{(2)}_{\mathbf{3}}$ being necessary as before.

After the weighton develops its vev, the superpotential for the charged lepton masses takes the form

$$\begin{aligned} W_e &= \alpha_e e^c_1 \tilde{\phi}^4 (LY^{(2)}_{\mathbf{3}})_{\mathbf{1}} H_d + \beta_e e^c_2 \tilde{\phi}^2 (LY^{(2)}_{\mathbf{3}})_{\mathbf{1'}} H_d + \gamma_e e^c_3 \tilde{\phi} (LY^{(2)}_{\mathbf{3}})_{\mathbf{1''}} H_d \\ &= \alpha_e e^c_1 \tilde{\phi}^4 (L_1Y_1 + L_2Y_3 + L_3Y_2) H_d + \beta_e e^c_2 \tilde{\phi}^2 (L_3Y_3 + L_1Y_2 + L_2Y_1) H_d \\ &\quad + \gamma_e e^c_3 \tilde{\phi} (L_2Y_2 + L_3Y_1 + L_1Y_3) H_d \,, \end{aligned} \tag{6.32}$$

which gives a charged lepton Yukawa matrix similar to Eq.6.26, except that it involves powers of $\tilde{\phi}$ controlling the hierarchies,

$$Y_e = \begin{pmatrix} \alpha_e\tilde{\phi}^4\, Y_1 & \alpha_e\tilde{\phi}^4\, Y_3 & \alpha_e\tilde{\phi}^4\, Y_2 \\ \beta_e\tilde{\phi}^2 Y_2 & \beta_e\tilde{\phi}^2 Y_1 & \beta_e\tilde{\phi}^2 Y_3 \\ \gamma_e\tilde{\phi} Y_3 & \gamma_e\tilde{\phi} Y_2 & \gamma_e\tilde{\phi} Y_1 \end{pmatrix} \tag{6.33}$$

For example, $\tau_T = i\infty$ implies $Y^{(2)}_{\mathbf{3}} \propto (1, 0, 0)^T$, leading to a diagonal and naturally hierarchical charged lepton Yukawa matrix with $m_e : m_\mu : m_\tau = \alpha_e\tilde{\phi}^4 : \beta_e\tilde{\phi}^2 : \gamma_e\tilde{\phi}$. The empirically observed

charged lepton mass ratios $m_e/m_\mu = 1/207$ and $m_\mu/m_\tau = 1/17$ suggest that we fix $\tilde{\phi} \approx 1/15$ to account for the charged lepton mass hierarchy, with the mass ratios $m_e/m_\mu \sim \tilde{\phi}^2$ and $m_\mu/m_\tau \sim \tilde{\phi}$, assuming order one coefficients $\alpha_e, \beta_e, \gamma_e \sim 1$. The small parameter $\tilde{\phi} \approx 1/15$ defined to to be the ratio of scales in Eq.6.31 now provides an explanation for the charged lepton mass hierarchies.

However now there will be additional terms corresponding to higher weight modular forms, $Y_{\mathbf{3}}^{(4)}$, compensated by extra powers of weighton fields ϕ, which will give corrections to the charged lepton superpotential,

$$\begin{aligned}\Delta W_e &= \alpha'_e e^c_1 \tilde{\phi}^6 (L Y_{\mathbf{3}}^{(4)})_{\mathbf{1}} H_d + \beta'_e e^c_2 \tilde{\phi}^4 (L Y_{\mathbf{3}}^{(4)})_{\mathbf{1}'} H_d + \gamma'_e e^c_3 \tilde{\phi}^3 (L Y_{\mathbf{3}}^{(4)})_{\mathbf{1}''} H_d \\ &= \alpha'_e e^c_1 \tilde{\phi}^6 (L_1 Y_1^{(4)} + L_2 Y_3^{(4)} + L_3 Y_2^{(4)}) H_d + \beta'_e e^c_2 \tilde{\phi}^4 (L_3 Y_3^{(4)} + L_1 Y_2^{(4)} + L_2 Y_1^{(4)}) H_d \\ &\quad + \gamma'_e e^c_3 \tilde{\phi}^3 (L_2 Y_2^{(4)} + L_3 Y_1^{(4)} + L_1 Y_3^{(4)}) H_d \,, \end{aligned} \tag{6.34}$$

where from Eq.6.21 the weight 4 Yukawa couplings are given in terms of the weight 2 Yukawa couplings,

$$Y_1^{(4)} = Y_1^2 - Y_2 Y_3, \quad Y_2^{(4)} = Y_3^2 - Y_1 Y_2, \quad Y_3^{(4)} = Y_2^2 - Y_1 Y_3. \tag{6.35}$$

This yields the additive correction to the charged lepton mass matrix in Eq.6.33,

$$\Delta Y_e = \begin{pmatrix} \alpha'_e \tilde{\phi}^6 \, Y_1^{(4)} & \alpha'_e \tilde{\phi}^6 \, Y_3^{(4)} & \alpha'_e \tilde{\phi}^6 \, Y_2^{(4)} \\ \beta'_e \tilde{\phi}^4 Y_2^{(4)} & \beta'_e \tilde{\phi}^4 Y_1^{(4)} & \beta'_e \tilde{\phi}^4 Y_3^{(4)} \\ \gamma'_e \tilde{\phi}^3 Y_3^{(4)} & \gamma'_e \tilde{\phi}^3 Y_2^{(4)} & \gamma'_e \tilde{\phi}^3 Y_1^{(4)} \end{pmatrix} \tag{6.36}$$

where $\alpha'_e, \beta'_e, \gamma'_e$ are new free complex coefficients (also assumed to be of order unity) while the weight 4 Yukawa couplings are given in Eq.6.35. For example, $\tau_T = i\infty$ implies $Y_{\mathbf{3}}^{(2)} \propto (1,0,0)^T$, implies that the higher order corrections also take the form of a diagonal charged lepton Yukawa matrix. However these are just the leading corrections. There will also be further corrections from even higher weight modular forms, such as $Y_{\mathbf{3}}^{(6)}$, compensated by extra powers of weighton fields ϕ, which will give further corrections to the charged lepton Yukawa matrix. However, since $\tilde{\phi} \approx 1/15$, we find all such corrections to be very suppressed, and have a negligible effect on the numerical results.

Since the modular weights of L and N^c are unchanged, and their representations are the same, we expect the seesaw neutrino matrices to be the same as in the original model at lowest order, where no weighton field ϕ appears and $f_N(Y) \propto Y_{\mathbf{3}}^{(2)}$ and $f_M(Y) \propto Y_{\mathbf{3}}^{(2)}$ as in Eq.6.28. Thus the seesaw matrices in this model are exactly the same as in Eq.6.29. However now there

	Q	d^c_3	d^c_2	d^c_1	u^c_3	u^c_2	u^c_1	$H_{u,d}$	ϕ
A_4	$\mathbf{3}$	$\mathbf{1'}$	$\mathbf{1''}$	$\mathbf{1}$	$\mathbf{1'}$	$\mathbf{1''}$	$\mathbf{1}$	$\mathbf{1}$	$\mathbf{1}$
k_I	1	$0,2,4$	-2	-3	$5,3,1$	$-1,2,4$	-3	0	1

Table 6.3: Natural A_4 models of quarks with a weighton ϕ. All 27 combinations of modular weights are considered in the text. Note that each supermultiplet has a modular weight $-k_I$.

will higher order corrections involving weightons, the leading correction being suppressed by $\tilde{\phi}^2$,

$$\begin{aligned}\Delta W_\nu &= g_1'\tilde{\phi}^2((N^c\,L)_{\mathbf{3}_S}Y^{(4)}_{\mathbf{3}})_{\mathbf{1}}H_u + g_2'\tilde{\phi}^2((N^c\,L)_{\mathbf{3}_A}Y^{(4)}_{\mathbf{3}})_{\mathbf{1}}H_u + \Lambda'\tilde{\phi}^2((N^cN^c)_{\mathbf{3_S}}\,Y^{(4)}_{\mathbf{3}})_{\mathbf{1}}\\
&= g_1'\tilde{\phi}^2\big[(2N^c_1L_1 - N^c_2L_3 - N^c_3L_2)Y^{(4)}_1 + (2N^c_3L_3 - N^c_1L_2 - N^c_2L_1)Y^{(4)}_3\\
&\quad + (2N^c_2L_2 - N^c_3L_1 - N^c_1L_3)Y^{(4)}_2\big]H_u\\
&\quad + g_2'\tilde{\phi}^2\big[(N^c_2L_3 - N^c_3L_2)Y^{(4)}_1 + (N^c_1L_2 - N^c_2L_1)Y^{(4)}_3 + (N^c_3L_1 - N^c_1L_3)Y^{(4)}_2\big]H_u\\
&\quad + 2\Lambda'\tilde{\phi}^2\big[(N^c_1N^c_1 - N^c_2N^c_3)Y^{(4)}_1 + (N^c_3N^c_3 - N^c_1N^c_2)Y^{(4)}_3 + (N^c_2N^c_2 - N^c_1N^c_3)Y^{(4)}_2\big]\,, \quad (6.37)\end{aligned}$$

which is of the same form as in Eq.6.28, yielding additive corrections to the seesaw matrices of the same form as in Eq.6.29 but suppressed by $\tilde{\phi}^2$ and with the primed Yukawa couplings given by Eq.6.35. As before, since $\tilde{\phi} \approx 1/15$, these corrections are expected to be about 0.5%, so in the neutrino sector we can safely ignore these corrections and use the same results as before. Thus we expect that the modulus best fit to point to be the same value quoted as before, approximating the fixed point case $\tau_T = i\infty$.

6.4.3 Natural Models of Quarks

Quarks have been considered with A_4 modular symmetry in [192]. However there has been no attempt to explain the quark mass hierarchy. Using similar ideas developed in the previous section for the charged leptons, we now consider models for the down type quark Yukawa matrix with $m_d : m_s : m_b \sim \tilde{\phi}^4 : \tilde{\phi}^3 : \tilde{\phi}$, which turns out to be a good description of the down quark mass hierarchies as we shall see. As in the charged lepton sector, the weighton is assumed to develop a vacuum expectation value (vev) so that the corresponding terms are suppressed by powers of $\tilde{\phi} = \langle\phi\rangle/M_{fl}$, where M_{fl} is a dimensionful cut-off flavour scale, which we assume to be the same scale as for the charged leptons.

We introduce the quark modular weights in Table 6.3 which can achieve this, using the same weighton ϕ as in the charged lepton sector. We assign the quark doublets Q to a triplet of A_4 with $k_Q = 1$ analogous to the lepton doublets. The three RH down type quarks $d^c_{3,2,1}$ are assigned to three different singlets $\mathbf{1'}$, $\mathbf{1''}$ and $\mathbf{1}$ of A_4, analogous to how the charged lepton Yukawa matrix was constructed.

Unlike in the charged lepton sector, here we allow higher weight modular forms in the quark

sector, which will prove necessary to describe quark mixing. We therefore have more freedom in assigning various modular weights to $d^c_{3,2,1}$ such that powers of ϕ with $k_\phi = 1$ are required compensate the terms, with the combinations $d^c_3\phi, d^c_2\phi^3, d^c_1\phi^4$ appearing, analogous to the charged lepton assignments. This generates the down type quark mass hierarchy naturally, with $m_{b,s,d} \propto \tilde{\phi}, \tilde{\phi}^3, \tilde{\phi}^4$.

After the weighton develops its VEV, the superpotential for the down type quark masses with $k_{d^c_{3,2,1}} = 0, -2, -3$ takes the form

$$\begin{aligned} W_d &= \alpha_d d^c_1 \tilde{\phi}^4 (Q Y^{(2)}_{\mathbf{3}})_{\mathbf{1}} H_d + \beta_d d^c_2 \tilde{\phi}^3 (Q Y^{(2)}_{\mathbf{3}})_{\mathbf{1}'} H_d + \gamma_d d^c_3 \tilde{\phi} (Q Y^{(2)}_{\mathbf{3}})_{\mathbf{1}''} H_d \\ &= \alpha_d d^c_1 \tilde{\phi}^4 (Q_1 Y_1 + Q_2 Y_3 + Q_3 Y_2) H_d + \beta_d d^c_2 \tilde{\phi}^3 (Q_3 Y_3 + Q_1 Y_2 + Q_2 Y_1) H_d \\ &\quad + \gamma_d d^c_3 \tilde{\phi} (Q_2 Y_2 + Q_3 Y_1 + Q_1 Y_3) H_d \,, \end{aligned} \tag{6.38}$$

which gives a similar form of Yukawa matrix for the down type quarks as for the charged leptons in Eq.6.33, albeit the second row being more suppressed than before,

$$Y^I_d = \begin{pmatrix} \alpha_d \tilde{\phi}^4 Y_1 & \alpha_d \tilde{\phi}^4 Y_3 & \alpha_d \tilde{\phi}^4 Y_2 \\ \beta_d \tilde{\phi}^3 Y_2 & \beta_d \tilde{\phi}^3 Y_1 & \beta_d \tilde{\phi}^3 Y_3 \\ \gamma_d \tilde{\phi} Y_3 & \gamma_d \tilde{\phi} Y_2 & \gamma_d \tilde{\phi} Y_1 \end{pmatrix} \tag{6.39}$$

where without loss of generality we may take $\alpha_d, \beta_d, \gamma_u$ to be real. However now there will be additional terms corresponding to higher weight modular forms, $Y^{(4)}_{\mathbf{3}}$, compensated by extra powers of weighton fields ϕ, which will give corrections to the down type quark superpotential, analogous to the higher order corrections to the charged lepton superpotential in Eq.6.34. Since these corrections will yield a matrix with a similar structure to the lowest order matrix but with each element having an additional correction be suppressed by a relative power of $\tilde{\phi}^2$. This yields

the additive correction to the down type quark mass matrix in Eq.6.39,

$$\Delta Y_d = \begin{pmatrix} \alpha'_d \tilde{\phi}^6 Y_1^{(4)} & \alpha'_d \tilde{\phi}^6 Y_3^{(4)} & \alpha'_d \tilde{\phi}^6 Y_2^{(4)} \\ \beta'_d \tilde{\phi}^5 Y_2^{(4)} & \beta'_d \tilde{\phi}^5 Y_1^{(4)} & \beta'_d \tilde{\phi}^5 Y_3^{(4)} \\ \gamma'_d \tilde{\phi}^3 Y_3^{(4)} & \gamma'_d \tilde{\phi}^3 Y_2^{(4)} & \gamma'_d \tilde{\phi}^3 Y_1^{(4)} \end{pmatrix} \tag{6.40}$$

where $\alpha'_d, \beta'_d, \gamma'_d$ are new free complex coefficients (also assumed to be of order unity) while the weight 4 Yukawa couplings are given in Eq.6.35.

Other alternatives include $k_{d^c_{3,2,1}} = 2, -2, -3$:

$$Y_d^{II} = \begin{pmatrix} \alpha_d \tilde{\phi}^4 Y_1 & \alpha_d \tilde{\phi}^4 Y_3 & \alpha_d \tilde{\phi}^4 Y_2 \\ \beta_d \tilde{\phi}^3 Y_2 & \beta_d \tilde{\phi}^3 Y_1 & \beta_d \tilde{\phi}^3 Y_3 \\ \gamma_d \tilde{\phi} Y_3^{(4)} & \gamma_d \tilde{\phi} Y_2^{(4)} & \gamma_d \tilde{\phi} Y_1^{(4)} \end{pmatrix} \tag{6.41}$$

Also we consider $k_{d^c_{3,2,1}} = 4, -2, -3$:

$$Y_d^{III} = \begin{pmatrix} \alpha_d \tilde{\phi}^4 Y_1 & \alpha_d \tilde{\phi}^4 Y_3 & \alpha_d \tilde{\phi}^4 Y_2 \\ \beta_d \tilde{\phi}^3 Y_2 & \beta_d \tilde{\phi}^3 Y_1 & \beta_d \tilde{\phi}^3 Y_3 \\ \gamma_d^I \tilde{\phi} Y_{3,I}^{(6)} + \gamma_d^{II} \tilde{\phi} Y_{3,II}^{(6)} & \gamma_d^I \tilde{\phi} Y_{2,I}^{(6)} + \gamma_d^{II} \tilde{\phi} Y_{2,II}^{(6)} & \gamma_d^I \tilde{\phi} Y_{1,I}^{(6)} + \gamma_d^{II} \tilde{\phi} Y_{1,II}^{(6)} \end{pmatrix} \tag{6.42}$$

It is worth noting that we have achieved a single power of suppression $\tilde{\phi}$ for the third down type family in several ways, by choosing an even weight for $k_{d^c_3} = 0, 2, 4, \ldots$ so that $d^c_3 \tilde{\phi} Q$ is also

even and may be compensated by a Yukawa coupling modular form of weight $2, 4, 6, \ldots$, leading to the three possibilities for the third row of the down type Yukawa matrix as above (with more possibilities at even higher weight). On the other hand higher powers of suppression such as $\tilde{\phi}^3, \tilde{\phi}^4$ for the first two families may only be achieved at lowest order by a Yukawa coupling modular form of weight 2.

Turning to the up type quark sector, we first consider $m_u : m_c : m_t \sim \tilde{\phi}^4 : \tilde{\phi}^2 : 1$, assuming $\tilde{\phi} \approx 1/15$ as before. In order to achieve this, the up type quarks are assigned the modular weights as shown in Table 6.3. The three RH up type quarks $u^c_{3,2,1}$ are assigned to three different singlets $\mathbf{1}'$, $\mathbf{1}''$ and $\mathbf{1}$ of A_4. In this case the up type quark mass hierarchy is much stronger and the top quark Yukawa coupling is of order unity, which suggests that it should be unsuppressed without any weighton field being involved. Moreover, as shown in [192], the lowest weight modular forms $Y^{(2)}_{\mathbf{3}}$ are not sufficient to describe quark mixing so here we shall utilise weight 6 modular form $Y^{(6)}_{\mathbf{3}}$ for only the third family (whereas in in [192] weight 6 modular forms were assumed for all three families of quarks). If we had used the lowest weight modular forms $Y^{(2)}_{\mathbf{3}}$ for all three families then the up quark Yukawa matrix would have rows proportional to that of the down quark Yukawa matrix, leading to zero quark mixing angles, so we need to use higher weight modular forms for the up Yukawa matrix, at least for the second or third families, and here we use weight 6 only for the third family. This motivates the assignments $k_{u^c_{3,2,1}} = 5, -1, -3$ such that the combinations $Qu^c_3, Qu^c_2\phi^2, Qu^c_1\phi^4$ imply the modular forms $Y^{(6)}_{\mathbf{3}}$, $Y^{(2)}_{\mathbf{3}}$, $Y^{(2)}_{\mathbf{3}}$, respectively, where powers of ϕ with $k_\phi = 1$ are required. Actually there are two independent weight 6 modular forms $Y^{(6)}_{\mathbf{3},I}$ and $Y^{(6)}_{\mathbf{3},II}$ and both must be considered as contributing independently.

Although the above assignments satisfies our requirements, we need to check that these are indeed the leading order terms. Firstly Qu^c_3 has weight -6 so the leading term is $Y^{(6)}_{\mathbf{3}}$, with the higher order correction $Qu^c_3\phi^2$ having weight -8 and requiring $Y^{(8)}_{\mathbf{3}}$ (the lower weight modular forms $Y^{(2)}_{\mathbf{3}}$ and $Y^{(4)}_{\mathbf{3}}$ are forbidden at all orders). Secondly, although Qu^c_2 has weight zero, this term is forbidden since it is an A_4 triplet and $Y^{(0)}_{\mathbf{3}}$ does not exist. Therefore the leading allowed term is $Qu^c_2\phi^2$ with weight -2, compensated by $Y^{(2)}_{\mathbf{3}}$, with the higher order term $Qu^c_2\phi^4$ with weight -4 compensated by $Y^{(4)}_{\mathbf{3}}$ being suppressed. Thirdly Qu^c_1 has weight 2 and cannot be compensated by a modular form with positive weight. While $Qu^c_1\phi^2$ has weight zero it is forbidden since it is an A_4 triplet and triplet modular forms cannot have zero weight. Therefore the leading term is $Qu^c_1\phi^4$ with weight -2 which is compensated by $Y^{(2)}_{\mathbf{3}}$, with the higher order correction $Qu^c_1\phi^6$ having weight -4 compensated by $Y^{(4)}_{\mathbf{3}}$ being suppressed.

After the weighton develops its vev, the leading order superpotential for the up type quark masses takes the form

$$\begin{aligned} W_u &= \alpha_u u^c_1 \tilde{\phi}^4 (QY^{(2)}_{\mathbf{3}})_{\mathbf{1}} H_u + \beta_u u^c_2 \tilde{\phi}^2 (QY^{(2)}_{\mathbf{3}})_{\mathbf{1}'} H_u + \gamma^I_u u^c_3 (QY^{(6)}_{\mathbf{3},I})_{\mathbf{1}''} H_u + \gamma^{II}_u u^c_3 (QY^{(6)}_{\mathbf{3},II})_{\mathbf{1}''} H_u \\ &= \alpha_u u^c_1 \tilde{\phi}^4 (Q_1 Y_1 + Q_2 Y_3 + Q_3 Y_2) H_u + \beta_u u^c_2 \tilde{\phi}^2 (Q_3 Y_3 + Q_1 Y_2 + Q_2 Y_1) H_u \\ &+ \gamma^I_u u^c_3 (Q_2 Y^{(6)}_{2,I} + Q_3 Y^{(6)}_{1,I} + Q_1 Y^{(6)}_{3,I}) H_u + \gamma^{II}_u u^c_3 (Q_2 Y^{(6)}_{2,II} + Q_3 Y^{(6)}_{1,II} + Q_1 Y^{(6)}_{3,II}) H_u \,, \end{aligned}$$

Thus $k_{u^c_{3,2,1}} = 5, -1, -3$ leads to the up quark Yukawa matrix,

$$Y_u^I = \begin{pmatrix} \alpha_u \tilde{\phi}^4 Y_1 & \alpha_u \tilde{\phi}^4 Y_3 & \alpha_u \tilde{\phi}^4 Y_2 \\ \beta_u \tilde{\phi}^2 Y_2 & \beta_u \tilde{\phi}^2 Y_1 & \beta_u \tilde{\phi}^2 Y_3 \\ \gamma_u^I Y^{(6)}_{3,I} + \gamma_u^{II} Y^{(6)}_{3,II} & \gamma_u^I Y^{(6)}_{2,I} + \gamma_u^{II} Y^{(6)}_{2,II} & \gamma_u^I Y^{(6)}_{1,I} + \gamma_u^{II} Y^{(6)}_{1,II} \end{pmatrix} \tag{6.43}$$

where the weight 6 Yukawa couplings are given in Eq.6.22. This is consistent with a diagonal and naturally hierarchical up type quark Yukawa matrix with $m_u : m_c : m_t \sim \tilde{\phi}^4 : \tilde{\phi}^2 : 1$, where without loss of generality we may take $\alpha_u, \beta_u, \gamma_u^I$ to be real, while in general γ_u^{II} can be complex.

Before performing a numerical study of this case, we recall that, $\tau_T = i\infty$ implies $Y^{(2)}_{\mathbf{3}} \propto (1,0,0)^T$, $Y^{(4)}_{\mathbf{3}} \propto (1,0,0)^T$, $Y^{(6)}_{\mathbf{3},I} \propto (1,0,0)^T$, $Y^{(6)}_{\mathbf{3},II} \propto (0,0,0)^T$ so near this limit $Y^{(6)}_{\mathbf{3},II}$ will not contribute. However we need to go away from this limit to explain quark mixing angles. There is a potential problem with the Yukawa structures in Eqs.6.39,6.43 since analytically (ignoring third family mixing angles) we expect $\theta^d_{12} \sim \theta^u_{12} \sim Y_2/Y_1$, so the physical Cabibbo angle $\theta_{12} \sim \theta^d_{12} - \theta^d_{12} \sim 0$ due to cancellation.

To avoid this problem we also consider an alternative model with the assignments $k_{u^c_{3,2,1}} = 5, 2, -3$ (i.e. only differing by the assignment $k_{u^c_2} = 2$) such that the combinations $Qu^c_3, Qu^c_2\phi, Qu^c_1\phi^4$ imply the modular forms $Y^{(6)}_{\mathbf{3}}$, $Y^{(4)}_{\mathbf{3}}$, $Y^{(2)}_{\mathbf{3}}$, respectively, where powers of ϕ with $k_\phi = 1$ are required. This may avoid the cancellation problem of the Cabibbo angle, since now $\theta^u_{12} \sim Y^{(4)}_2/Y^{(4)}_1$ is different from $\theta^d_{12} \sim Y_2/Y_1$, but is slightly less natural, being consistent with a diagonal and naturally hierarchical up type quark Yukawa matrix with $m_u : m_c : m_t \sim \tilde{\phi}^4 : \tilde{\phi} : 1$. Thus $k_{u^c_{3,2,1}} = 5, 2, -3$ leads to:

$$Y_u^{II} = \begin{pmatrix} \alpha_u \tilde{\phi}^4 Y_1 & \alpha_u \tilde{\phi}^4 Y_3 & \alpha_u \tilde{\phi}^4 Y_2 \\ \beta_u \tilde{\phi} Y^{(4)}_2 & \beta_u \tilde{\phi} Y^{(4)}_1 & \beta_u \tilde{\phi} Y^{(4)}_3 \\ \gamma_u^I Y^{(6)}_{3,I} + \gamma_u^{II} Y^{(6)}_{3,II} & \gamma_u^I Y^{(6)}_{2,I} + \gamma_u^{II} Y^{(6)}_{2,II} & \gamma_u^I Y^{(6)}_{1,I} + \gamma_u^{II} Y^{(6)}_{1,II} \end{pmatrix} \tag{6.44}$$

The analysis of the alternative model using the up quark Yukawa matrix in Eq.6.44 is very similar

to that using the up quark Yukawa matrix in Eq.6.43, but we expect that the Cabibbo angle will be reproduced more easily, with the down quark Yukawa matrix in Eq.6.39 being the same in both cases.

We also consider a third model with the assignments $k_{u^c_{3,2,1}} = 5, 4, -3$ (i.e. differing by the assignment $k_{u^c_2} = 4$) such that the combinations $Qu^c_3, Qu^c_2\phi, Qu^c_1\phi^4$ imply the modular forms $Y^{(6)}_{\mathbf{3}}$, $Y^{(6)}_{\mathbf{3}}$, $Y^{(2)}_{\mathbf{3}}$, respectively, where powers of ϕ with $k_\phi = 1$ are required. Thus with $k_{u^c_{3,2,1}} = 5, 4, -3$ we have:

$$Y_u^{III} = \begin{pmatrix} \alpha_u\tilde{\phi}^4\, Y_1 & \alpha_u\tilde{\phi}^4\, Y_3 & \alpha_u\tilde{\phi}^4\, Y_2 \\ \beta^I_u\tilde{\phi}Y^{(6)}_{2,I} + \beta^{II}_u\tilde{\phi}Y^{(6)}_{2,II} & \beta^I_u\tilde{\phi}Y^{(6)}_{1,I} + \beta^{II}_u\tilde{\phi}Y^{(6)}_{1,II} & \beta^I_u\tilde{\phi}Y^{(6)}_{3,I} + \beta^{II}_u\tilde{\phi}Y^{(6)}_{3,II} \\ \gamma^I_u Y^{(6)}_{3,I} + \gamma^{II}_u Y^{(6)}_{3,II} & \gamma^I_u Y^{(6)}_{2,I} + \gamma^{II}_u Y^{(6)}_{2,II} & \gamma^I_u Y^{(6)}_{1,I} + \gamma^{II}_u Y^{(6)}_{1,II} \end{pmatrix} \tag{6.45}$$

All the above three possibilities for the up quark Yukawa matrices have the third family controlled by a weight 6 modular form, resulting from the choice $k_{u^c_3} = 5$. We now consider third family modular forms of weight 4 corresponding to the choice $k_{u^c_3} = 3$. This would lead to three more possibilities as shown below.

With $k_{u^c_{3,2,1}} = 3, -1, -3$ we have:

$$Y_u^{IV} = \begin{pmatrix} \alpha_u\tilde{\phi}^4\, Y_1 & \alpha_u\tilde{\phi}^4\, Y_3 & \alpha_u\tilde{\phi}^4\, Y_2 \\ \beta_u\tilde{\phi}^2 Y_2 & \beta_u\tilde{\phi}^2 Y_1 & \beta_u\tilde{\phi}^2 Y_3 \\ \gamma_u Y^{(4)}_3 & \gamma_u Y^{(4)}_2 & \gamma_u Y^{(4)}_1 \end{pmatrix} \tag{6.46}$$

With $k_{u^c_{3,2,1}} = 3, 2, -3$ we have:

$$Y_u^V = \begin{pmatrix} \alpha_u \tilde{\phi}^4\, Y_1 & \alpha_u \tilde{\phi}^4\, Y_3 & \alpha_u \tilde{\phi}^4\, Y_2 \\ \beta_u \tilde{\phi} Y_2^{(4)} & \beta_u \tilde{\phi} Y_1^{(4)} & \beta_u \tilde{\phi} Y_3^{(4)} \\ \gamma_u Y_3^{(4)} & \gamma_u Y_2^{(4)} & \gamma_u Y_1^{(4)} \end{pmatrix} \tag{6.47}$$

With $k_{u^c_{3,2,1}} = 3, 4, -3$ we have:

$$Y_u^{VI} = \begin{pmatrix} \alpha_u \tilde{\phi}^4\, Y_1 & \alpha_u \tilde{\phi}^4\, Y_3 & \alpha_u \tilde{\phi}^4\, Y_2 \\ \beta_u^I \tilde{\phi} Y_{2,I}^{(6)} + \beta_u^{II} \tilde{\phi} Y_{2,II}^{(6)} & \beta_u^I \tilde{\phi} Y_{1,I}^{(6)} + \beta_u^{II} \tilde{\phi} Y_{1,II}^{(6)} & \beta_u^I \tilde{\phi} Y_{3,I}^{(6)} + \beta_u^{II} \tilde{\phi} Y_{3,II}^{(6)} \\ \gamma_u Y_3^{(4)} & \gamma_u Y_2^{(4)} & \gamma_u Y_1^{(4)} \end{pmatrix} \tag{6.48}$$

Finally we also consider third family modular forms of weight 2 corresponding to the choice $k_{u^c_3} = 1$. This would lead to three final possibilities as shown below.

With $k_{u^c_{3,2,1}} = 1, -1, -3$ we have:

$$Y_u^{VII} = \begin{pmatrix} \alpha_u \tilde{\phi}^4\, Y_1 & \alpha_u \tilde{\phi}^4\, Y_3 & \alpha_u \tilde{\phi}^4\, Y_2 \\ \beta_u \tilde{\phi}^2 Y_2 & \beta_u \tilde{\phi}^2 Y_1 & \beta_u \tilde{\phi}^2 Y_3 \\ \gamma_u Y_3 & \gamma_u Y_2 & \gamma_u Y_1 \end{pmatrix} \tag{6.49}$$

With $k_{u^c_{3,2,1}} = 1, 2, -3$ we have:

$$Y_u^{VIII} = \begin{pmatrix} \alpha_u \tilde{\phi}^4 Y_1 & \alpha_u \tilde{\phi}^4 Y_3 & \alpha_u \tilde{\phi}^4 Y_2 \\ \beta_u \tilde{\phi} Y_2^{(4)} & \beta_u \tilde{\phi} Y_1^{(4)} & \beta_u \tilde{\phi} Y_3^{(4)} \\ \gamma_u Y_3 & \gamma_u Y_2 & \gamma_u Y_1 \end{pmatrix} \tag{6.50}$$

With $k_{u^c_{3,2,1}} = 1, 4, -3$ we have:

$$Y_u^{IX} = \begin{pmatrix} \alpha_u \tilde{\phi}^4 Y_1 & \alpha_u \tilde{\phi}^4 Y_3 & \alpha_u \tilde{\phi}^4 Y_2 \\ \beta_u^I \tilde{\phi} Y_{2,I}^{(6)} + \beta_u^{II} \tilde{\phi} Y_{2,II}^{(6)} & \beta_u^I \tilde{\phi} Y_{1,I}^{(6)} + \beta_u^{II} \tilde{\phi} Y_{1,II}^{(6)} & \beta_u^I \tilde{\phi} Y_{3,I}^{(6)} + \beta_u^{II} \tilde{\phi} Y_{3,II}^{(6)} \\ \gamma_u Y_3 & \gamma_u Y_2 & \gamma_u Y_1 \end{pmatrix} \tag{6.51}$$

Note that there is only one possibility for the first family of up quarks since the required suppression $\tilde{\phi}^4$ can only be achieved by modular forms of weight 2.

In the the next section we perform a numerical analysis of our models. First we check the lepton sector results, based on the matrices in Eqs.6.29,6.33, then go on to the quark sector using one of the Yukawa matrices in Eq.6.39,6.41 or 6.42 combined with one of Eq.6.43-6.51. Without loss of generality we take $\alpha_{e,d,u}, \beta_{e,d,u}, \gamma_{e,d,u}$ to be real, with β_u^I, γ_u^I real while $\beta_u^{II}, \gamma_u^{II}$ are complex. We allow $\tilde{\phi}$ to be free but find that the numerical fits prefer $\tilde{\phi} \approx 1/15$, as expected.

6.5 Numerical and Analytical Results

6.5.1 Input Data and Global Analysis

The charged fermion mass matrices are given by

$$M_e = Y_e \frac{v_d}{\sqrt{2}} = Y_e \cos\beta \frac{v_H}{\sqrt{2}}, \quad M_d = Y_d \frac{v_d}{\sqrt{2}} = Y_d \cos\beta \frac{v_H}{\sqrt{2}}, \quad M_u = Y_u \frac{v_u}{\sqrt{2}} = Y_u \sin\beta \frac{v_H}{\sqrt{2}}, \tag{6.52}$$

where the ratio of Higgs VEVs is $\tan\beta = v_u/v_d$ and the SM Higgs VEV is $v_H = \sqrt{v_u^2 + v_d^2} = 246$ GeV, and Y_e, Y_d, Y_u represent the Yukawa matrices predicted by the models, namely Eq.6.33, for the charged lepton Yukawa matrix, Eqs.6.39,6.41 or 6.42 for the down quark Yukawa matrix and Eqs.6.43-6.51 for the up quark Yukawa matrix.

The scale of Yukawa couplings in this model is given by the string compactification scale, and hence we use couplings calculated at the GUT scale from a minimal SUSY breaking scenario, with $\tan\beta = 5$, as done in [192, 197, 217]. Similarly, we use the CKM parameters also at this scale as derived by the same authors. For the charged lepton and down type Yukawa masses, the physical particle masses are given by $m_i^{MSSM} = y_i^{MSSM} v_d/\sqrt{2}$, for $i = (e, \mu, \tau, d, s, b)$, and for the up quarks, $m_j^{MSSM} = y_j^{MSSM} v_u/\sqrt{2}$, for $j = (u, c, t)$. The numerical eigenvalues calculated from our input Yukawa matrices Y_e, Y_d, Y_u are matched to y^{MSSM}. Below we list $\tilde{y}_i \equiv y_i^{MSSM}\cos\beta$ and $\tilde{y}_j \equiv y_j^{MSSM}\sin\beta$ for $\tan\beta = 5$, together with the quark mixing parameters,[1]

$$
\begin{aligned}
&\tilde{y}_e = (1.97 \pm 0.0236)\times 10^{-6}, \quad \tilde{y}_\mu = (4.16 \pm 0.0497)\times 10^{-4}, \quad \tilde{y}_\tau = (7.07 \pm 0.0727)\times 10^{-3},\\
&\tilde{y}_d = (4.81 \pm 1.06)\times 10^{-6}, \quad \tilde{y}_s = (9.52 \pm 1.03)\times 10^{-5}, \quad \tilde{y}_b = (6.95 \pm 0.175)\times 10^{-3},\\
&\tilde{y}_u = (2.92 \pm 1.81)\times 10^{-6}, \quad \tilde{y}_c = (1.43\pm 0.100)\times 10^{-3}, \quad \tilde{y}_t = 0.534 \pm 0.0341 \ ,\\
&\theta_{12}^q = 13.027^\circ \pm 0.0814^\circ, \quad \theta_{23}^q = 2.054^\circ \pm 0.384^\circ, \quad \theta_{13}^q = 0.1802^\circ \pm 0.0281^\circ \ ,\\
&\delta^q = 69.21^\circ \pm 6.19^\circ.
\end{aligned}
\tag{6.53}
$$

For the neutrino parameters, we use the data from NuFit 4.1 (2019) [198], without Super-Kamiokande (SK) atmospheric data, which we summarise below for Normal Ordering (NO), where we write eorrs in brackets, which correspond to the average of positive and negative 1σ deviations.

$$
\begin{aligned}
&\sin^2\theta_{12} = 0.310(13), \quad \sin^2\theta_{13} = 0.02241(66), \quad \sin^2\theta_{23} = 0.558(26),\\
&\frac{\Delta m^2_{21}}{10^{-5}\ \text{eV}^2} = 7.39(21), \quad \frac{\Delta m^2_{31}}{10^{-3}\ \text{eV}^2} = 2.525(31), \quad \delta/\pi = 1.23(18)
\end{aligned}
\tag{6.54}
$$

For our numerical study, we follow a procedure similar to that described in [4], but here generalised to the quark sector, to find the minimum $\chi^2_{\text{min,Q}}$ contribution from the CKM and quark Yukawa pulls. We consider all 27 combinations of $Y_d^I Y_u^I, \ldots, Y_d^{III} Y_u^{IX}$, restricting τ to be within a range which is acceptable to the lepton sector, based on the matrices in Eqs.6.29,6.33, which is approximately the same as found in [185], model $\mathcal{D}_{10}$ in their notation.

We display our best fit points in table 6.4, for all 27 models. From this table it is clear that we find unacceptably high $\chi^2_{\text{min}} \gtrsim 50$ for all permutations besides $Y_d^{III} Y_u^{VI}$ and $Y_d^{II} Y_u^{III}$, for which we found an arbitrarily good $\chi^2_{\text{min,Q}} < 1$, where the subscript "Q" refers to the partial χ^2 from the quark sector alone, and note the total χ^2_{min} across both the quark and lepton sectors observables

[1] These values do not change significantly for $\tan\beta = 10$. For larger values of $\tan\beta$, threshold corrections become increasingly important.

	Y_u^I	Y_u^{II}	Y_u^{III}	Y_u^{IV}	Y_u^V	Y_u^{VI}	Y_u^{VII}	Y_u^{VIII}	Y_u^{IX}
Y_d^I	118	194	123	420	337	98.4	183	244	122
Y_d^{II}	79.1	78.9	**0.00**	248	279	142	413	479	93
Y_d^{III}	118	186	135	79.8	79.5	**0.00**	117	190	135

Table 6.4: $\chi^2_{\text{min,Q}}$ for all 27 combinations of $Y_u,\ Y_d$

is ≈ 1. For the remainder of this chapter, we will focus on these two successful models, and do not list the benchmark points for the other models which do not well reproduce data.

6.5.2 Model Y_u^{VI}, Y_d^{III}

Numerical Study

We find two combinations of down and up quark Yukawa matrices has an acceptable $\chi^2_{\text{min,Q}}$ value, from Y_u^{VI} in combination with Y_d^{III}, which we study in this section and $Y_u^{III},\ Y_d^{II}$ which we study in the next [2] In Tab. 6.5 we write the input and output parameters, both for the quark and lepton sectors for our best fit point in this model. Since the neutrino sector is the same as found in [185], model $\mathcal{D}_{10}$, and charged lepton Yukawa matrix a similar form besides the addition of weightons, the lepton observables and predictions are similar to what is seen by Ding, et. al. However, the quark sector is entirely new of our own construction. Here we see that by tuning the $\alpha_i,\ \beta_i,\ \gamma_i$ parameters to match SM fermion Yukawa couplings (at GUT scale), we also find very strong agreement with the CKM angles and phase.

To explain why this is the case, we first look at numerical motivations and then go on to study the analytic properties of this point. Firstly, we list the two numerical mixing matrices which produce the CKM for our best fit point found in Tab. 6.5 are as follows. Defining $U_L^{u,VI\dagger}(Y_u^{VI\dagger}Y_u^{VI})U_L^{u,VI} = Y_u^{VI\,diag}$, and similarly for the down sector we find the following two diagonalising matrices,

$$U_L^{u,VI} = \begin{pmatrix} 0.981 & -0.193 & -0.00283 \\ -0.149 + 0.122i & -0.758 + 0.622i & -0.0433 - 0.00328i \\ 0.00411 - 0.00522i & 0.0355 - 0.0244i & -0.988 - 0.15i \end{pmatrix}, \tag{6.55}$$

$$U_L^{d,III} = \begin{pmatrix} -0.999 & 0.0436 & -0.00277 \\ -0.0434 - 0.00329i & -0.996 - 0.0736i & 0.00225 + 0.0273i \\ -0.0028 - 0.00043i & -0.00319 - 0.0272i & 0.962 - 0.273i \end{pmatrix}. \tag{6.56}$$

[2] We have also tested these models with a different $\tan\beta = 10$, to check we are not overly sensitive to this initial choice.

Lepton observable	value (pull)
$\Delta m^2_{21} \cdot 10^5$ (eV^2)	7.39 (0.0)
$\Delta m^2_{31} \cdot 10^3$ (eV^2)	2.52 (0.0)
$\sin^2\theta_{12}$	0.310 (0.0)
$\sin^2\theta_{13}$	0.0224 (0.0)
$\sin^2\theta_{23}$	0.562 (0.2)
δ/π	1.58 (1.9)
$y_e \cdot 10^5$	1.00 (0.0)
$y_\mu \cdot 10^3$	2.12 (0.0)
$y_\tau \cdot 10^2$	3.61 (0.0)
$\chi^2_{\rm min,L}$	3.67
Lepton prediction	value
m_1 (eV)	0.11
m_2 (eV)	0.11
m_3 (eV)	0.12
α_{21}/π	0.013
α_{31}/π	1.01
m_{ee} (eV)	0.11
MO	NO
Lepton Input	value
Re(g_2/g_1)	0.4185
Im(g_2/g_1)	1.048
$g_1^2 v_u^2/\Lambda$ (eV)	0.05506
α_e	-0.9778
β_e	-0.6615
γ_e	-0.6360

Quark Observable	value(pull)
θ^q_{12}	0.227 (0.0)
θ^q_{13}	0.00314 (0.0)
θ^q_{23}	0.0358 (0.0)
δ^q/π	1.21 (0.0)
$y_u \cdot 10^5$	1.49 (0.0)
$y_c \cdot 10^3$	7.29 (0.0)
y_t	2.72 (0.0)
$y_d \cdot 10^5$	2.45 (0.0)
$y_s \cdot 10^4$	4.85 (0.0)
$y_b \cdot 10^2$	3.54 (0.0)
$\chi^2_{\rm min,Q}$	0.0
Quark input	value
α_u	-1.476
β_u^I	-0.1264
β_u^{II}	$0.2697 - 0.1971i$
γ_u	2.720
α_d	-2.387
β_d	2.672
γ_d^I	0.6253
γ_d^{II}	$0.4958 - 0.2187i$

Common Input	value
Re(τ)	0.03610
Im(τ)	2.352
$\tilde{\phi}$	0.05663

Table 6.5: Results of the fit to lepton and quark data for model combining M_ν, Y_e, Y_u^{VI}, Y_d^{III}. In the left panel are the lepton observables and pulls (in fractions of 1σ), the $\chi^2_{\rm min,L}$ contribution from the lepton sector, as well as predictions for neutrino masses, phases, neutrinoless double beta decay and MO. The inputs for the lepton sector are displayed at the bottom. In the right panel we have the quark observables and pulls, the $\chi^2_{\rm min,Q}$ quark contribution, and quark inputs. At the bottom right we list the τ and ϕ inputs which are common to both sectors. We note that $\tilde{\phi} = 1/15 = 0.06667$ for example may be fixed exactly to find an equivalently good benchmark point.

We can see that the Cabbibo angle, θ_{12} is mostly generated by the mixing in the up sector, since $U_L^{u\,1,2} \gg U_L^{d\,1,2}$, however both sectors will play a similar role in generating the other two angles, with the imaginary part playing a significant role for θ_{23}. To examine this further, we turn to an analytic study of the structure of our up and down Yukawa matrices.

Analytic Results

We may approximate the analytic forms of our successful model of Y_u^{VI}, Y_d^{III} rewriting the weighton and weight two modular forms as follows, using Eq.6.19, and writing the higher weight forms directly in terms of these weight two approximations as in Eqs. 6.21, 6.22,

$$\tilde{\phi} \simeq 0.057 \equiv \epsilon_1, \tag{6.57}$$

$$\begin{pmatrix} Y_1(\tau) \\ Y_2(\tau) \\ Y_3(\tau) \end{pmatrix} = \begin{pmatrix} 1 + \mathcal{O}(q) \\ -6q^{1/3} + \mathcal{O}(q) \\ -18q^{2/3} + \mathcal{O}(q) \end{pmatrix} \simeq \begin{pmatrix} 1.00 \\ -0.043 - 0.0033i \\ -0.00094 - 0.00014i \end{pmatrix} \equiv \begin{pmatrix} 1 \\ \epsilon_2 \\ \epsilon_3 \end{pmatrix}. \tag{6.58}$$

where $q = e^{2\pi i \tau}$. We find numerically that ϵ_1^2 is a similar order to ϵ_2^2, and to ϵ_3. Consequently, we may take the first non-trivial term at the order $\mathcal{O}(\epsilon_i) \sim \mathcal{O}(\epsilon_1) \sim \mathcal{O}(\epsilon_2) \sim \mathcal{O}(\epsilon_3^{1/2})$, dropping higher corrections in each entry of our successful model. We find the following results for the up and down quark Yukawa matrices, respectively, making a leading order approximation for each element of the matrix,

$$Y_u^{VI} \simeq \begin{pmatrix} \epsilon_1^4 \alpha_u & \epsilon_1^4 \epsilon_3 \alpha_u & \epsilon_1^4 \epsilon_2 \alpha_u \\ \epsilon_1 \epsilon_2 \left(2\beta_u^{II} + \beta_u^I\right) & \epsilon_1 \beta_u^I & \epsilon_1 \left(2\epsilon_2^2 \beta_u^{II} + \epsilon_3 \beta_u^I\right) \\ \left(\epsilon_2^2 - \epsilon_3\right) \gamma_u & -\epsilon_2 \gamma_u & \gamma_u \end{pmatrix}, \tag{6.59}$$

$$Y_d^{III} \simeq \begin{pmatrix} \epsilon_1^4 \alpha_d & \epsilon_1^4 \epsilon_3 \alpha_d & \epsilon_1^4 \epsilon_2 \alpha_d \\ \epsilon_1^3 \epsilon_2 \beta_d & \epsilon_1^3 \beta_d & \epsilon_1^3 \epsilon_3 \beta_d \\ \epsilon_1 \left(2\epsilon_2^2 \gamma_d^{II} + \epsilon_3 \gamma_d^I\right) & \epsilon_1 \epsilon_2 \left(2\gamma_d^{II} + \gamma_d^I\right) & \epsilon_1 \gamma_d^I \end{pmatrix}. \tag{6.60}$$

Since the matrices are hierarchical, we can make an estimate for the three mixing angles as follows, which accurately reproduces the fully calculated CKM angles. We then express ϵ_2, ϵ_3 by using the q-expansions, for which the first order reproduces well the full Dedekind-eta value for our best fit point.

$$\theta_{12} \simeq \left| \frac{Y_u^{2,1}}{Y_u^{2,2}} - \frac{Y_d^{2,1}}{Y_d^{2,2}} \right| = \left| 2\epsilon_2 \frac{\beta_u^{II}}{\beta_u^I} \right| = 12 e^{-\frac{2}{3}\pi \,\mathrm{Im}(\tau)} \left| \frac{\beta_u^{\mathrm{II}}}{\beta_u^{\mathrm{I}}} \right| \tag{6.61}$$

$$\theta_{13} \simeq \left| \frac{Y_u^{3,1}}{Y_u^{3,3}} - \frac{Y_d^{3,1}}{Y_d^{3,3}} \right| = \left| \epsilon_2^2 \frac{\gamma_d^I - 2\gamma_d^{II}}{\gamma_d^I} - 2\epsilon_3 \right| = 72 e^{-\frac{4}{3}\pi \,\mathrm{Im}(\tau)} \left| 1 - \frac{\gamma_d^{II}}{\gamma_d^I} \right| \tag{6.62}$$

$$\theta_{23} \simeq \left| \frac{Y_u^{3,2}}{Y_u^{3,3}} - \frac{Y_d^{3,2}}{Y_d^{3,3}} \right| = \left| 2\epsilon_2 \frac{\gamma_d^I + \gamma_d^{II}}{\gamma_d^I} \right| = 12 e^{-\frac{2}{3}\pi \,\mathrm{Im}(\tau)} \left| 1 + \frac{\gamma_d^{II}}{\gamma_d^I} \right| \tag{6.63}$$

The above approximations reproduce the numerical values of the quark mixing angles well, to two significant figures for $\theta_{12},\ \theta_{23}$, but only within a factor of two for θ_{13}. This is because it is the smallest angle, and hence sensitive to additional contributions. For the two larger angles, there are several reasons why the above expressions well reproduce data. To begin with, quark mixing angles are all small, so a small angle approximation is valid. Furthermore, overall factors and phases cancel in the ratios such as $\frac{Y_u^{2,1}}{Y_u^{2,2}}$ and $\frac{Y_d^{2,1}}{Y_d^{2,2}}$, since each row of the Yukawa matrices is controlled by a particular modular form, therefore the physical CKM angles are identified as the difference in these two ratios, with no arbitrary relative phase. This is quite different from a traditional FN model based on an Abelian symmetry, where mixing angle predictions would depend on arbitrary coefficients and phases. It implies that partial cancellations occur between $\frac{Y_u^{2,1}}{Y_u^{2,2}}$ and $\frac{Y_d^{2,1}}{Y_d^{2,2}}$ in constructing θ_{12}, which leads to a particularly simple form without β_u^I in the numerator. It also implies that the mixing angles are independent of ϵ_1 which cancels in the ratios, so the only role of ϵ_1 is to control mass hierarchies. The mixing angles are therefore completely controlled by ϵ_2 and ϵ_3, which however are not independent parameters, being related by the expansion of the A_4 triplet modular forms in Eq.6.19. This dependence is manifested in the final expressions on the RH sides of the Eqs.6.61,6.62,6.63 based on the truncations in Eq.6.58, which are valid for small $q = e^{2\pi i \tau}$ when the imaginary part of τ is large. Despite the large prefactors, the CKM angles are therefore small due to an exponential suppression arising from the best fit point τ having a large imaginary part. One can see that in the limit $\tau \to i\infty$ the CKM angles go to zero, which is expected as this would correspond to diagonal Yukawa matrices. Given $\mathcal{O}(1)$ input parameters, we then see the required value of τ to match the observed CKM values must be near $\tau \simeq 2.35i$.

6.5.3 Model Y_u^{III}, Y_d^{II}

Numerical Study

We now study a second successful model, comprised of Y_u^{III}, Y_d^{II}, with input and output parameters found in Tab. 6.6. This section will proceed analagously to the previous one.

Lepton observable	value (pull)
$\Delta m^2_{21} \cdot 10^5$ (eV^2)	7.39 (0.0)
$\Delta m^2_{31} \cdot 10^3$ (eV^2)	2.52 (0.0)
$\sin^2\theta_{12}$	0.310 (0.0)
$\sin^2\theta_{13}$	0.0224 (0.0)
$\sin^2\theta_{23}$	0.562 (0.2)
δ/π	1.58 (1.9)
$y_e \cdot 10^5$	1.00 (0.0)
$y_\mu \cdot 10^3$	2.12 (0.0)
$y_\tau \cdot 10^2$	3.61 (0.0)
$\chi^2_{\text{min,L}}$	3.67
Lepton prediction	value
m_1 (eV)	0.11
m_2 (eV)	0.11
m_3 (eV)	0.12
α_{21}/π	0.012
α_{31}/π	1.01
m_{ee} (eV)	0.11
MO	NO
Lepton Input	value
$\text{Re}(g_2/g_1)$	0.4185
$\text{Im}(g_2/g_1)$	1.038
$g_1^2 v_u^2/\Lambda$ (eV)	0.05508
α_e	-0.4658
β_e	-0.4566
γ_e	0.5284

Quark Observable	value(pull)
θ^q_{12}	0.227 (0.0)
θ^q_{13}	0.00314 (0.0)
θ^q_{23}	0.0358 (0.0)
δ^q/π	1.21 (0.0)
$y_u \cdot 10^5$	1.49 (0.0)
$y_c \cdot 10^3$	7.29 (0.0)
y_t	2.72 (0.0)
$y_d \cdot 10^5$	2.45 (0.0)
$y_s \cdot 10^4$	4.85 (0.0)
$y_b \cdot 10^2$	3.54 (0.0)
$\chi^2_{\text{min,Q}}$	0.0
Quark input	value
α_u	-1.137
β_u^I	-0.1048
β_u^{II}	$0.1937 + 0.1985i$
γ_u^I	2.722
γ_u^{II}	$-1.697 - 0.4260i$
α_d	-1.137
β_d	-1.533
γ_d	-0.5194

Common Input	value
$\text{Re}(\tau)$	0.03610
$\text{Im}(\tau)$	2.353
$\tilde{\phi}$	-0.06816

Table 6.6: Results of the fit to lepton and quark data for model combining M_ν, Y_e, Y_u^{III}, Y_d^{II}. In the left panel are the lepton observables and pulls (in fractions of 1σ), the $\chi^2_{\text{min,L}}$ contribution from the lepton sector, as well as predictions for neutrino masses, phases, neutrinoless double beta decay and MO. The inputs for the lepton sector are displayed at the bottom. In the right panel we have the quark observables and pulls, the $\chi^2_{\text{min,Q}}$ quark contribution, and quark inputs. At the bottom right we list the τ and ϕ inputs which are common to both sectors. We note that $\tilde{\phi} = 1/15 = 0.06667$ for example may be fixed exactly to find an equivalently good benchmark point.

We first present the two numerical diagonalising matrices as before. The numerical values of this model are similar to the previous scenario, where θ_{12} is dominated by the contribution from the up quark sector.

$$U_L^{u,III} = \begin{pmatrix} -0.98 - 0.0000121i & 0.198 + 0.000225i & 0.00312 - 0.00123i \\ 0.102 + 0.17i & 0.506 + 0.84i & -0.00896 + 0.0148i \\ -0.00166 - 0.00417i & 0.00782 - 0.0152i & -0.999 + 0.047i \end{pmatrix}, \tag{6.64}$$

$$U_L^{d,II} = \begin{pmatrix} 0.999 - 0.000038i & 0.0437 + 0.000215i & -0.00275 + 0.00068i \\ 0.0434 + 0.00329i & -0.995 - 0.0803i & -0.0428 + 0.00722i \\ -0.00467 - 0.000712i & 0.0428 + 0.00673i & -0.995 + 0.091i \end{pmatrix}. \tag{6.65}$$

Analytic Results

We again proceed with the same analytic approach as before, and will find very similar analytic approximations as with the previous scenario. For the new scenario (with slightly different input values of $(\varphi,\ \tau)$), we again see the relation $\mathcal{O}(\epsilon_i) \sim \mathcal{O}(\epsilon_1) \sim \mathcal{O}(\epsilon_2) \sim \mathcal{O}(\epsilon_3^{1/2})$, and take the lowest non trivial order in each entry in the two Yukawa matrices.

$$\tilde{\phi} \simeq -0.068 \equiv \epsilon_1, \tag{6.66}$$

$$\begin{pmatrix} Y_1(\tau) \\ Y_2(\tau) \\ Y_3(\tau) \end{pmatrix} = \begin{pmatrix} 1 + \mathcal{O}(q) \\ -6q^{1/3} + \mathcal{O}(q) \\ -18q^{2/3} + \mathcal{O}(q) \end{pmatrix} \simeq \begin{pmatrix} 1.00 \\ -0.043 - 0.0033i \\ -0.00093 - 0.00014i \end{pmatrix} \equiv \begin{pmatrix} 1 \\ \epsilon_2 \\ \epsilon_3 \end{pmatrix}. \tag{6.67}$$

$$Y_u^{III} \simeq \begin{pmatrix} \epsilon_1^4 \alpha_u & \epsilon_1^4 \epsilon_3 \alpha_u & \epsilon_1^4 \epsilon_2 \alpha_u \\ \epsilon_1 \epsilon_2 \left(2\beta_u^{II} + \beta_u^I\right) & \epsilon_1 \beta_u^I & \epsilon_1 \left(2\epsilon_2^2 \beta_u^{II} + \epsilon_3 \beta_u^I\right) \\ \epsilon_3 \gamma_u^I + 2\epsilon_2^2 \gamma_u^{II} & \epsilon_2 \left(\gamma_u^I + 2\gamma_u^{II}\right) & \gamma_u^I \end{pmatrix} \tag{6.68}$$

$$Y_d^{II} \simeq \begin{pmatrix} \epsilon_1^4\alpha_d & \epsilon_1^4\epsilon_3\alpha_d & \epsilon_1^4\epsilon_2\alpha_d \\ \epsilon_1^3\epsilon_2\beta_d & \epsilon_1^3\beta_d & \epsilon_1^3\epsilon_3\beta_d \\ \epsilon_1\gamma_d\left(\epsilon_2^2-\epsilon_3\right) & -\epsilon_1\epsilon_2\gamma_d & \epsilon_1\gamma_d \end{pmatrix}. \tag{6.69}$$

We now follow the same procedure to approximate the three CKM mixing angles, and replace $\epsilon_{2,3}$ with the q-expansions to first order.

$$\theta_{12} \simeq \left|\frac{Y_u^{2,1}}{Y_u^{2,2}} - \frac{Y_d^{2,1}}{Y_d^{2,2}}\right| = \left|2\epsilon_2\frac{\beta_u^{II}}{\beta_u^I}\right| = 12e^{-\frac{2}{3}\pi\,\mathrm{Im}(\tau)}\left|\frac{\beta_u^{\mathrm{II}}}{\beta_u^{\mathrm{I}}}\right| \tag{6.70}$$

$$\theta_{13} \simeq \left|\frac{Y_u^{3,1}}{Y_u^{3,3}} - \frac{Y_d^{3,1}}{Y_d^{3,3}}\right| = \left|\epsilon_2^2\frac{\gamma_u^I - 2\gamma_u^{II}}{\gamma_u^I} - 2\epsilon_3\right| = 72e^{-\frac{4}{3}\pi\,\mathrm{Im}(\tau)}\left|1 - \frac{\gamma_u^{II}}{\gamma_u^I}\right| \tag{6.71}$$

$$\theta_{23} \simeq \left|\frac{Y_u^{3,2}}{Y_u^{3,3}} - \frac{Y_d^{3,2}}{Y_d^{3,3}}\right| = \left|2\epsilon_2\frac{\gamma_u^I + \gamma_u^{II}}{\gamma_u^I}\right| = 12e^{-\frac{2}{3}\pi\,\mathrm{Im}(\tau)}\left|1 + \frac{\gamma_u^{II}}{\gamma_u^I}\right| \tag{6.72}$$

The analytic forms here are identical to the previous model, exchanging γ_d previously seen with γ_u here. In this scenario, the weight six entries previously found in the third row of Y_d^{VI} are instead found in the third row of Y_u^{III}. In this scenario, the mixing angles are even more controlled by the up sector than beore.

It can now be understood that these two specific models are both successful, as they both predict the same expressions for the CKM mixing angles above, for which values of α_i, β_i, γ_i that explain well the Yukawa couplings of the quarks also well reproduce the observed mixings in the quark sector.

6.5.4 Analytic Expansion of the Lepton Matrices

Finally, it is interesting to apply the same analytic expansion procedure used for the quarks, also to the leptons. For the charged lepton Yukawa matrix in Eq.6.33, we find (without dropping any

terms since the leading order matrix arises at weight 2),

$$Y_e \simeq \begin{pmatrix} \alpha_e\epsilon_1^4 & \alpha_e\epsilon_1^4\,\epsilon_3 & \alpha_e\epsilon_1^4\,\epsilon_2 \\ \beta_e\epsilon_1^2\epsilon_2 & \beta_e\epsilon_1^2 & \beta_e\epsilon_1^2\epsilon_3 \\ \gamma_e\epsilon_1\epsilon_3 & \gamma_e\epsilon_1\epsilon_2 & \gamma_e\epsilon_1 \end{pmatrix}. \tag{6.73}$$

This structure provides a natural explanation of the charged lepton mass hierarchy, namely $m_e : m_\mu : m_\tau = \alpha_e\epsilon_1^4 : \beta_e\epsilon_1^2 : \gamma_e\epsilon_1$.

After the seesaw mechanism, by inputting and expanding the matrices in Eq.6.29 we find the effective neutrino mass matrix,

$$M_\nu \simeq g_1^2\frac{v_u^2}{\Lambda}\begin{pmatrix} -2 & \epsilon_3 & \epsilon_2 \\ \epsilon_3 & -2\epsilon_2 & 1 \\ \epsilon_2 & 1 & -2\epsilon_3 \end{pmatrix} + g_2^2\frac{v_u^2}{\Lambda}\begin{pmatrix} 0 & -2\epsilon_2^2+\epsilon_3 & \epsilon_2 \\ -2\epsilon_2^2 & 2\epsilon_2 & -1 \\ \epsilon_2 & -1 & -2\epsilon_2^2+2\epsilon_3 \end{pmatrix}. \tag{6.74}$$

The parameters g_1, g_2 and ϵ_2, ϵ_3 are determined by the fit to the neutrino mass squared differences and PMNS mixing parameters, which arise predominantly from the neutrino sector, due to the very small charged lepton mixing corrections. The large elements in the neutrino mass matrix occurring in the $(1,1)$ and $(2,3)$ positions, controlled by g_1, g_2, are responsible for the quasi-degenerate neutrino masses $m_1 \sim m_2 \sim 0.11$ eV, and $m_3 \sim 0.12$ eV, with the neutrinoless double beta becay parameter $m_{ee} \sim 0.11$ eV in the sensitivity region of current experiments, and the cosmological sum of neutrino masses $\sum m_i \sim 0.34$ eV being in the disfavoured region. Either this lepton model will be discovered soon or it will be excluded in the near future. In any case we remark that the neutrino sector considered here is identical to that of the Feruglio model, being independent of the weighton ϕ, and hence ϵ_1.

6.6 Chapter Summary

In this chapter we have shown how quark and lepton mass hierarchies can be reproduced in the framework of modular symmetry. The mechanism we have proposed is analogous to the FN

mechanism, but without requiring any Abelian symmetry to be introduced, nor any SM singlet flavon to break it. The modular weights of fermion fields play the role of FN charges, and SM singlet fields with non-zero modular weight called weightons play the role of flavons.

We have illustrated the mechanism by analysing A_4 (modular level 3) models of quark and lepton (including neutrino) masses and mixing, with a single modulus field. We showed how a previously proposed A_4 modular model of leptons can be recast in natural form by introducing a single weighton, then applied similar ideas to 27 possible models in the quark sector. We analysed all the quark models, combined with the natural lepton model, and identified two viable combinations, which can successfully describe all quark and lepton (including neutrino) masses and mixing, using a single modulus field τ, and in which all charged fermion mass hierarchies originate from a single weighton.

We have discussed these two particular examples in some detail, both numerically and analytically, showing how both fermion mass and mixing hierarchies emerge from the modular symmetry. The analytic results clearly show how the fermion mass hierarchies are controlled by the powers of the weighton field which multiply a particular row of the Yukawa matrix, while the smallness of the quark mixing angles arises because of the proximity of the modulus field to the fixed point case $\tau_T = i\infty$, which results in exponentially suppressed entries within a particular row of the Yukawa matrix. This leads to a simple analytic understanding of the smallness of quark mixing angles.

We emphasise that the mechanism introduced in this chapter is quite unlike the traditional FN mechanism, based on an Abelian symmetry, in which the suppression of both rows and columns of the Yukawa matrices arises from FN charges. In the present approach, fermion mass hierarchies and small quark mixing angles emerge from different aspects of the modular symmetry, without having to introduce an extra Abelian symmetry and an additional flavon to break it. The A_4 flavour symmetry arises as a finite subgroup of the underlying modular symmetry, and the weightons responsible for the charged fermion mass hierarchies are A_4 singlets which do not break the flavour symmetry.

Finally we note that the class of modular level 3 (with even weight modular forms) examples of the mechanism we present here are by no means exhaustive. The new mechanism may be be applied to other levels and choices of weights, and to models with any number of moduli fields and weightons.

Chapter 7

Conclusion

Naturalness may take many forms in modern day BSM theories. In this thesis we have considered quantitative measures of naturalness, such as the Barbieri-Giudice (BG) metric for the BLSSM, as well as concepts such as unification as a guiding principle and finally explicitly theories which solve the flavour problem, with natural ($\mathcal{O}(1)$) parameters.

In chapter 2 we began by considering the SUSY extension of the $U(1)_{B-L}$ model. We used two metrics of FT, both a high scale BG metric, as well as a low (SUSY) scale one to compare the BLSSM to the CMSSM. We found here that both models have a similar level of FT, but slightly higher for the BLSSM at GUT scale, in the presence of all available constraints. This was largely driven by the requirement for a high Z' mass of 4 TeV from non-observation in searches, which sets generally larger allowed unification masses, which was somewhat reflected by a higher mass low energy spectra of sparticles. Considering low energy FT, the BLSSM and MSSM are somewhat more similar. In addition to FT, we considered the DM candidates of each model for our given parameter scan. There are several candidates which appear in the BLSSM but not MSSM which can well accommodate all DM constraints so far. In addition to the bino which was present in both models, the extra $B-L$ neutralinos (the $U(1)_{B-L}$ gaugino, $\tilde{B}'$ and two Higgsinos $\tilde{\eta}$) may be cold DM candidates. In addition we found the superpartner to the RH neutrino, the RH sneutrino, was an ideal candidate.

In chapter 3 we built on the previous chapter's finding of a RH sneutrino acting as a cold DM candidate and inspected its properties. Here we saw that the current and near future (15 year) tests of indirect detection could begin to touch the available parameter space. If such a signal were to be established, then by examining the shape of the photon flux distribution, there exists the possibility to discriminate different DM species consequently. For example, the scalar sneutrino may be distinguishable from the fermionic neutralino DM given the different flux shapes, for the same given DM mass. We also explored the possibility of detecting sneutrinos at the LHC through unique signatures. In addition to the usual mono-X searches, we found there were options involving multi-lepton final states, with and without jets in addition to the missing transverse energy. Finally, we saw that the exact details depended on the hierarchy of mass states in a particular spectrum.

We then shifted focus from DM to a more subtle problem in chapter 4. Here we compared two similar models, the $U(1)_Y \times U(1)_{B-L}$ model of the previous two chapters, versus the $U(1)_R \times U(1)_{B-L}$ model arising from $SO(10)$. One of the first discovery modes of both models was from their Z', and in this chapter we investigated the ability to use forward-backward asymmetry to differentiate the two models. Since the BLR has axial couplings rather than just vector as in the usual $B-L$ case, such a test to discern from which a Z' belongs is possible. These findings may provide hints towards unification at high scales.

In the remaining two chapters, 5 and 6, we considered the flavour problem. In the framework of Modular Symmetry, inspired by string theory, we provided several models which explain the observed neutrino masses and mixing. In the first chapter we considered a model with natural parameters for the charged lepton masses, in addition to explaining neutrino data. We considered seven scenarios across two different modular levels, 4 and 5, corresponding to the discrete groups S_4 and A_5. All of these seven models had good fits to data, in addition to natural charged lepton masses. In chapter 6 we extended this idea to the quark sector, using a pre-existing model of neutrino masses, but attempting to determine all quark and lepton masses using natural input parameters. We found two such model scenarios which were able to satisfy all neutrino and quark masses and mixing angles, providing an elegant solution to the flavour puzzle.

Looking ahead, there are many possible directions which still remain to be explored. Firstly, the obvious dark matter problem requires a solution which cannot be provided by the SM. Despite the beauty of the WIMP scenario, there is no argument which prevents a huge span of DM masses, over fifty orders of magnitude, which may prevent any terrestrial interaction. However, we have shown that even typical SUSY WIMP scenarios may perfectly evade current experimental efforts, and require further study to fully explore its parameter space. From the collider perspective, so far there has been no BSM physics discovered, though many natural, $\mathcal{O}$(TeV) scale models may still be hiding in the data, and require ~ 3000 fb^{-1}, or more, to be seen. Undiscussed in this thesis are the alluring hints of new physics from both $g-2$ (electron and muon) and also the ever-present $b-$anomalies, where a coherent picture of all flavour sectors has yet to emerge, though the next few years of experiments will shed light on the final story here. There are also the less well known anomalies, such as from the Atomki group, which have proven if nothing else that $\mathcal{O}(10)$ MeV bosons may be added to the SM consistently with all current experimental data, and that new physics might be hiding at low-scale. Arguably the only BSM problem which directly requires a solution is neutrino physics. Much is still unknown in this sector though: the absolute scale, MO and CP-violating phase are yet to be directly measured, and the remaining parameters have much more precision to be gained. Neutrino masses may be the key to solving the whole flavour puzzle, which is perhaps the most compelling problem which still remains with the SM. With new directions like modular symmetry, there is clearly much more to be explored in this age old problem, and this is largely dependent on new directions from theorists. In summary there are a great many worthy directions to pursue as a modern day BSM physicist, and with numerous experiments operating in a multitude of sectors, the current status of particle physics is an exciting one.

Appendix A

Higgs Self-Energy Correction

In this section, we briefly derive the correction to the Higgs mass term from a fermion. We begin with the Feynman rule for a fermion propagator, and two useful trace theorems.

$$\frac{i(\not{p}+m)}{p^2-m^2+i\epsilon}$$

Feynman rule for fermion propagator

$$\mathrm{Tr}\left[(\not{k})^2\right] = \mathrm{Tr}\left[k_\mu\gamma^\mu k_\nu\gamma^\nu\right] = \mathrm{Tr}\left[k_\mu k_\nu(-\gamma^\nu\gamma^\mu + \{\gamma^m u, \gamma^\nu\})\right] = \mathrm{Tr}\left[-\not{k}^2 + 2k_\mu k_\nu g^{\mu\nu}\right], \quad \text{(A.1)}$$

$$2\mathrm{Tr}\left[(\not{k})^2\right] = \mathrm{Tr}\left[2k^2\mathbb{1}\right] \to \mathrm{Tr}\left[(\not{k})^2\right] = 4k^2. \quad \text{(A.2)}$$

We may now draw the relevant loop diagram for the correction to the Higgs mass from a fermion loop, and calculate the mass correction given N_c colours.

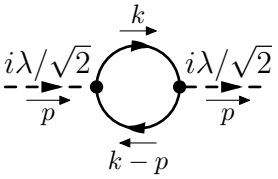

$$= -i\Delta m_H^2 \quad \text{(A.3)}$$

$$-i\Delta m_H^2 = N_c(-1)\left(\frac{i\lambda}{\sqrt{2}}\right)^2\int_{-\infty}^{\infty}\frac{\mathrm{d}^4k}{(2\pi)^4}\mathrm{Tr}\left[\frac{i(\not{k}+m)}{k^2-m^2+i\epsilon}\frac{i(-\not{p}+\not{k}+m)}{(k-p)^2-m^2+i\epsilon}\right] \quad \text{(A.4)}$$

$$= -N_c\frac{\lambda^2}{2}\int_{-\infty}^{\infty}\frac{\mathrm{d}^4k}{(2\pi)^4}\mathrm{Tr}\left[\frac{(\not{k})}{k^2}\frac{(\not{k})}{k^2}\right] = -\frac{\lambda^2}{2}\int_{-\infty}^{\infty}\frac{\mathrm{d}^4k}{(2\pi)^4}\frac{4}{k^2} \quad \text{(A.5)}$$

$$-i\Delta m_H^2 = -N_c(-i)_{wick\ rotation}\frac{\lambda^2}{2}2\pi^2\int_{-\infty}^{\infty}\frac{\mathrm{d}k_E}{(2\pi)^4}k_E^3\frac{4}{k_E^2} = \frac{i\lambda^2}{4\pi^2}\int_{-\infty}^{\infty}\mathrm{d}k_E k_E \quad \text{(A.6)}$$

$$\Delta m_H^2 = \frac{-N_c\lambda^2}{4\pi^2}\int_0^{\Lambda_{UV}}\mathrm{d}k_E k_E = -N_c\frac{\lambda^2}{8\pi^2}\Lambda_{UV}^2 + \ldots \quad \text{(A.7)}$$

We finally see the leading order mass correction scales with the square of the cut-off, which will lead to very large FT of the bare mass term.

Appendix B

β Functions for the BLSSM

We complete the list of the β functions giving those concerning the soft masses of the scalar fields H_u, H_d and η_1, η_2. These are given, at one-loop, by

$$\begin{aligned}
\beta_{m^2_{H_u}} &= -\frac{6}{5}\left(g_1^2(M_1^2+\tilde{M}^2)+\tilde{g}^2({M_1'}^2+\tilde{M}^2)+2g_1\tilde{g}(M_1+M_1')\tilde{M}\right)-6g_2^2M_W^2, \\
&- 3(g_1^2+\tilde{g}^2)\sigma_1-\frac{3\sqrt{10}}{4}g_{BL}\tilde{g}\sigma_2+6\left(m^2_{H_u}+m^2_{q_{33}}+m^2_{u_{33}}\right)Y_t^2+6T_t^2 \qquad \text{(B.1)} \\
\beta_{m^2_{H_d}} &= -\frac{6}{5}\left(g_1^2(M_1^2+\tilde{M}^2)+\tilde{g}^2({M_1'}^2+\tilde{M}^2)+2g_1\tilde{g}(M_1+M_1')\tilde{M}\right)-6g_2^2M_W^2, \\
&+ 3(g_1^2+\tilde{g}^2)\sigma_1+\frac{3\sqrt{10}}{4}g_{BL}\tilde{g}\sigma_2+6\left(m^2_{H_d}+m^2_{q_{33}}+m^2_{d_{33}}\right)Y_b^2+6T_b^2 \qquad \text{(B.2)} \\
\beta_{m^2_{\eta_1}} &= -12{g_{BL}}^2({M_1'}^2+\tilde{M}^2)+4m^2_{\eta_1}\mathrm{tr}(Y_N^2)+4\mathrm{tr}(T^2_{Y_N})+8\mathrm{tr}(m^2_{\nu_R}Y_N^2), \\
&+ 3\sqrt{\frac{2}{5}}g_{BL}\tilde{g}\sigma_1+\frac{3}{2}{g_{BL}}^2\sigma_2, \qquad \text{(B.3)} \\
\beta_{m^2_{\eta_2}} &= -12{g_{BL}}^2({M_1'}^2+\tilde{M}^2)-3\sqrt{\frac{2}{5}}g_{BL}\tilde{g}\sigma_1-\frac{3}{2}{g_{BL}}^2\sigma_2, \qquad \text{(B.4)}
\end{aligned}$$

where, for the sake of simplicity, we have neglected all the Yukawa couplings but top- and bottom-quark Y_t, Y_b and the heavy-neutrinos Y_N. We have also assumed real parameters.

Appendix C

Linear Seesaw and β Functions for the BLR

The linear seesaw is similar to an inverse seesaw, but with $\mu \to 0$ and a new term coupling a LH neutrino to the scalar singlet S:

$$\begin{pmatrix} 0 & Yv & Fv_L \\ Y^T v & 0 & \tilde{F}v_R \\ F^T v_L & \tilde{F}^T v_R & 0 \end{pmatrix} \equiv \begin{pmatrix} 0 & m_D & \epsilon \\ m_D^T & 0 & M_\chi \\ \epsilon^T & M_\chi^T & 0 \end{pmatrix}. \tag{C.1}$$

Each element here corresponds to a 3×3 block. Solving this in block diagonal form, assuming $\epsilon \ll m_D \ll M_\chi$, one finds

$$\begin{pmatrix} M_\chi + m_D^T m_D M_\chi^{-1} & 0 & 0 \\ 0 & -(M_\chi + m_D^T m_D M_\chi^{-1}) & 0 \\ 0 & 0 & -\epsilon \frac{m_D^T}{M_\chi} \end{pmatrix}. \tag{C.2}$$

So the light and heavy physical masses are

$$M_{\nu_L} = -\epsilon \frac{m_D^T}{M_\chi} + \text{h.c.} \tag{C.3}$$

$$M_{N_1} \sim M_{N_2} \sim M_\chi + m_D^T m_D M_\chi^{-1} + \text{h.c.} \tag{C.4}$$

Here we have the light neutrinos, ν_L, as observed in oscillation experiments, and $N_{1,2}$ are the heavier neutral fermions. The smallness of ϵ may allow for a low (TeV) scale M_χ, which is a fundamental feature of all low-scale seesaw mechanisms. Unlike the inverse seesaw, we see that M_{ν_l} is linear in m_D, which is proportional to the Yukawa couplings, hence the name "linear" seesaw.

Coefficient	GUT normalisation	Value	Scale	
$b^{BLR}_{R,R}$	1	15/2	$M_{\rm SUSY} < Q < M_{\rm GUT}$	Abelian
		13/3	$M_{\rm BLR} < Q < M_{\rm SUSY}$	
$b^{BLR}_{(B-L),(B-L)}$	3/8	27/4	$M_{\rm SUSY} < Q < M_{\rm GUT}$	
		17/4	$M_{\rm BLR} < Q < M_{\rm SUSY}$	
$b^{BLR}_{R,B-L} = b^{BLR}_{B-L,R}$	$\sqrt{3/8}$	$-\sqrt{3/8}$	$M_{\rm SUSY} < Q < M_{\rm GUT}$	
		$-1/\sqrt{24}$	$M_{\rm BLR} < Q < M_{\rm SUSY}$	
B^{BLR}_3	1	-3	$M_{\rm SUSY} < Q < M_{\rm GUT}$	Non-Abelian
	1	-7	$M_{\rm BLR} < Q < M_{\rm SUSY}$	
	1	-7	$M_{\rm EW} < Q < M_{\rm BLR}$	
B^{BLR}_2	1	1	$M_{\rm SUSY} < Q < M_{\rm GUT}$	
	1	-19/6	$M_{\rm BLR} < Q < M_{\rm SUSY}$	
	1	-19/6	$M_{\rm EW} < Q < M_{\rm BLR}$	

Table C.1: Beta function coefficients for Abelian and non-Abelian gauge groups in the BLR model

C.1 RGEs

Beta functions for the non-Abelian and Abelian groups, respectively, are [123]

$$\frac{\mathrm{d}g_a}{\mathrm{d}t} = \frac{B_a g_a^3}{16\pi^2}\ , \quad \frac{dg_{lm}}{dt} = \frac{g_{lk}}{16\pi^2} b_{ij} g_{ik} g_{jm}, \tag{C.5}$$

where the index a runs over the non-Abelian groups $SU(2)_L$ and $SU(3)_c$, $a = 2, 3$ and (i, j, k, l, m) run over the $U(1)_R$, $U(1)_{B-L}$, and mixed $U(1)_R \times U(1)_{B-L}$ and $U(1)_{B-L} \times U(1)_R$ groups, $(i, j, k, l, m) = (R, B - L)$ and Einstein summation convention is assumed. For our RGE section, we make a rotation on the coupling matrix G, such that it is set in upper triangular form [58]

$$G = \begin{pmatrix} g_{11} & g_{12} \\ g_{21} & g_{22} \end{pmatrix} \tag{C.6}$$

$$\tilde{G} = GO_R^T = \begin{pmatrix} g & \tilde{g} \\ 0 & g' \end{pmatrix} = \begin{pmatrix} \frac{g_{11}g_{22} - g_{12}g_{21}}{\sqrt{g_{21}^2 + g_{22}^2}} & \frac{g_{11}g_{21} + g_{12}g_{22}}{\sqrt{g_{21}^2 + g_{22}^2}} \\ 0 & \sqrt{g_{21}^2 + g_{22}^2} \end{pmatrix} \tag{C.7}$$

One may consequently find the RGE in terms of $g,\ g',\ \tilde{g}$ by differentiating these expressions and then replacing the differentials dg_{ij}/dt with the beta functions as calculated with eq. C.5, then replacing g_{11}, g_{12}, g_{22} in terms of $g,\ g',\ \tilde{g}$.

C.2 Derivation of Renormalisation Factors

In N=1 SUSY, for the renormalisation of a single gauge coupling at one loop, one finds the standard expression [218]

$$\frac{\mathrm{d}g}{\mathrm{d}t} = \frac{g^3}{16\pi^2}(S(R)^{Ch} - 3C(G)) \tag{C.8}$$

where $S(R)^{Ch}$ is the Dynkin index summed over all chiral multiplets and for a single multiplet is defined as

$$\delta^{ab}S(R) = \mathrm{tr}(t^a t^b), \tag{C.9}$$

and $C(G)$ is the quadratic Casimir invariant of the adjoint representation of group G. This is trivial to determine and is simply N for $SU(N)$ and 0 for a $U(N)$. The Dynkin index can be quickly found knowing the particle content of a model and the quantum numbers under the different gauge groups of a theory; thus one may immediately determine how couplings run in SUSY theories with no calculation of any Feynman diagrams, unlike the SM. This is because in SUSY one is only concerned with wave-function renormalisation [219]. We now go through some specific examples of how one calculates the Dynkin indices. In our notation $b_{ij} = S(R)_{ij}$ as the Casimir invariant is 0 for $U(1)$ gauge groups. Before we discuss the Dynkin index for the Abelian sector which interests us, we will quickly discuss how to calculate this in the non-Abelian sector. As an example, we will use $SU(2)$. For an $SU(N)$ group, in any representation

$$\delta^{ab}S(R)^{SU(N)} = \mathrm{tr}(t^a t^b) \tag{C.10}$$

$$\delta_{ab}\delta^{ab}S(R)^{SU(N)} = \delta_{ab}\mathrm{tr}(t^a t^b) \tag{C.11}$$

$$(N^2-1)S(R)^{SU(N)} = \mathrm{tr}(t^a t^a) = (N^2-1)\mathrm{tr}(t^3 t^3) \tag{C.12}$$

$$S(R)^{SU(N)} = \mathrm{tr}(t^3 t^3) \tag{C.13}$$

Where we note that the number of generators is fixed for any representation, and equal to N^2-1, and consequently $\delta^{ab}\delta_{ab} = N^2 - 1$. Also, for $SU(N)$, though this holds more generally for any compact Lie group, $\mathrm{tr}(t^1 t^1) = \mathrm{tr}(t^2 t^2) = ...$, we choose to consider the T^3 but are at liberty to choose any of the generators. As a concrete example, we consider $SU(2)$ and the 2 and 3 dimensional representations. We find

$$S(2)^{SU(2)} = \mathrm{tr}(T^3 T^3) = \frac{1}{4}\mathrm{tr}(\sigma^3\sigma^3) = \frac{1}{4}\mathrm{tr}(I_2) = \frac{1}{2} \tag{C.14}$$

$$S(3)^{SU(2)} = \mathrm{tr}(J^3 J^3) = 2 \tag{C.15}$$

where $J_3 = [1,0,0;0,0,0;0,0,-1]$, and $T^a = \frac{1}{2}\sigma^a$, the Pauli matrices. So, for a non-Abelian group, one then sums over all the chiral multiplets

Coefficient	$S(R)^{Ch}$	GUT normalisation	C(G)	S(R)$^{GN}_{Ch}$ -3C(G) [1]	Scale
b_3^{BLR}	$1/2 \times \sum_i C_i = 6$	1	3	-3	$M_{SUSY} < \mathrm{Q} < M_{GUT}$
b_L^{BLR}	$1/2 \times \sum_i L_i = 7$	1	2	+1	
$b_{R,R}^{BLR}$	$\sum_i T^2_{3R\ i} = 15/2$	1	0	15/2	
$b_{BL,BL}^{BLR}$	$\sum_i (B-L)_i^2 = 18$	3/8	0	27/4	
$b_{R,BL}^{BLR}$	$\sum_i ((B-L)T_{3R})_i = -1$	$\sqrt{3/8}$	0	-$\sqrt{3/8}$	
$b_{BL,R}^{BLR}$	$\sum_i ((B-L)T_{3R})_i = -1$	$\sqrt{3/8}$	0	-$\sqrt{3/8}$	
$b_{\chi,\chi}^{\chi}$	$\sum_i (T_\chi^2)_i = 153/8$	1/10	0	153/80	
$b_{Y,Y}^{\chi}$	$\sum_i (T_Y^2)_i = 11$	3/5	0	33/5	
$b_{Y,\chi}^{\chi}$	$\sum_i (T_Y T_\chi)_i = 6$	$1/\sqrt{10} \times \sqrt{3/5}$	0	$3\sqrt{6}/5$	
$b_{\chi,Y}^{\chi}$	$\sum_i (T_\chi T_Y)_i = 6$	$1/\sqrt{10} \times \sqrt{3/5}$	0	$3\sqrt{6}/5$	
$SU(3)_c$	-	-	-	[2] $b_3^{SM} = -7$	$10^2\mathrm{GeV} < \mathrm{Q} < 10^3\mathrm{GeV}$
$SU(2)_L$	-	-	-	[3] $b_L^{SM} = -19/6$	$10^2\mathrm{GeV} < \mathrm{Q} < 10^3\mathrm{GeV}$
$U(1)_Y$	-	-	-	[4] $b_1^{SM} = 41/10$	$10^2\mathrm{GeV} < \mathrm{Q} < 10^3\mathrm{GeV}$

Table C.2: Beta function coefficients for the BLR model

C.2.1 Derivation of β Function Coefficients

Beta function for non-Abelian and Abelian groups, respectively are [123]

$$\frac{\mathrm{d}g}{\mathrm{d}t} = \frac{Bg^3}{16\pi^2}\ , \quad \frac{dg_{lm}}{dt} = \frac{g_{lk}}{(4\pi)^2} b_{ij} g_{ik} g_{jm}. \tag{C.16}$$

$$\frac{dg_{11}}{dt} = \frac{b_{11}g_{11}\left(g_{11}^2+g_{12}^2\right) + b_{12}g_{21}\left(g_{11}^2+g_{12}^2\right) + \left(g_{11}g_{21}+g_{12}g_{22}\right)\left(b_{21}g_{11}+b_{22}g_{21}\right)}{16\pi^2} \tag{C.17}$$

$$\frac{dg_{12}}{dt} = \frac{b_{11}g_{12}\left(g_{11}^2+g_{12}^2\right) + b_{21}g_{12}\left(g_{11}g_{21}+g_{12}g_{22}\right) + g_{22}\left(b_{12}\left(g_{11}^2+g_{12}^2\right) + b_{22}\left(g_{11}g_{21}+g_{12}g_{22}\right)\right)}{16\pi^2} \tag{C.18}$$

$$\frac{dg_{21}}{dt} = \frac{b_{11}g_{11}\left(g_{11}g_{21}+g_{12}g_{22}\right) + b_{12}g_{21}\left(g_{11}g_{21}+g_{12}g_{22}\right) + \left(g_{21}^2+g_{22}^2\right)\left(b_{21}g_{11}+b_{22}g_{21}\right)}{16\pi^2} \tag{C.19}$$

$$\frac{dg_{22}}{dt} = \frac{b_{11}g_{12}\left(g_{11}g_{21}+g_{12}g_{22}\right) + b_{21}g_{12}\left(g_{21}^2+g_{22}^2\right) + g_{22}\left(b_{12}\left(g_{11}g_{21}+g_{12}g_{22}\right) + b_{22}\left(g_{21}^2+g_{22}^2\right)\right)}{16\pi^2} \tag{C.20}$$

[1] $b_3^{SM} = (-(11/3)N^c + (2N_f^c)/3)$; $N^c = 3$, N_f^c is the number of fermions with factor (1/2): (ie 6: (1/2)*(u_L,..,t_R)).
[2] $b_2^{SM} = (-(11/3)N^L + (2N_f^c)/3) + (n_{sc}T(R_{sc}))/3)$; $N^L = 2$, N_f^c is the number of SU(2) doublets = (1/2)*(3+9)=6, $n_{sc} = 1$, $T(R_{cs}) = 1/2$
[3] $b_Y = (1/2) \times 10 + (1/4) \times (2) \times (1/2)^2 = 41/6$. $b_1 = 3/5 \times b_Y = 41/10$
[4] S(R)^{GN} = S(R) × GUT normalisation

C.2.2 Calculating GUT normalisations

Hypercharge

$SU(5) \to SU(3)_c \times SU(2)_L \times U(1)_Y$. Begin with an SU(5) 5-plet, which contains three down quarks of different colours and a lepton doublet.

$$\begin{pmatrix} d^r \\ d^b \\ d^g \\ \begin{pmatrix} \nu \\ e \end{pmatrix} \end{pmatrix} \tag{C.21}$$

The generator of this group must be traceless and have the first three quantum numbers the same, and the last two. (eg a,a,a,b,b where 3a+2b=0). As an example we choose twos and threes.

$$T_Y = x \begin{pmatrix} 2 & 0 & 0 & 0 & 0 \\ 0 & 2 & 0 & 0 & 0 \\ 0 & 0 & 2 & 0 & 0 \\ 0 & 0 & 0 & -3 & 0 \\ 0 & 0 & 0 & 0 & -3 \end{pmatrix} \tag{C.22}$$

For the fundamental representation of $SU(N)$, $\mathrm{tr}(T^a T^a)$=1/2. This determines the normalisation parameter, x.

$$\mathrm{tr}(T_Y T_Y) = 1/2 = x^2(30) \to x = 1/\sqrt{60}. \tag{C.23}$$

In the SM, the hypercharge of a lepton doublet is $Y(L) = Y(Q - T_{3L}) = -1/2$, and so $Y(L)^2 = +1/4$. In our GUT normalisation, we would have $Y(L)_{GUT} = \frac{-3}{\sqrt{60}} \to Y(L)^2_{GUT} = 3/20$. So we find that $\frac{Y(L)^2_{GUT}}{Y(L)^2_{SM}} = \frac{3}{5}$. Since the Lagrangian contains terms like $(igYB_\mu)$, then $\frac{(g_Y^{GUT})^2}{(g_Y^{SM})^2} = \frac{(\alpha_Y^{GUT}) \equiv \alpha_1}{(\alpha_Y^{SM})} = \frac{5}{3}$ In a similar fashion, to find the normalisation for $B - L$, we recall that this gauge group is obtained from a PS, $SU(4)_{PS} \to SU(3)_c \times U(1)_{B-L}$, so our SU(4) 4-plet will take the form:

$$T_{B-L} = \frac{1}{\sqrt{24}} \begin{pmatrix} 1 & 0 & 0 & 0 \\ 0 & 1 & 0 & 0 \\ 0 & 0 & 1 & 0 \\ 0 & 0 & 0 & -3 \end{pmatrix} \tag{C.24}$$

and so we may compare the squared $B-L$ normalisation for the SM and GUT normalised to find:

$$\frac{(B-L)^2_{GUT}}{(B-L)^2_{SM}} = \frac{(9/24)}{1} = \frac{3}{8} \tag{C.25}$$

Previously, we found the relation $1/g_Y^2 = 1/g_R^2 + 1/g_{BL}^2 \rightarrow \alpha_Y^{-1} = \alpha_R^{-1} + \alpha_{BL}^{-1}$, which holds with with a $g_{BL}(B-L)/2$ normalisation, which is equivalent to $g_{BL^*}(B-L)$ where $g_{BL^*} = g_{BL}/2$. Using this, along with $\alpha_1^{-1} = \frac{3}{5}\alpha_Y^{-1}$ and $\alpha_{BL'}^{-1} = \frac{3}{8}\alpha_{BL*}^{-1} = \frac{12}{8}\alpha_{BL}$, we find

$$\alpha_1^{-1} = \frac{3}{5}\alpha_R^{-1} + \frac{2}{5}\alpha_{BL'}^{-1}. \tag{C.26}$$

This is used to fix the value of our α_1^{-1} coupling at the breaking scale v_R

C.3 Gauge Kinetic Mixing

C.3.1 Removing Mixed Kinetic Term

The kinetic sector for a gauge group $U(1)_1 \times U(1)_2$ will have a mixed term:

$$\mathcal{L} = -\frac{1}{4}F^{A_1}_{\mu\nu}F^{\mu\nu}_{A_1} - \frac{1}{4}F^{A_2}_{\mu\nu}F^{\mu\nu}_{A_2} - \frac{\kappa}{2}F^{A_1}_{\mu\nu}F^{\mu\nu}_{A_2} \tag{C.27}$$

with κ parametrising the strength of the mixing and

$$F^{A_i}_{\mu\nu} = \partial_\mu A^i_\nu - \partial_\nu A^i_\mu \tag{C.28}$$

(with no anti-commutation term as the two groups are Abelian). We may eliminate the mixing term in the kinetic Lagrangian by performing a rotation on the gauge fields:

$$\begin{pmatrix} A^1_\mu \\ A^2_\mu \end{pmatrix} = \begin{pmatrix} \cos(\phi) & -\sin(\phi) \\ \sin(\phi) & \cos(\phi) \end{pmatrix} \begin{pmatrix} \bar{B}^1_\mu \\ \bar{B}^2_\mu \end{pmatrix} \tag{C.29}$$

One finds the mixed term in the $\bar{B}$ basis

$$\mathcal{L}_{kin} \supset 2\partial^2(\bar{B}^1_\mu \bar{B}^\mu_2)(\cos^2(\theta) - \sin^2(\theta)) \tag{C.30}$$

Which may be removed by setting $\theta = \pi/4$. The kinetic Lagrangian then takes the form

$$\mathcal{L}_{\text{kin}} = -\frac{1-\kappa}{4}F^{\bar{B}_1}_{\mu\nu}F^{\mu\nu}_{\bar{B}_1} - \frac{1+\kappa}{4}F^{\bar{B}_2}_{\mu\nu}F^{\mu\nu}_{\bar{B}_2} \tag{C.31}$$

To take the canonical form (kinetically diagonal basis), one may rescale the fields:

$$\begin{pmatrix} \bar{B}^1_\mu \\ \bar{B}^2_\mu \end{pmatrix} = \begin{pmatrix} \frac{1}{\sqrt{1-\kappa}} & 0 \\ 0 & \frac{1}{\sqrt{1+\kappa}} \end{pmatrix} \begin{pmatrix} B^1_\mu \\ B^2_\mu \end{pmatrix} \tag{C.32}$$

So the rotated and rescaled Lagrangian takes the form

$$\mathcal{L} = -\frac{1}{4} F^{B_1}_{\mu\nu} F^{\mu\nu}_{B_1} - \frac{1}{4} F^{B_2}_{\mu\nu} F^{\mu\nu}_{B_2} \tag{C.33}$$

under the total transformation

$$\begin{pmatrix} A^1_\mu \\ A^2_\mu \end{pmatrix} = \begin{pmatrix} \cos(\pi/4) & -\sin(\pi/4) \\ \sin(\pi/4) & \cos(\pi/4) \end{pmatrix} \begin{pmatrix} \frac{1}{\sqrt{1-\kappa}} & 0 \\ 0 & \frac{1}{\sqrt{1+\kappa}} \end{pmatrix} \begin{pmatrix} B^1_\mu \\ B^2_\mu \end{pmatrix} \tag{C.34}$$

$$= \underbrace{\frac{1}{\sqrt{2}} \begin{pmatrix} \frac{1}{\sqrt{1-\kappa}} & -\frac{1}{\sqrt{1-\kappa}} \\ \frac{1}{\sqrt{1+\kappa}} & \frac{1}{\sqrt{1+\kappa}} \end{pmatrix}}_{\equiv \mathcal{R}_\kappa} \begin{pmatrix} B^1_\mu \\ B^2_\mu \end{pmatrix} \tag{C.35}$$

C.3.2 Consequences for Gauge Interactions

The fermion interaction Lagrangian is given by

$$\mathcal{L}_{\text{int}} = \bar{\psi}_f \gamma_\mu Q^1_f g_1 A^\mu_1 \psi_f + \bar{\psi}_f \gamma_\mu Q^2_f g_2 A^\mu_2 \psi_f \tag{C.36}$$

where the fermions ψ_f have charges Q^i_f and the gauge coupling is g_{ii} under the gauge group $U(1)_i$. To make the transformation into the new (kinetic mixing free) basis more obvious, we may write this interaction Lagrangian in a more suggestive way

$$\mathcal{L}_{\text{int}} = \bar{\psi}_f \gamma_\mu \begin{pmatrix} Q^1_f & Q^2_f \end{pmatrix} \begin{pmatrix} g_1 & 0 \\ 0 & g_2 \end{pmatrix} \begin{pmatrix} A^\mu_1 \\ A^\mu_2 \end{pmatrix} \psi_f \tag{C.37}$$

Under the transformation C.35, the interaction now becomes

$$\mathcal{L}_{\text{int}} = \bar{\psi}_f \gamma_\mu \begin{pmatrix} Q^1_f & Q^2_f \end{pmatrix} \begin{pmatrix} g_1 & 0 \\ 0 & g_2 \end{pmatrix} \frac{1}{\sqrt{2}} \begin{pmatrix} \frac{1}{\sqrt{1-\kappa}} & -\frac{1}{\sqrt{1-\kappa}} \\ \frac{1}{\sqrt{1+\kappa}} & \frac{1}{\sqrt{1+\kappa}} \end{pmatrix} \begin{pmatrix} B^\mu_1 \\ B^\mu_2 \end{pmatrix} \psi_f \tag{C.38}$$

We define

$$G = \begin{pmatrix} g_1 & 0 \\ 0 & g_2 \end{pmatrix} \frac{1}{\sqrt{2}} \begin{pmatrix} \frac{1}{\sqrt{1-\kappa}} & -\frac{1}{\sqrt{1-\kappa}} \\ \frac{1}{\sqrt{1+\kappa}} & \frac{1}{\sqrt{1+\kappa}} \end{pmatrix} \equiv \begin{pmatrix} g_{11} & g_{12} \\ g_{21} & g_{22} \end{pmatrix} \tag{C.39}$$

So the interaction Lagrangian takes the form

$$\mathcal{L}_{\text{int}} = \bar{\psi}_f \gamma_\mu (g_{11} Q_f^1 + g_{21} Q_f^2) B_1 \psi_f^\mu + \bar{\psi}_f \gamma_\mu (g_{12} Q_f^1 + g_{22} Q_f^2) B_2^\mu \psi_f \tag{C.40}$$

At this point, we may choose to work in this basis, but we may perform an extra rotation on the fields B_1, B_2 to parametrise the matrix G, in terms of only three independent parameters. By making the rotation (which is a function of $(g_1,\ g_2,\ \kappa)$):

$$\begin{pmatrix} B_1^\mu \\ B_2^\mu \end{pmatrix} = \underbrace{\frac{1}{\sqrt{g_{22}^2 + g_{21}^2}} \begin{pmatrix} g_{22} & g_{21} \\ -g_{21} & g_{22} \end{pmatrix}}_{O} \begin{pmatrix} B^\mu \\ B'^\mu \end{pmatrix} \tag{C.41}$$

One finds

$$OG = \begin{pmatrix} \frac{-g_{12}g_{21} + g_{11}g_{22}}{\sqrt{g_{21}^2 + g_{22}^2}} & \frac{g_{11}g_{21} + g_{12}g_{22}}{\sqrt{g_{21}^2 + g_{22}^2}} \\ 0 & \sqrt{g_{21}^2 + g_{22}^2} \end{pmatrix} \equiv \begin{pmatrix} g & \tilde{g} \\ 0 & g' \end{pmatrix} \tag{C.42}$$

and we may thus write the interaction Lagrangian as

$$\mathcal{L}_{\text{int}} = \bar{\psi}_f \gamma_\mu (g Q_f^1 + \tilde{g} Q_f^2) B^\mu \psi_f + \bar{\psi}_f \gamma_\mu (g' Q_f^2) B'^\mu \psi_f \tag{C.43}$$

One may question whether this spoils the kinetic Lagrangian and introduce mixed terms, but it does not, the mixed terms cancel and leave the kinetic part of the Lagrangian is found to be

$$\mathcal{L} = -\frac{1}{4} F_{\mu\nu}^B F_B^{\mu\nu} - \frac{1}{4} F_{\mu\nu}^{B'} F_{B'}^{\mu\nu} \tag{C.44}$$

C.4 β-Functions for Two $U(1)$ Groups

This discussion of the derivation of the beta functions follow the procedure in eq 12-14 in [123], noting simplicity due to working in a SUSY framework. We use the basis with g_{ij} (rather than $\tilde{g}$ found in eq. C.40). We first rewrite the interaction Lagrangian of fermions with gauge bosons using a slightly different notation (but still in this basis), which we will use henceforth

$$\mathcal{L}_{\text{int}} = \bar{\psi}_f \gamma_\mu Q_f^r \psi_f g_{rb} B_b^\mu \tag{C.45}$$

where the indices f, s refers to fermions, scalars respectively and the repeated indices imply a sum over all fermion/scalar fields. For our two-field case, $r, b = 1, 2$ (for a specific case, eg $U(1)_R \times U(1)_{B-L}$ one would say $r, b = R, (B-L)$). If one expands this expression, one will recover the interaction Lagrangian, C.40. The β-functions determine how these couplings run with energy, and will take the form (in our case) of a system comprised of four differential equations

$$\frac{dg_{ij}}{dt} = f_{ij}(g) \tag{C.46}$$

where i, j labels the fields and the RHS is a function of all other fields at order g^3. One must then solve the system of differential equations to find how each of the i fields run.

$$g_{kb} = Q_k^r g_{rb} \tag{C.47}$$

$$\frac{dg_{kb}}{dt} = g_{ka}\beta_{ab} \tag{C.48}$$

$$\beta_{ab} = \frac{1}{(4\pi)^2}\left(\frac{4}{3}\kappa g_{fa}g_{fb} + \frac{1}{3}\eta g_{sa}g_{sb}\right) \tag{C.49}$$

where g_{kb} is a reduced coupling that evolves according to $\frac{dg_{kb}}{dt}$, where k labels the fields (fermions / scalars) that carry U(1) charges. There is an explanation of the origin of eq. C.49 in the appendix. We may expand eq.C.49, a

$$\beta_{ab} = \frac{1}{(4\pi)^2}\left(\frac{4}{3}\kappa Q_f^r Q_f^p g_{ra}g_{rb} + \frac{1}{3}\eta Q_s^r Q_s^p g_{ra}g_{rb}\right) \tag{C.50}$$

$$= \frac{1}{(4\pi)^2}\sum_{i,j} b^{ij} g_{ia}g_{jb} \tag{C.51}$$

where we have defined

$$b^{ij} = \left(\frac{4}{3}\kappa Q_f^i Q_f^j + \frac{1}{3}\eta Q_s^i Q_s^j\right) \tag{C.52}$$

One thus finds a general expression for the four beta functions as

$$\frac{dg_{11}}{dt} = \frac{b_{11}g_{11}\left(g_{11}^2+g_{12}^2\right) + b_{12}g_{21}\left(g_{11}^2+g_{12}^2\right) + \left(g_{11}g_{21}+g_{12}g_{22}\right)\left(b_{21}g_{11}+b_{22}g_{21}\right)}{16\pi^2} \tag{C.53}$$

$$\frac{dg_{12}}{dt} = \frac{b_{11}g_{12}\left(g_{11}^2+g_{12}^2\right) + b_{21}g_{12}\left(g_{11}g_{21}+g_{12}g_{22}\right) + g_{22}\left(b_{12}\left(g_{11}^2+g_{12}^2\right) + b_{22}\left(g_{11}g_{21}+g_{12}g_{22}\right)\right)}{16\pi^2} \tag{C.54}$$

$$\frac{dg_{21}}{dt} = \frac{b_{11}g_{11}\left(g_{11}g_{21}+g_{12}g_{22}\right) + b_{12}g_{21}\left(g_{11}g_{21}+g_{12}g_{22}\right) + \left(g_{21}^2+g_{22}^2\right)\left(b_{21}g_{11}+b_{22}g_{21}\right)}{16\pi^2} \tag{C.55}$$

$$\frac{dg_{22}}{dt} = \frac{b_{11}g_{12}\left(g_{11}g_{21}+g_{12}g_{22}\right) + b_{21}g_{12}\left(g_{21}^2+g_{22}^2\right) + g_{22}\left(b_{12}\left(g_{11}g_{21}+g_{12}g_{22}\right) + b_{22}\left(g_{21}^2+g_{22}^2\right)\right)}{16\pi^2} \tag{C.56}$$

In SUSY, one may easily find b_{ij}, without using any diagrams, by counting the charges. Examples of the calculation of these parameters are discussed in appendix C.2.

We have four charges, $g_{11},\ g_{12},\ g_{21},\ g_{22}$, corresponding to the

$$(U(1)_R)^2,\ U(1)_R U(1)_{B-L},\ U(1)_{B-L}U(1)_R,\ (U(1)_{B-L})^2 \tag{C.57}$$

groups. For the beta-function coefficients, we find

$$\beta_{11} = \frac{b_{11}}{(4\pi)^2}, \quad b_{11} = 15/2 \tag{C.58}$$

$$\beta_{12} = \frac{b_{12}}{(4\pi)^2}, \quad b_{12} = -1 \tag{C.59}$$

$$\beta_{21} = \frac{b_{21}}{(4\pi)^2}, \quad b_{21} = -1 \tag{C.60}$$

$$\beta_{22} = \frac{b_{22}}{(4\pi)^2}, \quad b_{22} = 18 \tag{C.61}$$

so we now have

$$\frac{dg_{11}}{dt} = \frac{1}{(4\pi)^2}\left(b_{11}g_{11}^3 + b_{21}g_{12}g_{21}^2\right) \tag{C.62}$$

$$\frac{dg_{12}}{dt} = \frac{1}{(4\pi)^2}\left(b_{12}g_{11}g_{12}^2 + b_{22}g_{12}g_{22}^2\right) \tag{C.63}$$

$$\frac{dg_{21}}{dt} = \frac{1}{(4\pi)^2}\left(b_{11}g_{21}g_{11}^2 + b_{21}g_{22}g_{21}^2\right) \tag{C.64}$$

$$\frac{dg_{22}}{dt} = \frac{1}{(4\pi)^2}\left(b_{12}g_{21}g_{12}^2 + b_{22}g_{22}^3\right). \tag{C.65}$$

C.5 Rotation into $\tilde{g}$ Basis

This section follows that of section 3 of [58]. We now rotate our coupling matrix:

$$G = \begin{pmatrix} g_{11} & g_{12} \\ g_{21} & g_{22} \end{pmatrix} \tag{C.66}$$

$$O_R = \begin{pmatrix} \cos\theta & -\sin\theta \\ \sin\theta & \cos\theta \end{pmatrix} = \frac{1}{\sqrt{g_{22}^2 + g_{21}^2}} \begin{pmatrix} g_{22} & -g_{21} \\ g_{21} & g_{22} \end{pmatrix} \tag{C.67}$$

$$\tilde{G} = GO_R^T = \begin{pmatrix} g & \tilde{g} \\ 0 & g' \end{pmatrix} = \begin{pmatrix} \frac{g_{11}g_{22}-g_{12}g_{21}}{\sqrt{g_{21}^2+g_{22}^2}} & \frac{g_{11}g_{21}+g_{12}g_{22}}{\sqrt{g_{21}^2+g_{22}^2}} \\ 0 & \sqrt{g_{21}^2 + g_{22}^2} \end{pmatrix} \tag{C.68}$$

$$g_{11} \to g = \frac{g_{11}g_{22} - g_{12}g_{21}}{\sqrt{g_{21}^2 + g_{22}^2}} \tag{C.69}$$

$$g_{12} \to \tilde{g} = \frac{g_{11}g_{21} + g_{12}g_{22}}{\sqrt{g_{21}^2 + g_{22}^2}} \tag{C.70}$$

$$g_{21} \to 0 \tag{C.71}$$

$$g_{22} \to g' = \sqrt{g_{21}^2 + g_{22}^2} \tag{C.72}$$

Appendix D

Finite Modular Groups

D.1 Finite Modular Group Γ_4 and Level 4 Modular Forms

The finite modular group Γ_4 is isomorphic to S_4, the symmetric group of permutations of four objects. It has 24 elements and five irreducible representations: **1**, **1′**, **2**, **3** and **3′**. It admits a presentation in terms of two generators S and T:

$$S^2 = (ST)^3 = T^4 = \mathbb{1} \,. \tag{D.1}$$

In this paper we use an explicit realization of the elements S and T for the different representations, obtained from the one in Ref. [220], with the identification [186]: $S = S'T'^2$ and $T = S'$, where the primed generators are those given in Ref. [220]. We also use the CGn coefficients listed in Ref. [220].

The linear space of weight 2 and level 4 modular forms has dimension 5 (see, e.g., [174]). These forms can be constructed in terms of the Dedekind eta function [186]:

$$\eta(\tau) \equiv q^{1/24} \prod_{n=1}^{\infty} (1-q^n) \,, \qquad q = e^{2\pi i \tau} \,. \tag{D.2}$$

Defining

$$\begin{aligned} Y(c_1, \ldots, c_6|\tau) \equiv \frac{\mathrm{d}}{\mathrm{d}\tau} \Bigg[& c_1 \log\eta\left(\tau + \frac{1}{2}\right) + c_2 \log\eta\left(4\tau\right) + c_3 \log\eta\left(\frac{\tau}{4}\right) \\ & + c_4 \log\eta\left(\frac{\tau+1}{4}\right) + c_5 \log\eta\left(\frac{\tau+2}{4}\right) + c_6 \log\eta\left(\frac{\tau+3}{4}\right) \Bigg] \,, \end{aligned} \tag{D.3}$$

with $c_1 + \cdots + c_6 = 0$, the basis of the modular forms of weight 2 reads [186],

$$Y_1(\tau) \equiv i\, Y(1, 1, \omega, \omega^2, \omega, \omega^2|\tau)\,, \tag{D.4a}$$
$$Y_2(\tau) \equiv i\, Y(1, 1, \omega^2, \omega, \omega^2, \omega|\tau)\,, \tag{D.4b}$$
$$Y_3(\tau) \equiv i\, Y(1, -1, -1, -1, 1, 1|\tau)\,, \tag{D.4c}$$
$$Y_4(\tau) \equiv i\, Y(1, -1, -\omega^2, -\omega, \omega^2, \omega|\tau)\,, \tag{D.4d}$$
$$Y_5(\tau) \equiv i\, Y(1, -1, -\omega, -\omega^2, \omega, \omega^2|\tau)\,, \tag{D.4e}$$

with $\omega \equiv e^{2\pi i/3}$. Notice here, we have an extra factor of i compared to the definition of Ref. [186]. It has been shown that $Y_1(\tau)$ and $Y_2(\tau)$ form a doublet transforming in the $\mathbf{2}$ of S_4, while the three remaining modular forms make up a triplet transforming in $\mathbf{3'}$ of S_4. Doublet and the triplet will be denoted by

$$Y_{\mathbf{2}}(\tau) \equiv \begin{pmatrix} Y_1(\tau) \\ Y_2(\tau) \end{pmatrix}\,, \qquad Y_{\mathbf{3'}}(\tau) \equiv \begin{pmatrix} Y_3(\tau) \\ Y_4(\tau) \\ Y_5(\tau) \end{pmatrix}\,. \tag{D.5}$$

The q-expansions ($q \equiv e^{i2\pi\tau}$) for Eq. (D.4) can be found in [186]. In our analysis we use the full analytic form. The modular forms of higher weights $k = 4,\, 6, \ldots$ are homogeneous polynomials in the variables $Y_i(\tau)$, $i = 1, \ldots, 5$.

Under CP, Eq. (5.9), modular forms of level 4 and weight 2 transform as [187]:

$$Y_{\mathbf{2}}(-\tau^*) = X_{\mathbf{2}}\, [Y_{\mathbf{2}}(\tau)]^* \quad, \qquad Y_{\mathbf{3'}}(-\tau^*) = X_{\mathbf{3'}}\, [Y_{\mathbf{3'}}(\tau)]^* \quad, \tag{D.6}$$

where $X_{\mathbf{2}}$ and $X_{\mathbf{3'}}$ are the matrices:

$$X_{\mathbf{2}} = \begin{pmatrix} 0 & 1 \\ 1 & 0 \end{pmatrix} \quad, \qquad X_{\mathbf{3'}} = -\frac{1}{3} \begin{pmatrix} -1 & 2\omega & 2\omega^2 \\ 2\omega & 2\omega^2 & -1 \\ 2\omega^2 & -1 & 2\omega \end{pmatrix}\,. \tag{D.7}$$

By decomposing products of representations in their irreducible components we find that a consistent action of CP on chiral multiplets $\varphi_{\mathbf{r}}$ transforming in the representation $\mathbf{r}$ ($\mathbf{r} = \mathbf{1}, \mathbf{1'}, \mathbf{2}, \mathbf{3}, \mathbf{3'}$) of Γ_4 is given by:

$$\varphi_{\mathbf{r}} \xrightarrow{CP} X_{\mathbf{r}}\, \varphi_{\mathbf{r}}^* \quad, \tag{D.8}$$

with $X_{\mathbf{2}}$ and $X_{\mathbf{3'}}$ given above and

$$X_{\mathbf{1}} = -X_{\mathbf{1'}} = 1 \quad, \qquad X_{\mathbf{3}} = X_{\mathbf{3'}} \quad. \tag{D.9}$$

This set of matrices satisfy the consistency conditions

$$X_{\mathbf{r}}\ \rho^{*}_{\mathbf{r}}(\gamma)\ X^{-1}_{\mathbf{r}} = \rho_{\mathbf{r}}(\gamma') \quad , \qquad (\gamma,\gamma') \in \Gamma \quad , \tag{D.10}$$

as can be checked by working with the generators $\gamma = (S,T)$. We find $S' = S^{-1}$ and $T' = T^{-1}$. The conditions for the VEV $(\varphi_1, \varphi_2, \varphi_3)$ of a triplet to preserve CP read:

$$\mathrm{Im}(\varphi_1) = \sqrt{3}\mathrm{Re}(\varphi_2 - \varphi_3) \ , \quad \mathrm{Im}(\varphi_2) = \sqrt{3}\mathrm{Re}(\varphi_1 - \varphi_2) \ , \quad \mathrm{Im}(\varphi_3) = \sqrt{3}\mathrm{Re}(\varphi_3 - \varphi_1) \ . \tag{D.11}$$

In our basis, the requirement of CP conservation on a modular invariant supersymmetric theory at level 4, adopting the above CP transformations on the chiral multiplets, amounts to having all Lagrangian parameters real.

D.2 Finite Modular Group Γ_5 and Level 5 Modular Forms

The finite modular group Γ_5 is isomorphic to A_5, the group of even permutations of five objects. It has 60 elements and five irreducible representations: **1**, **3**, **3′**, **4** and **5**. It admits a presentation in terms of two generators of S and T:

$$S^2 \ = \ (ST)^3 \ = \ T^5 \ = \ I \, . \tag{D.12}$$

In this paper we use the explicit realisation of the elements S and T for the different representations given in Ref. [196], where we can also find the corresponding CG coefficients.

Level 5 modular forms of weight 2 have been built in Ref. [189], making use of the Jacobi theta function:

$$\theta_3(u,\tau) \equiv \theta_{0,0}(u,\tau) = \sum_{n=-\infty}^{\infty} p^{n^2} e^{2\pi i n u} \quad , \tag{D.13}$$

where $p \equiv e^{\pi i \tau}$. Defining the seed functions:

$$\begin{aligned}
\alpha_{1,-1}(\tau) &\equiv \theta_3\left(\frac{\tau+1}{2}, 5\tau\right) , & \alpha_{2,-1}(\tau) &\equiv e^{2\pi i\tau/5}\,\theta_3\left(\frac{3\tau+1}{2}, 5\tau\right) , \\
\alpha_{1,0}(\tau) &\equiv \theta_3\left(\frac{\tau+9}{10}, \frac{\tau}{5}\right) , & \alpha_{2,0}(\tau) &\equiv \theta_3\left(\frac{\tau+7}{10}, \frac{\tau}{5}\right) , \\
\alpha_{1,1}(\tau) &\equiv \theta_3\left(\frac{\tau}{10}, \frac{\tau+1}{5}\right) , & \alpha_{2,1}(\tau) &\equiv \theta_3\left(\frac{\tau+8}{10}, \frac{\tau+1}{5}\right) , \\
\alpha_{1,2}(\tau) &\equiv \theta_3\left(\frac{\tau+1}{10}, \frac{\tau+2}{5}\right) , & \alpha_{2,2}(\tau) &\equiv \theta_3\left(\frac{\tau+9}{10}, \frac{\tau+2}{5}\right) , \\
\alpha_{1,3}(\tau) &\equiv \theta_3\left(\frac{\tau+2}{10}, \frac{\tau+3}{5}\right) , & \alpha_{2,3}(\tau) &\equiv \theta_3\left(\frac{\tau}{10}, \frac{\tau+3}{5}\right) , \\
\alpha_{1,4}(\tau) &\equiv \theta_3\left(\frac{\tau+3}{10}, \frac{\tau+4}{5}\right) , & \alpha_{2,4}(\tau) &\equiv \theta_3\left(\frac{\tau+1}{10}, \frac{\tau+4}{5}\right) ,
\end{aligned} \tag{D.14}$$

and the functions,

$$Y(c_{1,-1},\ldots,c_{1,4};c_{2,-1},\ldots,c_{2,4}|\tau) \equiv \sum_{i,j} c_{i,j}\frac{\mathrm{d}}{\mathrm{d}\tau}\log\alpha_{i,j}(\tau)\,, \quad \text{with } \sum_{i,j} c_{i,j} = 0\,, \tag{D.15}$$

then the modular forms of weight two are divided into the following multiplets of A_5,

$$Y_{\mathbf{5}}(\tau) = \begin{pmatrix} Y_1(\tau) \\ Y_2(\tau) \\ Y_3(\tau) \\ Y_4(\tau) \\ Y_5(\tau) \end{pmatrix} \equiv \begin{pmatrix} -\frac{1}{\sqrt{6}}Y\left(-5,1,1,1,1,1;-5,1,1,1,1,1|\tau\right) \\ Y(0,1,\zeta^4,\zeta^3,\zeta^2,\zeta\,;\,0,1,\zeta^4,\zeta^3,\zeta^2,\zeta\,|\,\tau) \\ Y(0,1,\zeta^3,\zeta,\zeta^4,\zeta^2\,;\,0,1,\zeta^3,\zeta,\zeta^4,\zeta^2\,|\,\tau) \\ Y(0,1,\zeta^2,\zeta^4,\zeta,\zeta^3\,;\,0,1,\zeta^2,\zeta^4,\zeta,\zeta^3\,|\,\tau) \\ Y(0,1,\zeta,\zeta^2,\zeta^3,\zeta^4\,;\,0,1,\zeta,\zeta^2,\zeta^3,\zeta^4\,|\,\tau) \end{pmatrix}, \tag{D.16}$$

$$Y_{\mathbf{3}}(\tau) = \begin{pmatrix} Y_6(\tau) \\ Y_7(\tau) \\ Y_8(\tau) \end{pmatrix} \equiv \begin{pmatrix} \frac{1}{\sqrt{2}}Y\left(-\sqrt{5},-1,-1,-1,-1,-1;\sqrt{5},1,1,1,1,1|\tau\right) \\ Y(0,1,\zeta^4,\zeta^3,\zeta^2,\zeta\,;\,0,-1,-\zeta^4,-\zeta^3,-\zeta^2,-\zeta\,|\,\tau) \\ Y(0,1,\zeta,\zeta^2,\zeta^3,\zeta^4\,;\,0,-1,-\zeta,-\zeta^2,-\zeta^3,-\zeta^4\,|\,\tau) \end{pmatrix}, \tag{D.17}$$

$$Y_{\mathbf{3}'}(\tau) = \begin{pmatrix} Y_9(\tau) \\ Y_{10}(\tau) \\ Y_{11}(\tau) \end{pmatrix} \equiv \begin{pmatrix} \frac{1}{\sqrt{2}}Y\left(\sqrt{5},-1,-1,-1,-1,-1;-\sqrt{5},1,1,1,1,1|\tau\right) \\ Y(0,1,\zeta^3,\zeta,\zeta^4,\zeta^2\,;\,0,-1,-\zeta^3,-\zeta,-\zeta^4,-\zeta^2\,|\,\tau) \\ Y(0,1,\zeta^2,\zeta^4,\zeta,\zeta^3\,;\,0,-1,-\zeta^2,-\zeta^4,-\zeta,-\zeta^3\,|\,\tau) \end{pmatrix}, \tag{D.18}$$

where $\zeta = e^{2\pi i/5}$. The first few terms of the q-expansions of these modular forms can be found in Ref. [189]. Our numerical results have made use of q-expansions up to $\mathcal{O}(q^{100})$, but the results are unchanged when using up to $\mathcal{O}(q^5)$.

D.3 Numerical Results in Fundamental Region

The models studied in chapter 5 are modular invariant and it is always possible to map the Lagrangian referred to a certain value τ of the modulus to an equivalent Lagrangian where the modulus τ' is inside the fundamental region $|\mathrm{Re}(\tau')| \leq 1/2$, $|\tau'| \geq 1$. By definition there exists a modular transformation γ such that $\tau' = \gamma\tau$. Together with the transformation $\tau \to \gamma\tau$, we consider the field redefinition mapping all chiral multiplets except L into the modular transformed ones, after setting to zero all their weights. We find that the low-energy superpotential

$$w = -\frac{v^2}{2\Lambda} L^T \ \mathcal{W}(\tau) \ L - \frac{v}{\sqrt{2}} E^{cT} \ \mathcal{Y}(\varphi) \ L \tag{D.19}$$

becomes

$$w = -\frac{v^2}{2\Lambda} L^T \ \mathcal{W}(\gamma\tau) \ L - \frac{v}{\sqrt{2}} E^{cT} \ \mathcal{Y}(\varphi) \ \rho_L^\dagger(\gamma) L \quad , \tag{D.20}$$

where

$$\mathcal{W}(\gamma\tau) = (c\tau + d)^2 \rho_L(\gamma)^* \ \mathcal{W}(\tau) \ \rho_L^\dagger(\gamma) \quad . \tag{D.21}$$

Neutrino and charged lepton mass matrices are now:

$$m_\nu = \frac{v^2}{\Lambda} \ \mathcal{W}(\gamma\tau) \quad , \qquad m_e^\dagger m_e = \frac{v^2}{2} \rho_L(\gamma) \ \mathcal{Y}(\varphi)^\dagger \mathcal{Y}(\varphi) \ \rho_L^\dagger(\gamma) \quad . \tag{D.22}$$

The lepton mixing matrix is unchanged. We list here the transformations needed to map the values of τ found by our minimisation procedure to points inside the fundamental region.

	Input parameters - fundamental region									
Case	$\gamma\tau$	Re(τ)	Im(τ)	Re(φ_1)	Im(φ_1)	Re(φ_2)	Im(φ_2)	Re(φ_3)	Im(φ_3)	$1/\Lambda$ (eV^{-1})
$4WV$	$ST^{-1}\tau$	-0.1579	0.9957	2/3	0	1/6	$1/2\sqrt{3}$	-1/3	$1/\sqrt{3}$	0.003223
$4SV$	$T^{-1}\tau$	-0.1564	0.9968	-1/3	$-1/\sqrt{3}$	-1/3	$1/\sqrt{3}$	-1/3	0	0.7672
$4WC$	$T^{-1}ST^{-3}\tau$	-0.07915	1.055	-0.3947	0.5774	0.6974	-0.05315	0.1053	0.1824	0.0007030
$4SC$	$T^{-1}ST^{-3}\tau$	-0.1667	0.9966	-0.2709	0.5774	0.6355	0.05406	0.2291	0.3968	0.06993

Table D.1: Parameters τ and φ in the fundamental region for level 4 models.

	Input parameters - fundamental region									
Case	$\gamma\tau$	Re(τ)	Im(τ)	Re(φ_1)	Im(φ_1)	Re(φ_2)	Im(φ_2)	Re(φ_3)	Im(φ_3)	$1/\Lambda$ (eV^{-1})
$5WC3$	$S\tau$	0.01908	1.007	-0.3301	0	-0.7188	0	-1.096	0	0.007958
$5WC3p$	$T^{-2}S\tau$	-0.3908	3.902	-0.1618	0	0.1621	0.4990	0.2911	-0.8960	0.0007302
$5SC$	$T^{-2}S\tau$	-0.08591	1.277	0.1812	0	0.4561	0.3314	0.7194	-0.5227	0.002804

Table D.2: Parameters τ and φ in the fundamental region for level 5 models.

Bibliography

[1] Luigi Delle Rose, Shaaban Khalil, Simon J. D. King, Carlo Marzo, Stefano Moretti, and Cem S. Un. "Naturalness and dark matter in the supersymmetric B-L extension of the standard model". In: *Phys. Rev. D* 96.5 (2017), p. 055004. DOI: 10.1103/PhysRevD.96.055004. arXiv: 1702.01808 [hep-ph].

[2] Luigi Delle Rose, Shaaban Khalil, Simon J. D. King, Suchita Kulkarni, Carlo Marzo, Stefano Moretti, and Cem S. Un. "Sneutrino Dark Matter in the BLSSM". In: *JHEP* 07 (2018), p. 100. DOI: 10.1007/JHEP07(2018)100. arXiv: 1712.05232 [hep-ph].

[3] Simon J. D. King, Stephen F. King, and Stefano Moretti. "$SO(10)$ inspired Z' models at the LHC". In: *Phys. Rev. D* 97.11 (2018), p. 115027. DOI: 10.1103/PhysRevD.97.115027. arXiv: 1712.01279 [hep-ph].

[4] Juan Carlos Criado, Ferruccio Feruglio, and Simon J. D. King. "Modular Invariant Models of Lepton Masses at Levels 4 and 5". In: *JHEP* 02 (2020), p. 001. DOI: 10.1007/JHEP02(2020)001. arXiv: 1908.11867 [hep-ph].

[5] Simon J. D. King and Stephen F. King. "Fermion mass hierarchies from modular symmetry". In: *JHEP* 09 (2020), p. 043. DOI: 10.1007/JHEP09(2020)043. arXiv: 2002.00969 [hep-ph].

[6] Stephen F. King. "Models of Neutrino Mass, Mixing and CP Violation". In: *J. Phys.* G42 (2015), p. 123001. DOI: 10.1088/0954-3899/42/12/123001. arXiv: 1510.02091 [hep-ph].

[7] Shaaban Khalil. "TeV-scale gauged B-L symmetry with inverse seesaw mechanism". In: *Phys. Rev.* D82 (2010), p. 077702. DOI: 10.1103/PhysRevD.82.077702. arXiv: 1004.0013 [hep-ph].

[8] Howard Georgi and C. Jarlskog. "A New Lepton - Quark Mass Relation in a Unified Theory". In: *Phys. Lett.* 86B (1979), pp. 297–300. DOI: 10.1016/0370-2693(79)90842-6.

[9] Graham Ross and Mario Serna. "Unification and fermion mass structure". In: *Phys. Lett.* B664 (2008), pp. 97–102. DOI: 10.1016/j.physletb.2008.05.014. arXiv: 0704.1248 [hep-ph].

[10] Stefan Antusch and Martin Spinrath. "New GUT predictions for quark and lepton mass ratios confronted with phenomenology". In: *Phys. Rev.* D79 (2009), p. 095004. DOI: 10.1103/PhysRevD.79.095004. arXiv: 0902.4644 [hep-ph].

[11] Jogesh C. Pati and Abdus Salam. "Lepton Number as the Fourth Color". In: *Phys. Rev.* D10 (1974). [Erratum: Phys. Rev.D11,703(1975)], pp. 275–289. DOI: 10.1103/PhysRevD.10.275,10.1103/PhysRevD.11.703.2.

[12] S. F. King. "Unified Models of Neutrinos, Flavour and CP Violation". In: *Prog. Part. Nucl. Phys.* 94 (2017), pp. 217–256. DOI: 10.1016/j.ppnp.2017.01.003. arXiv: 1701.04413 [hep-ph].

[13] Stefan Antusch, Stephen F. King, and Martin Spinrath. "GUT predictions for quark-lepton Yukawa coupling ratios with messenger masses from non-singlets". In: *Phys. Rev.* D89.5 (2014), p. 055027. DOI: 10.1103/PhysRevD.89.055027. arXiv: 1311.0877 [hep-ph].

[14] Aharon Davidson. "$B - L$ as the fourth color within an $\mathrm{SU}(2)_L \times \mathrm{U}(1)_R \times \mathrm{U}(1)$ model". In: *Phys. Rev. D* 20 (1979), p. 776. DOI: 10.1103/PhysRevD.20.776.

[15] Rabindra N. Mohapatra and R. E. Marshak. "Local B-L Symmetry of Electroweak Interactions, Majorana Neutrinos and Neutron Oscillations". In: *Phys. Rev. Lett.* 44 (1980). [Erratum: Phys.Rev.Lett. 44, 1643 (1980)], pp. 1316–1319. DOI: 10.1103/PhysRevLett.44.1316.

[16] Albert M Sirunyan et al. "Search for supersymmetry in multijet events with missing transverse momentum in proton-proton collisions at 13 TeV". In: *Phys. Rev.* D96.3 (2017), p. 032003. DOI: 10.1103/PhysRevD.96.032003. arXiv: 1704.07781 [hep-ex].

[17] Philip Bechtle et al. "Killing the cMSSM softly". In: *Eur. Phys. J.* C76.2 (2016), p. 96. DOI: 10.1140/epjc/s10052-015-3864-0. arXiv: 1508.05951 [hep-ph].

[18] Howard Baer, Vernon Barger, Dan Mickelson, and Maren Padeffke-Kirkland. "SUSY models under siege: LHC constraints and electroweak fine-tuning". In: *Phys. Rev.* D89.11 (2014), p. 115019. DOI: 10.1103/PhysRevD.89.115019. arXiv: 1404.2277 [hep-ph].

[19] D. S. Akerib et al. "Results on the Spin-Dependent Scattering of Weakly Interacting Massive Particles on Nucleons from the Run 3 Data of the LUX Experiment". In: *Phys. Rev. Lett.* 116.16 (2016), p. 161302. DOI: 10.1103/PhysRevLett.116.161302. arXiv: 1602.03489 [hep-ex].

[20] W. Abdallah and S. Khalil. "MSSM Dark Matter in Light of Higgs and LUX Results". In: *Adv. High Energy Phys.* 2016 (2016), p. 5687463. DOI: 10.1155/2016/5687463. arXiv: 1509.07031 [hep-ph].

[21] G. Hinshaw et al. "Nine-Year Wilkinson Microwave Anisotropy Probe (WMAP) Observations: Cosmological Parameter Results". In: *Astrophys. J. Suppl.* 208 (2013), p. 19. DOI: 10.1088/0067-0049/208/2/19. arXiv: 1212.5226 [astro-ph.CO].

[22] P. A. R. Ade et al. "Planck 2015 results. XIII. Cosmological parameters". In: *Astron. Astrophys.* 594 (2016), A13. DOI: 10.1051/0004-6361/201525830. arXiv: 1502.01589 [astro-ph.CO].

[23] Shaaban Khalil. "Low scale $B - L$ extension of the Standard Model at the LHC". In: *J. Phys.* G35 (2008), p. 055001. DOI: 10.1088/0954-3899/35/5/055001. arXiv: hep-ph/0611205 [hep-ph].

[24] Lorenzo Basso, Alexander Belyaev, Stefano Moretti, and Claire H. Shepherd-Themistocleous. "Phenomenology of the minimal B-L extension of the Standard model: Z' and neutrinos". In: *Phys. Rev.* D80 (2009), p. 055030. DOI: 10.1103/PhysRevD.80.055030. arXiv: 0812.4313 [hep-ph].

[25] L. Basso, A. Belyaev, S. Moretti, G. M. Pruna, and C. H. Shepherd-Themistocleous. "Phenomenology of the minimal B-L extension of the Standard Model". In: *PoS* EPS-HEP2009 (2009), p. 242. DOI: 10.22323/1.084.0242. arXiv: 0909.3113 [hep-ph].

[26] Lorenzo Basso, Stefano Moretti, and Giovanni Marco Pruna. "Phenomenology of the minimal $B-L$ extension of the Standard Model: the Higgs sector". In: *Phys. Rev.* D83 (2011), p. 055014. DOI: 10.1103/PhysRevD.83.055014. arXiv: 1011.2612 [hep-ph].

[27] L. Basso, A. Belyaev, S. Moretti, and G. M. Pruna. "Higgs phenomenology in the minimal $B - L$ extension of the Standard Model at LHC". In: *J. Phys. Conf. Ser.* 259 (2010), p. 012062. DOI: 10.1088/1742-6596/259/1/012062. arXiv: 1009.6095 [hep-ph].

[28] Swarup Kumar Majee and Narendra Sahu. "Dilepton Signal of a Type-II Seesaw at CERN LHC: Reveals a TeV Scale B-L Symmetry". In: *Phys. Rev.* D82 (2010), p. 053007. DOI: 10.1103/PhysRevD.82.053007. arXiv: 1004.0841 [hep-ph].

[29] Tong Li and Wei Chao. "Neutrino Masses, Dark Matter and B-L Symmetry at the LHC". In: *Nucl. Phys.* B843 (2011), pp. 396–412. DOI: 10.1016/j.nuclphysb.2010.10.004. arXiv: 1004.0296 [hep-ph].

[30] Pavel Fileviez Perez, Tao Han, and Tong Li. "Testability of Type I Seesaw at the CERN LHC: Revealing the Existence of the B-L Symmetry". In: *Phys. Rev.* D80 (2009), p. 073015. DOI: 10.1103/PhysRevD.80.073015. arXiv: 0907.4186 [hep-ph].

[31] W. Emam and S. Khalil. "Higgs and Z-prime phenomenology in B-L extension of the standard model at LHC". In: *Eur. Phys. J.* C52 (2007), pp. 625–633. DOI: 10.1140/epjc/s10052-007-0411-7. arXiv: 0704.1395 [hep-ph].

[32] S. Khalil and S. Moretti. "Heavy neutrinos, Z' and Higgs bosons at the LHC: new particles from an old symmetry". In: *J. Mod. Phys.* 4.1 (2013), pp. 7–10. DOI: 10.4236/jmp.2013.41002. arXiv: 1207.1590 [hep-ph].

[33] S. Khalil and S. Moretti. "A simple symmetry as a guide toward new physics beyond the Standard Model". In: *Front.in Phys.* 1 (2013), p. 10. DOI: 10.3389/fphy.2013.00010. arXiv: 1301.0144 [physics.pop-ph].

[34] Shaaban Khalil. "Radiative symmetry breaking in supersymmetric $B - L$ models with an inverse seesaw mechanism". In: *Phys. Rev.* D94.7 (2016), p. 075003. DOI: 10.1103/PhysRevD.94.075003. arXiv: 1606.09292 [hep-ph].

[35] S. Khalil and A. Masiero. "Radiative B-L symmetry breaking in supersymmetric models". In: *Phys. Lett.* B665 (2008), pp. 374–377. DOI: 10.1016/j.physletb.2008.06.063. arXiv: 0710.3525 [hep-ph].

[36] Pavel Fileviez Perez and Sogee Spinner. "The Fate of R-Parity". In: *Phys. Rev.* D83 (2011), p. 035004. DOI: 10.1103/PhysRevD.83.035004. arXiv: 1005.4930 [hep-ph].

[37] J. E. Camargo-Molina, B. O'Leary, W. Porod, and F. Staub. "The Stability Of R-Parity In Supersymmetric Models Extended By $\mathrm{U}(1)_{B-L}$". In: *Phys. Rev.* D88 (2013), p. 015033. DOI: 10.1103/PhysRevD.88.015033. arXiv: 1212.4146 [hep-ph].

[38] Tatsuru Kikuchi and Takayuki Kubo. "Radiative B-L symmetry breaking and the Z-prime mediated SUSY breaking". In: *Phys. Lett.* B666 (2008), pp. 262–268. DOI: 10.1016/j.physletb.2008.07.059. arXiv: 0804.3933 [hep-ph].

[39] Renato M. Fonseca, Michal Malinsky, Werner Porod, and Florian Staub. "Running soft parameters in SUSY models with multiple U(1) gauge factors". In: *Nucl. Phys.* B854 (2012), pp. 28–53. DOI: 10.1016/j.nuclphysb.2011.08.017. arXiv: 1107.2670 [hep-ph].

[40] A. Elsayed, S. Khalil, and S. Moretti. "Higgs Mass Corrections in the SUSY B-L Model with Inverse Seesaw". In: *Phys. Lett.* B715 (2012), pp. 208–213. DOI: 10.1016/j.physletb.2012.07.066. arXiv: 1106.2130 [hep-ph].

[41] Lorenzo Basso and Florian Staub. "Enhancing $h \to \gamma\gamma$ with staus in SUSY models with extended gauge sector". In: *Phys. Rev.* D87.1 (2013), p. 015011. DOI: 10.1103/PhysRevD.87.015011. arXiv: 1210.7946 [hep-ph].

[42] Ben O'Leary, Werner Porod, and Florian Staub. "Mass spectrum of the minimal SUSY B-L model". In: *JHEP* 05 (2012), p. 042. DOI: 10.1007/JHEP05(2012)042. arXiv: 1112.4600 [hep-ph].

[43] L. Basso, A. Belyaev, D. Chowdhury, M. Hirsch, S. Khalil, S. Moretti, B. O'Leary, W. Porod, and F. Staub. "Proposal for generalised Supersymmetry Les Houches Accord for see-saw models and PDG numbering scheme". In: *Comput. Phys. Commun.* 184 (2013), pp. 698–719. DOI: 10.1016/j.cpc.2012.11.004. arXiv: 1206.4563 [hep-ph].

[44] A. Elsayed, S. Khalil, S. Moretti, and A. Moursy. "Right-handed sneutrino-antisneutrino oscillations in a TeV scale Supersymmetric B-L model". In: *Phys. Rev.* D87.5 (2013), p. 053010. DOI: 10.1103/PhysRevD.87.053010. arXiv: 1211.0644 [hep-ph].

[45] S. Khalil and S. Moretti. "The $B - L$ Supersymmetric Standard Model with Inverse Seesaw at the Large Hadron Collider". In: *Rept. Prog. Phys.* 80.3 (2017), p. 036201. DOI: 10.1088/1361-6633/aa50e6. arXiv: 1503.08162 [hep-ph].

[46] W. Abdallah, S. Khalil, and S. Moretti. "Double Higgs peak in the minimal SUSY B-L model". In: *Phys. Rev.* D91.1 (2015), p. 014001. DOI: 10.1103/PhysRevD.91.014001. arXiv: 1409.7837 [hep-ph].

[47] Lorenzo Basso, Ben O'Leary, Werner Porod, and Florian Staub. "Dark matter scenarios in the minimal SUSY B-L model". In: *JHEP* 09 (2012), p. 054. DOI: 10.1007/JHEP09(2012)054. arXiv: 1207.0507 [hep-ph].

[48] W. Abdallah, J. Fiaschi, S. Khalil, and S. Moretti. "Z'-induced invisible right-handed sneutrino decays at the LHC". In: *Phys. Rev.* D92 (2015), p. 055029. DOI: 10.1103/PhysRevD.92.055029. arXiv: 1504.01761 [hep-ph].

[49] W. Abdallah, J. Fiaschi, S. Khalil, and S. Moretti. "Mono-jet, -photon and -Z signals of a supersymmetric (B - L) model at the Large Hadron Collider". In: *JHEP* 02 (2016), p. 157. DOI: 10.1007/JHEP02(2016)157. arXiv: 1510.06475 [hep-ph].

[50] A. Hammad, S. Khalil, and S. Moretti. "LHC signals of a B-L supersymmetric standard model CP -even Higgs boson". In: *Phys. Rev.* D93.11 (2016), p. 115035. DOI: 10.1103/PhysRevD.93.115035. arXiv: 1601.07934 [hep-ph].

[51] A. Hammad, S. Khalil, and S. Moretti. "Higgs boson decays into $\gamma\gamma$ and Zγ in the MSSM and the B-L supersymmetric SM". In: *Phys. Rev.* D92.9 (2015), p. 095008. DOI: 10.1103/PhysRevD.92.095008. arXiv: 1503.05408 [hep-ph].

[52] Riccardo Barbieri and Alessandro Strumia. "About the fine tuning price of LEP". In: *Phys. Lett.* B433 (1998), pp. 63–66. DOI: 10.1016/S0370-2693(98)00577-2. arXiv: hep-ph/9801353 [hep-ph].

[53] G. Cacciapaglia, C. Csaki, G. Marandella, and A. Strumia. "The Minimal Set of Electroweak Precision Parameters". In: *Phys. Rev.* D74 (2006), p. 033011. DOI: 10.1103/PhysRevD.74.033011. arXiv: hep-ph/0604111 [hep-ph].

[54] R. Wendell et al. "Atmospheric neutrino oscillation analysis with sub-leading effects in Super-Kamiokande I, II, and III". In: *Phys. Rev.* D81 (2010), p. 092004. DOI: 10.1103/PhysRevD.81.092004. arXiv: 1002.3471 [hep-ex].

[55] Charanjit S. Aulakh, Alejandra Melfo, Andrija Rasin, and Goran Senjanovic. "Seesaw and supersymmetry or exact R-parity". In: *Phys. Lett.* B459 (1999), pp. 557–562. DOI: 10.1016/S0370-2693(99)00708-X. arXiv: hep-ph/9902409 [hep-ph].

[56] Bob Holdom. "Two U(1)'s and Epsilon Charge Shifts". In: *Phys. Lett.* 166B (1986), pp. 196–198. DOI: 10.1016/0370-2693(86)91377-8.

[57] Shaaban Khalil and Cem Salih Un. "Muon Anomalous Magnetic Moment in SUSY B-L Model with Inverse Seesaw". In: *Phys. Lett.* B763 (2016), pp. 164–168. DOI: 10.1016/j.physletb.2016.10.035. arXiv: 1509.05391 [hep-ph].

[58] Claudio Coriano, Luigi Delle Rose, and Carlo Marzo. "Constraints on abelian extensions of the Standard Model from two-loop vacuum stability and $U(1)_{B-L}$". In: *JHEP* 02 (2016), p. 135. DOI: 10.1007/JHEP02(2016)135. arXiv: 1510.02379 [hep-ph].

[59] Florian Staub. "SARAH 4 : A tool for (not only SUSY) model builders". In: *Comput. Phys. Commun.* 185 (2014), pp. 1773–1790. DOI: 10.1016/j.cpc.2014.02.018. arXiv: 1309.7223 [hep-ph].

[60] Werner Porod. "SPheno, a program for calculating supersymmetric spectra, SUSY particle decays and SUSY particle production at e+ e- colliders". In: *Comput. Phys. Commun.* 153 (2003), pp. 275–315. DOI: 10.1016/S0010-4655(03)00222-4. arXiv: hep-ph/0301101 [hep-ph].

[61] Elena Accomando, Claudio Coriano, Luigi Delle Rose, Juri Fiaschi, Carlo Marzo, and Stefano Moretti. "Z', Higgses and heavy neutrinos in U(1)' models: from the LHC to the GUT scale". In: *JHEP* 07 (2016), p. 086. DOI: 10.1007/JHEP07(2016)086. arXiv: 1605.02910 [hep-ph].

[62] Vardan Khachatryan et al. "Search for narrow resonances in dilepton mass spectra in proton-proton collisions at $\sqrt{s} = 13$ TeV and combination with 8 TeV data". In: *Phys. Lett.* B768 (2017), pp. 57–80. DOI: 10.1016/j.physletb.2017.02.010. arXiv: 1609.05391 [hep-ex].

[63] Philip Bechtle, Oliver Brein, Sven Heinemeyer, Georg Weiglein, and Karina E. Williams. "HiggsBounds: Confronting Arbitrary Higgs Sectors with Exclusion Bounds from LEP and the Tevatron". In: *Comput. Phys. Commun.* 181 (2010), pp. 138–167. DOI: 10.1016/j.cpc.2009.09.003. arXiv: 0811.4169 [hep-ph].

[64] Philip Bechtle, Oliver Brein, Sven Heinemeyer, Georg Weiglein, and Karina E. Williams. "HiggsBounds 2.0.0: Confronting Neutral and Charged Higgs Sector Predictions with Exclusion Bounds from LEP and the Tevatron". In: *Comput. Phys. Commun.* 182 (2011), pp. 2605–2631. DOI: 10.1016/j.cpc.2011.07.015. arXiv: 1102.1898 [hep-ph].

[65] Philip Bechtle, Oliver Brein, Sven Heinemeyer, Oscar Stal, Tim Stefaniak, Georg Weiglein, and Karina E. Williams. "HiggsBounds-4: Improved Tests of Extended Higgs Sectors against Exclusion Bounds from LEP, the Tevatron and the LHC". In: *Eur. Phys. J.* C74.3 (2014), p. 2693. DOI: 10.1140/epjc/s10052-013-2693-2. arXiv: 1311.0055 [hep-ph].

[66] Philip Bechtle, Sven Heinemeyer, Oscar Stal, Tim Stefaniak, and Georg Weiglein. "Applying Exclusion Likelihoods from LHC Searches to Extended Higgs Sectors". In: *Eur. Phys. J.* C75.9 (2015), p. 421. DOI: 10.1140/epjc/s10052-015-3650-z. arXiv: 1507.06706 [hep-ph].

[67] Philip Bechtle, Sven Heinemeyer, Oscar Stal, Tim Stefaniak, and Georg Weiglein. "HiggsSignals: Confronting arbitrary Higgs sectors with measurements at the Tevatron and the LHC". In: *Eur. Phys. J.* C74.2 (2014), p. 2711. DOI: 10.1140/epjc/s10052-013-2711-4. arXiv: 1305.1933 [hep-ph].

[68] K. A. Olive et al. "Review of Particle Physics". In: *Chin. Phys.* C38 (2014), p. 090001. DOI: 10.1088/1674-1137/38/9/090001.

[69] G. Belanger, F. Boudjema, A. Pukhov, and A. Semenov. "MicrOMEGAs 2.0: A Program to calculate the relic density of dark matter in a generic model". In: *Comput. Phys. Commun.* 176 (2007), pp. 367–382. DOI: 10.1016/j.cpc.2006.11.008. arXiv: hep-ph/0607059 [hep-ph].

[70] G. Belanger, F. Boudjema, A. Pukhov, and A. Semenov. "micrOMEGAs$_3$: A program for calculating dark matter observables". In: *Comput. Phys. Commun.* 185 (2014), pp. 960–985. DOI: 10.1016/j.cpc.2013.10.016. arXiv: 1305.0237 [hep-ph].

[71] D. S. Akerib et al. "Results from a search for dark matter in the complete LUX exposure". In: *Phys. Rev. Lett.* 118.2 (2017), p. 021303. DOI: 10.1103/PhysRevLett.118.021303. arXiv: 1608.07648 [astro-ph.CO].

[72] Toby Falk, Keith A. Olive, and Mark Srednicki. "Heavy sneutrinos as dark matter". In: *Phys. Lett.* B339 (1994), pp. 248–251. DOI: 10.1016/0370-2693(94)90639-4. arXiv: hep-ph/9409270 [hep-ph].

[73] Greg W. Anderson and Diego J. Castano. "Measures of fine tuning". In: *Phys. Lett.* B347 (1995), pp. 300–308. DOI: 10.1016/0370-2693(95)00051-L. arXiv: hep-ph/9409419 [hep-ph].

[74] Greg W. Anderson and Diego J. Castano. "Naturalness and superpartner masses or when to give up on weak scale supersymmetry". In: *Phys. Rev.* D52 (1995), pp. 1693–1700. DOI: 10.1103/PhysRevD.52.1693. arXiv: hep-ph/9412322 [hep-ph].

[75] Greg W. Anderson and Diego J. Castano. "Challenging weak scale supersymmetry at colliders". In: *Phys. Rev.* D53 (1996), pp. 2403–2410. DOI: 10.1103/PhysRevD.53.2403. arXiv: hep-ph/9509212 [hep-ph].

[76] Greg W. Anderson, Diego J. Castano, and Antonio Riotto. "Naturalness lowers the upper bound on the lightest Higgs boson mass in supersymmetry". In: *Phys. Rev.* D55 (1997), pp. 2950–2954. DOI: 10.1103/PhysRevD.55.2950. arXiv: hep-ph/9609463 [hep-ph].

[77] Paolo Ciafaloni and Alessandro Strumia. "Naturalness upper bounds on gauge mediated soft terms". In: *Nucl. Phys.* B494 (1997), pp. 41–53. DOI: 10.1016/S0550-3213(97)00138-7. arXiv: hep-ph/9611204 [hep-ph].

[78] Kwok Lung Chan, Utpal Chattopadhyay, and Pran Nath. "Naturalness, weak scale supersymmetry and the prospect for the observation of supersymmetry at the Tevatron and at the CERN LHC". In: *Phys. Rev.* D58 (1998), p. 096004. DOI: 10.1103/PhysRevD.58.096004. arXiv: hep-ph/9710473 [hep-ph].

[79] Leonardo Giusti, Andrea Romanino, and Alessandro Strumia. "Natural ranges of supersymmetric signals". In: *Nucl. Phys.* B550 (1999), pp. 3–31. DOI: 10.1016/S0550-3213(99)00153-4. arXiv: hep-ph/9811386 [hep-ph].

[80] J. A. Casas, J. R. Espinosa, and I. Hidalgo. "The MSSM fine tuning problem: A Way out". In: *JHEP* 01 (2004), p. 008. DOI: 10.1088/1126-6708/2004/01/008. arXiv: hep-ph/0310137 [hep-ph].

[81] J. A. Casas, J. R. Espinosa, and I. Hidalgo. "A Relief to the supersymmetric fine tuning problem". In: *String phenomenology. Proceedings, 2nd International Conference, Durham, UK, July 29-August 4, 2003*. 2004, pp. 76–85. DOI: 10.1142/9789812702463_0011. arXiv: hep-ph/0402017 [hep-ph].

[82] J. A. Casas, J. R. Espinosa, and I. Hidalgo. "Implications for new physics from fine-tuning arguments. 1. Application to SUSY and seesaw cases". In: *JHEP* 11 (2004), p. 057. DOI: 10.1088/1126-6708/2004/11/057. arXiv: hep-ph/0410298 [hep-ph].

[83] J. A. Casas, J. R. Espinosa, and I. Hidalgo. "Expectations for LHC from naturalness: modified versus SM Higgs sector". In: *Nucl. Phys.* B777 (2007), pp. 226–252. DOI: 10.1016/j.nuclphysb.2007.04.024. arXiv: hep-ph/0607279 [hep-ph].

[84] Ryuichiro Kitano and Yasunori Nomura. "A Solution to the supersymmetric fine-tuning problem within the MSSM". In: *Phys. Lett.* B631 (2005), pp. 58–67. DOI: 10.1016/j.physletb.2005.10.003. arXiv: hep-ph/0509039 [hep-ph].

[85] Peter Athron and D. J. Miller. "A New Measure of Fine Tuning". In: *Phys. Rev.* D76 (2007), p. 075010. DOI: 10.1103/PhysRevD.76.075010. arXiv: 0705.2241 [hep-ph].

[86] Howard Baer, Vernon Barger, Peisi Huang, Azar Mustafayev, and Xerxes Tata. "Radiative natural SUSY with a 125 GeV Higgs boson". In: *Phys. Rev. Lett.* 109 (2012), p. 161802. DOI: 10.1103/PhysRevLett.109.161802. arXiv: 1207.3343 [hep-ph].

[87] John R. Ellis, K. Enqvist, Dimitri V. Nanopoulos, and F. Zwirner. "Aspects of the Superunification of Strong, Electroweak and Gravitational Interactions". In: *Nucl. Phys.* B276 (1986), pp. 14–70. DOI: 10.1016/0550-3213(86)90015-5.

[88] Riccardo Barbieri and G. F. Giudice. "Upper Bounds on Supersymmetric Particle Masses". In: *Nucl. Phys.* B306 (1988), pp. 63–76. DOI: 10.1016/0550-3213(88)90171-X.

[89] Graham G. Ross, Kai Schmidt-Hoberg, and Florian Staub. "Revisiting fine-tuning in the MSSM". In: *JHEP* 03 (2017), p. 021. DOI: 10.1007/JHEP03(2017)021. arXiv: 1701.03480 [hep-ph].

[90] Howard Baer, Vernon Barger, Peisi Huang, and Xerxes Tata. "Natural Supersymmetry: LHC, dark matter and ILC searches". In: *JHEP* 05 (2012), p. 109. DOI: 10.1007/JHEP05(2012)109. arXiv: 1203.5539 [hep-ph].

[91] Howard Baer, Vernon Barger, Peisi Huang, Dan Mickelson, Azar Mustafayev, and Xerxes Tata. "Radiative natural supersymmetry: Reconciling electroweak fine-tuning and the Higgs boson mass". In: *Phys. Rev.* D87.11 (2013), p. 115028. DOI: 10.1103/PhysRevD.87.115028. arXiv: 1212.2655 [hep-ph].

[92] Matthew W. Cahill-Rowley, JoAnne L. Hewett, Ahmed Ismail, and Thomas G. Rizzo. "The Higgs Sector and Fine-Tuning in the pMSSM". In: *Phys. Rev.* D86 (2012), p. 075015. DOI: 10.1103/PhysRevD.86.075015. arXiv: 1206.5800 [hep-ph].

[93] Jonathan L. Feng and David Sanford. "A Natural 125 GeV Higgs Boson in the MSSM from Focus Point Supersymmetry with A-Terms". In: *Phys. Rev.* D86 (2012), p. 055015. DOI: 10.1103/PhysRevD.86.055015. arXiv: 1205.2372 [hep-ph].

[94] Zhaofeng Kang, Jinmian Li, and Tianjun Li. "On Naturalness of the MSSM and NMSSM". In: *JHEP* 11 (2012), p. 024. DOI: 10.1007/JHEP11(2012)024. arXiv: 1201.5305 [hep-ph].

[95] Howard Baer, Vernon Barger, and Dan Mickelson. "How conventional measures overestimate electroweak fine-tuning in supersymmetric theory". In: *Phys. Rev.* D88.9 (2013), p. 095013. DOI: 10.1103/PhysRevD.88.095013. arXiv: 1309.2984 [hep-ph].

[96] Howard Baer, Vernon Barger, and Dan Mickelson. "Direct and indirect detection of higgsino-like WIMPs: concluding the story of electroweak naturalness". In: *Phys. Lett.* B726 (2013), pp. 330–336. DOI: 10.1016/j.physletb.2013.08.060. arXiv: 1303.3816 [hep-ph].

[97] Kamila Kowalska and Enrico Maria Sessolo. "Natural MSSM after the LHC 8 TeV run". In: *Phys. Rev.* D88.7 (2013), p. 075001. DOI: 10.1103/PhysRevD.88.075001. arXiv: 1307.5790 [hep-ph].

[98] Genevieve Belanger, Diptimoy Ghosh, Rohini Godbole, and Suchita Kulkarni. "Light stop in the MSSM after LHC Run 1". In: *JHEP* 09 (2015), p. 214. DOI: 10.1007/JHEP09(2015)214. arXiv: 1506.00665 [hep-ph].

[99] M. Abbas and S. Khalil. "Neutrino masses, mixing and leptogenesis in TeV scale B - L extension of the standard model". In: *JHEP* 04 (2008), p. 056. DOI: 10.1088/1126-6708/2008/04/056. arXiv: 0707.0841 [hep-ph].

[100] Ben O'Leary, Werner Porod, and Florian Staub. "Mass spectrum of the minimal SUSY B-L model". In: *JHEP* 05 (2012), p. 042. DOI: 10.1007/JHEP05(2012)042. arXiv: 1112.4600 [hep-ph].

[101] Shaaban Khalil, Hiroshi Okada, and Takashi Toma. "Right-handed Sneutrino Dark Matter in Supersymmetric B-L Model". In: *JHEP* 07 (2011), p. 026. DOI: 10.1007/JHEP07(2011)026. arXiv: 1102.4249 [hep-ph].

[102] Elena Accomando, Luigi Delle Rose, Stefano Moretti, Emmanuel Olaiya, and Claire H. Shepherd-Themistocleous. "Novel SM-like Higgs decay into displaced heavy neutrino pairs in $U(1)'$ models". In: *JHEP* 04 (2017), p. 081. DOI: 10.1007/JHEP04(2017)081. arXiv: 1612.05977 [hep-ph].

[103] Elena Accomando, Luigi Delle Rose, Stefano Moretti, Emmanuel Olaiya, and Claire H. Shepherd-Themistocleous. "Extra Higgs boson and Z' as portals to signatures of heavy neutrinos at the LHC". In: *JHEP* 02 (2018), p. 109. DOI: 10.1007/JHEP02(2018)109. arXiv: 1708.03650 [hep-ph].

[104] C. Patrignani et al. "Review of Particle Physics". In: *Chin. Phys.* C40.10 (2016), p. 100001. DOI: 10.1088/1674-1137/40/10/100001.

[105] Hye-Sung Lee, Konstantin T. Matchev, and Salah Nasri. "Revival of the thermal sneutrino dark matter". In: *Phys. Rev.* D76 (2007), p. 041302. DOI: 10.1103/PhysRevD.76.041302. arXiv: hep-ph/0702223 [HEP-PH].

[106] Lars Bergstrom, Piero Ullio, and James H. Buckley. "Observability of gamma-rays from dark matter neutralino annihilations in the Milky Way halo". In: *Astropart. Phys.* 9 (1998), pp. 137–162. DOI: 10.1016/S0927-6505(98)00015-2. arXiv: astro-ph/9712318.

[107] Torbjorn Sjostrand. "High-energy physics event generation with PYTHIA 5.7 and JETSET 7.4". In: *Comput. Phys. Commun.* 82 (1994), pp. 74–90. DOI: 10.1016/0010-4655(94)90132-5.

[108] M. Ackermann et al. "Searching for Dark Matter Annihilation from Milky Way Dwarf Spheroidal Galaxies with Six Years of Fermi Large Area Telescope Data". In: *Phys. Rev. Lett.* 115.23 (2015), p. 231301. DOI: 10.1103/PhysRevLett.115.231301. arXiv: 1503.02641 [astro-ph.HE].

[109] J. Alwall, R. Frederix, S. Frixione, V. Hirschi, F. Maltoni, O. Mattelaer, H. S. Shao, T. Stelzer, P. Torrielli, and M. Zaro. "The automated computation of tree-level and next-to-leading order differential cross sections, and their matching to parton shower simulations". In: *JHEP* 07 (2014), p. 079. DOI: 10.1007/JHEP07(2014)079. arXiv: 1405.0301 [hep-ph].

[110] Stephen F. King. "Flavourful Z' models for $R_{K^{(*)}}$". In: *JHEP* 08 (2017), p. 019. DOI: 10.1007/JHEP08(2017)019. arXiv: 1706.06100 [hep-ph].

[111] S. F. King and T. Yanagida. "Testing the see-saw mechanism at collider energies". In: *Prog. Theor. Phys.* 114 (2006), pp. 1035–1043. DOI: 10.1143/PTP.114.1035. arXiv: hep-ph/0411030 [hep-ph].

[112] Giorgio Arcadi, Manfred Lindner, Yann Mambrini, Mathias Pierre, and Farinaldo S. Queiroz. "GUT Models at Current and Future Hadron Colliders and Implications to Dark Matter Searches". In: *Phys. Lett.* B771 (2017), pp. 508–514. DOI: 10.1016/j.physletb.2017.05.023. arXiv: 1704.02328 [hep-ph].

[113] Elena Accomando, Alexander Belyaev, Luca Fedeli, Stephen F. King, and Claire Shepherd-Themistocleous. "Z' physics with early LHC data". In: *Phys. Rev.* D83 (2011), p. 075012. DOI: 10.1103/PhysRevD.83.075012. arXiv: 1010.6058 [hep-ph].

[114] Paul Langacker. "The Physics of Heavy Z' Gauge Bosons". In: *Rev. Mod. Phys.* 81 (2009), pp. 1199–1228. DOI: 10.1103/RevModPhys.81.1199. arXiv: 0801.1345 [hep-ph].

[115] Michal Malinsky, J. C. Romao, and J. W. F. Valle. "Novel supersymmetric SO(10) seesaw mechanism". In: *Phys. Rev. Lett.* 95 (2005), p. 161801. DOI: 10.1103/PhysRevLett.95.161801. arXiv: hep-ph/0506296 [hep-ph].

[116] M. Hirsch, S. Morisi, and J. W. F. Valle. "A4-based tri-bimaximal mixing within inverse and linear seesaw schemes". In: *Phys. Lett.* B679 (2009), pp. 454–459. DOI: 10.1016/j.physletb.2009.08.003. arXiv: 0905.3056 [hep-ph].

[117] Valentina De Romeri, Martin Hirsch, and Michal Malinsky. "Soft masses in SUSY SO(10) GUTs with low intermediate scales". In: *Phys. Rev.* D84 (2011), p. 053012. DOI: 10.1103/PhysRevD.84.053012. arXiv: 1107.3412 [hep-ph].

[118] M. Hirsch, M. Malinsky, W. Porod, L. Reichert, and F. Staub. "Hefty MSSM-like light Higgs in extended gauge models". In: *JHEP* 02 (2012), p. 084. DOI: 10.1007/JHEP02(2012)084. arXiv: 1110.3037 [hep-ph].

[119] Martin Hirsch, Werner Porod, Laslo Reichert, and Florian Staub. "Phenomenology of the minimal supersymmetric $U(1)_{B-L} \times U(1)_R$ extension of the standard model". In: *Phys. Rev.* D86 (2012), p. 093018. DOI: 10.1103/PhysRevD.86.093018. arXiv: 1206.3516 [hep-ph].

[120] Mariana Frank and Özer Özdal. "Exploring the supersymmetric $U(1)_{B-L} \times U(1)_R$ model with dark matter, muon $g-2$ and Z' mass limits". In: *Phys. Rev.* D97.1 (2018), p. 015012. DOI: 10.1103/PhysRevD.97.015012. arXiv: 1709.04012 [hep-ph].

[121] Joydeep Chakrabortty and Amitava Raychaudhuri. "GUTs with dim-5 interactions: Gauge Unification and Intermediate Scales". In: *Phys. Rev.* D81 (2010), p. 055004. DOI: 10.1103/PhysRevD.81.055004. arXiv: 0909.3905 [hep-ph].

[122] Manuel E. Krauss, Werner Porod, and Florian Staub. "SO(10) inspired gauge-mediated supersymmetry breaking". In: *Phys. Rev.* D88.1 (2013), p. 015014. DOI: 10.1103/PhysRevD.88.015014. arXiv: 1304.0769 [hep-ph].

[123] Stefano Bertolini, Luca Di Luzio, and Michal Malinsky. "Intermediate mass scales in the non-supersymmetric SO(10) grand unification: A Reappraisal". In: *Phys. Rev.* D80 (2009), p. 015013. DOI: 10.1103/PhysRevD.80.015013. arXiv: 0903.4049 [hep-ph].

[124] Morad Aaboud et al. "Search for high-mass new phenomena in the dilepton final state using proton-proton collisions at $\sqrt{s} = 13$ TeV with the ATLAS detector". In: *Phys. Lett.* B761 (2016), pp. 372–392. DOI: 10.1016/j.physletb.2016.08.055. arXiv: 1607.03669 [hep-ex].

[125] Elena Accomando, Alexander Belyaev, Juri Fiaschi, Ken Mimasu, Stefano Moretti, and Claire Shepherd-Themistocleous. "Forward-backward asymmetry as a discovery tool for Z' bosons at the LHC". In: *JHEP* 01 (2016), p. 127. DOI: 10.1007/JHEP01(2016)127. arXiv: 1503.02672 [hep-ph].

[126] Elena Accomando, Alexander Belyaev, Juri Fiaschi, Ken Mimasu, Stefano Moretti, and Claire Shepherd-Themistocleous. "A_{FB} as a discovery tool for Z' bosons at the LHC". In: *Nuovo Cim.* C38.4 (2016), p. 153. DOI: 10.1393/ncc/i2015-15153-7. arXiv: 1504.03168 [hep-ph].

[127] Juri Fiaschi, Elena Accomando, Alexander Belyaev, Ken Mimasu, Stefano Moretti, and Claire H. Shepherd-Themistocleous. "Complementarity of Forward-Backward Asymmetry for discovery of Z' bosons at the Large Hadron Collider". In: *PoS* EPS-HEP2015 (2015), p. 176. DOI: 10.22323/1.234.0176. arXiv: 1510.05892 [hep-ph].

[128] F. Gianotti et al. "Physics potential and experimental challenges of the LHC luminosity upgrade". In: *Eur. Phys. J.* C39 (2005), pp. 293–333. DOI: 10.1140/epjc/s2004-02061-6. arXiv: hep-ph/0204087 [hep-ph].

[129] Benoit Hespel, David Lopez-Val, and Eleni Vryonidou. "Higgs pair production via gluon fusion in the Two-Higgs-Doublet Model". In: *JHEP* 09 (2014), p. 124. DOI: 10.1007/JHEP09(2014)124. arXiv: 1407.0281 [hep-ph].

[130] Shahram Hamidi and Cumrun Vafa. "Interactions on Orbifolds". In: *Nucl. Phys.* B279 (1987), pp. 465–513. DOI: 10.1016/0550-3213(87)90006-X.

[131] Lance J. Dixon, Daniel Friedan, Emil J. Martinec, and Stephen H. Shenker. "The Conformal Field Theory of Orbifolds". In: *Nucl. Phys.* B282 (1987), pp. 13–73. DOI: 10.1016/0550-3213(87)90676-6.

[132] J. Lauer, J. Mas, and Hans Peter Nilles. "Duality and the Role of Nonperturbative Effects on the World Sheet". In: *Phys. Lett.* B226 (1989), pp. 251–256. DOI: 10.1016/0370-2693(89)91190-8.

[133] J. Lauer, J. Mas, and Hans Peter Nilles. "Twisted sector representations of discrete background symmetries for two-dimensional orbifolds". In: *Nucl. Phys.* B351 (1991), pp. 353–424. DOI: 10.1016/0550-3213(91)90095-F.

[134] J. Erler, D. Jungnickel, and J. Lauer. "Dependence of Yukawa couplings on the axionic background moduli of Z(N) orbifolds". In: *Phys. Rev.* D45 (1992), pp. 3651–3668. DOI: 10.1103/PhysRevD.45.3651.

[135] Luis E. Ibanez. "Hierarchy of Quark - Lepton Masses in Orbifold Superstring Compactification". In: *Phys. Lett.* B181 (1986), pp. 269–272. DOI: 10.1016/0370-2693(86)90044-4.

[136] J. A. Casas, F. Gomez, and C. Munoz. "Complete structure of Z(n) Yukawa couplings". In: *Int. J. Mod. Phys.* A8 (1993), pp. 455–506. DOI: 10.1142/S0217751X93000187. arXiv: hep-th/9110060 [hep-th].

[137] Oleg Lebedev. "The CKM phase in heterotic orbifold models". In: *Phys. Lett.* B521 (2001), pp. 71–78. DOI: 10.1016/S0370-2693(01)01180-7. arXiv: hep-th/0108218 [hep-th].

[138] Tatsuo Kobayashi and Oleg Lebedev. "Heterotic Yukawa couplings and continuous Wilson lines". In: *Phys. Lett.* B566 (2003), pp. 164–170. DOI: 10.1016/S0370-2693(03)00560-4. arXiv: hep-th/0303009 [hep-th].

[139] D. Cremades, L. E. Ibanez, and F. Marchesano. "Yukawa couplings in intersecting D-brane models". In: *JHEP* 07 (2003), p. 038. DOI: 10.1088/1126-6708/2003/07/038. arXiv: hep-th/0302105 [hep-th].

[140] Ralph Blumenhagen, Mirjam Cvetic, Paul Langacker, and Gary Shiu. "Toward realistic intersecting D-brane models". In: *Ann. Rev. Nucl. Part. Sci.* 55 (2005), pp. 71–139. DOI: 10.1146/annurev.nucl.55.090704.151541. arXiv: hep-th/0502005 [hep-th].

[141] Steven A. Abel and Mark D. Goodsell. "Realistic Yukawa Couplings through Instantons in Intersecting Brane Worlds". In: *JHEP* 10 (2007), p. 034. DOI: 10.1088/1126-6708/2007/10/034. arXiv: hep-th/0612110 [hep-th].

[142] Ralph Blumenhagen, Boris Kors, Dieter Lust, and Stephan Stieberger. "Four-dimensional String Compactifications with D-Branes, Orientifolds and Fluxes". In: *Phys. Rept.* 445 (2007), pp. 1–193. DOI: 10.1016/j.physrep.2007.04.003. arXiv: hep-th/0610327 [hep-th].

[143] Fernando Marchesano. "Progress in D-brane model building". In: *Fortsch. Phys.* 55 (2007), pp. 491–518. DOI: 10.1002/prop.200610381. arXiv: hep-th/0702094 [HEP-TH].

[144] Ignatios Antoniadis, Alok Kumar, and Binata Panda. "Fermion Wavefunctions in Magnetized branes: Theta identities and Yukawa couplings". In: *Nucl. Phys.* B823 (2009), pp. 116–173. DOI: 10.1016/j.nuclphysb.2009.08.002. arXiv: 0904.0910 [hep-th].

[145] Tatsuo Kobayashi, Satoshi Nagamoto, and Shohei Uemura. "Modular symmetry in magnetized/intersecting D-brane models". In: *PTEP* 2017.2 (2017), 023B02. DOI: 10.1093/ptep/ptw184. arXiv: 1608.06129 [hep-th].

[146] D. Cremades, L. E. Ibanez, and F. Marchesano. "Computing Yukawa couplings from magnetized extra dimensions". In: *JHEP* 05 (2004), p. 079. DOI: 10.1088/1126-6708/2004/05/079. arXiv: hep-th/0404229 [hep-th].

[147] Hiroyuki Abe, Kang-Sin Choi, Tatsuo Kobayashi, and Hiroshi Ohki. "Non-Abelian Discrete Flavor Symmetries from Magnetized/Intersecting Brane Models". In: *Nucl. Phys.* B820 (2009), pp. 317–333. DOI: 10.1016/j.nuclphysb.2009.05.024. arXiv: 0904.2631 [hep-ph].

[148] S. Ferrara, D. Lust, Alfred D. Shapere, and S. Theisen. "Modular Invariance in Supersymmetric Field Theories". In: *Phys. Lett.* B225 (1989), p. 363. DOI: 10.1016/0370-2693(89)90583-2.

[149] S. Ferrara, .D. Lust, and S. Theisen. "Target Space Modular Invariance and Low-Energy Couplings in Orbifold Compactifications". In: *Phys. Lett.* B233 (1989), pp. 147–152. DOI: 10.1016/0370-2693(89)90631-X.

[150] Philippe Brax and Marc Chemtob. "Flavor changing neutral current constraints on standard - like orbifold models". In: *Phys. Rev.* D51 (1995), pp. 6550–6571. DOI: 10.1103/PhysRevD.51.6550. arXiv: hep-th/9411022 [hep-th].

[151] Pierre Binetruy and Emilian Dudas. "Dynamical mass matrices from effective superstring theories". In: *Nucl. Phys.* B451 (1995), pp. 31–52. DOI: 10.1016/0550-3213(95)00345-S. arXiv: hep-ph/9505295 [hep-ph].

[152] E. Dudas, S. Pokorski, and Carlos A. Savoy. "Soft scalar masses in supergravity with horizontal U(1)-x gauge symmetry". In: *Phys. Lett.* B369 (1996), pp. 255–261. DOI: 10.1016/0370-2693(95)01536-1. arXiv: hep-ph/9509410 [hep-ph].

[153] Emilian Dudas. "Dynamical mass matrices from moduli fields". In: *5th Hellenic School and Workshops on Elementary Particle Physics (CORFU 1995) Corfu, Greece, September 3-24, 1995*. 1996, pp. 504–508. arXiv: hep-ph/9602231 [hep-ph].

[154] G. K. Leontaris and N. D. Tracas. "Modular weights, $U(1)'$s and mass matrices". In: *Phys. Lett.* B419 (1998), pp. 206–210. DOI: 10.1016/S0370-2693(97)01412-3. arXiv: hep-ph/9709510 [hep-ph].

[155] Thomas Dent. "CP violation and modular symmetries". In: *Phys. Rev.* D64 (2001), p. 056005. DOI: 10.1103/PhysRevD.64.056005. arXiv: hep-ph/0105285 [hep-ph].

[156] Thomas Dent. "On the modular invariance of mass eigenstates and CP violation". In: *JHEP* 12 (2001), p. 028. DOI: 10.1088/1126-6708/2001/12/028. arXiv: hep-th/0111024 [hep-th].

[157] C.A. Lutken and Graham G. Ross. "Duality in the quantum Hall system". In: *Phys. Rev. B* 45.20 (1992), p. 11837. DOI: 10.1103/PhysRevB.45.11837.

[158] Andrea Cappelli and Guillermo R. Zemba. "Modular invariant partition functions in the quantum Hall effect". In: *Nucl. Phys. B* 490 (1997), pp. 595–632. DOI: 10.1016/S0550-3213(97)00110-7. arXiv: hep-th/9605127.

[159] Brian P. Dolan. "Modular invariance, universality and crossover in the quantum Hall effect". In: *Nucl. Phys. B* 554 (1999), p. 487. DOI: 10.1016/S0550-3213(99)00326-0. arXiv: cond-mat/9809294.

[160] Brian P. Dolan. "Duality and the modular group in the quantum Hall effect". In: *J. Phys. A* 32 (1999), p. L243. DOI: 10.1088/0305-4470/32/21/101. arXiv: cond-mat/9805171.

[161] C.P. Burgess and Brian P. Dolan. "Particle vortex duality and the modular group: Applications to the quantum Hall effect and other 2-D systems". In: *Phys. Rev. B* 63 (2001), p. 155309. DOI: 10.1103/PhysRevB.63.155309. arXiv: hep-th/0010246.

[162] C.P. Burgess and Brian P. Dolan. "Duality and nonlinear response for quantum Hall systems". In: *Phys. Rev. B* 65 (2002), p. 155323. DOI: 10.1103/PhysRevB.65.155323. arXiv: cond-mat/0105621.

[163] C.P. Burgess and Brian P. Dolan. "The Quantum Hall effect in graphene: Emergent modular symmetry and the semi-circle law". In: *Phys. Rev. B* 76 (2007), p. 113406. DOI: 10.1103/PhysRevB.76.113406. arXiv: cond-mat/0612269.

[164] C.A. Lutken and G.G. Ross. "Geometric scaling in the quantum Hall system". In: *Phys. Lett. B* 653 (2007), pp. 363–365. DOI: 10.1016/j.physletb.2007.08.022. arXiv: 0706.2467 [cond-mat.mes-hall].

[165] C.A. Lutken and G.G. Ross. "Experimental probes of emergent symmetries in the quantum Hall system". In: *Nucl. Phys. B* 850 (2011), pp. 321–338. DOI: 10.1016/j.nuclphysb.2011.04.020. arXiv: 1008.5257 [cond-mat.str-el].

[166] Y. Reyimuaji and A. Romanino. "Can an unbroken flavour symmetry provide an approximate description of lepton masses and mixing?" In: *JHEP* 03 (2018), p. 067. DOI: 10.1007/JHEP03(2018)067. arXiv: 1801.10530 [hep-ph].

[167] Guido Altarelli and Ferruccio Feruglio. "Discrete Flavor Symmetries and Models of Neutrino Mixing". In: *Rev. Mod. Phys.* 82 (2010), pp. 2701–2729. DOI: 10.1103/RevModPhys.82.2701. arXiv: 1002.0211 [hep-ph].

[168] Hajime Ishimori, Tatsuo Kobayashi, Hiroshi Ohki, Yusuke Shimizu, Hiroshi Okada, and Morimitsu Tanimoto. "Non-Abelian Discrete Symmetries in Particle Physics". In: *Prog. Theor. Phys. Suppl.* 183 (2010), pp. 1–163. DOI: 10.1143/PTPS.183.1. arXiv: 1003.3552 [hep-th].

[169] D. Hernandez and A. Yu. Smirnov. "Lepton mixing and discrete symmetries". In: *Phys. Rev.* D86 (2012), p. 053014. DOI: 10.1103/PhysRevD.86.053014. arXiv: 1204.0445 [hep-ph].

[170] Stephen F. King and Christoph Luhn. "Neutrino Mass and Mixing with Discrete Symmetry". In: *Rept. Prog. Phys.* 76 (2013), p. 056201. DOI: 10.1088/0034-4885/76/5/056201. arXiv: 1301.1340 [hep-ph].

[171] Stephen F. King, Alexander Merle, Stefano Morisi, Yusuke Shimizu, and Morimitsu Tanimoto. "Neutrino Mass and Mixing: from Theory to Experiment". In: *New J. Phys.* 16 (2014), p. 045018. DOI: 10.1088/1367-2630/16/4/045018. arXiv: 1402.4271 [hep-ph].

[172] Ferruccio Feruglio. "Pieces of the Flavour Puzzle". In: *Eur. Phys. J.* C75.8 (2015), p. 373. DOI: 10.1140/epjc/s10052-015-3576-5. arXiv: 1503.04071 [hep-ph].

[173] Claudia Hagedorn. "Theories of Leptonic Flavor". In: *Proceedings, Prospects in Neutrino Physics (NuPhys2016): London, UK, December 12-14, 2016*. 2017. arXiv: 1705.00684 [hep-ph].

[174] Ferruccio Feruglio. "Are neutrino masses modular forms?" In: *From My Vast Repertoire ...: Guido Altarelli's Legacy*. Ed. by Aharon Levy, Stefano Forte, and Giovanni Ridolfi. 2019, pp. 227–266. DOI: 10.1142/9789813238053_0012. arXiv: 1706.08749 [hep-ph].

[175] P. P. Novichkov, J. T. Penedo, S. T. Petcov, and A. V. Titov. "Generalised CP Symmetry in Modular-Invariant Models of Flavour". In: *JHEP* 07 (2019), p. 165. DOI: 10.1007/JHEP07(2019)165. arXiv: 1905.11970 [hep-ph].

[176] Alexander Baur, Hans Peter Nilles, Andreas Trautner, and Patrick K. S. Vaudrevange. "Unification of Flavor, CP, and Modular Symmetries". In: *Phys. Lett.* B795 (2019), pp. 7–14. DOI: 10.1016/j.physletb.2019.03.066. arXiv: 1901.03251 [hep-th].

[177] Alexander Baur, Hans Peter Nilles, Andreas Trautner, and Patrick K. S. Vaudrevange. "A String Theory of Flavor and CP". In: *Nucl. Phys.* B947 (2019), p. 114737. DOI: 10.1016/j.nuclphysb.2019.114737. arXiv: 1908.00805 [hep-th].

[178] Ivo de Medeiros Varzielas, Stephen F. King, and Ye-Ling Zhou. "Multiple modular symmetries as the origin of flavor". In: *Phys. Rev.* D101.5 (2020), p. 055033. DOI: 10.1103/PhysRevD.101.055033. arXiv: 1906.02208 [hep-ph].

[179] Tatsuo Kobayashi, Satoshi Nagamoto, Shintaro Takada, Shio Tamba, and Takuya H. Tatsuishi. "Modular symmetry and non-Abelian discrete flavor symmetries in string compactification". In: *Phys. Rev.* D97.11 (2018), p. 116002. DOI: 10.1103/PhysRevD.97.116002. arXiv: 1804.06644 [hep-th].

[180] Tatsuo Kobayashi, Kentaro Tanaka, and Takuya H. Tatsuishi. "Neutrino mixing from finite modular groups". In: *Phys. Rev.* D98.1 (2018), p. 016004. DOI: 10.1103/PhysRevD.98.016004. arXiv: 1803.10391 [hep-ph].

[181] Tatsuo Kobayashi, Yusuke Shimizu, Kenta Takagi, Morimitsu Tanimoto, Takuya H. Tatsuishi, and Hikaru Uchida. "Finite modular subgroups for fermion mass matrices and baryon/lepton number violation". In: *Phys. Lett.* B794 (2019), pp. 114–121. DOI: 10.1016/j.physletb.2019.05.034. arXiv: 1812.11072 [hep-ph].

[182] Juan Carlos Criado and Ferruccio Feruglio. "Modular Invariance Faces Precision Neutrino Data". In: *SciPost Phys.* 5.5 (2018), p. 042. DOI: 10.21468/SciPostPhys.5.5.042. arXiv: 1807.01125 [hep-ph].

[183] Tatsuo Kobayashi, Naoya Omoto, Yusuke Shimizu, Kenta Takagi, Morimitsu Tanimoto, and Takuya H. Tatsuishi. "Modular A_4 invariance and neutrino mixing". In: *JHEP* 11 (2018), p. 196. DOI: 10.1007/JHEP11(2018)196. arXiv: 1808.03012 [hep-ph].

[184] P. P. Novichkov, S. T. Petcov, and M. Tanimoto. "Trimaximal Neutrino Mixing from Modular A4 Invariance with Residual Symmetries". In: *Phys. Lett.* B793 (2019), pp. 247–258. DOI: 10.1016/j.physletb.2019.04.043. arXiv: 1812.11289 [hep-ph].

[185] Gui-Jun Ding, Stephen F. King, and Xiang-Gan Liu. "Modular A_4 symmetry models of neutrinos and charged leptons". In: *JHEP* 09 (2019), p. 074. DOI: 10.1007/JHEP09(2019)074. arXiv: 1907.11714 [hep-ph].

[186] J. T. Penedo and S. T. Petcov. "Lepton Masses and Mixing from Modular S_4 Symmetry". In: *Nucl. Phys.* B939 (2019), pp. 292–307. DOI: 10.1016/j.nuclphysb.2018.12.016. arXiv: 1806.11040 [hep-ph].

[187] P. P. Novichkov, J. T. Penedo, S. T. Petcov, and A. V. Titov. "Modular S_4 models of lepton masses and mixing". In: *JHEP* 04 (2019), p. 005. DOI: 10.1007/JHEP04(2019)005. arXiv: 1811.04933 [hep-ph].

[188] Stephen F. King and Ye-Ling Zhou. "Trimaximal TM_1 mixing with two modular S_4 groups". In: *Phys. Rev.* D101.1 (2020), p. 015001. DOI: 10.1103/PhysRevD.101.015001. arXiv: 1908.02770 [hep-ph].

[189] P. P. Novichkov, J. T. Penedo, S. T. Petcov, and A. V. Titov. "Modular A_5 symmetry for flavour model building". In: *JHEP* 04 (2019), p. 174. DOI: 10.1007/JHEP04(2019)174. arXiv: 1812.02158 [hep-ph].

[190] Gui-Jun Ding, Stephen F. King, and Xiang-Gan Liu. "Neutrino mass and mixing with A_5 modular symmetry". In: *Phys. Rev.* D100.11 (2019), p. 115005. DOI: 10.1103/PhysRevD.100.115005. arXiv: 1903.12588 [hep-ph].

[191] Hiroshi Okada and Morimitsu Tanimoto. "CP violation of quarks in A_4 modular invariance". In: *Phys. Lett.* B791 (2019), pp. 54–61. DOI: 10.1016/j.physletb.2019.02.028. arXiv: 1812.09677 [hep-ph].

[192] Hiroshi Okada and Morimitsu Tanimoto. "Towards unification of quark and lepton flavors in A_4 modular invariance". In: (2019). arXiv: 1905.13421 [hep-ph].

[193] Francisco J. de Anda, Stephen F. King, and Elena Perdomo. "$SU(5)$ grand unified theory with A_4 modular symmetry". In: *Phys. Rev.* D101.1 (2020), p. 015028. DOI: 10.1103/PhysRevD.101.015028. arXiv: 1812.05620 [hep-ph].

[194] Tatsuo Kobayashi, Yusuke Shimizu, Kenta Takagi, Morimitsu Tanimoto, and Takuya H. Tatsuishi. "Modular S_3 invariant flavor model in SU(5) GUT". In: *PTEP* 2020.5 (2020), 053B05. DOI: 10.1093/ptep/ptaa055. arXiv: 1906.10341 [hep-ph].

[195] Xiang-Gan Liu and Gui-Jun Ding. "Neutrino Masses and Mixing from Double Covering of Finite Modular Groups". In: *JHEP* 08 (2019), p. 134. DOI: 10.1007/JHEP08(2019)134. arXiv: 1907.01488 [hep-ph].

[196] Gui-Jun Ding, Lisa L. Everett, and Alexander J. Stuart. "Golden Ratio Neutrino Mixing and A_5 Flavor Symmetry". In: *Nucl. Phys.* B857 (2012), pp. 219–253. DOI: 10.1016/j.nuclphysb.2011.12.004. arXiv: 1110.1688 [hep-ph].

[197] Stefan Antusch and Vinzenz Maurer. "Running quark and lepton parameters at various scales". In: *JHEP* 11 (2013), p. 115. DOI: 10.1007/JHEP11(2013)115. arXiv: 1306.6879 [hep-ph].

[198] Ivan Esteban, M. C. Gonzalez-Garcia, Alvaro Hernandez-Cabezudo, Michele Maltoni, and Thomas Schwetz. "Global analysis of three-flavour neutrino oscillations: synergies and tensions in the determination of θ_{23}, δ_{CP}, and the mass ordering". In: *JHEP* 01 (2019), p. 106. DOI: 10.1007/JHEP01(2019)106. arXiv: 1811.05487 [hep-ph].

[199] M. Tanabashi et al. "Review of Particle Physics". In: *Phys. Rev.* D98.3 (2018), p. 030001. DOI: 10.1103/PhysRevD.98.030001.

[200] C. D. Froggatt and Holger Bech Nielsen. "Hierarchy of Quark Masses, Cabibbo Angles and CP Violation". In: *Nucl. Phys.* B147 (1979), pp. 277–298. DOI: 10.1016/0550-3213(79)90316-X.

[201] S. F. King and Graham G. Ross. "Fermion masses and mixing angles from SU(3) family symmetry". In: *Phys. Lett.* B520 (2001), pp. 243–253. DOI: 10.1016/S0370-2693(01)01139-X. arXiv: hep-ph/0108112 [hep-ph].

[202] Ferruccio Feruglio and Andrea Romanino. "Neutrino Flavour Symmetries". In: (2019). arXiv: 1912.06028 [hep-ph].

[203] Jun-Nan Lu and Gui-Jun Ding. "Alternative Schemes of Predicting Lepton Mixing Parameters from Discrete Flavor and CP Symmetry". In: *Phys. Rev.* D95.1 (2017), p. 015012. DOI: 10.1103/PhysRevD.95.015012. arXiv: 1610.05682 [hep-ph].

[204] Cai-Chang Li, Jun-Nan Lu, and Gui-Jun Ding. "Toward a unified interpretation of quark and lepton mixing from flavor and CP symmetries". In: *JHEP* 02 (2018), p. 038. DOI: 10.1007/JHEP02(2018)038. arXiv: 1706.04576 [hep-ph].

[205] Jun-Nan Lu and Gui-Jun Ding. "Quark and lepton mixing patterns from a common discrete flavor symmetry with a generalized CP symmetry". In: *Phys. Rev.* D98.5 (2018), p. 055011. DOI: 10.1103/PhysRevD.98.055011. arXiv: 1806.02301 [hep-ph].

[206] Jun-Nan Lu and Gui-Jun Ding. "Dihedral flavor group as the key to understand quark and lepton flavor mixing". In: *JHEP* 03 (2019), p. 056. DOI: 10.1007/JHEP03(2019)056. arXiv: 1901.07414 [hep-ph].

[207] Mu-Chun Chen, Saúl Ramos-Sánchez, and Michael Ratz. "A note on the predictions of models with modular flavor symmetries". In: *Phys. Lett.* B801 (2020), p. 135153. DOI: 10.1016/j.physletb.2019.135153. arXiv: 1909.06910 [hep-ph].

[208] Hiroshi Okada and Yuta Orikasa. "Modular S_3 symmetric radiative seesaw model". In: *Phys. Rev.* D100.11 (2019), p. 115037. DOI: 10.1103/PhysRevD.100.115037. arXiv: 1907.04716 [hep-ph].

[209] Takaaki Nomura and Hiroshi Okada. "A two loop induced neutrino mass model with modular A_4 symmetry". In: (2019). arXiv: 1906.03927 [hep-ph].

[210] Gui-Jun Ding, Stephen F. King, Xiang-Gan Liu, and Jun-Nan Lu. "Modular S_4 and A_4 symmetries and their fixed points: new predictive examples of lepton mixing". In: *JHEP* 12 (2019), p. 030. DOI: 10.1007/JHEP12(2019)030. arXiv: 1910.03460 [hep-ph].

[211] Tatsuo Kobayashi, Yusuke Shimizu, Kenta Takagi, Morimitsu Tanimoto, and Takuya H. Tatsuishi. "New A_4 lepton flavor model from S_4 modular symmetry". In: *JHEP* 02 (2020), p. 097. DOI: 10.1007/JHEP02(2020)097. arXiv: 1907.09141 [hep-ph].

[212] Jun-Nan Lu, Xiang-Gan Liu, and Gui-Jun Ding. "Modular symmetry origin of texture zeros and quark lepton unification". In: *Phys. Rev.* D101.11 (2020), p. 115020. DOI: 10.1103/PhysRevD.101.115020. arXiv: 1912.07573 [hep-ph].

[213] Bobby Samir Acharya, D. Bailin, A. Love, W. A. Sabra, and Steven Thomas. "Spontaneous breaking of CP symmetry by orbifold moduli". In: *Phys. Lett.* B357 (1995). [Erratum: Phys. Lett.B407,451(1997)], pp. 387–396. DOI: 10.1016/0370-2693(95)00945-H,10.1016/S0370-2693(97)00912-X. arXiv: hep-th/9506143 [hep-th].

[214] Joel Giedt. "CP violation and moduli stabilization in heterotic models". In: *Mod. Phys. Lett.* A17 (2002), pp. 1465–1473. DOI: 10.1142/S0217732302007879. arXiv: hep-ph/0204017 [hep-ph].

[215] Tatsuo Kobayashi and Shio Tamba. "Modular forms of finite modular subgroups from magnetized D-brane models". In: *Phys. Rev.* D99.4 (2019), p. 046001. DOI: 10.1103/PhysRevD.99.046001. arXiv: 1811.11384 [hep-th].

[216] Tatsuo Kobayashi and Hajime Otsuka. "Classification of discrete modular symmetries in Type IIB flux vacua". In: *Phys. Rev.* D101.10 (2020), p. 106017. DOI: 10.1103/PhysRevD.101.106017. arXiv: 2001.07972 [hep-th].

[217] Fredrik Björkeroth, Francisco J. de Anda, Ivo de Medeiros Varzielas, and Stephen F. King. "Towards a complete $A_4 \times SU(5)$ SUSY GUT". In: *JHEP* 06 (2015), p. 141. DOI: 10.1007/JHEP06(2015)141. arXiv: 1503.03306 [hep-ph].

[218] Stephen P. Martin and Michael T. Vaughn. "Regularization dependence of running couplings in softly broken supersymmetry". In: *Phys. Lett.* B318 (1993), pp. 331–337. DOI: 10.1016/0370-2693(93)90136-6. arXiv: hep-ph/9308222 [hep-ph].

[219] G. F. Giudice and R. Rattazzi. "Extracting supersymmetry breaking effects from wave function renormalization". In: *Nucl. Phys.* B511 (1998), pp. 25–44. DOI: 10.1016/S0550-3213(97)00647-0. arXiv: hep-ph/9706540 [hep-ph].

[220] Federica Bazzocchi, Luca Merlo, and Stefano Morisi. "Fermion Masses and Mixings in a S(4)-based Model". In: *Nucl. Phys.* B816 (2009), pp. 204–226. DOI: 10.1016/j.nuclphysb.2009.03.005. arXiv: 0901.2086 [hep-ph].